⊿\E<

Laboratório Nacional de Engenharia Civil

NUMERICAL MODELLING OF IRREGULAR WAVE PROPAGATION IN THE NEARSHORE REGION

Londres, Maio 1997

Filipa Simões de Brito Ferreira de Oliveira

I&D
TESE
HIDRÁULICA

University of London

Imperial College of Science,
Technology and Medicine

Department of Civil Engineering

NUMERICAL MODELLING OF IRREGULAR WAVE PROPAGATION IN THE NEARSHORE REGION

Filipa Simões de Brito Ferreira de Oliveira

Licenciada em Engenharia Civil pela Universidade de Coimbra
Mestre em Rios, Estuários e Engenharia Costeira pela University of London

Acknowledgements

The author would like to express her gratitude to Dr K. Anastasiou for his supervision, advice, and support which have been essential to carry out this study.

The author would also like to thank to Dr Y. Zhao for discussions and comments on issues encountered in this study, and to her colleagues in the same research group for their kindness and friendship.

Contents

List of Figures

List of Tables

Table no.	Chapter	Title	Page
5.1	5	Test conditions for non-breaking series.	148
6.1	6	Test conditions for the breaking series.	198

List of Symbols

Symbol	Definition
a	Wave amplitude
a, b, e	Coefficients in singular perturbation difference equation
C	Wave celerity; phase velocity
C_g	Group velocity
d	Water depth (from bottom sea to SWL)
d_b	Water depth at breaking
E	Mean wave energy density
F	Function in multigrid system
f	Wave frequency
f_D	Dissipation factor
f_p	Peak frequency of the energy spectrum
G	Grid system in multigrid method
g	Gravitational acceleration
H	Wave height
H_0	Offshore wave height
H_b	Breaking wave height
H_{rms}	Root mean square wave height
H_s	Significant wave height
h	Mean water depth and mesh size in multigrid system
i	Imaginary unit ($\sqrt{-1}$)
k	Wave number ($2\pi/L$)

L	Wave length and partial difference operator
L_0	Offshore wave length
Q	Flux; vertically integrated function of particle velocity
Q_x	Flux in x direction
Q_y	Flux in y direction
T	Wave period
t	time
Ur	Ursell parameter
u, v, w	x, y, z direction velocity components
x	Coordinate axis: horizontal, normal to shore, positive to front when facing shore
y	Coordinate axis: horizontal, parallel to shore, positive to left when facing shore
α	Wave direction and reflection coefficient
α_0	Incident wave angle
ε	Energy dissipation rate per unit surface and per unit of time
π	Constant = 3.14159 ...
ρ	Sea water density
Ψ	Logarithm of velocity potential function
ϕ	Velocity potential
ω	Wave angular frequency
Ω	Calculation domain
$\partial\Omega$	Boundary of calculation domain
η	Displacement of water surface relative to SWL by passage of a wave
θ	Wave phase angle
Λ	Partial difference operator on boundary

Chapter 1

Introduction

1.1 - The subject of study

Waves play a dominant role in the field of coastal engineering. They are a major component of the design of coastal structures, harbour planning, and beach protection works. Information about the wave field for a certain area of interest is important as input data in order to evaluate the nearshore hydrodynamics (wave processes are responsible for large fluid motions which drive currents) and also the nearshore morphodynamics (the consequent sediment transport and bed evolution). More attention has been devoted to this topic since the 70's, which has led to significant progress being achieved in its understanding and consequent modelling.

This particular study is centralised on the modelling of the wave field. The quantification of the nearshore wave climate usually produces information such as wave height and wave direction. The estimation of the wave field is done because in general the locations where the wave conditions are known are different from the locations at which the design wave conditions are desired and so it is necessary to calculate the transformation of waves from one depth to another in order to obtain the design wave conditions at the particular area of interest. Such wave transformations occurring in the nearshore region involve processes such as shoaling, refraction, diffraction, reflection and breaking.

The sea state is a random process with the repercussion that its modelling is a complex task. Physical and numerical models have been developed all over the world to improve the realism and accuracy of wave transformation predictions

although aspects like wave interactions, mostly non - linear, remain still poorly understood. Physical models are usually quite expensive, therefore the use of numerical models is currently on the increase with the advantage of their immediate use in industry for more than one application.

Wave transformation modelling techniques and mathematical models of wave climate have been reviewed by Hamm et al. (1993) and Yoo et al. (1989). Since the last decade the mild - slope equation derived by Berkhoff (1972, 1976) for linear waves, has become the most popular mathematical model to predict the wave field in the nearshore region. It describes wave transformations from deep water through to shallow water in terms of the velocity potential function, including the processes of refraction, diffraction and reflection.

The above equation is a departure from the traditional approach based on a wave averaged energy conservation law, which is the main component of pure refraction wave ray models, derived by integrating basic equations of fluid motion over the depth and averaging over a wave period. Ray models have the advantage that they can be applied to large areas with relatively small computational storage requirements. Nevertheless, the majority of such models cannot describe satisfactorily wave transformation in caustic zones because the underlying technique does not allow for the diffraction process. More recently, this limitation has been overcome in a model proposed by Yoo and O'Connor (1986) by introducing a term that accounts for diffraction into the kinematic energy conservation equation. However, like other ray models it is only valid for fully progressive waves, that is; it excludes the effects of reflection.

The mild - slope equation has been successfully applied to a wide range of water depths, although it loses some accuracy in shallow water and for very steep waves. It is also accepted that in shallow water the Boussinesq equation gives better results than the mild-slope equation because in the latter the linear wave assumption is not applicable in shallow water. Nevertheless, this disadvantage can be somewhat overcome by introducing a certain degree of non - linearity into the model with the inclusion of a non - linear term based on an empirically formulated dispersion relationship. Other phenomena like wave - current interaction (Kirby, 1984) and

energy dissipation (Dalrymple et al, 1984) have also been recently implemented into the original equation.

Numerical solution methods for the mild - slope equation have been the subject of constant investigation since its derivation, and in order to develop more efficient models several researchers have derived different formulations of the mild - slope equation, namely parabolic, hyperbolic and elliptic. In this work the wave field is solved adopting the elliptic form of the mild - slope equation. Part of the work is dedicated to developing an efficient numerical model capable of solving the problem with a minimum computational cost and simultaneously without imposing any mathematical restriction that would lead to inadequate description of the physics involved. The rest of the work is dedicated to its application to a random wave field. The process of energy dissipation through wave breaking has been introduced into the model where the randomness of the wave field is dealt with by a spectral component approach, which consists of dividing the spectrum into a finite number of independent components in the frequency domain over a certain range of directions.

1.2 - Original contributions of this work

The original contributions of this work can be summarised as follows:

1) An efficient numerical model to solve the elliptic formulation of the mild - slope equation based on a robust iterative method that can be applied to large areas with a reasonable computational cost.

2) An improved numerical model based on a hyperbolic form of the mild - slope equation achieved by incorporating sponge filters into the numerical boundaries so as to increase their efficiency in dealing with outgoing waves.

3) An evaluation of the effects on the performance of the numerical model based on the elliptic form of the mild - slope equation of incorporating sponge filters

into the model and upgrading the radiation boundary conditions from first to higher orders of accuracy.

4) A numerical model based on a non - linear transformation of the mild - slope equation which is solved by an iterative process which has its convergence behaviour accelerated by a multigrid technique.

5) A numerical model for irregular wave propagation in the nearshore region that does not include the energy dissipation process due to wave breaking, based on (1) above and on the linear superposition of independent spectral components.

6) Two numerical models for irregular wave propagation in the nearshore region that incorporate the phenomenon of wave breaking based on different formulations.

1.3 - Layout of the thesis

This thesis is divided in 7 chapters. Each of chapters 2, 3, 4, 5 and 6 deals with a different subject although there is a logical sequence linking them. In each of the chapters one or more numerical models are described, developed and validated. An introduction to the particular subject is given at the beginning of each chapter followed by a description of its mathematical formulation and then a literature survey on work previously done on its modelling. There follows a mathematical description of the model proposed, the tests performed to validate the model or models together with a discussion of the results obtained, and finally each chapter is concluded with a brief summary. In the last chapter, chapter 7, conclusions about the work undertaken are established and some recommendations for further work based on these conclusions are put forward.

In chapter 2 two robust algorithms are implemented in two iterative numerical models of the elliptic form of the mild - slope equation. Chapter 3 is devoted to improving the performance of models based on the mild - slope equation by implementing and testing different types of radiation boundary conditions for

outgoing waves. Different proposals are examined and implemented, and their effects evaluated. In chapter 4 a numerical model based on a non - linear formulation of the mild - slope equation is solved iteratively and a multigrid technique is used to accelerate its convergence. In chapter 5 a numerical model for random waves based on the model previously obtained for monochromatic waves is developed. Finally in chapter 6 two different approaches for incorporating the breaking phenomenon are put forward in the numerical model for random waves and the performance of the two numerical models generated is evaluated.

Chapter 2

The Mild-Slope Equation
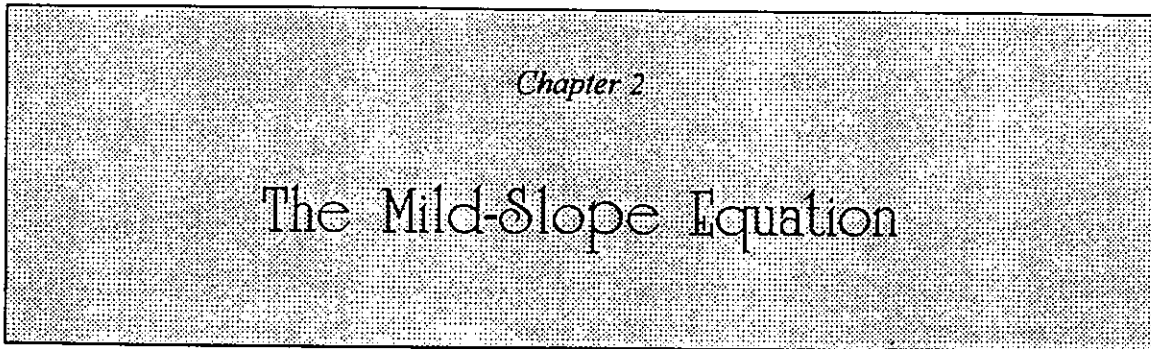
2.1 - Introduction

2.1.1 - Chapter layout

In this chapter is described the initial part of the research work done on modelling wave propagation. The goal was to develop a numerical model for the mild - slope equation that approaches the phenomenon of regular wave propagation accurately and efficiently without compromising the physics involved. The elliptic form of the mild -slope equation was chosen because it is the one that best satisfies the above requirements as will be explained in the chapter.

To develop an efficient model, it is crucial to implement a suitable algorithm that iteratively solves the linear system of equations generated from the governing equation. Thus, two numerical models with different algorithms were developed.

The present chapter is organised as follows:

- This section introduces the mild-slope equation and discusses its validity. It includes a description of refraction and diffraction together with a general survey of previous models that approach both phenomena.
- Section 2.2 is dedicated to the derivation of the mild-slope equation and a literature survey on the existing models.
- In section 2.3 a numerical model based on an elliptic form of the mild-slope equation is proposed. The governing equation and the boundary conditions are described. The mathematical methods to solve the linear system generated are extensively discussed and finally the two algorithms implemented are presented.

- In section 2.4 the validation of the models (which differ in terms of the implemented algorithm that solves the linear system iteratively) is done. Both are verified for the case of waves propagating over an elliptic shoal and for harbour resonance.

- In section 2.5 the two numerical models are compared in terms of efficiency.

- To close the present chapter a summarised discussion of the work here developed is done in section 2.6.

2.1.2 - General concepts

Linear waves are the first approximation of a complete theoretical description of monochromatic or regular wave behaviour. They are symmetrical about the SWL and as they are pure oscillatory waves, which means that water particles move in closed orbits for each wave period, the fluid is assumed not to move in the direction of wave advance. In order to legitimately apply the linear wave theory the wave steepness, H/L, and the Ursell or Stokes parameter defined by Stokes (1847) as $Ur = L^2 H/d^3$, should be small. Short waves are classified by $H/L \ll 1$ and $Ur \leq 75$. Waves can be classified based on the ratio of water depth to wave length as

Classification	d/L
Shallow water waves	<1/20
Intermediate water depth waves	1/20 to 1/2
Deep water waves	>1/2

However, Goda (1983) summarised these parameters in the form of the Ursell parameter and suggested the following classification:

Short waves	when	$Ur \leq 75$
Long waves	when	$Ur \geq 75$

Commonly waves are classified as short for periods less then around 22 sec and long for periods from 22 sec up to 10 min.

Before the derivation of the mild-slope equation refraction and diffraction were treated separately for short waves although some authors attempted to describe the combined phenomenon mathematically. The shortcomings of these equations was that they did not reduce to the linear shallow water equation in the case of small water depth, and they did not reduce to the appropriate refraction equations, the eiconal equation (defining the path of a wave ray) and the energy flux equation (from which can be derived the law of conservation of energy flux between two rays), when neglecting diffraction (or the curvature $\nabla^2 a$ of the amplitude function).

Refraction can be caused by variations on the bathymetry or by any sort of interference on the wave propagation that causes one part of a wave to travel faster or slower than another. This phenomenon is described in several text books dedicated to wave mechanics and it is approached by a ray theory or geometrical optics theory, assuming that wave rays can be defined as a family of curves to which the wave number vectors are tangential and the wave energy flux is conserved between two adjacent wave rays. Neglecting the presence of currents and for coastlines with straight parallel contours refraction analysis has been done for several years based on Snell's law by two basic techniques, graphical and numerical.

Diffraction is the phenomenon of diffusion or transverse flow of wave energy. As a dynamic process, different from the kinematic process of wave refraction it can only be investigated through the fundamental equations of fluid motion. Diffraction effects can occur due to the presence of an obstacle or if there is an abrupt change in orthogonal spacing along the wave crest. In practice, the second factor can be neglected for the pure refraction case but one should bear in mind that it can affect the resulting wave height by diminishing the effect of wave refraction on wave height variation along a wave crest. Water wave diffraction is analogous to the diffraction of light, therefore Penny and Price (1952) derived a solution for the Helmholtz equation based on Sommerfeld's theory of the diffraction of light for the case of surface waves. They were able to predict the wave crest pattern and height variation for diffracted water waves. Wiegel (1962) applied the exact solution presented by Penny and Price (1952) to calculate the diffraction coefficient for each point behind a structure as a function of its position relatively to the lee of the structure and the characteristics of the incident wave. This method can be applied to evaluate the effects of diffraction for a detached breakwater provided the length

of the breakwater is equal to or greater than a few wave lengths. Johnson (1952, 1953) studied wave passing through a gap for different gap width to incident wave length ratios and calculated diffraction coefficient contours in the lee of a gap whose width is smaller than about five times the incident wave length. For a greater gap width the diffraction effects of the structure on each side of the gap can be considered independent and therefore the theory for diffraction at the end of each single structure can be used for each side. For both types of structures, single and with a gap, diffraction diagrams can be found in several text books (U.S. Army Corps of Engineers, 1984).

2.2 - The mild-slope equation

The mild-slope equation can be derived based on the principle of conservation of energy under the assumption that the bed is mildly sloping ($\nabla h/kh = O(\varepsilon) << 1$)), that is that the rate of change of water depth is small within a characteristic wave length, and the water motion is irrotational, which allows the introduction of a wave potential function. Wind action, wave breaking, bottom friction and bed percolation were neglected. It is a vertically integrated model for wave motion therefore the governing equation is 2-D. It is valid for a time-harmonic or periodic wave motion and it can be considered on its time-dependent or time independent form. It reduces to the Helmholtz equation for constant water depth and to the long wave equation for shallow water. It is approximate in intermediate depth and exact in both deep and shallow water. Booij (1983) comparing results obtained from the mild-slope equation discretised by a finite elements technique with the full linear equations (3-D model) reported favourably on the use of the mild-slope for quite large slopes like 1:3 or even the order of unity for certain circumstances. Several other authors like Copeland (1985), Smith and Sprinks (1975) presented a formal derivation of the mild-slope equation and a more brief description can be seen in several text books like Mei (1989), Massel (1989)and Dean and Dalrymple (1984).

2.2 1 - The existing models

Since the 70's the mild-slope equation has been widely used because it can both deal with generally complex wave fields (practical flexibility) and guarantee good agreement with experimental data (accuracy).

Several numerical models were proposed to solve the elliptic form of the mild-slope equation by a finite elements technique (Berkhoff 1972, Bettess and Zienkiewicz 1977, Houston 1981, Tsay and Liu 1983) which were verified by comparison with analytical solutions like Hom-ma 's results for the long wave equation for plane waves incident upon an island, measurements from a hydraulic model and different numerical models available. Others proposed solutions obtained by a finite differences technique (Williams et al 1980). All these numerical models give reasonably good results although they require a certain minimum number of grid nodes, 8 or 10, per wave length. This limits the applicability of the model to a large coastal area due to its computational cost in terms of memory and time requirements. These models were efficient for domains of applicability of the order of a few wave lengths. Although a discretisation of the partial differential equation using finite elements has the theoretical advantage of flexibility in terms of dimensions of grid elements and therefore allowing a more detailed solution for a particular area of interest, in practice, due to the requirement of a minimum number of grid nodes per wave length, a finite differences discretisation can be a more simple numerical technique to achieve the same accuracy for the approximate solution, with less computational effort involved, in this particular elliptic form of the mild - slope equation.

Nevertheless, in order to overcome the computational effort to solve the mild-slope equation on its elliptic form and obtain a solution for larger domains, several authors proposed a model based on the transient or time dependent form of the mild-slope equation (Copeland 1975, Madsen and Larsen 1987). Copeland's model is described in chapter 3. These mathematical models consist of a set of first order differential equations derived from the elliptic form by Ito and Tanimoto (1972) for a steady state harmonic solution. The derived hyperbolic system contains the equation of motion and continuity and it is similar in form to the shallow water equations. The number of grid nodes per wave length necessary to obtain valid results is of the same order as for the elliptic form. The disadvantage of this model is that for large domains the

amount cf computer time required to reach a steady state is considerable since the time step allowed by the explicit finite differences method is controlled by the Courant number criterion.

Dong and Al-Mashouk (1989) compared the hyperbolic or transient model (initial value problem) with the elliptic or steady state model (boundary value problem) and in fact they did not conclude on the superiority of one of the models over the other. Nevertheless, for some particular problems like harbour resonance, the hyperbolic model requires a considerable amount of time to reach a steady state, and thus can be less efficient.

Another way to solve the mild-slope equation using a more economic model was suggested by Radder(1979) with a parabolic approximation. Parabolic approximations are widely used because they can be used in wave propagation studies over an area of 10 to 100 wave lengths. The disadvantage of such a formulation concerns the inadequate description of the underlying physics. Wave reflections and diffraction effects (curvature of the wave amplitude) in the direction of wave propagation are neglected. This means that only diffraction effects along the wave front (line of equal phase) are taken into account and that the main direction of propagation has to be maintained. Such considerations can be of extreme importance in harbours and therefore limit the applicability of the model in those circumstances.

Pursuing the goal of finding approximate solutions of the mild-slope equation suitable for large coastal areas, Panchang et al (1988) developed a model based on the elliptic form of the mild-slope equation transformed by Radder (1979), the reduced wave equation, which is solved by an Error Vector Propagation or marching method implemented in finite differences. The advantage over the parabolic form is that reflections are considered allowing therefore its applicability when the bathymetry or structures reflect the energy in the main propagation direction. However, the physics is still compromised regarding diffraction.

Another attempt to address the problem was suggested by Ebersole (1985) with a model in which the set of governing equations was derived from the elliptic form. It consists of an initial value problem with a finite differences solution. The author claims

that it can be applied without the parabolic models constrains for areas two orders of magnitude larger than the areas were a model based on the elliptic form as a boundary value problem is applied.

Radder (1979) and Li and Anastasiou (1992) proposed a numerical model based on a non-linear form of the mild-slope equation where the dependent variable is a slower varying function than the velocity potential. The advantage of this governing equation is that due to the characteristics of this new function the minimum number of nodes per wave length required to obtain reasonable results can be of the order of 3 in the absence of reflections. Thus, it allows the applicability of the model for larger coastal areas. Li and Anastasiou (1992) implemented a multigrid technique to accelerate the convergence process of the model. Further description and discussion is done in chapter 4.

A recent group of numerical models proposed by Panchang et al (1991), Li (1994) and Zhao and Anastasiou (1996) seem to be in the right direction to overcome the difficulty of solving the mild-slope equation for large coastal areas without compromising the physics involved in the phenomenon. All these models assume the elliptic form of the mild-slope equation as the governing equation and discretise it by a finite differences technique. The innovation of these models consists of solving the problem iteratively using powerful algorithms which have been more recently either developed or explored. A more detailed discussion of these models is done in section 2.3 because it would not be appropriate to do it here.

2.3 - Numerical treatment of the mild-slope equation

The original mild-slope as derived by Berkhoff (1972)

$$\nabla.\left(CC_g \nabla\phi\right) + \omega^2 \phi \frac{C}{C_g} = 0$$
(2.1)

can be written in its Helmholtz form without loss of generality (Radder, 1979), as

$$\nabla^2 \phi + k_c^2 \phi = 0 ,$$ (2.2)

also called the reduced wave equation, where k_c , the effective wave number is defined by

$$k_c^2 = k^2 - \frac{\nabla^2 (CC_g)^{\frac{1}{2}}}{(CC_g)^{\frac{1}{2}}} ,$$ (2.3)

k is the local wave number governed by the dispersion relation

$$\omega^2 = gk \tanh(kh) ,$$ (2.4)

ω is the wave angular frequency, h is the local water depth, g is the gravitational acceleration, $C=\omega/k$ is the phase velocity and $C_g=\partial\omega/\partial k$ is the group velocity.

Equation (2.2) is an elliptic equation, boundary value problem, that can be discretised by a 2nd order finite differences technique valid for the grid node i,j as follows,

$$\left(\frac{\phi_{i-1,j} - 2\phi_{i,j} + \phi_{i-1,j}}{\Delta x^2} \right) + \left(\frac{\phi_{i,j-1} - 2\phi_{i,j} + \phi_{i,j-1}}{\Delta y^2} \right) + k_c^2 \phi_{i,j} = 0$$ (2.5)

in a system of cartesian co-ordinates, where x is the direction normal to the shore and y is parallel to the shore.

Other forms of discretisation could have been used but this was chosen due to its simplicity, effectiveness and small number of variables involved.

In a boundary value problem the implementation of the most representative boundary conditions is essential to the performance of the model. An attempt to improve the order of accuracy of boundary conditions, as it is done in chapter 3, is a worthwhile investment aiming at improving the model.

Boundary conditions are extensively described in chapter 3, therefore in this chapter the subject will be restricted to a brief description of first order radiation boundary conditions. They can simulate outgoing waves in order to limit the area of computation with the minimum amount of artificial reflections or introduce a certain

reflectivity to simulate a possible obstacle. The radiation boundary conditions for waves approaching the boundary with a normal incidence are:

- Offshore driving boundary

$$\frac{\partial \phi}{\partial x} = ik_c \left(2\phi^i - \phi\right) \tag{2.6}$$

discretised as

$$\frac{\phi_{i-1,j} - \phi_{i,j}}{\Delta x} - ik_c \left(2\frac{\phi_{i-1,j}^i + \phi_{i,j}^i}{2} - \frac{\phi_{i-1,j} + \phi_{i,j}}{2}\right) = 0 \tag{2.7}$$

for i = 1 and j = 1,....,Ny

- Shoreward downstream boundary

$$\frac{\partial \phi}{\partial x} = ik_c \alpha\phi \tag{2.8}$$

discretised as

$$\frac{\phi_{i,j} - \phi_{i-1,j}}{\Delta x} - ik_c \alpha\left(\frac{\phi_{i,j} + \phi_{i-1,j}}{2}\right) = 0 \tag{2.9}$$

for i = Nx and j = 1,....,Ny

- Lateral downstream boundaries

$$\frac{\partial \phi}{\partial y} = ik_c \alpha\phi \tag{2.10}$$

discretised as

$$\frac{\phi_{i,j} - \phi_{i,j+1}}{\Delta y} - ik_c \alpha\left(\frac{\phi_{i,j} + \phi_{i,j+1}}{2}\right) = 0 \tag{2.11}$$

for i = 1,....,Nx and j = 1, and

$$\frac{\phi_{i,j} - \phi_{i,j-1}}{\Delta y} - ik_c \alpha\left(\frac{\phi_{i,j} + \phi_{i,j-1}}{2}\right) = 0 \tag{2.12}$$

for i = 1,...., Nx and j = Ny

where α is a reflection coefficient to be determined empirically and ϕ^i is the incident wave at the boundary.

The downwave formulations (2.8) and (2.10) were derived to produce an approximated solution at the boundaries that minimise reflection of the outgoing waves and simultaneously a solution of the Helmholtz equation in the form of a plane wave. Its derivation can be followed in Kirby's publication, 1989. The driving boundary condition, formulated by equation (2.6) is based on the same derivation as the downwave boundaries, but here the velocity potential is assumed to have two components, the incident and the backscattered potential

$$\phi = \phi^i + \phi^r,$$ (2.13)

and thus

$$\frac{\partial \phi}{\partial x} = ik_c\left(\phi^i - \phi^r\right) = ik_c\left(\phi^i - \left(\phi - \phi^i\right)\right) = ik_c\left(2\phi^i - \phi\right).$$

The discretisation of this boundary value problem generates a linear system of equations (Ax=b) that can be solved by a direct or indirect method.

Direct methods, like the Gaussian elimination method, produce the exact answer in a finite number of steps (in the absence of rounding error). They can be efficient for domains of approximately 10 wave lengths. However, bigger areas imply larger storage requirements which can make the problem prohibitive despite applying sparse matrix techniques.

Indirect or iterative methods produce a sequence of approximations which converge to the solution in the limit and can be more economical than direct methods for a large system of equations. Iterative methods were therefore chosen. They can be classified into stationary and gradient methods. For both cases trial values of variables are improved by iterative corrections until they satisfy a convergence criterion. It is the correction technique of the values of the variables that distinguishes the methods.

An iterative method is called stationary when the error propagation through one iteration step can be specified in the form

$$e^{(k+1)} = Me^{(k)},$$ (2.14)

where $e^{(k)}$ is the vector of errors in the approximation $x^{(k)}$ such that

$$x^{(k)} = x + e^{(k)}$$ (2.15)

and M is the iteration matrix, function of the coefficient matrix A, which does not vary from iteration to iteration.

An iterative gradient method of solving n simultaneous equations is equivalent to the process of finding the position of the minimum of an error function defined over an n - dimensional space. This is done by finding groups of vectors and directions that correspond to the solution. In each iteration a trial set of values for the variables generates a new set corresponding to a lower value of the error function. Here, in contrast with stationary methods, error vectors cannot be generated by means of an iteration matrix therefore the process is classified as non - stationary.

Finally comes the convergence criterion which, if satisfied, terminates the iterative process. The two most common criteria are: either a vector difference norm or a residual norm both associated with a tolerance chosen according to the degree of accuracy of the solution wanted.

For a vector difference norm the formulation is

$$\frac{\left\| x^{(k)} - x^{(k-1)} \right\|}{\left\| x^{(k)} \right\|} \leq \text{tolerance}.$$
(2.16)

For a residual norm the formulation is

$$\frac{\left\| r^{(k)} \right\|}{\left\| b \right\|} \leq \text{tolerance}$$
(2.17)

or

$$\frac{\left\| r^{(k)} \right\|}{\left\| x^{(k)} \right\|} \leq \text{tolerance},$$
(2.18)

where $r^{(k)}$ is the residual $b - Ax^{(k)}$.

The residual norm was the criterion chosen when solving the mild-slope equation for two reasons: it is known to be the more reliable of the two criteria since some iterations may have a slow convergence; also its use would be consistent with other authors like Panchang et al (1991), Li (1994) and Zhao and Anastasiou (1996), who used the same criterion. Consequently, the iterative process used to solve the mild-slope equation is terminated when

$$\frac{\sum \left\| \nabla^2 \phi + k_c^2 \phi \right\|^2}{\sum \left\| \phi \right\|^2} \le \text{tolerance} .$$
(2.19)

The difficulty of iterative methods is mainly related with the convergence process. Classical stationary methods like Gauss - Seidel, Jacobi and SOR (Successive Over Relaxation) do not guarantee convergence when applied to the present governing equation because:

a) A is not diagonally dominant. The sum of the coefficients of the non-diagonal elements in the matrix (which are 4, resulting from the first four terms) are usually larger in absolute value, than the coefficient of the diagonal element.

b) A is non-Hermitian hence not positive definite. For A to be Hermitian $\overline{A}^T = A$, that is $\overline{a_{kj}} = a_{jk}$, which is not true due to the boundary conditions.

Consequently other methods have to be considered in order to solve the mild - slope equation iteratively.

The conjugate gradient (CG) method converges only when A is symmetric ($A^T = A$ or $a_{kj} = a_{jk}$) and positive definite ($x^T A x > 0$, $\forall x \in C \ne 0$). To overcome this difficulty, Panchang (1991) reformulated the problem to produce a matrix A, which is symmetric and positive definite by using a Gauss transformation, i.e. by multiplying each side of the equation by the complex conjugate transpose of A. The matrix A was thus transformed to a normal matrix. Although the process was guaranteed to converge it was rather slow. Thus Panchang (1991) proposed to use a real matrix to precondition the governing equation and then apply the previous transformation. He then obtained an algorithm that requires more operations per iteration but claimed that convergence is reached after substantial fewer iterations, resulting in savings of computer time.

Li (1994) proposed a modified CG method named generalised conjugate gradient (GCG) method. As it was said, gradient methods are based on the idea of minimising an error function. The term conjugate means that the successive generated vectors that converge to the solution are orthogonal with respect to A. The difference between the CG and the GCG method is that they were derived based on a

different error function. This allows for the GCG method to be applied in a straight forward manner without having to transform the matrix A into a normal matrix. Li (1994) demonstrated that to solve the elliptic shoal case with a convergence criterion represented by equation (2.19), for a tolerance of 10^{-7} the CG without preconditioning requires 16800 iterations, with preconditioning requires 2000 iterations and the GCG requires 2500 iterations. He claimed that the rate of convergence of the GCG is as fast as that of normal equations with preconditioning and with less storage requirements.

In the present work two other gradient - like methods are studied and used to solve the mild-slope equation. They are the Biconjugate Gradient Stabilised (Bi-CGSTAB) method proposed by Van der Vorst (1992) and the Generalised Minimum Residual (GMRES) proposed by Saad and Schultz (1986). They were developed for non-Hermitian linear systems and the difference between these Krylov Subspace Methods is that while the GMRES iterates the approximate solution expressed in terms of Arnoldi vectors, the Bi-CGSTAB iterates the approximate solution expressed in terms of unsymmetric Lanczos vectors.

A subspace of R^m is a subset that is also a vector space and for a collection of vectors $a_1, ..., a_n \in R^m$, the set of all linear combinations of theses vectors is a subspace. Krylov subspaces are just the range spaces of the Krylov matrices which can be defined as follows: if $A \in R^{n \cdot n}$ and $v \in R^n$, then the Krylov matrix $K(A, v, j) \in R^{n \times j}$ is expressed as $K(A,v,j) = \left[v, Av, ..., A^{j-1}v\right]$.

Using the Arnoldi vectors or the unsymmetric Lanczos vectors are two ways to proceed in order to overcome the non symmetry of the matrix A which results in the non existence of the orthogonal tridiagonalisation $Q^T A Q = T$. In order to implement both algorithms, a partial triadiagonalisation of A is done. The Arnoldi algorithm allows the partial triadiagonalisation of A making use of only one set of orthogonal vectors, meaning that, the approach involves a column by column generation of an orthogonal Q such that $Q^T A Q = H$ is the Hessenberg reduction ($h_{ij} = 0$, i>j+1), with $Q^T Q = I$. The unsymmetric Lanczos algorithm makes use of 2 sets of biorthogonal

vectors for the triadiagonalisation of A. This approach computes the columns of $Q =$ $[q_1, ..., q_n]$ and $P = [p_1, ..., p_n]$ so that $P^T A Q = T$ is tridiagonal and $P^T Q = I_n$.

Both algorithms, for the Bi-CGSTAB and the GMRES methods, are described in the following sections.

2.3.1 - The Bi - CGSTAB method

The Biconjugate Gradient method (Bi-CG) was initially presented by Fletcher (1976) for solving general non-Hermitian systems. It is an extension of the Lanczos derivation of the Conjugate Gradient method by producing a sequence of iterates $\{x_k\}$ with the property that x_k belongs to $x_0 + k(A, r_0, k)$ and produces a residual that is orthogonal to $k(A^T, s_0, k)$ for some $s_0 \in R^n$, where the symbol k denotes subspace. However, in here, the matrix A is not symmetric therefore it is not possible to reduce it to tridiagonal. Thus the unsymmetric Lanczos process is used to generate bases for the two involved Krylov spaces. In particular, after k steps of the unsymmetric Lanczos algorithm we have: $Q_k, P_k \in R^{n \cdot k}$ such that $P_k^T Q_k = I_k$, a tridiagonal matrix $T_k = P_k^T A Q_k$ such that

$$AQ_k = Q_k T_k + r_k e_k^T \qquad P_k^T r_k = 0$$

$$A^T P_k = P_k T_k^T + s_k e_k^T \qquad Q_k^T s_k = 0,$$

and the Galerkin condition

$$P_k^T (b - A x_k) = P_k^T (r_0 - A Q_k y_k) = 0$$

is valid, $Q_k = [q_1, ..., q_k]$ and $P_k = [p_1, ..., p_k]$ are Lanczos vectors, that is a sequence of orthogonal vectors, $e_k = I_k(:,k)$ and y_k such that $T_k y_k = Q_k^T r_0$.

Because the Bi-CG method suffered from numerical instability due to its dependence on the unsymmetric Lanczos process, more stable algorithms were developed in order to overcome this shortcoming of the method. The most successful was the Conjugate 'Gradients-Squared (CG-S), a variant of the Bi-CG that steered the direction vector towards the solution. It is known for its favourable speed of convergence but it presents a quite irregular convergence behaviour particularly

when starting the iteration close to the solution. A new method which is more smoothly convergent was needed and so Van der Vorst (1992) proposed the Bi-CGSTAB method. This method is applied as follows:

a) Choose ϕ_0 and tolerance. Set the scalar $\bar{\omega}_0 = 1$, $\beta = 1$, $\alpha_0 = 1$, and the vectors $v_0 = q_0 = 0$.

b) Calculate $r_0 = b - A\phi_0$

c) For i=1,2,...

$$\bar{\beta} = (r_0, r_{i-1})$$

$$\omega_i = \frac{\bar{\beta} \, \bar{\omega}_{i-1}}{\beta \, \alpha_{i-1}}$$

$$q_i = r_{i-1} + \omega_i (q_{i-1} - \alpha_{i-1} v_{i-1})$$

$$v_i = Aq_i$$

$$\bar{\omega} = \frac{\bar{\beta}_i}{(r_0, v_i)}$$

$$s = r_{i-1} - \bar{\omega}_i v_i$$

$$t = As$$

$$\alpha_i = \frac{(t, s)}{(t, t)}$$

$$\phi_i = \phi_{i-1} + \bar{\omega}_i q_i + \alpha_i s$$

$$r_i = s - \alpha_i t$$

d) If $\|r_i\| / \|\phi_i\| <$ tolerance, stop. Otherwise, go to (c).

As a remark regarding the above notation used to describe the algorithm, it should be said that (x, y) denotes inner product of two complex vectors x and y, which is defined as $(x, y) = \bar{x}^T y$.

The language used to formulate the algorithm was Fortran 77. As it is also the case for any other computing language, the structure of the code is totally dependent on the ability of the programmer. Nevertheless, it is useful to state here some information regarding this particular aspect. The algorithm was written for complex variables in a total number of 68 lines. The main iteration process was written in a total of 42 lines that evoke twice a routine with 28 lines and 3 times another routine with 11 lines. Further information regarding computation time and number of iterations required to

solve a particular problem will be presented in the appropriate section, section 2.5, where a comparison with the same parameters concerning the GMRES algorithm will be established.

A useful final remark within this section is that, in his work, Van der Vorst (1992) established a comparison between the CG-S and the Bi-CGSTAB for several cases and demonstrated the better performance of the Bi-CGSTAB regarding efficiency and convergence behaviour.

2.3.2 - The GMRES method

The original GMRES was proposed by Saad and Shultz (1986) as an efficient iterative scheme to solve non-Hermitian linear systems of equations. Just as the unsymmetric Lanczos process underwrites the Bi-CG method, the Arnoldi process underwrites the GMRES method. In this method the iterate x_k minimises $\|b - Ax\|_2$ over the set $x_0 + K(A, r_0, k)$ and it is expressed in terms of Arnoldi vectors.

To overcome the difficulty of the original GMRES method in dealing with a matrix with complex coefficients Walker and Zhou (1994) proposed a modified scheme. This scheme was adopted by Zhao and Anastasiou (1996) who also proposed 3 other GMRES-based iterative methods. The GMRES scheme can be formulated as follows:

a) Choose initial $x_0 = \phi_0$ and tolerance.

b) Start $r_0 = b - Ax_0$, $\beta = \|r_0\|_2$, $r_0 = r_0/\beta$.

c) Apply the Arnoldi process

for j=1, ..., m do

- $v_j = Av_{j-1} \ \left(v_1 = Ar_0\right)$

- For l=1, ...j-1

$h_{l,j} = \left(v_j, v_l\right)$

$v_j = v_j - h_{l,j}.v_l$

- Compute $h_{j,j} = \|v_j\|_2$

$v_j = v_j/h_{j,j}$

- $p_j = (r, v_j)$

  $r = r - p_j . v_j$

d) Solve $H_m y_m = P$

  where $P = (p_1, p_2, ..., p_m)^T$.

  Form the approximate solution:

  $x_m = x_o + V_m y_m$

e) Restart,

  if satisfied, stop. Else $x_o = x_m$, go to (b).

$\|v_j\|_2$ denotes the 2-norm of vector v_j, i.e., if $v_j = (q_1, q_2, ..., q_n)^T$, then

$$\|v_j\|_2 = \sqrt{\sum_{i=1}^{n} q_i^2}.$$

The Arnoldi iteration number m is used to truncate the iteration process. For a large consecutive number of steps the round - off errors would accumulate leading to loss of orthogonality. Thus, the truncation of the process stabilises the algorithm. The value used here was m=15 to be consistent with Zhao and Anastasiou (1996).

The programming language used to code the algorithm was also Fortran 77. Bearing in mind what was said for the Bi-CGSTAB algorithm, also here some information regarding the writing of the computational code will be stated. The algorithm was written for complex variables in a total number of 123 lines. The main iteration process was written in a total of 98 lines that evoke three times a routine with 28 lines and 4 times another routine with 11 lines. The implementation of the GMRES algorithm is more complex than the implementation of he Bi-CGSTAB algorithm. Regarding computation time and number of iterations required to solve a particular problem, further information will be presented in the appropriate section, (section 2.5) where a comparison between both algorithms is established.

2.4 - Validation of the models

The two models differ on the algorithm that solves iteratively the linear system of equations. The system contains the governing equation, equation (2.5) and the boundary conditions, equations (2.7), (2.9), (2.11) and (2.12). It is a system of $Nx*Ny$ linear complex equations. The unknowns are the velocity potential at each grid node, and Nx and Ny are the total number of grid nodes in the x and y direction respectively. One model uses the Bi-CGSTAB as the iterative solver (from now on called the Bi-CGSTAB model) and the other the GMRES algorithm (from now on called the GMRES model). Both models will be validated for two cases: wave propagation over an elliptic shoal and harbour resonance. The choice of the above cases will be explained in each section.

2.4.1 - Verification of the models for wave propagation over an elliptic shoal

The elliptic shoal case is often used to demonstrate stability, accuracy and efficiency of numerical models used to predict the wave climate in the nearshore region because it involves the occurrence of a complex diffraction pattern behind the shoal, corresponding to a cusped caustic in the wave-ray approximation.

Berkhoff et al (1982) set an experiment for this case and because the results are so well documented allowing for the comparison with results obtained from numerical models this case became known as Berkhoff's shoal. Its geometry consists on an elliptic shoal that lays down over a mild slope of 1:50. The bottom lay - out is shown in Fig. 2.1 where a more detailed description of shoal dimensions and position can also be seen. The incident wave direction is slightly oblique to the bottom contours and to the minor axis of the elliptic shoal (20°). Both numerical models will be applied to predict the wave climate in this region.

The incident waves have a period of 1 sec and are normal to the offshore boundary. The models run on a numerical domain of 220*200 grid nodes in the x and y direction respectively. The grid spacing considered was $\Delta x = \Delta y = 0.1$ m. The cartesian co-

ordinates have the directions shown in Fig. 2.1 and the centre of the shoal has co-
ordinates $x = 11.0$ m and $y = 10.0$ m.

Equation (2.6) was used for the incoming or offshore boundary. For the outgoing
boundaries, equations (2.9), (2.11) and (2.12) were used with the coefficient $\alpha = 1$, to
simulate artificial boundary conditions. The convergence criterion used for the
iterative methods is expressed by equation (2.18) with a tolerance equal to 10^{-7}, to be
consistent with Panchang et al (1991).

The computational results are expressed in terms of normalised wave height, defined
as the wave amplitude at each node divided by the incident wave amplitude,
because this way is easier to analyse the amplification of the incident wave due to its
transformation. The two dimensional (2D) results obtained with the Bi-CGSTAB model
are shown in Fig. 2.2 and the ones obtained with the GMRES model are shown in Fig.
2.3. Both plots represent the results in terms of contours (lines of equal normalised
wave height). Sections taken from the region behind the shoal (Fig. 2.1) are
presented in Fig. 2.4.1 to Fig. 2.4.8 together with experimental data obtained by
Berkhoff et al (1982). These sections are numbered from 1 to 8 and are located at $x =$
12.0 m, $x = 14.0$ m, $x = 16.0$ m, $x = 18.0$ m, $x = 20.0$ m, $y = 8.0$ m, $y = 10.0$ m and $y = 12.0$
m, respectively.

The results obtained show that both numerical models, the Bi-CGSTAB and the
GMRES, describe reasonably well the physical process of wave propagation and
deformation over this particular bathymetry. The 2D contour plots, Figs. 2.2 and 2.3,
allow to observe that both models show an excellent agreement in terms of wave
pattern and amplification factor. This is confirmed by Figs. 2.4.1 to 2.4.8, which show in
more detail the computational results for the region behind the shoal together with
the experimental data available to validate the models. The physical transformation
that occurs behind the shoal can be described by two phases: the first is a
convergence or focusing of wave energy that occurs in an area up to 8 m (between
sections 4 and 5) just immediately behind the centre of the shoal, which is mainly due
to the refraction process originated by the presence of the shoal, and thus
producing a peak in the wave amplification factor; the second, at a greater
distance from the centre of the shoal, is mainly the diffraction process that slowly
tends to attenuate the effects caused by the presence of the shoal.

Comparing the computational with the experimental results, it can be observed that: at 1 m behind the centre of the shoal (section 1), its presence starts to be noticed and there is good agreement between numerical and experimental results, not only in terms of following the same trend but also having the same values. Then as we advance further from the shoal, section 2 and section 3, at 3 m and 5 m respectively from the centre of the shoal, both models start to overestimate the peak amplification factor within the convergence region and slightly underestimate the two regions at the sides of the peak. However this tendency starts to vanish at about 6 m from the centre of the shoal and now the calculated peak amplification factor · tends to be slightly underestimated and the two sides just adjacent to the peak overestimated as it can be seen in sections 4 and 5, at 7 m and 9 m from the centre of the shoal. These observations can be confirmed by the results obtained in sections 6, 7 and 8.

All the above considerations lead to the conclusions that both numerical models give very good results in terms of following the trend of the laboratory data and reasonable results in terms of accuracy. The numerical models slightly overpredict the convergence process that occurs behind the shoal and they seem to predict the attenuation of the effects caused by presence of the shoal at a faster rate than what really happens in the laboratory experiment. This mismatch between the numerical and experimental results is due mainly to non - linear effects and wave induced currents produced by differential wave pattern. Although no comments were made regarding the occurrence of breaking within the physical experiment it seems quite likely that it would have happened. Dissipation of energy due to bottom friction is also another non - linear effect that is responsible for the differences observed, although its influence should not be as important as the two previous phenomena, breaking and non - linear interactions, because laboratory experiments for a regular progressive wave with H = 2 m, T = 8 sec and h = 7 m give relative changes in the mean energy flux over one wave length due to bottom friction and percolation to 1.7% and 0.06% respectively (Svendsen and Jonsson, 1982). A final remark is that the trend of the numerical results is in very close agreement with that obtained from other linear models like those by Berkhoff et al (1982) and more recently by Panchang et al (1991).

2.4.2 - Verification of the models for harbour resonance

2.4.2.1 - Introduction

Harbour resonance is the phenomenon of enhancement of the water surface oscillation and depends on the wave frequency. Both numerical models are also tested for a rectangular harbour connected to the open sea. The reason why this case was chosen is to prove the applicability of these models to such an important case so common along coasts. Besides, this test allows to prove that the models not only can be applied for open nearshore areas, as it is the case of wave propagation over an elliptic shoal, but also for areas with closed reflective boundaries as it is the case of harbours. A rectangular harbour was chosen because it is a simple geometry and there exist theoretical and experimental results for comparison as this particular case has been studied before. It also allows to study the phenomenon of harbour resonance.

2.4.2.2 - Previous studies of the case

The intention of this section is not to deeply investigate the case of harbour resonance but to document it well enough to understand and support the available data which will be compared with the present results.

Many authors have studied the harbour resonance problem. Miles and Munk (1961) studied the case of a rectangular harbour connected directly to the open sea. They formulated the problem as an integral equation in terms of a Green's function including the effect of wave radiation from the harbour mouth to the open sea and found two important aspects of the phenomenon of harbour resonance: a) there is a limit of wave amplitude within the harbour even at resonance; b) the narrowing of the harbour entrance leads not to a reduction in the harbour oscillation but to its enhancement (harbour paradox).

Ippen and Goda (1963) also studied the problem of a rectangular harbour connected to the open sea. They approached the problem using two methods: a)

The Fourier transformation method to evaluate the waves radiated from the harbour entrance to the open sea; b) the method of separation of variables to evaluate the solution inside the harbour. At the harbour entrance the solution was obtained by matching average wave amplitudes from solutions in both regions. To validate their solution they set a laboratory experiment and compared results. Differences were observed at the peak amplitudes. The laboratory results were lower than the theoretical predictions and this can be due to several mechanisms like: radiation damping associated with energy escaping seaward from the harbour entrance; energy loss by friction at the harbour entrance boundaries; energy loss due to wave breaking in shallow water; and finite amplitude effects of energy transfer into higher harmonics. An interesting and unexpected result was the fluctuations in the response curve in the region of the first peak amplitude which indicate that the open sea condition was not properly physically simulated.

Lee (1971) proposed a theory to solve the problem for a harbour of arbitrary geometry by applying Weber's solution of the Helmholtz equation for both regions inside and outside the harbour. He then obtained the total solution by matching the wave amplitudes and their normal derivatives at the harbour entrance. Weber's solution of the Helmholtz equation is found by applying Green's identity formula for the area of interest and using the Hankel function of the first kind and zero order as the fundamental solution of the two-dimensional Helmholtz equation. In order to validate his solutions he compared them with experimental data from the laboratory. For the case of circular or rectangular harbours he also made comparisons with a different analytical solution obtained from a different theory. This theory consists of obtaining the solution of the Helmholtz equation in the region inside the harbour by the method of separation of variables and for the open sea region by Weber's solution. Once again both solutions were matched for the harbour entrance. These results will be used for comparison with the numerical results obtained in the present work. His experimental results were more accurate than the ones previously obtained by Ippen and Goda (1963), which was due to physical conditions like the wave basin dimensions.

Since those experiments, several authors like Mei (1989), Panchang et al (1991) and others have been validating their finite elements and finite differences numerical models for the case of a rectangular harbour because the achievement of

reasonable results for this particular case is a vote of confidence on the applicability of their numerical models.

2.4.2.3 - Numerical tests

Both numerical models were applied for a rectangular harbour connected to the open sea as shown in Fig. 2.5. The depth was considered constant and equal to 6 m. The grid spacing was taken as $\Delta x = \Delta y = 1.0$ m. The infinite ocean outside the harbour was represented by a finite rectangular region (Fig. 2.5) the same size as that used by Panchang (1991) and Zhao and Anastasiou (1996).

Equation (2.6) was used for the incoming boundary and equations (2.11) and (2.12) for the artificial lateral boundaries that simulate outgoing waves with a coefficient $\alpha=1$. For the solid boundaries, the shore and the harbour, totally reflective boundaries were assumed. Therefore equations (2.10) and (2.12) were used for the lateral walls of the harbour with $\alpha=0$ and equation (2.8) was used for the backwall of the harbour and the shoreline, also with $\alpha=0$.

The computed response of the fully open rectangular harbour (for several different wavelengths) at the centre of the backwall of the harbour is presented in Fig. 2.6 together with the theoretical results obtained by Lee (1971). The numerical results for both models, the Bi-CGSTAB and the GMRES, were obtained for the convergence criterion expressed by equation (2.18) with a tolerance equal to 10^{-12}. The abscissa is the parameter kl (where l is the length of the harbour); the ordinate is the amplification factor, defined as the wave amplitude at the centre of the backwall of the harbour divided by the standing wave amplitude at the harbour entrance when the entrance is closed. This representation of the results is consistent with Lee 's (1971) presentation and the input wavelengths were chosen within a range that allows comparison of the abscissa kl to be obtained within the limits of the data available.

The results obtained for the case of harbour resonance follow the trend of the theoretical results. The differences observed at the peaks, particularly at the first peak

(longer waves), where the results are shifted to the right, can be due to two factors. One is that the mild-slope equation was derived for short waves and therefore as the waves become longer the model simulates less well the phenomenon. The other is that this case is particularly sensitive to the position of the open sea boundary which separates the computational domain from the infinite sea and, therefore, a better simulation of the phenomenon requires this boundary to be located as far away as possible from the domain of interest.

2.5 - Algorithmic and performance aspects

Bearing in mind that it is intended to develop a numerical model for random waves based on a model for monochromatic waves it is important to analyse and compare the Bi-CGSTAB and the GMRES models. The efficiency of the models depends on the computational skills of the programmer that writes the code but most of all depends on the performance of the iterative methods. In the present case, the only difference between the models is associated exclusively with the iterative process. An evaluation of the convergence characteristics of both algorithms will be made in an attempt to compare their efficiency. A comparison criterion should be established. As each iteration involves a different set of operations, the amount of iterations required to achieve a certain convergence cannot be used. Instead, the number of operations is used. The number of operations per iteration for the Bi-CGSTAB is about 28 N and for the GMRES is about 525 N (considering each iteration with m=15 internal steps). N is the total number of grid nodes considered in the domain.

The computer runs here described were done on a Silicon Graphics ,IRIS 4000 workstation. The convergence criterion used is expressed by equation (2.18).

For Berkhoff's shoal and a tolerance of 10^{-7} the Bi-CGSTAB model requires a total of 883 iterations and about 2519 seconds of CPU time while the GMRES model requires a total of 85 iterations (each including an internal number of steps, m=15) and about 5384 seconds of CPU time. The Bi-CGSTAB algorithm is about 2.1 times faster than the GMRES algorithm and it required only about 55.4% of the total number of operations required by the GMRES algorithm.

Both iterative solvers proposed in this work, the Bi-CGSTAB and the GMRES methods, are more efficient than the one proposed by Panchang (1991), based on the CG method, and also that proposed by Li (1994), based on the GCG, as described in section 2.3. This statement is based on the numerical results obtained for Berkhoff's shoal case, and it is legitimate because the same convergence criterion and tolerance were used in each of the 4 solvers. Li (1994) proved that the GCG method is more efficient than the method proposed by Panchang (1991) based on the CG. However, it should be noted that although Li's method requires more iterations (2500) than the CG scheme (which requires 2000 iterations) to achieve the imposed tolerance, each iteration involves fewer operations. Nevertheless, the Bi-CGSTAB and the GMRES methods produce an even faster rate of convergence, because the GCG requires about 27 N operations per iteration, yielling a total number of operations larger than each of the aforementioned two methods.

In order to investigate further the performance of the models, Berkhoff's shoal was run for a convergence criterion with a tolerance of 10^{-16}. The total number of iterations required for the Bi-CGSTAB was 10585 while for the GMRES was 1402 (each including an internal number of steps, m=15). The Bi-CGSTAB required about 40% of the total number of operations than the GMRES. Results of the variation of the residual in the process of convergence are shown in Fig. 2.7. They are expressed in terms of the total number of operations involved.

The numerical experiments undertaken to compare the algorithms indicate that both perform reasonably well. The Bi-CGSTAB is considerable more efficient as the total number of operations required is about half the number of operations for the GMRES. The GMRES shows a better stability, that is, a more monotonic convergence but the overall convergence rate is lower.

2.6 - Closure

This chapter dealt with numerical modelling of monochromatic wave propagation in the nearshore region. The mathematical formulation chosen to simulate wave transformation is the mild - slope equation in its elliptic form because it allows to

approach ine phenomenon without physical constraints, that is, including the processes of shoaling, refraction, diffraction and reflection. The model was discretised using a finite differences technique. A new generation of robust iterative methods was chosen to be the most effective way to find an approximate solution for the problem. Two efficient algorithms, the Bi-CGSTAB and the GMRES, were implemented generating two different numerical models. Both models were tested for a complex bathymetry and harbour resonance. When the results were compared with experimental results some discrepancies due to the fact that the models do not allow for non - linearity were observed. However, the general good agreement obtained suggests that both models can be applied with confidence, not only for wave transformation in caustic zones where refraction and diffraction are the dominant processes, but also for cases where reflection plays a major role, like the case of harbour resonance. Nevertheless, efficiency in terms of computational time, was another parameter considered in the performance of the models, and regarding this parameter, the model based on the Bi-CGSATB algorithm performed better than the model based on the GMRES algorithm, although the last showed a better stability. As it is the intention to develop a model for random wave propagation that is an extension of these models in the sense that it will be based on the assumption of linear superposition of independent spectral components, both accuracy and efficiency play a very important role. Accuracy, because the results obtained for each transformed component will be accumulated, and efficiency because the model will be dealing with a large number of components.

PROFILE
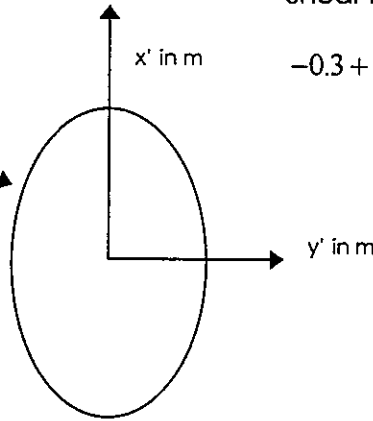
Shoal Thickness:

$$-0.3 + 0.5\sqrt{1 - \left(\frac{x'}{5}\right)^2 - \left(\frac{y'}{3.75}\right)^2}$$

x' in m

Shoal boundary:

$$\left(\frac{x'}{4}\right)^2 + \left(\frac{y'}{3}\right)^2 = 1$$

y' in m

Outside shoal:
h=0.45-0.02(5.84-y')

h=0.45m   slope 1:50

CONTOUR

T= 1 sec

y (in m)

x (in m)
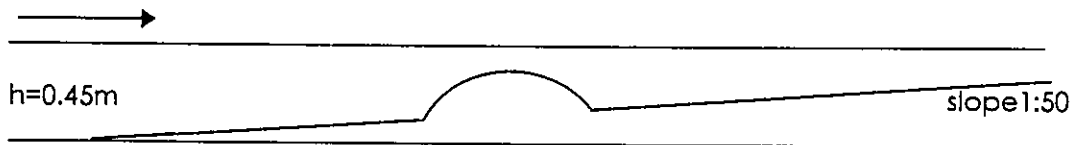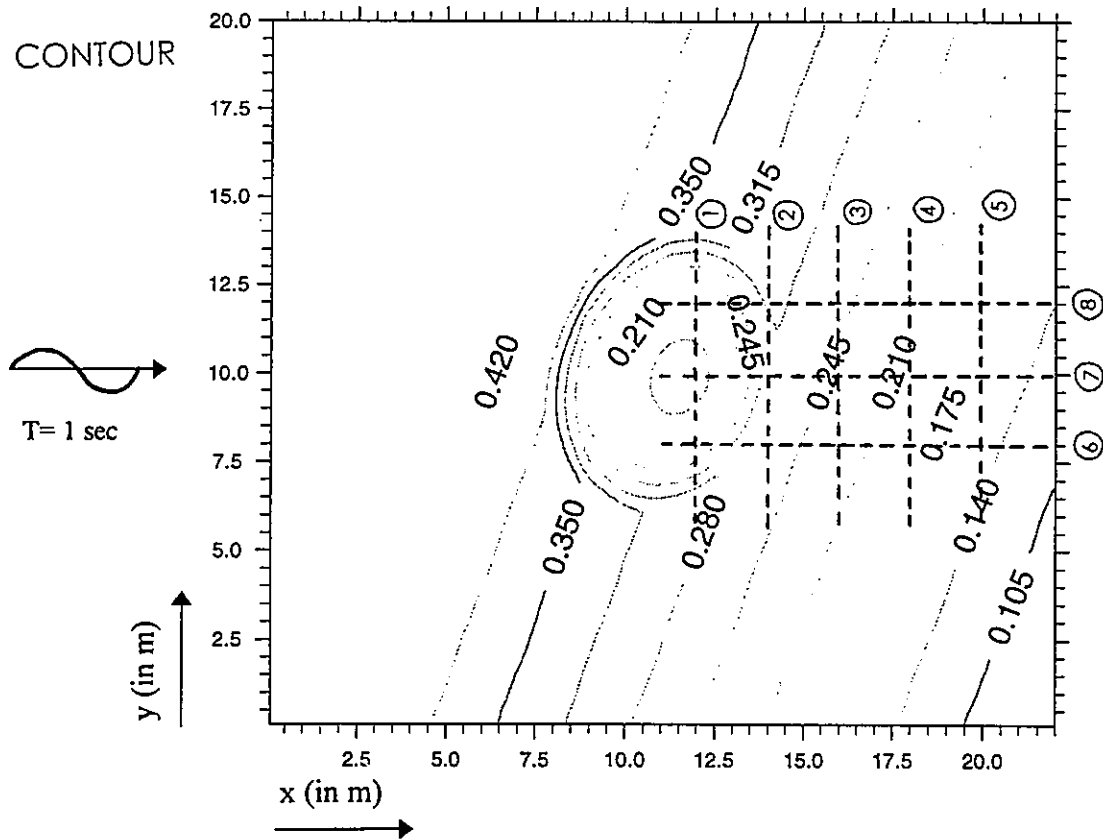
Fig. 2.1 - Elliptic shoal case; model bathymetry.
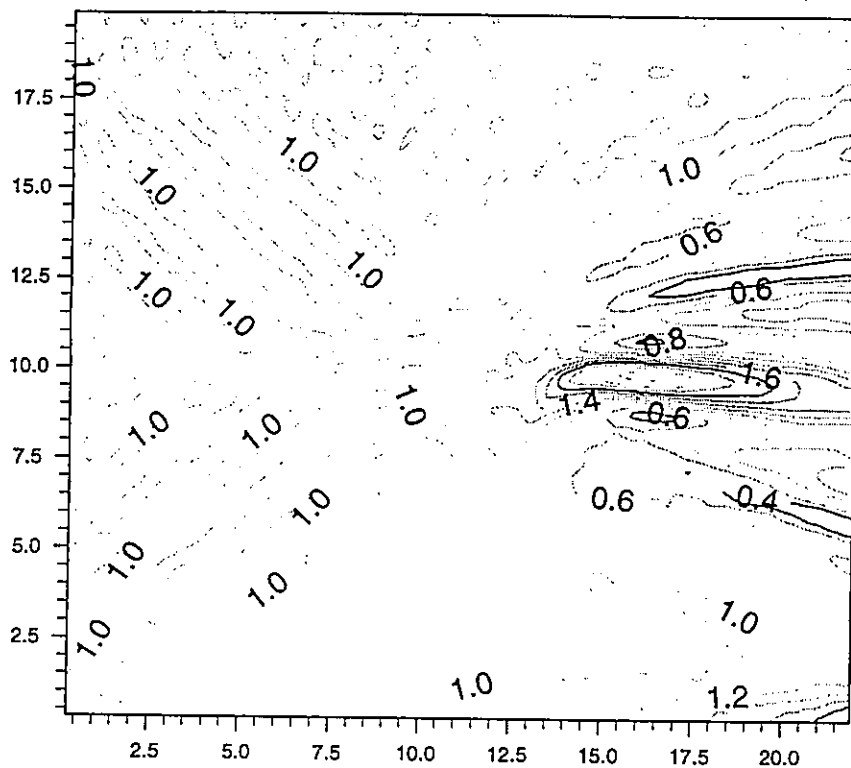
Fig. 2.2 - Wave height pattern of Bi-CGSTAB model.
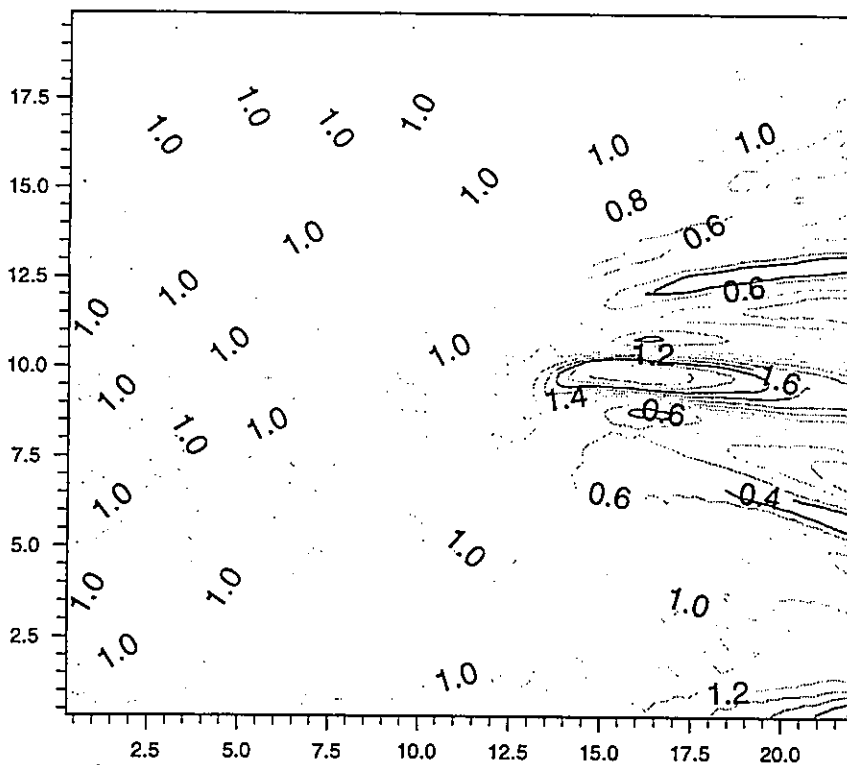
Fig. 2.3 - Wave height pattern of GMRES model.
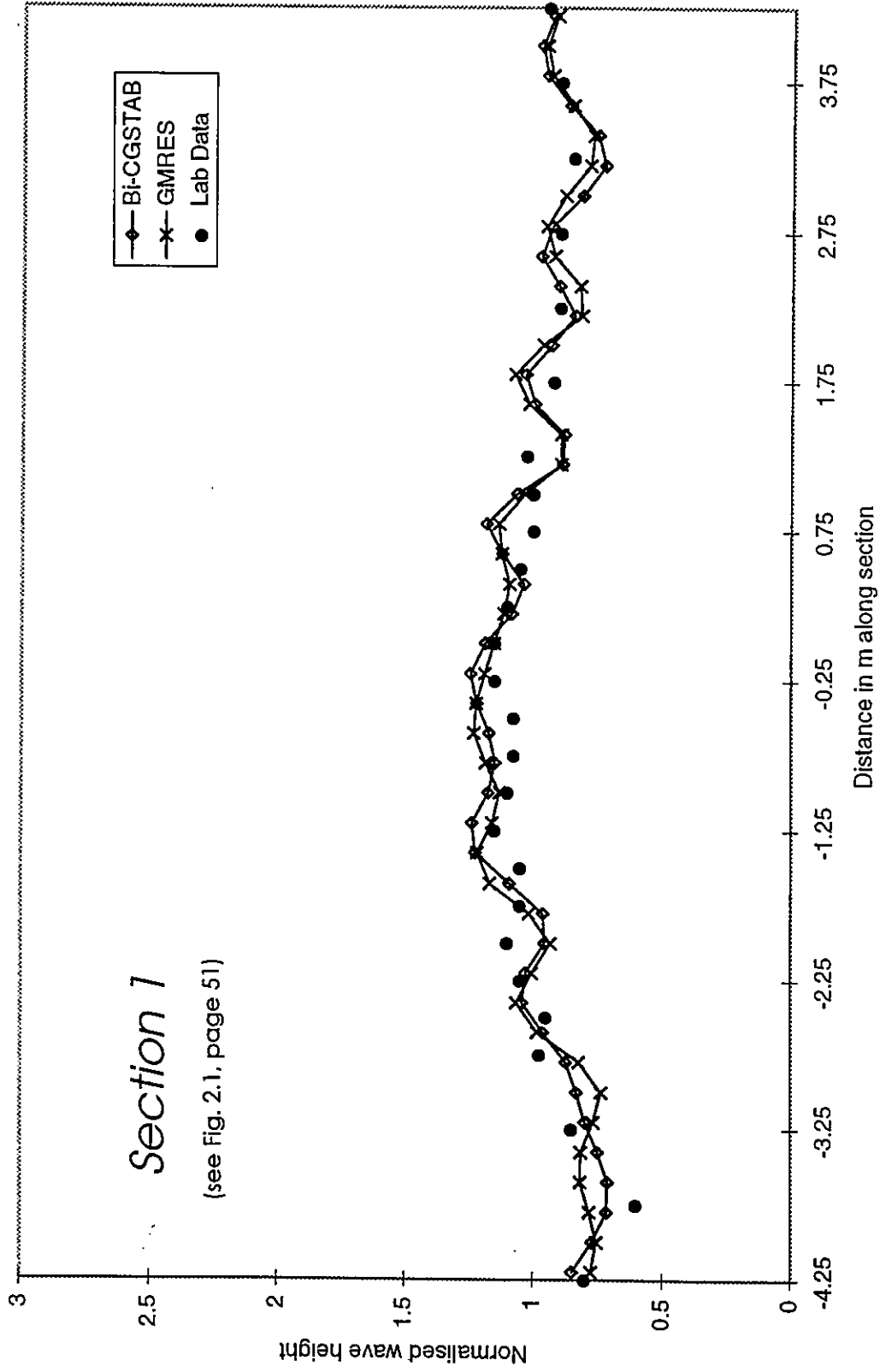
Fig. 2.4.1 - Comparison between experimental data of Berkhoff et al (1982) and computational results. Section 1.
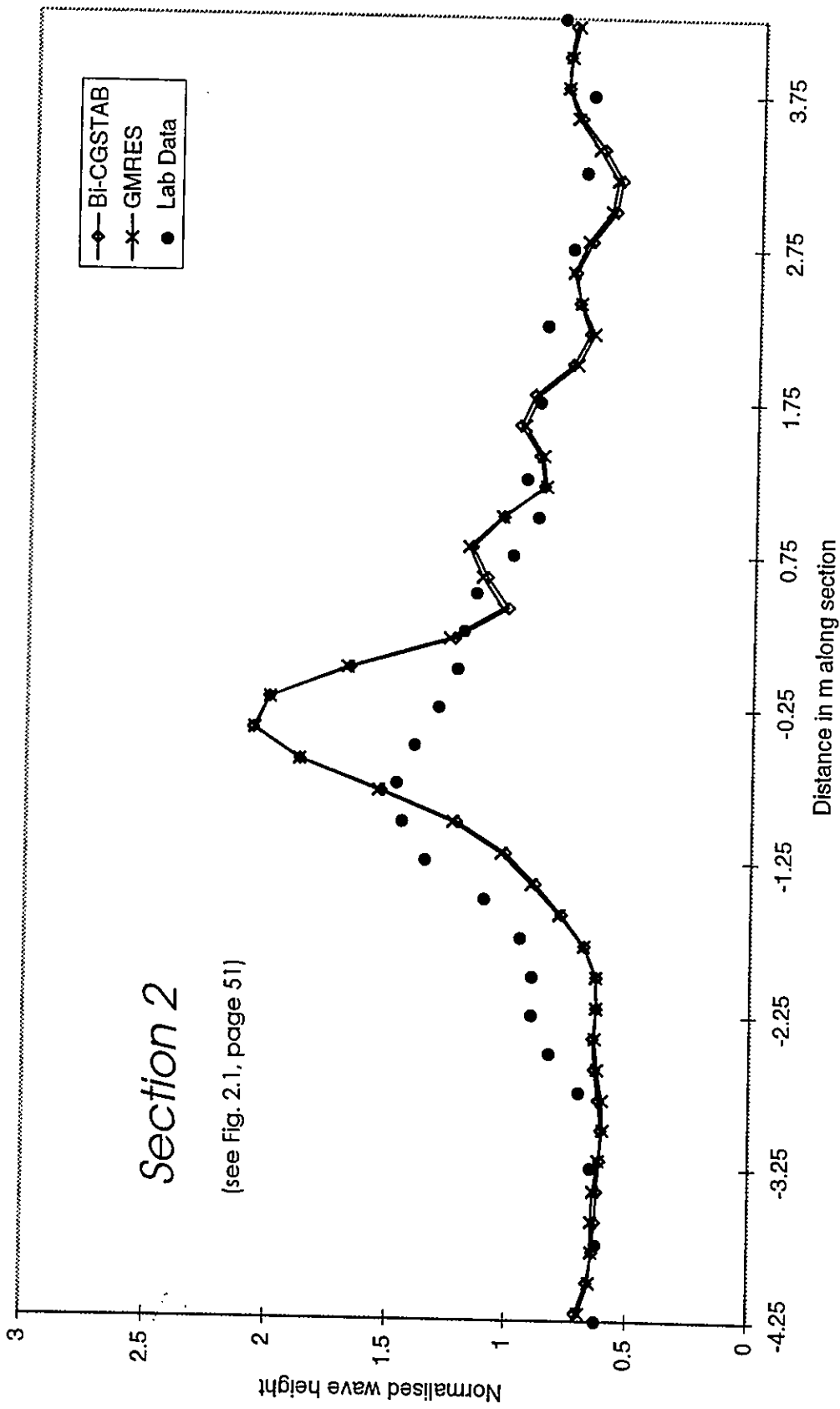
Fig. 2.4.2 - Comparison between experimental data of Berkhoff et al (1982) and computational results. Section 2.
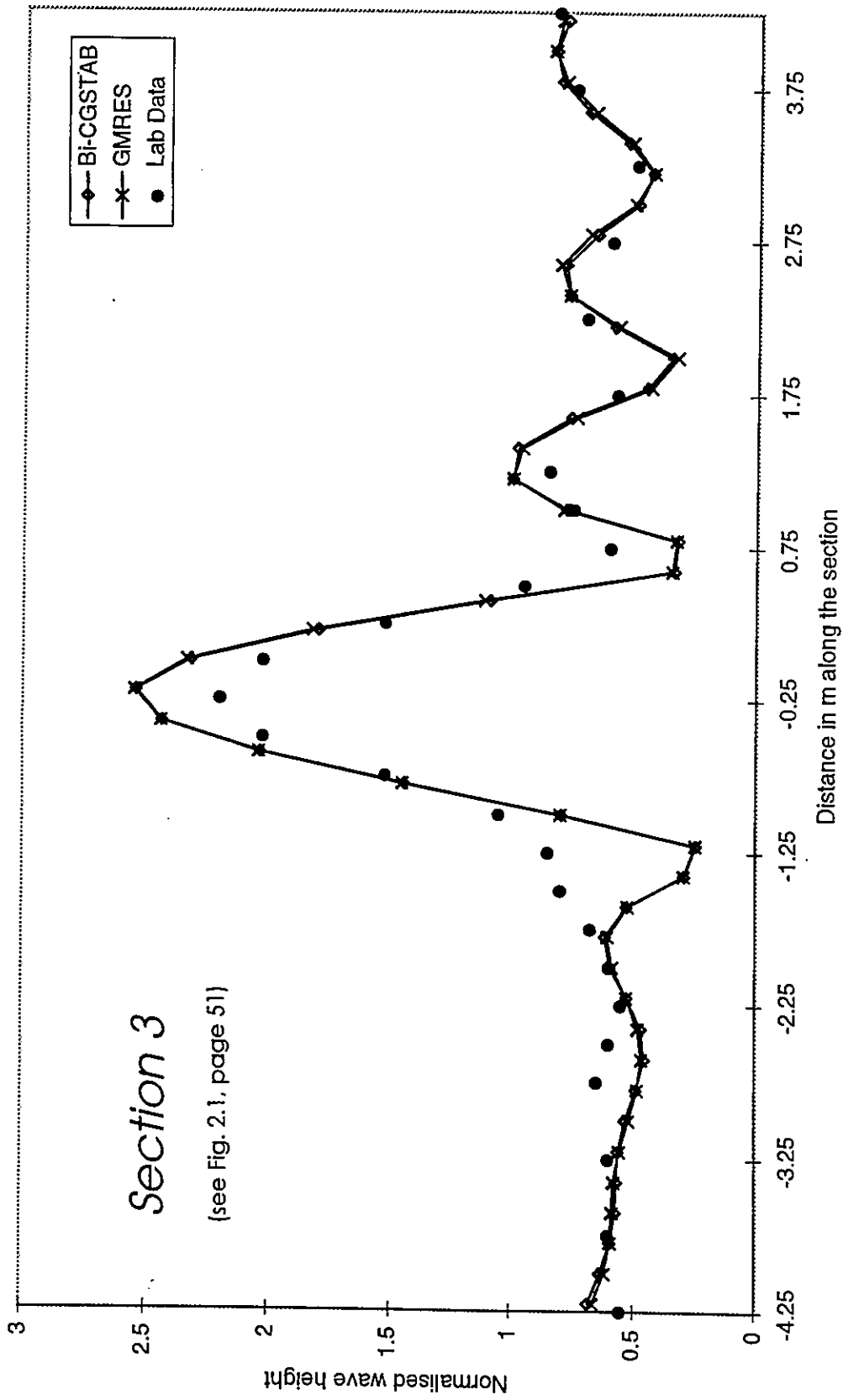
Fig. 2.4.3 - Comparison between experimental data of Berkhoff et al (1982) and computational results. Section 3.
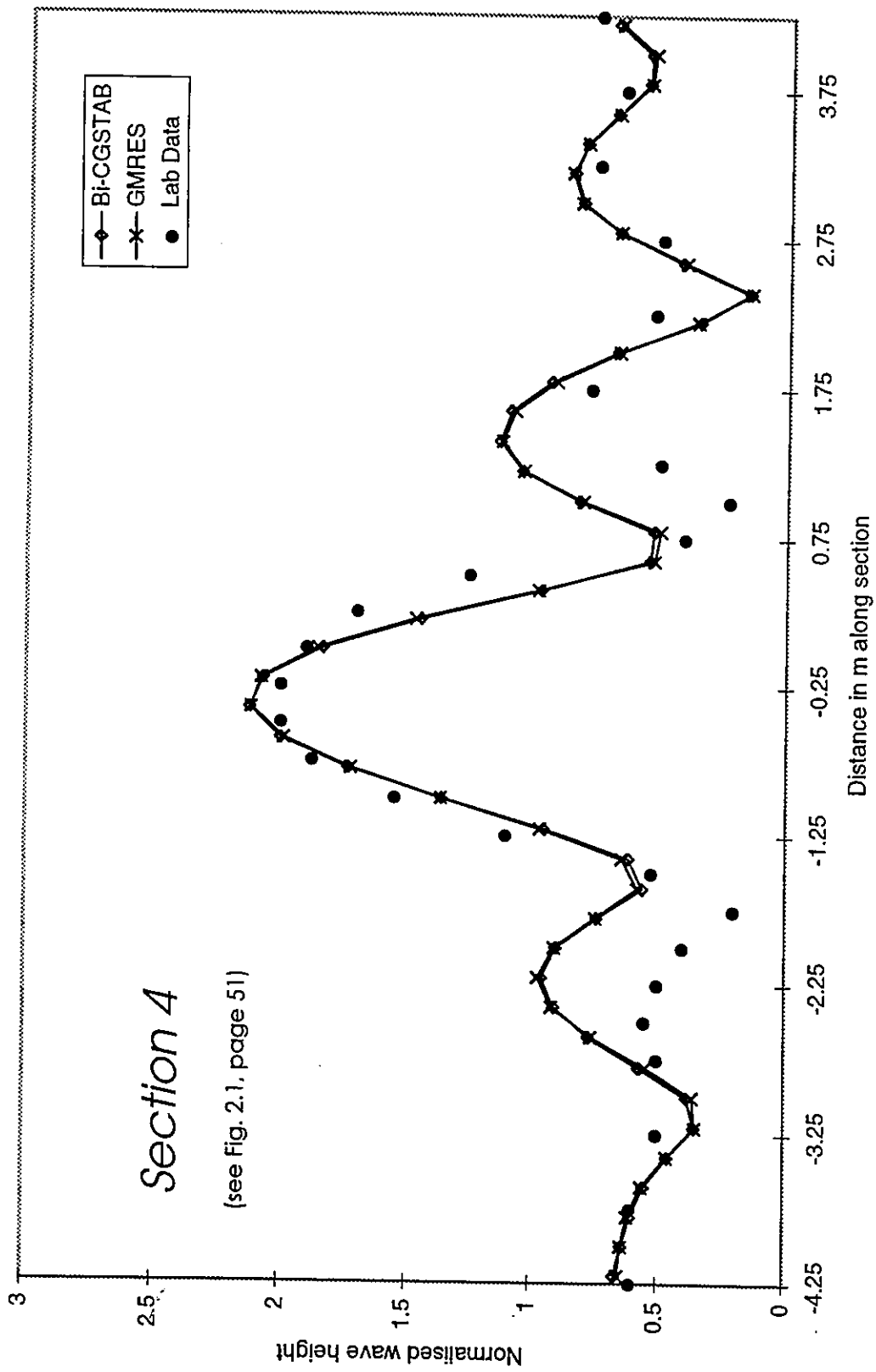
Fig. 2.4.4 - Comparison between experimental data of Berkhoff et al (1982) and computational results. Section 4.
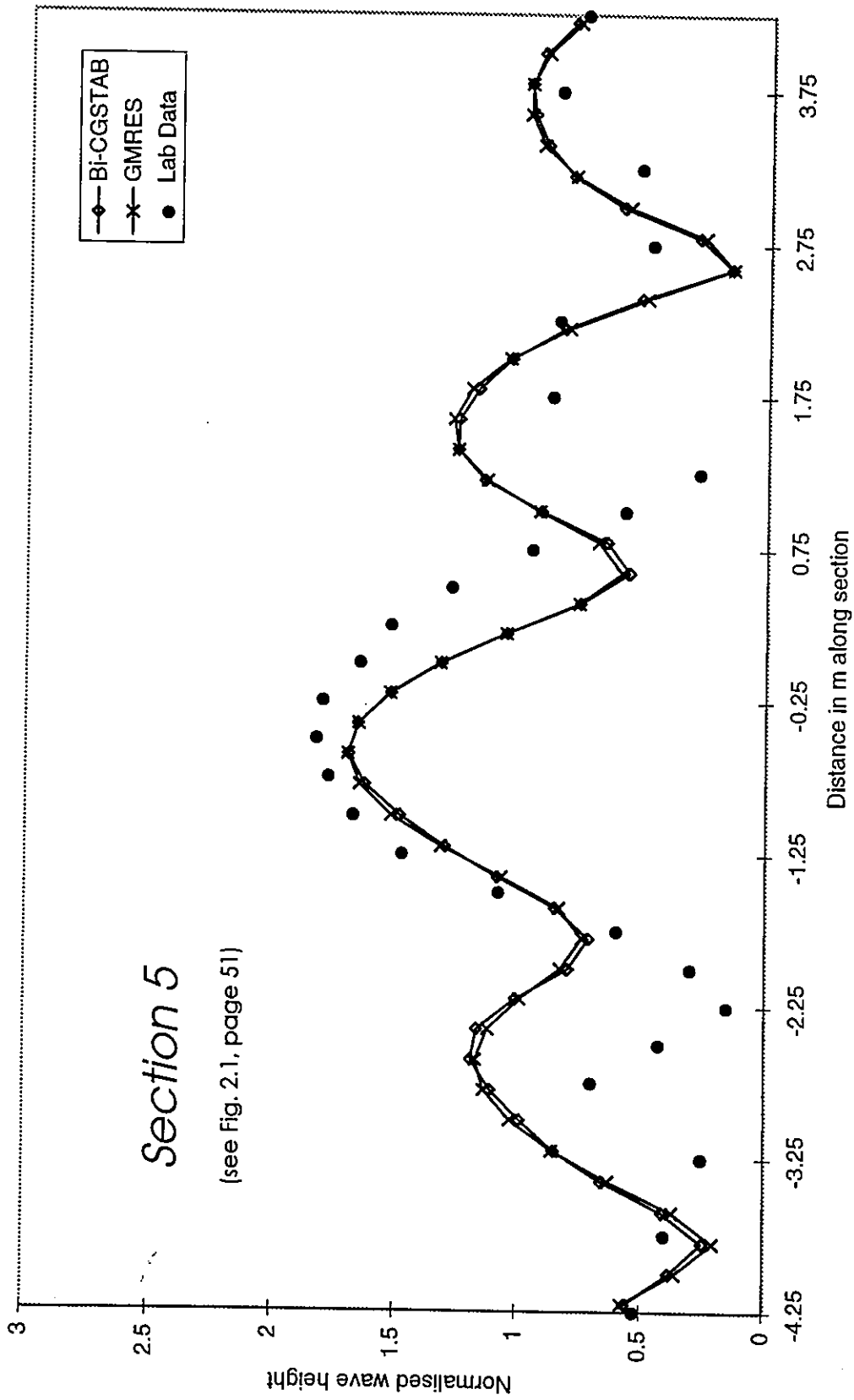
Fig. 2.4.5 - Comparison between experimental data of Berkhoff et al (1982) and computational results. Section 5.

Section 6

(see Fig. 2.1, page 51)

Normalised wave height

Distance in m along section

Bi-CGSTAB
GMRES
Lab Data
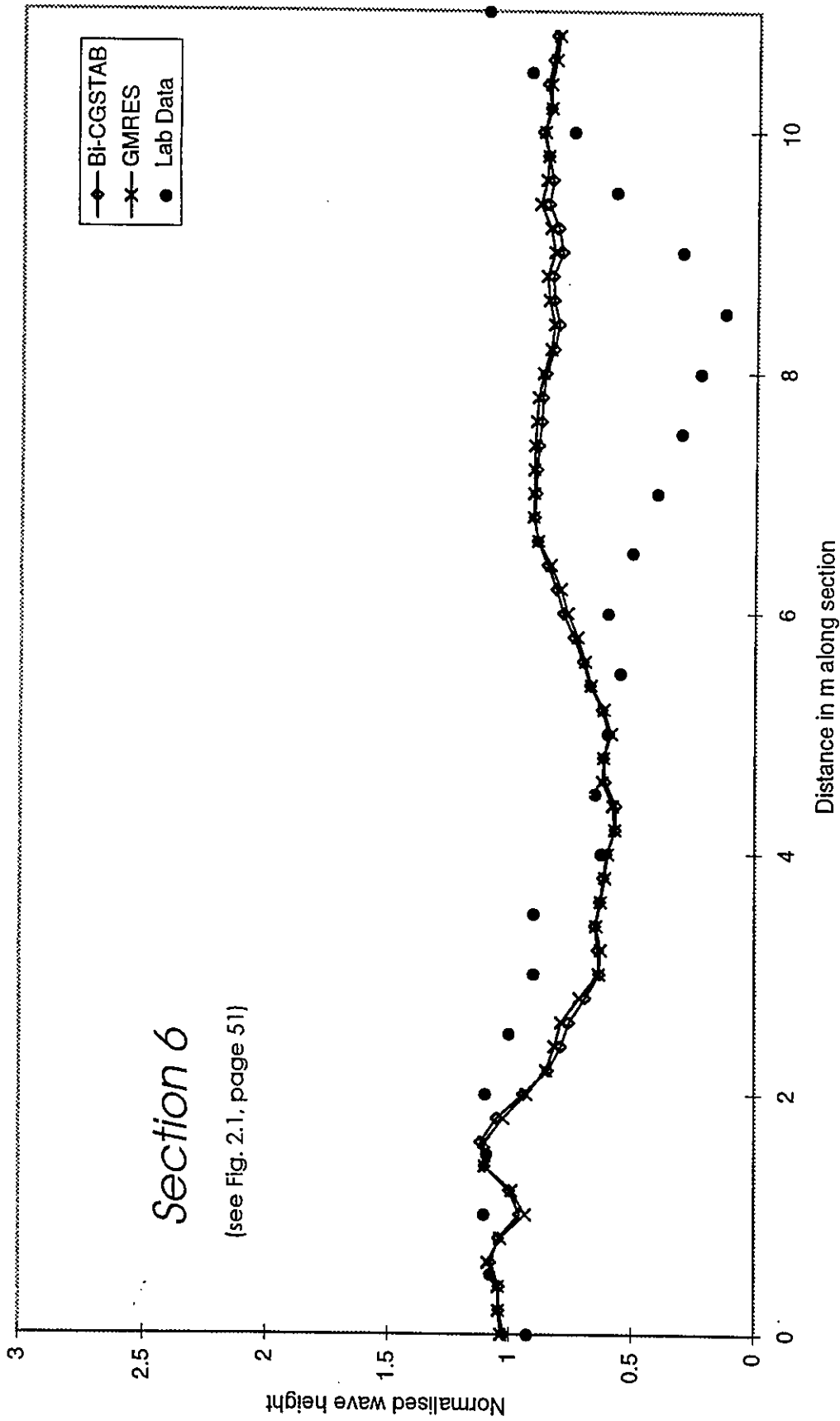
Fig. 2.4.6 - Comparison between experimental data of Berkhoff et al (1982) and computational results. Section 6.
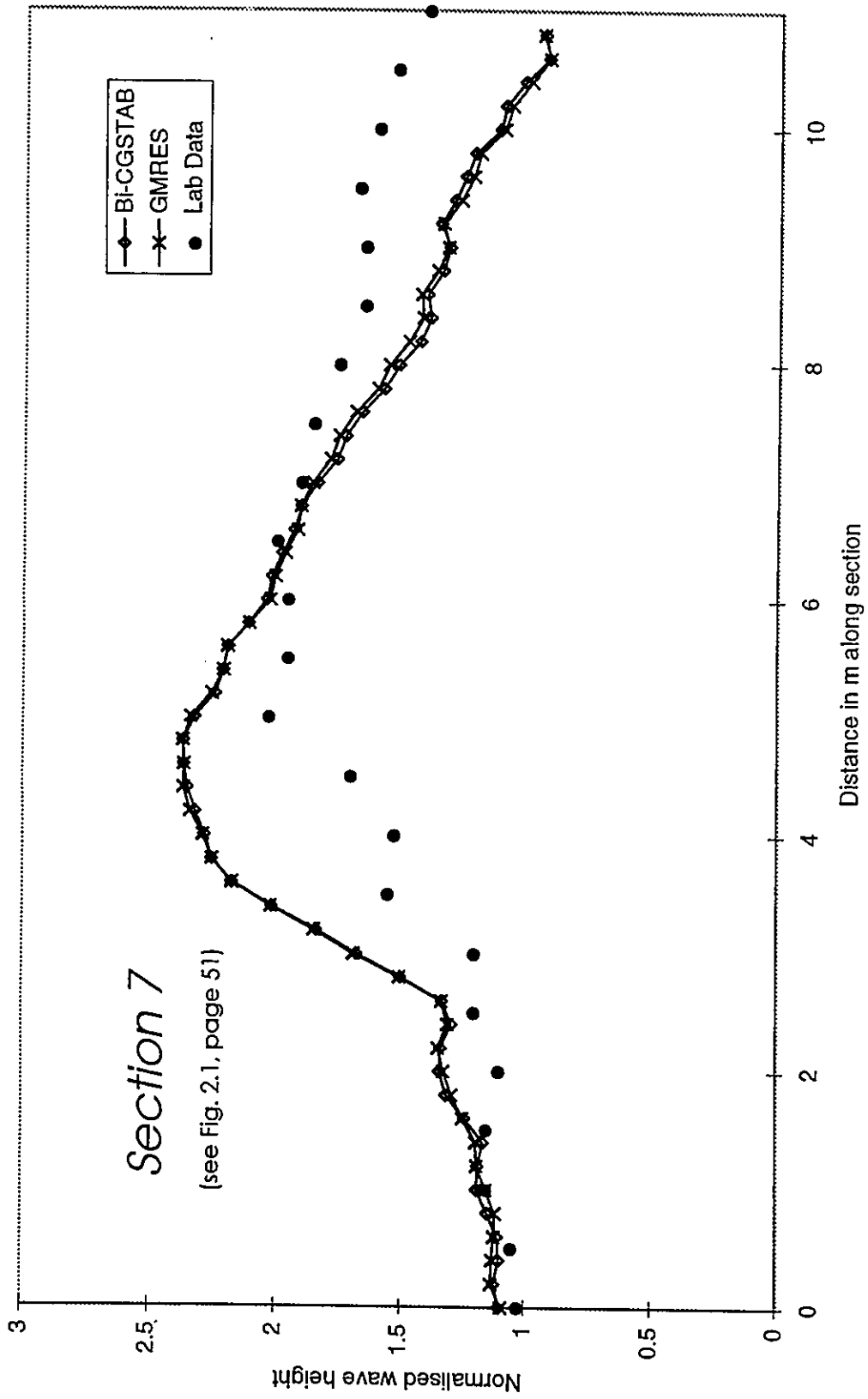
Fig. 2.4.7 - Comparison between experimental data of Berkhoff et al (1982) and computational results. Section 7.

Section 8

(see Fig. 2.1, page 51)
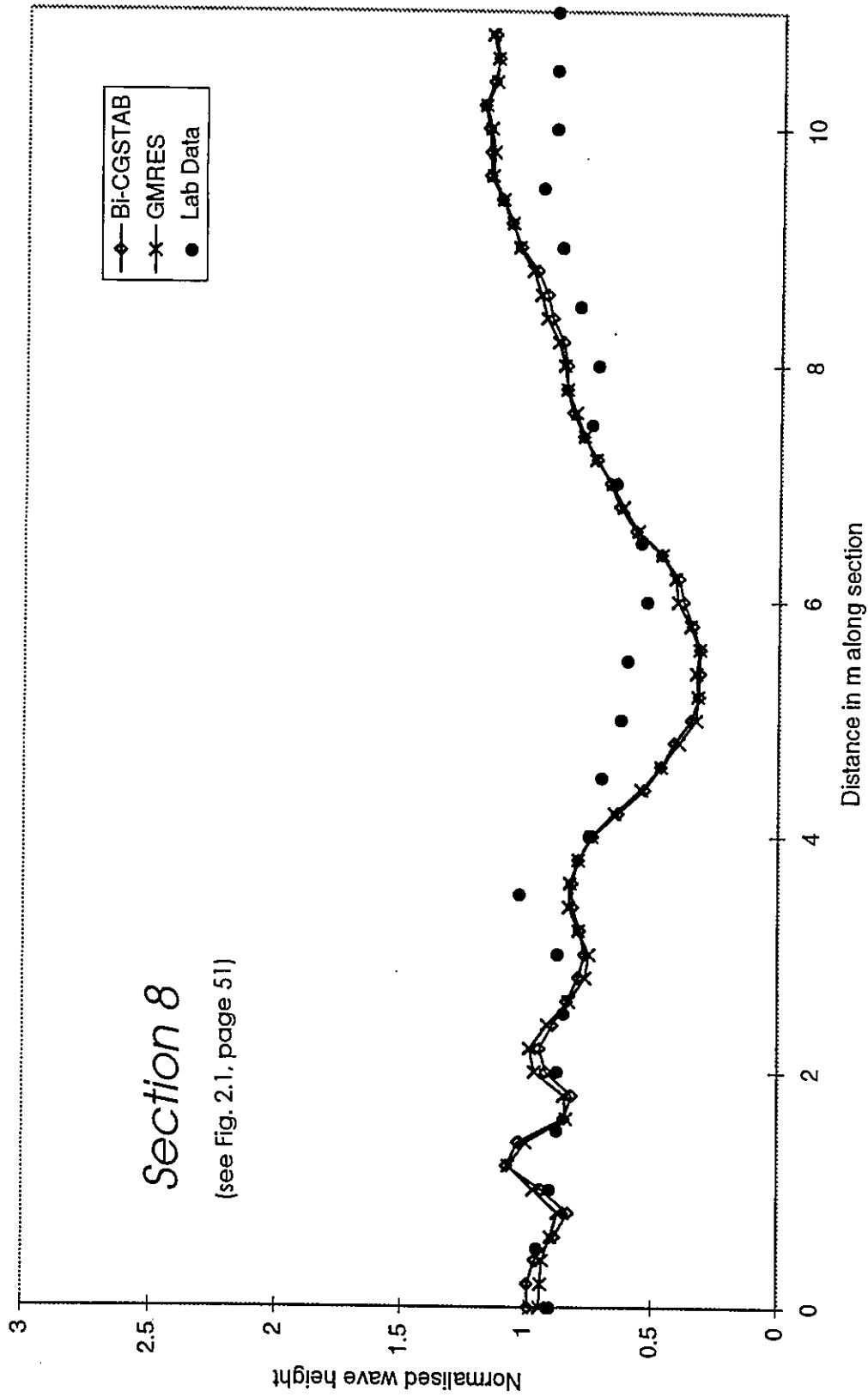
Fig. 2.4.8 - Comparison between experimental data of Berkhoff et al (1982) and computational results. Section 8.
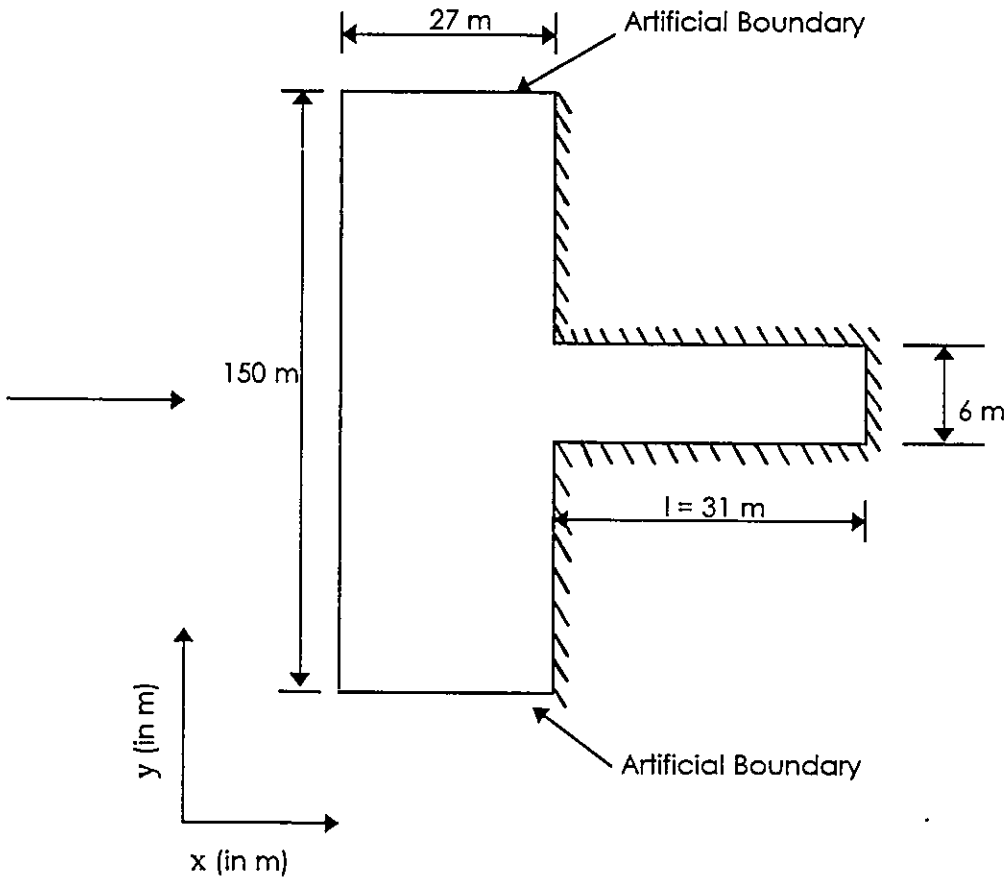
Fig. 2.5 - Harbour geometry for resonance simulation.
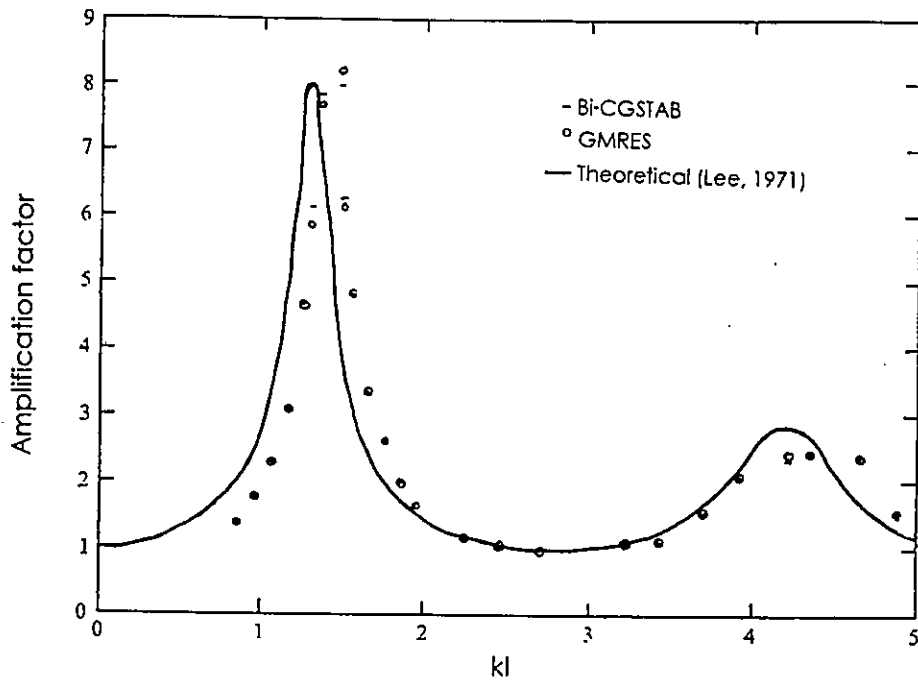
Fig. 2.6 - Response curve at the centre of the backwall.
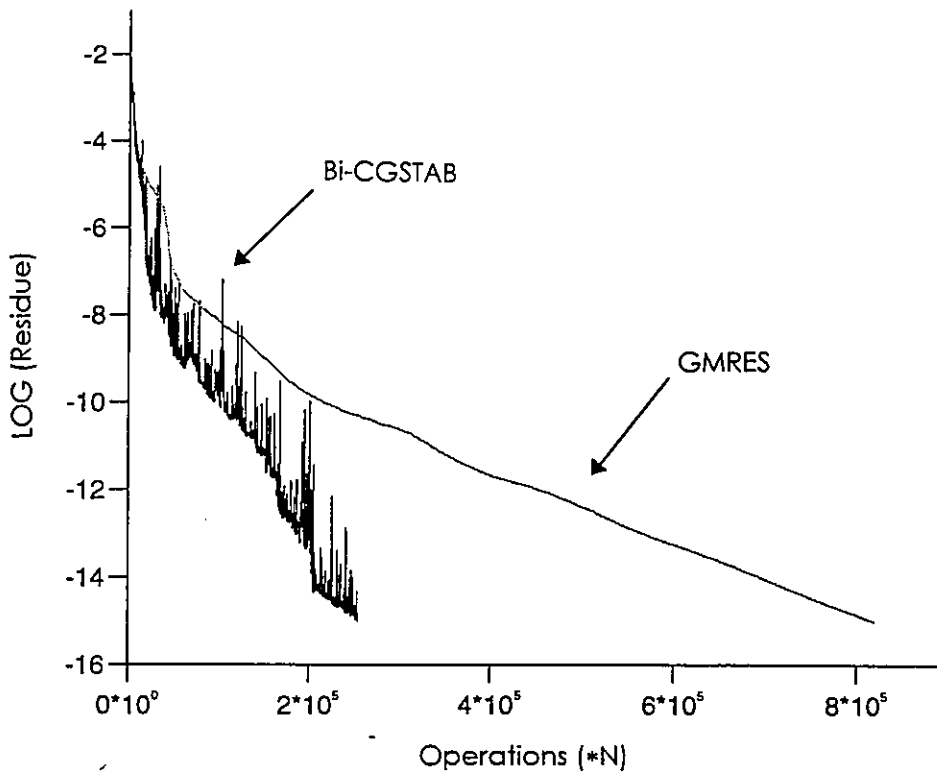
Fig. 2.7 - Comparison between the convergence of the two algorithms.

Chapter 3

Numerical Treatment of Boundary Conditions in Wave Propagation Models

3.1 - Introduction

The objective of this chapter is to improve the accuracy of the numerical model based on the mild-slope equation developed in the previous chapter by exploring different types of boundary conditions that simulate non-reflective boundaries.

The subject of numerical treatment of boundary conditions in wave propagation models is explored. Different formulations are investigated, and a numerical model based on a hyperbolic approximation of the mild - slope equation is also tested, in order to obtain a better understanding of the effects of the implementation of these boundary conditions in models based on different formulations of the mild - slope equation.

The chapter is organised as follows:

- In the following section the subject of boundary conditions is introduced and the mathematical formulation for the mild-slope equation is discussed.
- Section 3.3 is dedicated to a literature review of previous work in the field of non-reflective boundaries.
- In section 3.4 absorbing boundary conditions (sponge filters) combined with first order radiation boundary conditions are implemented in two models based on the mild-slope equation: a hyperbolic model and an elliptic model. A subsection describes the hyperbolic model and the implementation of the

sponge filters. Another subsection describes the implementation of the sponge filters in the elliptic model which has been extensively discussed in chapter 2.

- In section 3.5, parabolic radiation boundary conditions (higher order boundary conditions) for elliptic models of wave propagation are described.

- Section 3.6 is dedicated to the numerical tests done to evaluate the formulations proposed. The first group of tests reported concern the hyperbolic model and the second the elliptic model. The results obtained are here presented and discussed.

- Finally this chapter is closed with a critical summary regarding the work here developed.

3.2 - General concepts

In the sea there are three types of boundaries: the air - water interface or free surface, the sea bottom and natural or man made obstacles. When modelling the sea mathematically several conditions can be assumed at the physical boundaries and in general the more conditions that are imposed the more accurately the boundary is represented. For example, at the free surface (where the atmospheric pressure is taken as zero) the wind action can be neglected or not, at the sea bottom bed friction can be neglected or not, the bottom can be assumed as a impenetrable solid or a percolation layer. However a compromise is made when modelling the sea, and it involves analysing what conditions are more important to impose, meaning that if we have to neglect some of the physics involved or make some assumptions in order to have mathematical simplicity, we should be aware of the priority of the conditions in terms of their influence on the results.

The mild-slope equation was derived by Berkhoff (1972) assuming that the influx of energy through the water surface and bed is zero and that the bed slope is slowly varying. Due to the fact that it is a 2-dimensional equation applied over a certain domain the only physical boundaries that are left to be treated are the natural or man made obstacles. However there is a different type of boundary to consider when the propagation of waves is simulated numerically. For the mild - slope

equation discretised using a finite differences technique over a certain rectangular domain $R = \{(x, y) \mid x_l < x < x_r , y_l < y < y_r \}$, there are two types of boundaries ∂R that limit the region of study. They are solid boundaries like breakwaters or natural existing obstacles and open boundaries. The last ones are only implemented due to the need to limit the domain.

The mild-slope equation is an elliptic partial differential equation (PDE) also designated as a boundary value problem. It requires boundary conditions appropriate for this type of formulation, which can be expressed in the general form

$$A(x,y) \frac{\partial \phi}{\partial n} + B(x,y) \, \phi = C(x,y)$$ (3.1)

along ∂R where $\frac{\partial \phi}{\partial n}$ is the velocity potential gradient in the direction normal to the boundary in question.

When $A(x,y) = 0$ the condition is known as a Dirichlet condition and this means that the dependent variable is known along the boundary. This can happen for example when there are measurements available for a certain area that can be used as input data for the model.

When $B(x,y) = 0$ the condition is known as a Neumann condition and the velocity potential gradient is known along the normal to the boundary. For example, for the case of lateral boundaries, assuming there is no variation of the wave height H, in the direction normal to these boundaries and that Snell's law is valid along them, which means that outside the domain the bathymetry contour lines are parallel to the offshore boundary (y axis), then

$$\frac{\partial \eta}{\partial y} = 0 \;\Rightarrow\; \frac{\partial \phi}{\partial y} = 0 .$$ (3.2)

Another example is the wavemaker condition which can be used along the offshore boundary (y axis),

$$\frac{\partial \phi}{\partial x} = 0 .$$ (3.3)

Finally when $(A(x,y),\ B(x,y)) \neq 0$ the condition is known as elastic or Robbins boundary condition. This type of boundary condition can represent a sea wall, an open boundary or a coastline:

$$\frac{\partial \phi}{\partial n} - ik\alpha\phi = 0 \qquad (3.4)$$

where α is a reflection coefficient that varies with the type of boundary and may have to be determined empirically. For the case of $\alpha = 0$ we have fully reflection, for example a perfectly reflecting wall. For the case of $\alpha = 1$ we are dealing with outgoing waves as will be described later on. For α between 0 and 1 we are dealing with partially reflected / partially transmitted waves.

3.3 - Previous work on non-reflective boundary conditions

Radiation, outgoing, artificial and damping are four of the names given to the boundary conditions that limit the area of computation which is the open sea. The two main objectives when implementing radiation boundary conditions are that they do not affect the solution of the differential equation in question inside the domain and that they minimise the non - physical reflections that occur from the limits of the computational area. This problem is common in numerical simulations of local processes in the atmosphere and in the ocean. An appropriate mathematical expression to describe this open domain depends on the character of the equations of motion to be solved (hyperbolic, elliptic or parabolic). Romate (1992) and Santos and Neves (1991) reviewed works related with the subject.

For a problem where any disturbances that are generated in the domain of integration and in time leave the system (phenomenon which is characterised by an hyperbolic system), Sommerfeld's radiation boundary condition

$$\frac{\partial \phi}{\partial t} + C\frac{\partial \phi}{\partial y} = 0, \qquad (3.5)$$

where ϕ is any variable and C is the phase velocity of the waves, is well known as the solution to outgoing waves. It has been vastly used due to its efficiency. For

radiation boundary conditions the objective is to have a condition that is satisfied by outgoing waves but not by incoming waves and the above equation is based on the expectation that the wave approaching the boundary is non - dispersive and propagating normally to the boundary.

Aiming to improve the open boundaries, Orlanski (1976) proposed a slightly different approach to Sommerfeld's radiation boundary condition in which the evaluation of the phase velocity is performed in the vicinity of the boundary and extrapolated to the boundary instead of fixing a constant value. In fact, he uses Sommerfeld's condition to calculate the propagation velocity from the neighbouring grid points. The advantage is that the waves in the domain pass through the boundary without undergoing significant distortion and without influencing the interior solution. This idea is a good improvement to Sommerfeld's condition. Pursuing the same goal, Chapman (1985) and more recently Tang and Grimshaw (1996) carried on examining several other different approaches based on Sommerfeld's radiation boundary condition using a barotropic coastal ocean numerical model. They did not comment on the superiority of any particular formulation proposed and suggested that each formulation should be tested to fit the model in question. Basically, similarly to Orlanski (1976), they suggested different prescriptions for the phase velocity (or advection velocity), C. In fact, they produce several tests that confirm the improvements obtained by modifying the above parameter for different models. From all the above numerical experiments, it can be concluded that the phase velocity plays a crucial role in the accuracy of the radiation boundary conditions, and that an improvement on Sommerfeld's condition can be achieved if its value is not assumed as constant but made adjustable to the local conditions of the boundaries.

Engquist and Majda (1977) studied the problem of oblique incident waves. They derived the perfectly absorbing boundary condition based on a solution to the second order wave equation, but because it was impractical from a computational point of view they also derived a hierarchy of highly absorbing local boundary conditions that are approximations to the first one. The Sommerfeld condition is the first-order approximation to their solution when the incident wave is normal to the boundary. First and second order radiation boundary conditions are expressed as:

*1st order condition

$$\cos\alpha\,\frac{\partial\phi}{\partial t}+C\,\frac{\partial\phi}{\partial x}\bigg|_{x=0}=0$$

(3.6)

where α ($|\alpha|\leq\pi/2$) is the angle between the wave direction and the normal to the boundary which is the x axes;

*2nd order condition

$$a\,\frac{\partial^2\phi}{\partial t^2}+b\,\frac{\partial}{\partial t}\frac{\partial\phi}{\partial x}-C^2\,\frac{\partial^2\phi}{\partial y^2}+e\,\phi\bigg|_{x=0}=0$$

(3.7)

where

$$a=\cos\alpha_1\cos\alpha_2+\frac{C}{C_g}$$

(3.8)

$$b=C\left(\cos\alpha_1+\cos\alpha_2\right)$$

(3.9)

$$e=C^2\left(\frac{\omega^2}{CC_g}-k^2\right)$$

(3.10)

and α_1 and α_2 are the angles between the wave direction and the normal to each main cartesian axes, x and y. $|\alpha_i|\leq\pi/2$ (i = 1,2).

First and second order radiation boundary conditions were also tested by Broeze and Romate (1992) who solved the free surface wave problem by numerical experiments making use of a panel method. These numerical experiments confirm that an increase in the order of accuracy of the radiation boundary conditions improves the solutions in the numerical domain by minimising artificial reflections which occur at the boundaries. It can be observed in equation (3.7) that second order radiation boundary conditions give additional information regarding the conditions at the boundary. Now the advection term $\left(\frac{\partial}{\partial t}\frac{\partial\phi}{\partial x}=\frac{\partial u}{\partial t}=a_x\right)$ imposes a certain acceleration in the direction normal to the boundary, x, and some diffusion in the direction of the boundary ($\frac{\partial^2\phi}{\partial y^2}=\frac{\partial v}{\partial y}$) was also introduced.

The same conclusions were achieved by Bayliss et al (1982) and more recently by Johnsen and Lynch (1994) who implemented higher order radiation boundary conditions in their models discretised by a finite element technique on spherical co-ordinates. Bayliss et al (1982) solved the elliptic Laplace and Helmholtz equations and Johnsen and Lynch (1994) solved the shallow water equations.

All the investigated formulations here described were derived for a time dependent problem, as already mentioned. Nevertheless, elliptic formulations have the same requirements of minimising the artificial reflections that occur at the numerical boundaries. In fact, up to the present date, besides Kirby's (1989) investigation not much research work has been done for this particular problem. First order radiation boundary conditions, valid for normal incidence at the boundary, have been applied without evaluation of how much an increase in the order of the operators can improve the inside domain solution. As this subject will be investigated for the particular case of the elliptic formulation of the mild - slope equation, a description and discussion of Kirby's work will be done in section 3.4.

Other types of radiation boundary conditions are the so - called sponge filters combined with Sommerfeld's type radiation boundary condition. In practice they are absorbing boundaries where an artificial dissipation term is added implicitly or explicitly to the governing equation near the boundaries, so that outgoing waves are absorbed and therefore reflect as little as possible. Chapman (1985) did some work on this field based on an idea suggested by Israeli and Orszag (1981) by combining sponge filters with Orlanski type radiation boundary conditions imposed at the outer edge of the sponge filter. He implemented successfully these boundary conditions in a barotropic coastal ocean numerical model. Larsen and Dancy (1983) also used sponge filters successfully in a finite differences numerical model of the Boussinesq equation. The sponge filters combined with first order radiation boundary conditions are an efficient alternative to the implementation of higher order radiation boundary conditions. In fact, the third term of equation (3.7), introduces a certain diffusion that might bring some instability to the convergence process and the whole expression has a much higher computational demand than a first order radiation boundary condition. Sponge filters are of simple implementation and efficient. The only

disadvantage is that they require a certain wasted area of the numerical domain.

Based on the studies mentioned above, it can be concluded that while some type of open boundary conditions are satisfactory in a particular context they can be unreliable in a different context. Thus, an improvement in the accuracy of the solutions due to a better simulation of open boundaries requires a numerical experimentation and comparison of different types of open boundaries. Aiming to improve the accuracy of the results obtained by two numerical models based on the mild-slope equation, different non-reflective boundary conditions will be implemented in these models, in the following sections. Tests for different cases will be done to evaluate the suitability of these boundary conditions.

3.4 - Sponge filters

Sponge filters, described in the previous section, will be implemented in the numerical model described in chapter 2 and also in a numerical model based on a hyperbolic approximation of the mild - slope equation. The implementation of sponge filters in the hyperbolic model constitutes a good vehicle for testing these type of non - reflective boundaries because the model is well documented and the implementation of sponge filters in it is a relatively easy procedure, allowing a good understanding to be developed regarding the performance of sponge filters.

The following subsections are dedicated to the implementation of the sponge filters combined with first order radiation boundary conditions. The first subsection is dedicated to the hyperbolic model. The model with first order radiation boundary conditions is described followed by the description of the implementation of the sponge filters. The second subsection is dedicated to the implementation of the sponge filters in the elliptic model.

3.4.1 - Sponge filters in a hyperbolic model of the mild-slope equation

3.4.1.1 - The hyperbolic model

Like the model produced by Copeland (1985), this model is based on a transient or time dependent form of the mild-slope equation, which is a hyperbolic system of first order equations, the equation of continuity and the equation of motion and discretised using a finite differences scheme.

The mild-slope equation for transient conditions can be written as (Booij, 1981)

$$\nabla\left(C\,C_g\,\nabla\eta\right) + (k^2\,CC_g - \omega^2)\,\eta - \frac{\partial^2\eta}{\partial t^2} = 0. \tag{3.11}$$

The appropriate harmonic solution for a steady state condition is

$$\eta(x,y,t) = \phi\,(x,y)\,\exp(-i\omega t) \tag{3.12}$$

so

$$\frac{\partial^2\eta}{\partial t^2} = -\omega^2\eta \tag{3.13}$$

Substituting (3.13) in (3.11) gives

$$\nabla\left(CC_g\nabla\eta\right) + \left(k^2 CC_g - \omega^2\right)\left(-\frac{1}{\omega^2}\frac{\partial^2\eta}{\partial t^2}\right) - \frac{\partial^2\eta}{\partial t^2} = 0 \tag{3.14}$$

which is the same as

$$\nabla\left(CC_g\,\nabla\eta\right) - \frac{C_g}{C}\frac{\partial^2\eta}{\partial t^2} = 0. \tag{3.15}$$

From this equation, Ito and Tanimoto (1972) derived a pair of first order equations:

$$\nabla Q + \frac{C}{C_g}\frac{\partial\eta}{\partial t} = 0 \tag{3.16}$$

and

$$\frac{\partial Q}{\partial t} + CC_g\,\nabla\eta = 0 \tag{3.17}$$

where Q is the flux (vertically integrated function of particle velocity), $Q = C_g\,\eta$.

The first is the equation of continuity and the second the equation of motion.

This system contains the governing equations for the hyperbolic model and the first order derivatives are discretised by a finite difference technique:

$$\eta_{ij}^{t+\Delta t/2} = \eta_{ij}^{t-\Delta t/2} - \left(\frac{C}{C_g}\right)_{ij} \left[Qx_{i-1,j}^{t} - Qx_{ij}^{t}\right] \Delta t / \Delta x - \left(\frac{C}{C_g}\right)_{ij} \left[Qy_{i,j+1}^{t} - Qy_{ij}^{t}\right] \Delta t / \Delta y$$

$$(3.18)$$

$$Qx_{ij}^{t+\Delta t} = Qx_{ij}^{t} - \left(CC_g\right)_{ij} \left[\eta_{ij}^{t+\Delta t/2} - \eta_{i-1,j}^{t+\Delta t/2}\right] \Delta t / \Delta x \qquad (3.19)$$

$$Qy_{ij}^{t+\Delta t} = Qy_{ij}^{t} - \left(CC_g\right)_{ij} \left[\eta_{ij}^{t+\Delta t/2} - \eta_{i,j-1}^{t+\Delta t/2}\right] \Delta t / \Delta y \qquad (3.20)$$

where t is the instant time, i is the index of the nodes in the x direction and j is the index of the nodes in the y direction for each cell as follows:
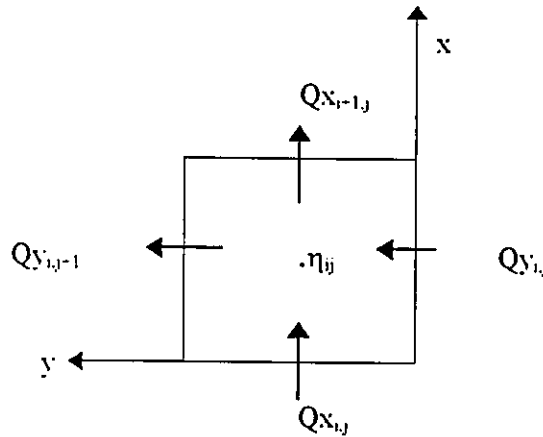
The fluxes in the x and y directions, Qx and Qy, are calculated at a time $\Delta t/2$ ahead of the corresponding values of η and are offset from the locations of η by $\Delta x/2$ and $\Delta y/2$, respectively.

The model considers two types of boundaries besides the solid boundaries created when in the presence of obstacles: driving boundaries and downwave boundaries.

For the first type, Copeland (1985) introduced what he called an ad-hoc physical approach equivalent to the most simple (first order) radiation boundary condition given by Engquist and Madja (1977) and mentioned in section 3.2, that is

$$\frac{\Delta Qx}{\Delta x} - \left(\frac{\cos\theta}{C}\right) \frac{\Delta Qx}{\Delta t}\bigg|_{x=0} = 0.$$

(3.22)

The reflected or backscattered wave travelling back towards the offshore boundary is absorbed at the boundary by calculating its value which is derived from decomposing the flux normal to this boundary, Qx, into the required driving function qx and the reflected wave.

The required driving function at the boundary at a time $t+\Delta t$ is

$$qx_{0,j}^{t-\Delta t} = \eta C_g \cos\theta,$$

(3.23)

where the water surface elevation is calculated as

$$\eta = \frac{H}{2} \sin\left(k\sin\theta \frac{\Delta y}{2} + k\cos\theta \frac{\Delta x}{2} - \omega(t+\Delta t)\right).$$

(3.24)

The reflected wave at the boundary, defined by QE at a time $t+\Delta t$, can be interpolated from the reflected wave at the previous time step t, calculated at the boundary (location 0,j), E1, and at the row adjacent to the boundary (location 1,j), E2, as it follows:

$$QE = E1 - (E1 - E2) \, C \frac{\Delta t}{\Delta x \cos\theta}$$

(3.25)

where

$$E1 = Qx_{0,j}^t - qx_{0,j}^t$$

(3.26)

and

$$E2 = Qx_{1,j}^t - qx_{1,j}^t.$$

(3.27)

Hence the value of the normal flux to the boundary used in the computation is

$$Qx_{0,j}^{t-\Delta t} = qx_{0,j}^{t-\Delta t} + QE.$$

(3.28)

For the second type, the downwave boundaries, the values of the flux at the boundary are calculated from the flux in the adjacent upwave grid row affected by a time delay τ and a weighting factor AF, both parameters calculated for a certain reflectivity. Copeland (1985) derived these two parameters and as a result the flux at the boundary at an instant t can be written as

$$Qx_{N,j}^{t} = AF \, Qx_{N-1,j}^{t-\tau} \tag{3.29}$$

considering (N,j) the location at the boundary and (N-1,j) the location at the adjacent upwave grid row.

3.4.1.2 - Implementation of the sponge filters

Sponge filters were described in section 3.2, therefore this section will explore their implementation in the hyperbolic model of the mild-slope equation.

The idea was to modify the governing equations in order to introduce a dissipation term that decreases the energy in the system near the downwave computational boundaries and therefore the outgoing waves are absorbed with as little reflection as possible. Hence the linear system of first order equations was modified for the computational area near these boundaries by introducing a dissipation term in the equation of motion (3.17), as follows:

$$\frac{\partial Q}{\partial t} + CC_g \, \nabla\eta + f_D Q = 0 \tag{3.34}$$

while the equation of continuity (3.16) remains the same, that is

$$\nabla Q + \frac{C}{C_g} \frac{\partial \eta}{\partial t} = 0. \tag{3.35}$$

Discretising using a finite differences technique the resulting equations for the interior domain remain the same as in 3.3.1.1 while for the grid cells at the downwave boundary they are now:

$$\eta_{ij}^{t-\Delta t \cdot 2} = \eta_{ij}^{t-\Delta t \cdot 2} - \left(\frac{C}{C_g}\right)_{ij} \left[Qx_{i+1,j}^{t} - Qx_{ij}^{t}\right] \Delta t / \Delta x - \left(\frac{C}{C_g}\right)_{ij} \left[Qy_{i,j+1}^{t} - Qy_{ij}^{t}\right] \Delta t / \Delta y \tag{3.36}$$

$$Qx_{ij}^{t-\Delta t} = Qx_{ij}^{t} - \left(CC_g\right)_{ij} \left[\eta_{ij}^{t-\Delta t \cdot 2} - \eta_{i-1,j}^{t-\Delta t \cdot 2}\right] \Delta t / \Delta x + f_D Qx_{i,j}^{t} \tag{3.37}$$

$$Qy_{ij}^{t-\Delta t} = Qy_{ij}^{t} - \left(CC_g\right)_{ij} \left[\eta_{ij}^{t-\Delta t \cdot 2} - \eta_{i,j-1}^{t-\Delta t \cdot 2}\right] \Delta t / \Delta y + f_D Qy_{i,j}^{t} \qquad (3.38)$$

where f_D is an empirical dissipation factor that should be determined by experimentation for each case in order to obtain the optimum performance of the sponge filters.

3.4.2 - Sponge filters in a elliptic model of the mild-slope equation

The elliptic model of the mild-slope equation was described in chapter 2, and sponge filters in section 3.3 of this chapter. This section concentrates on the implementation of the sponge filters into the elliptic model.

By introducing an energy dissipation term into the elliptic form of the mild - slope equation, the sponge filters can be simulated. The modified equation is applied at the downwave boundaries decreasing the energy in this area.

Booij (1981) showed that the inclusion in the original form of the mild-slope equation of the term $i\omega f_D \phi$, in which $i = \sqrt{-1}$, ω is the angular frequency and f_D a damping factor, results in wave damping. Based on this, Dalrymple, Kirby and Hwang (1984) tested the performance of this energy dissipation in wave damping in the region (interior domain) where the dissipation term was included for the parabolic model developed by Radder (1979).

Subsequently, when implementing a dissipation term in the model, the governing equation (2.2) can have the same expression but now k_c becomes

$$k_c = k^2 - \frac{\nabla\left(CC_g\right)^{1/2}}{\left(CC_g\right)^{1/2}} + \frac{i\omega f_D}{CC_g}. \qquad (3.39)$$

where f_D is the empirical damping or dissipation factor that must be established by experimentation to obtain the best results for each case studied.

3.5 - Higher order radiation boundary conditions in a elliptic model of the mild-slope equation

Elliptic partial differential equations are in general very sensitive to the formulation of the boundary conditions imposed to the computational domain due to its nature of being a boundary value problem. Aiming to improve the accuracy of the solutions, higher order parabolic radiation boundary conditions will be implemented in the elliptic model formulated by the reduced wave equation, as considered in chapter 2.

As mentioned in section 3.2, where existing formulations and their applicability for open boundary conditions were investigated and discussed, Kirby (1989) derived several parabolic approximations to radiation boundary conditions for elliptic wave equations that closely mirror Engquist and Majda's (1977) work. Both authors derived higher-order radiation boundary conditions, but for different applications. Engquist and Majda (1977) dealt with a time dependent formulation, or initial value problem, whereas Kirby (1989) dealt with an elliptic formulation (constant depth Helmholtz formulation), or boundary value problem. In this section, the higher-order radiation boundary conditions derived by Kirby (1989) will be applied to equation (2.2), where the effective wave number K_c is expressed by equation (2.3).

To derive the higher order radiation boundary conditions Kirby used a homogeneous solution for the constant depth Helmholtz formulation posed in a half - plan ($x \le 0$, $-\infty \le y \le \infty$). Based on the assumption that no reflections occur at this boundary, the above solution produces the following condition:

$$\phi_x = il\phi; \quad x = 0 \tag{3.40}$$

where l is a parameter related to the incident wave direction. As the order of approximation of this parameter increases, a more accurate expression can be derived for equation (3.40), generating a succession of downwave boundaries more transparent to the passage of obliquely incident waves. The simplest approximation for the parameter l produces the well known first order radiation boundary condition for normal incidence waves which is

$$\frac{\partial \phi}{\partial x} = ik\phi.$$

(3.41)

The lowest-order parabolic approximation can be written as

$$\frac{\partial \phi}{\partial x} = ik\left(\phi + \frac{1}{2k^2}\frac{\partial^2 \phi}{\partial y^2}\right)$$

(3.42)

and is derived by a binomial expansion of 1 (Kirby, 1989).

The next higher-order is

$$\frac{\partial \phi}{\partial x} + \frac{1}{4k^2}\frac{\partial^3 \phi}{\partial x \partial y^2} = ik\left(\phi + \frac{3}{4k^2}\frac{\partial^2 \phi}{\partial y^2}\right).$$

(3.43)

and is derived based on further improvement of 1 (Kirby, 1989).

Kirby (1989) performed numerical tests to evaluate the reflection coefficient of the backscattered waves based on the above formulations and his results show that each succeeding approximation provides an improvement at increasing angles of incidence but the most significant improvement is achieved when first order conditions are substituted by the lowest parabolic approximation, that is the next higher order. Based on these conclusions, the lowest-order parabolic approximation will be implemented in the present model.

3.6 - Numerical tests

This section presents a description of numerical tests performed and the results obtained using the models previously described. The first subsection concerns the tests undertaken with the hyperbolic model in order to evaluate the efficiency of sponge filters and develop a better understanding of their performance aspects. The second subsection concerns the tests undertaken with the elliptic model. The performance of sponge filters and higher order radiation boundary conditions implemented in order to improve the accuracy of the model developed in chapter 2, is also investigated.

3.6.1 - Hyperbolic model

The hyperbolic model described in section 3.4.1.2 was applied for cases where the incident wave direction is not normal to the offshore boundary or cases where even if it is normal, due to the bathymetry or the existence of obstacles, refraction and diffraction originate a change in the wave direction and consequently waves leave the domain with a direction that is no longer parallel to the lateral boundaries. For these cases, where there is flux normal to the lateral boundaries, the performance of the sponge filters was tested successfully. The above tests were also done when sponge filters were implemented at the shore (downwave) boundary but the results show that energy absorption or wave damping in this area disturbs the progressive wave propagation in the interior of the domain.

In order to check the performance of the sponge layers the tests chosen to verify the model were :
- wave diffraction around a semi-infinite breakwater over a domain of constant depth for an incident wave normal to the breakwater;
- wave entering through a breakwater gap of width equal to L over a domain of constant depth;
- wave entering through a breakwater gap of width equal to 2L over a domain of constant depth;

These were chosen because they are cases where there is a flux component normal to the lateral boundaries and there are results available for comparison. The computational results for the 3 cases presented here were obtained with the model with and without sponge layers. In order to verify both models, results were also compared with analytical results obtained by Wiegel (1962) and Johnson (1952).

The calibration of the model which includes sponge filters consisted of minimising the numerical error introduced by waves reflected from the boundaries into the solution for the area of interest. This was achieved by using a process of trial and error to find the optimal gradient of absorption within the sponge layer width, bearing in mind to obtain the least amount of reflections with the narrowest possible layer. It was observed that a smooth gradient of the absorption was

more efficient in reducing fast oscillations resulting from the presence of partial standing waves. However, as large sponge layers incur the cost of a wasted area of calculation, the compromise of obtaining the least amount of reflections with the narrowest possible sponges has to be considered. The model was calibrated for an incident wave angle (between the wave direction and the normal to the offshore boundary) in the range 0° (normal to the offshore) to 45° propagating over uniform depth. For an angle of 45° the relative numerical error for the wave height results is 4%. Experience from running the model for this application suggests that good results can be obtained for sponge widths between L/2 and L.

The case of normal wave incidence to a semi-infinite breakwater over a uniform depth of 40 m was tested for the hyperbolic model with first order radiation boundary conditions as described in section 3.3.1.1 and for the hyperbolic model with first order radiation boundary conditions combined with sponge layers. The above tests were done on a computational area of about 100*200 grid nodes (x and y directions respectively) for the model without sponge filters and 100*230 grid nodes (x and y direction respectively) for the model with sponge filters. The number of grid nodes per wave length used was 10. For both applications the grid spacing considered was about L/10*L/10 m². The sponge layers width was one wave length. An incident wave of height 1 m and period 8 sec was propagated normally to the offshore boundary. The computed results for the models with and without sponge filters in terms of contour plots for the normalised wave height are shown in Fig. 3.1 and 3.2, respectively. In order to verify the models, results can be compared with analytical results obtained by Wiegel (1962), Fig. 3.3. For a better analysis, sections taken from a distance 4 L and 8 L behind the breakwater can be shown in Fig. 3.4 and 3.5, respectively.

For the cases of a wave propagating through a breakwater gap of widths L and 2 L over a uniform dept of 40 m tests were again done for the hyperbolic model in the presence and absence of sponge layers. The numerical domain covered an area of 200*200 grid nodes for the model without sponge layers and an area of 200*230 grid nodes (x and y direction respectively) for the model with sponge layers. The number of grid nodes per wave length used was 10 and the grid spacing considered was L/10*L/10 m². The sponge layer width was equal to L. The incident waves of height 1 m and period 8 sec were made normal to the offshore

boundary which included the totally reflecting breakwater. The computed results are shown in terms of contour plots for the normalised wave height in Fig. 3.6, 3.7, 3.11 and 3.12. The results can be compared with the ones obtained by Johnson (1952) shown in Fig. 3.8 and 3.13. For better analysis sections taken from a distance 6 L and 10 L behind the breakwater are shown in Fig. 3.9 and 3.10 respectively, for the case where the breakwater gap is equal to L and in Fig. 3.14 and 3.15 respectively, for the case where the breakwater gap is equal to 2 L.

Both hyperbolic models, one where the open boundaries are treated as first order radiation boundary conditions and the other where they are treated as a combination of first order radiation boundary conditions with sponge filters, give good results for wave propagation in the vicinity of an obstacle, that is, simulate well the wave transformation process of diffraction. The computed results obtained from the models show good agreement with the analytical solutions obtained by Wiegel (1962) for the case of the semi-infinite breakwater, and Johnson (1952) for both cases of breakwater gap. The computational results for the 3 cases of study plotted in terms of contours (lines of equal normalised wave height), show that the wave pattern of the diffracted solution can be predicted well by both models. A generally correct quantitative evaluation of the transformed waves due to the presence of the structures can also be seen in the same plots. Nevertheless, the sections located behind the structures at positions previously identified, allow a more detailed evaluation of these results. A common characteristic observed in all the sections is that the hyperbolic model with first order radiation boundary conditions combined with sponge filters reduces the amplitude of the oscillations that can be observed in the model in the absence of sponges. The amplitude of the oscillations is proportional to the average value of the solution and oscillations are less noticeable when the gradient of the solution reaches its maximum value, that is, when there is a faster variation of the wave height, which occurs in front of the lee of the structures. The results obtained for the model with first order radiation boundary conditions combined with sponge filters are considerably smoother and in better agreement with the analytical results. Sponge filters in the hyperbolic model are therefore efficient in reducing the partial standing waves arising from the boundaries.

3.6.2 - Elliptic model

The two elliptic models, one with first order radiation boundary conditions combined with sponge filters, as described in section 3.4.2, and the other with higher order radiation boundary conditions (lowest-order parabolic approximation), as described in section 3.5, were run for Berkhoff's elliptic shoal.

Similarly to the hyperbolic model, a process of trial and error was undertaken in order to investigate the sensitivity of the model to the introduction of the sponge filters. The gradient of absorption within the sponge filters was made to vary linearly along the width. The width of the sponges was about 3.5 L at the lateral downwave boundaries and about 2 L at the shore boundary. For these conditions, the maximum dissipation factor, f_{Dmax}, at the outer sponge edge was made to vary within interval [0.1, 4]. The sensitivity of the solutions to this variation is shown from Fig. 3.16.1 to Fig. 3.16.8, for the same eight sections considered in chapter 2 for the Berkhoff's shoal. The computational results that best represent this variation were obtained for an f_{Dmax} equal to 0.4, 0.5, 0.6, 0.8, 1.0, 1.5, 2.0 and 3.0. To avoid repetition, the bathymetry and numerical conditions are the same as described in chapter 2, Fig. 2.1. The width of the sponges was established based on using the maximum area available around the domain of interest, which for this case was considered to be precisely the area were the eight sections are allocated.

For the model with higher order radiation boundary conditions, the lowest-order parabolic approximation, described and discussed in section 3.5 and expressed by equation (3.42), was implemented. It was derived for downstream conditions, thus for upstream conditions it can be written as

$$\frac{\partial \phi}{\partial x} = -ik\left(\phi + \frac{1}{2k^2} \frac{\partial^2 \phi}{\partial y^2} \right).$$
(3.44)

Bearing in mind that $\phi = \phi^i + \phi^r$, and $\dfrac{\partial \phi}{\partial x} = \dfrac{\partial \phi^i}{\partial x} + \dfrac{\partial \phi^r}{\partial x}$, where ϕ^i and ϕ^r are the incident and backscattered velocity potential components respectively, the implementation of the boundary condition was established as follows:

- Offshore/driving boundary

$$\frac{\partial \phi}{\partial x} = \frac{\partial \phi^i}{\partial x} + \left(ik_c \phi^i + \frac{i}{2k_c} \frac{\partial^2 \phi^i}{\partial y^2} \right) - \left(ik_c \phi + \frac{i}{2k_c} \frac{\partial^2 \phi}{\partial y^2} \right)$$ (3.45)

for $x = 1$ and $1 < y < Ny$.

- Lateral/driving boundary

$$\frac{\partial \phi}{\partial y} = \frac{\partial \phi^i}{\partial y} + \left(ik_c \phi^i + \frac{i}{2k_c} \frac{\partial^2 \phi^i}{\partial x^2} \right) - \left(ik_c \phi + \frac{i}{2k_c} \frac{\partial^2 \phi}{\partial x^2} \right)$$ (3.46)

for $y = 1$ or $y = Ny$ and $1 < x < Nx$.

- Shore/downwave boundary

$$\frac{\partial \phi}{\partial x} = ik_c \left(\phi + \frac{1}{2k_c^2} \frac{\partial^2 \phi}{\partial y^2} \right)$$ (3.47)

for $x = Nx$ and $1 < y < Ny$.

- Lateral/downwave boundary

$$\frac{\partial \phi}{\partial y} = ik_c \left(\phi + \frac{1}{2k_c^2} \frac{\partial^2 \phi}{\partial x^2} \right)$$ (3.48)

for $y = 1$ or $y = Ny$ and $1 < x < Nx$.

Driving boundary conditions are radiation boundary conditions plus the incoming waves.

Once again the model was applied to Berkhoff's shoal. The computational results for the eight sections behind the shoal are shown from Fig. 3.17.1 to Fig. 3.17.8.

The objective of implementing sponge filters within the elliptic model with first order radiation boundary conditions was to improve the accuracy of the numerical solutions by introducing a dissipation area adjacent to the boundaries that would minimise the backscattered waves. However, what was observed was that the introduction of the sponge filters only decreases the wave energy within the sponge layers and that for the area of interest, which is the region behind the shoal, they tend to produce sharper variations of the results. Thus, it can be concluded that sponge filters do not produce a successful improvement when

dealing with open boundary conditions for this particular mathematical formulation.

Computed solutions of the elliptic model with higher order radiation boundary conditions show a better agreement with the experimental data obtained by Berkhoff (1982) than the solutions of the model with first order radiation boundary conditions. A higher accuracy was expected to be achieved as the lowest order parabolic approximation makes downwave open boundaries more transparent to the passage of oblique incident waves. Nevertheless, the finite differences scheme, described in chapter 2, requires a 9 points stencil instead of a 5 points one, due to the introduction of the terms $\dfrac{\partial^2 \phi}{\partial y^2}$ and $\dfrac{\partial^2 \phi}{\partial x^2}$, that bring instability to the numerical scheme if only a 5 points stencil is used. This requirement increases the computational cost to solve the problem, in terms of time and memory, and taking into account that the improvement of the results is not so significant, it seems that the applicability of the elliptic model with higher order radiation boundary conditions is somewhat questionable. That is, if the model is simply to be applied for a sea state representative of regular waves then the investment can be worthwhile, but if the objective is to further extend the model for irregular wave propagation assuming a superposition of independent spectral components then its application can be computationally very expensive.

3.7 - Closure

This chapter dealt with numerical formulations that simulate open boundary conditions in a numerical domain for wave propagation. The importance of a correct simulation of outgoing waves with a minimum of artificial reflections into the domain of interest is crucial with regard to eliminating errors due to the presence of partial standing waves in the domain of interest. An investigation was undertaken to establish the state of the art regarding not only formulations for radiation boundary conditions, but also their implementation in different wave propagation numerical models. The behaviour of two different formulations, based on the mild - slope equation, for non - reflective boundary conditions was

investigated. These two formulations, elliptic and hyperbolic, are the ones that best deal with the phenomenon of wave propagation because they do not impose any physical constraint, therefore it is important to optimise their performance, noting that further work will be presented regarding only the elliptic formulation.

For the hyperbolic formulation, first order time dependent radiation boundary conditions and first order time dependent radiation boundary conditions combined with sponge filters were implemented. The objective was to develop a good understanding of the performance of sponge filters in a numerical model where their implementation is a reasonably easy procedure, thus undertaking a more complete investigation regarding this type of non - reflective boundary conditions. Results obtained from applying the two models to 3 different cases for which existing data were available for comparison, showed that first order radiation boundary conditions combined with sponge filters constitute a worthwhile improvement.

For the elliptic formulation, the behaviour of the model for three types of non - reflective boundary conditions was studied. The objective was to improve the accuracy of the model developed in chapter 2. These boundaries were simulated by first order radiation boundary conditions, higher order radiation boundary conditions, and first order radiation boundary conditions combined with sponge filters. Once again tests were performed to evaluate the efficiency of these formulations in improving the accuracy of the solutions. The results obtained with the model where sponge filters combined with first order radiation boundary conditions were implemented did not show an improvement over the results obtained from using simply first order radiation boundary conditions. However, higher order radiation boundary conditions showed to be more effective when dealing with eliminating the backscattered waves. Nevertheless, the last model incurs an higher computational cost in comparison with the model which is based on first order radiation boundary conditions. Owing to the fact that it is intended to extend this model to irregular waves under the assumption of linear superposition of independent spectral components, and the improvements obtained regarding the accuracy of the solutions are not very significant, this

research work led to the conclusion that the most efficient model for the stated purpose is the model with first order radiation boundary conditions.
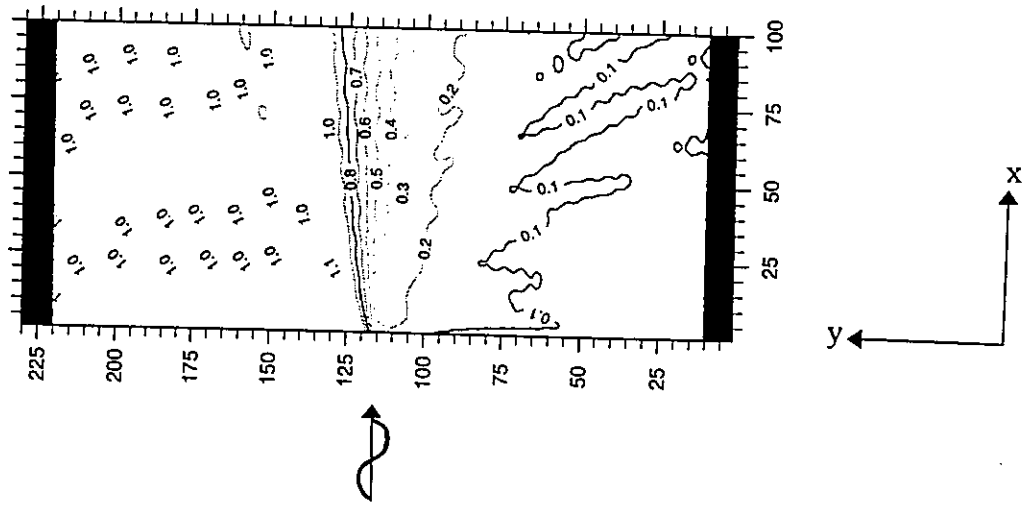
Fig. 3.1 - Semi-infinite breakwater. Wave diffraction diagram obtained with the hyperbolic model with sponge filters.

Fig. 3.2 - Semi-infinite breakwater. Wave diffraction diagram obtained with the hyperbolic model in the absence of sponge filters.
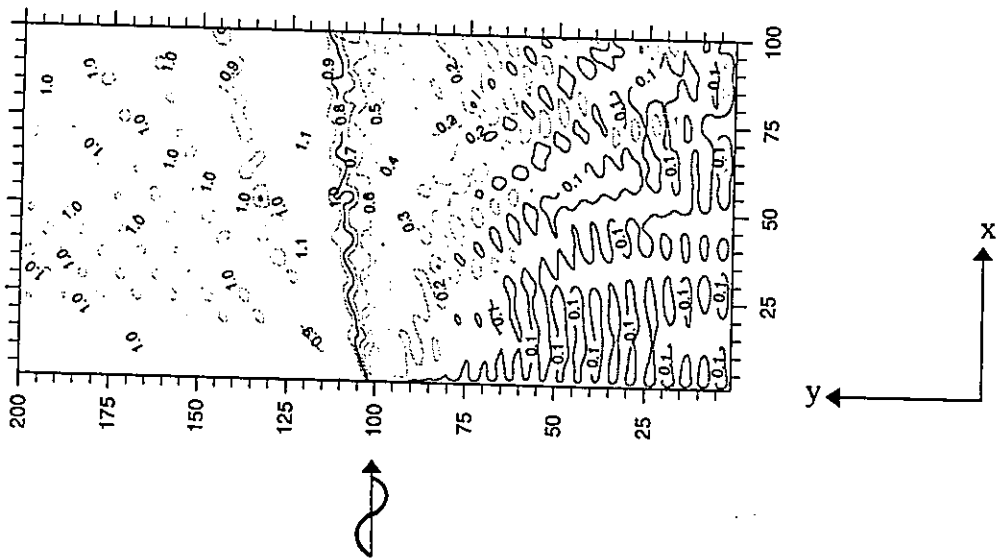
Fig. 3.3 – Semi-infinite breakwater. Wave diffraction diagram. Results obtained by Wiegel (1962).
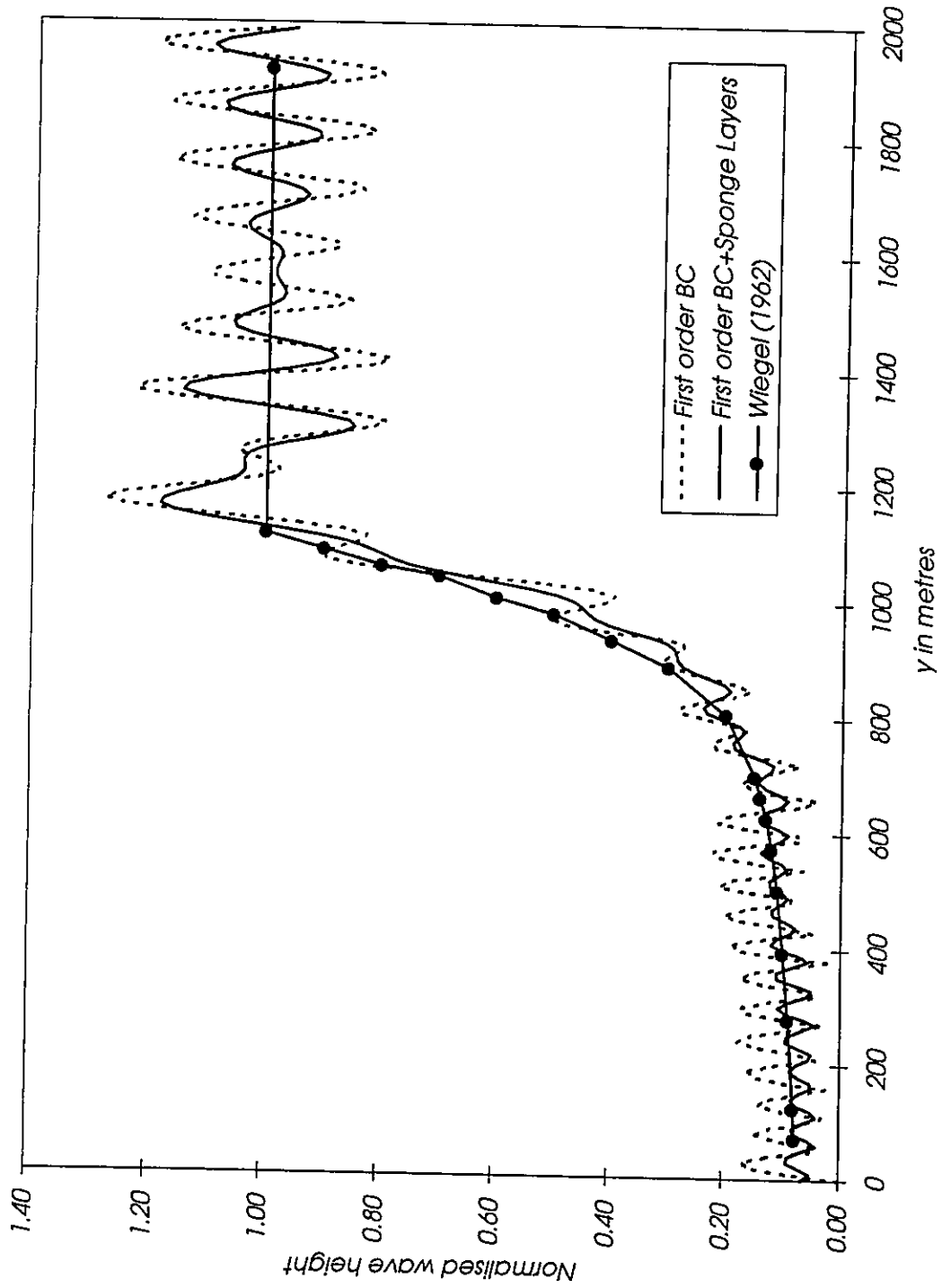
Fig. 3.4 - Normalised wave height at a distance x = 4 L behind the semi-infinite breakwater.
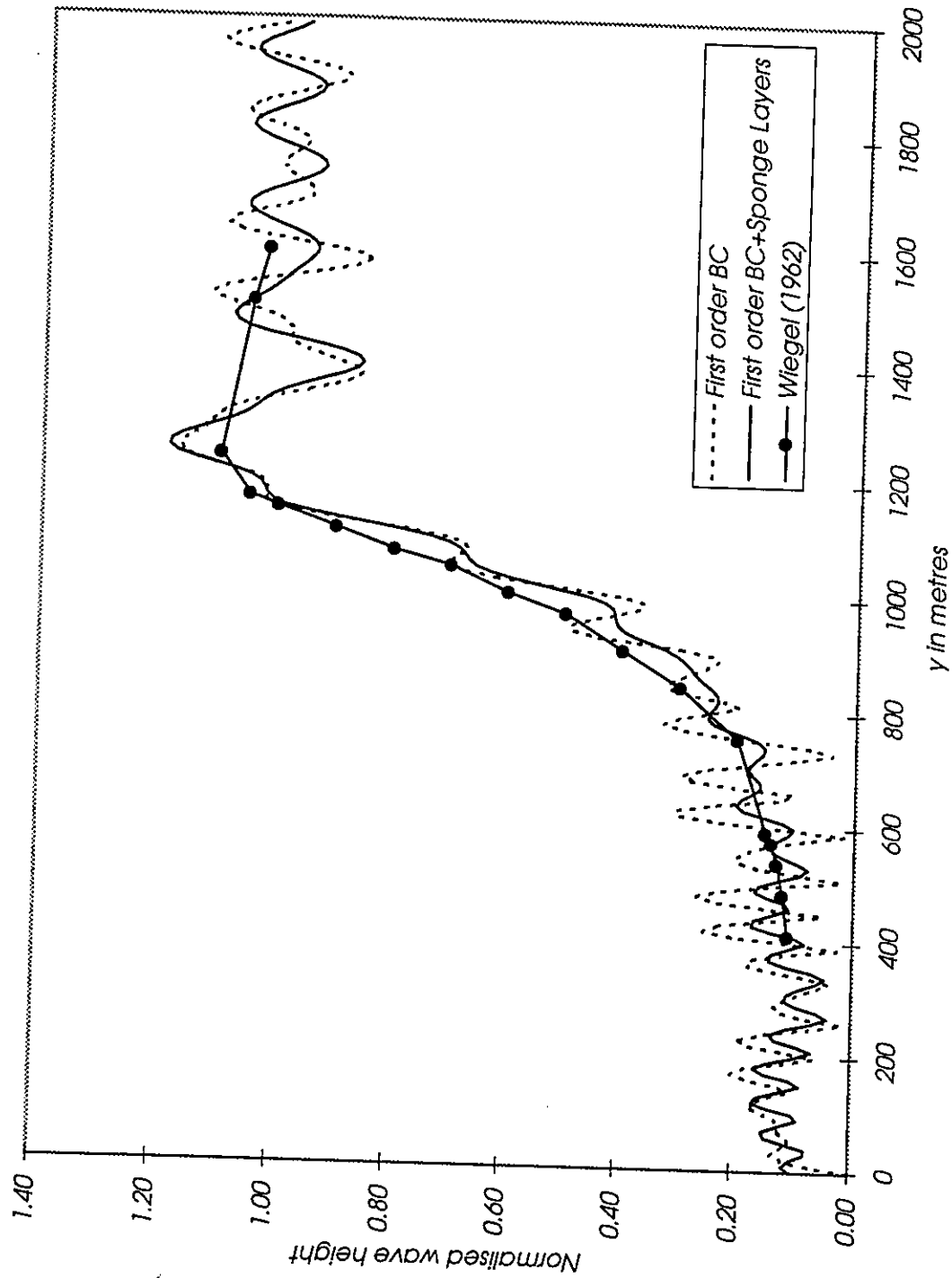
Fig. 3.5 - Normalised wave height at a distance x = 8 L behind the semi-infinite breakwater.
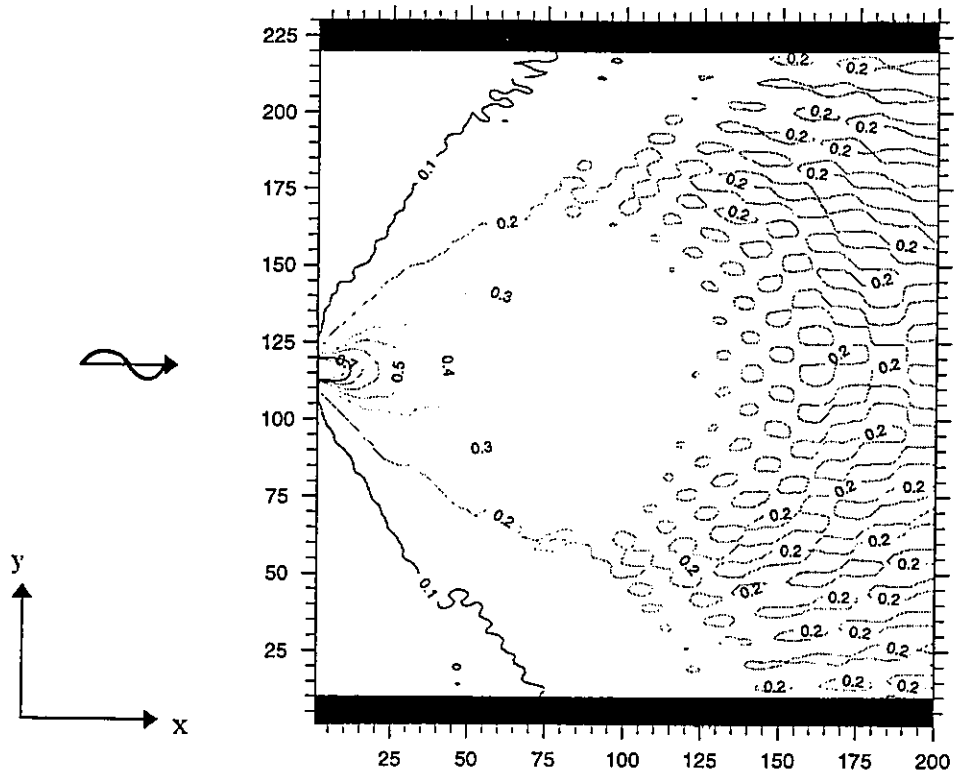
Fig. 3.6 - Breakwater gap width of one wave length. Wave diffraction diagram obtained with the hyperbolic model with sponge filters.
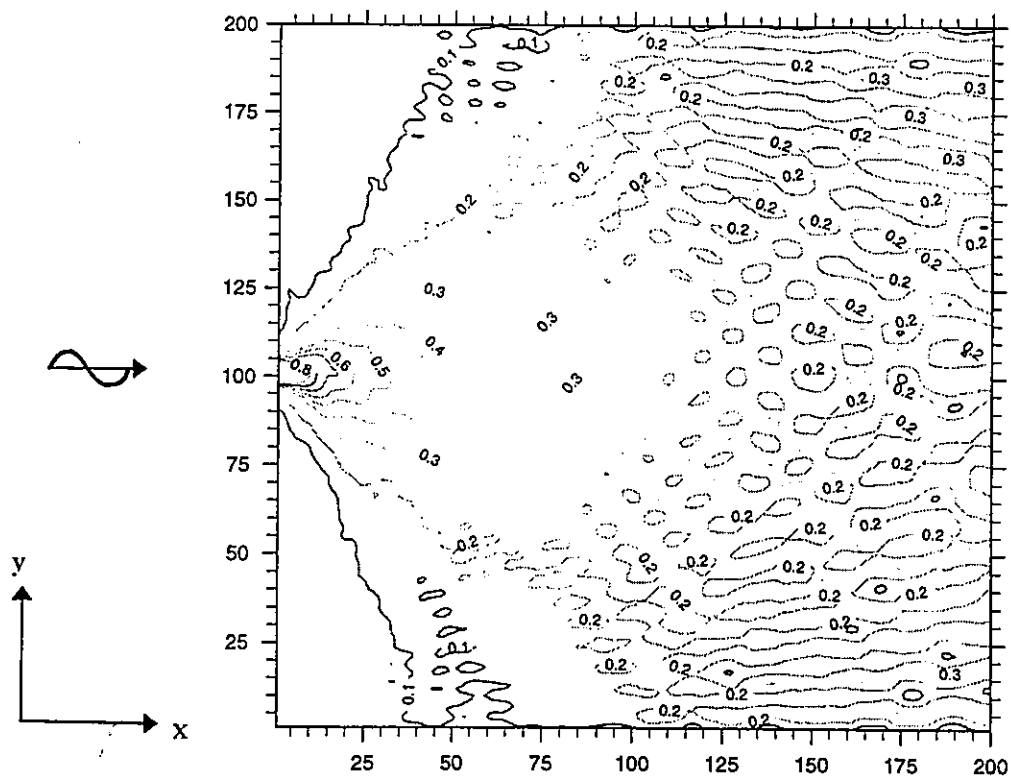
Fig. 3.7 - Breakwater gap width of one wave length. Wave diffraction diagram obtained with the hyperbolic model in the absence of sponge filters.
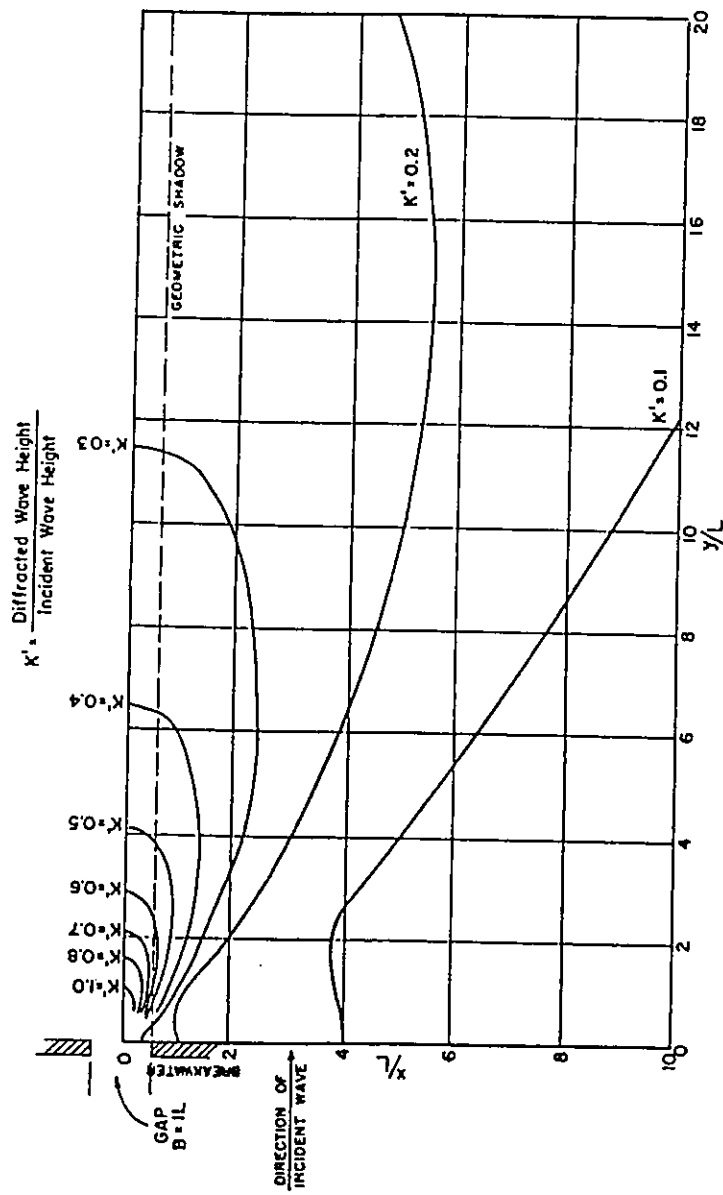
Fig. 3.8 - Breakwater gap width of one wave length. Wave diffraction diagram. Results obtained by Johnson (1952).
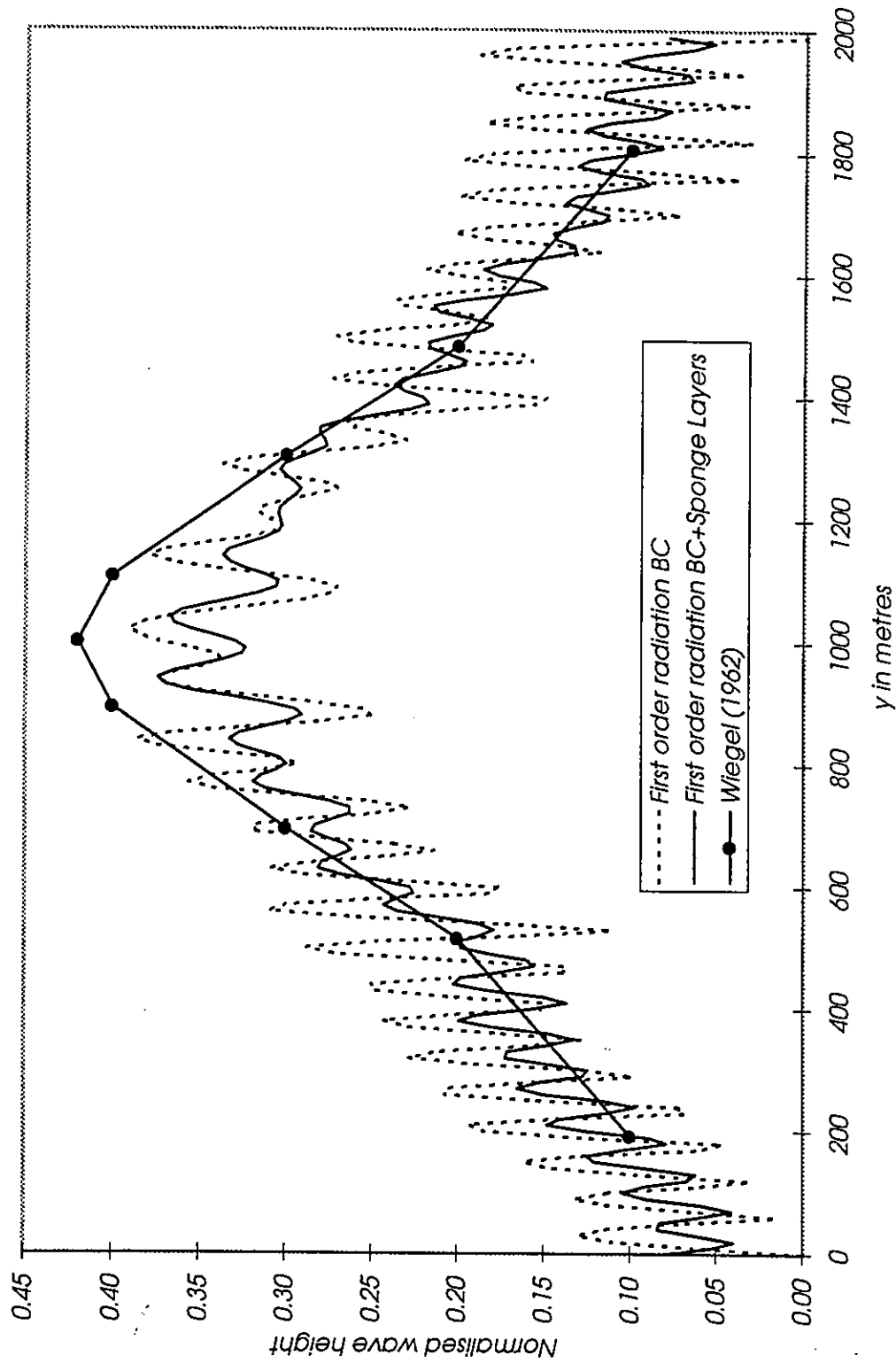
Fig. 3.9 - Normalised wave height at a distance x = 6 L behind the breakwater gap width of one wave length.
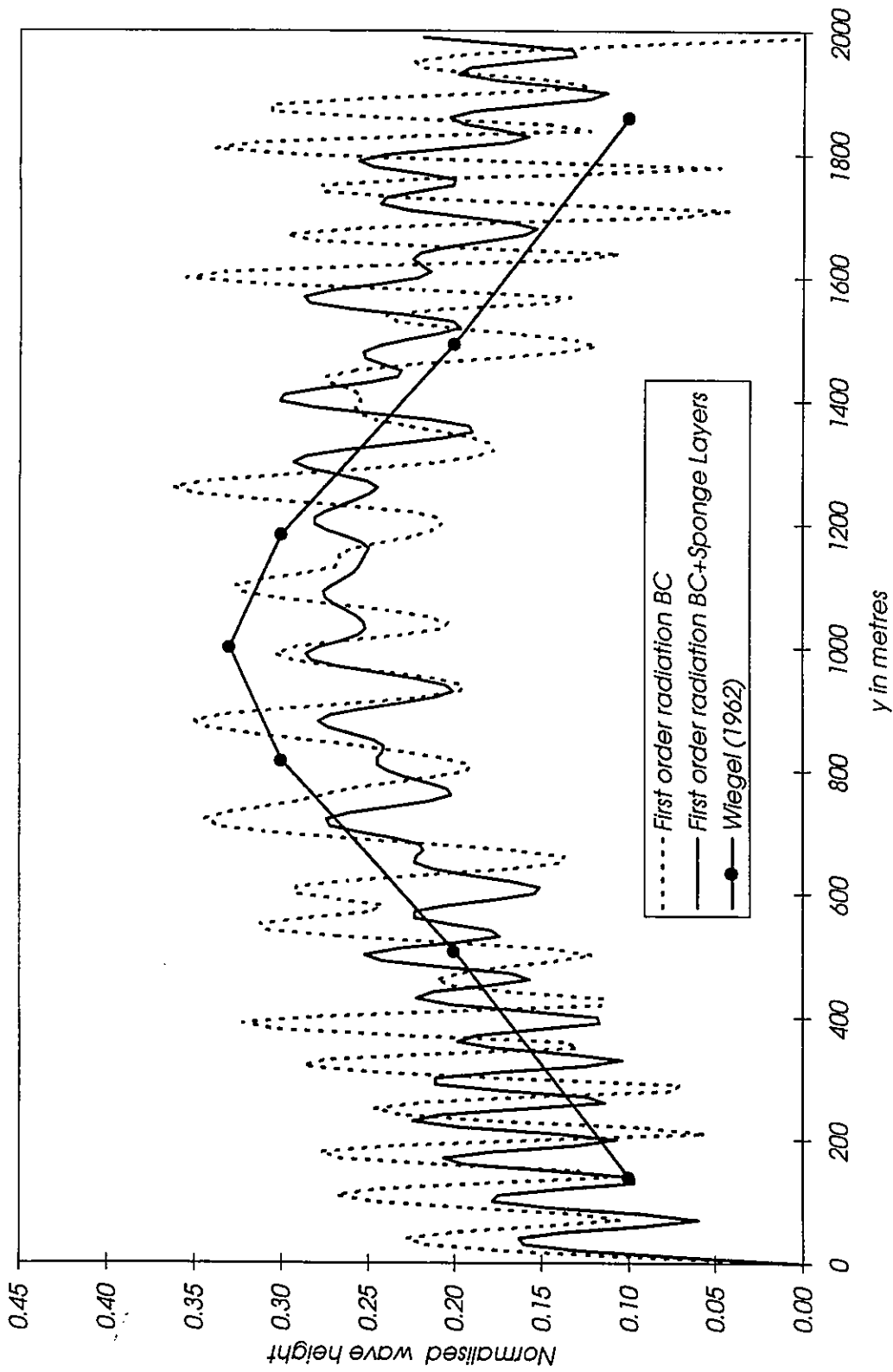
Fig. 3.10 - Normalised wave height at a distance x = 10 L behind the breakwater gap width of one wave length.
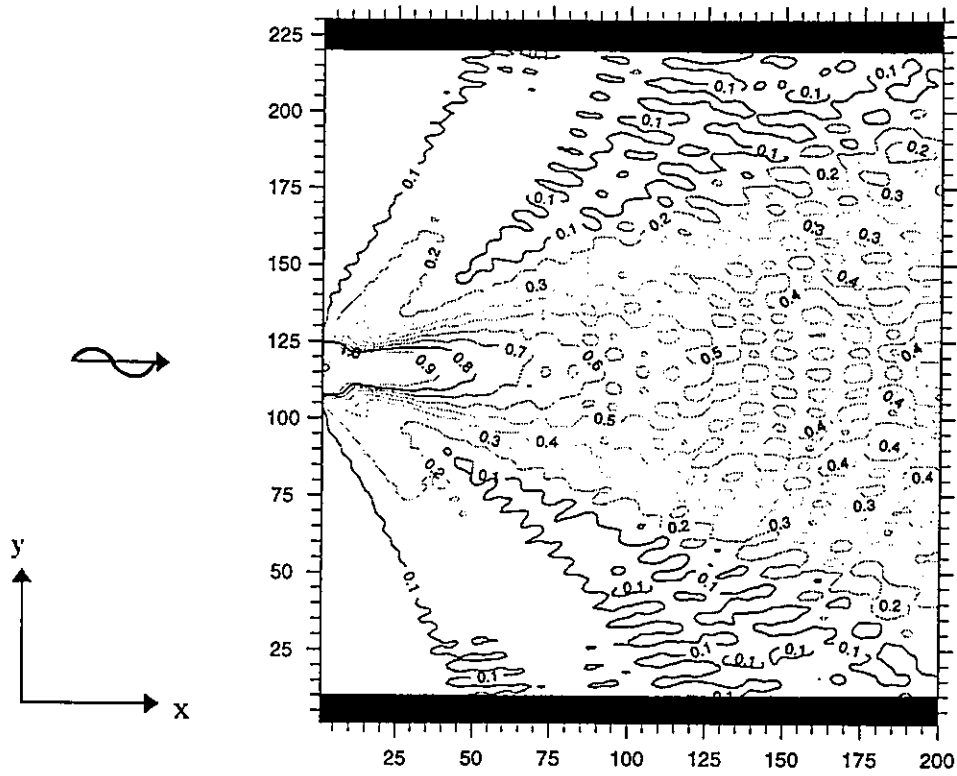
Fig. 3.11 - Breakwater gap width of two wave length. Wave diffraction diagram obtained with the hyperbolic model with sponge filters.
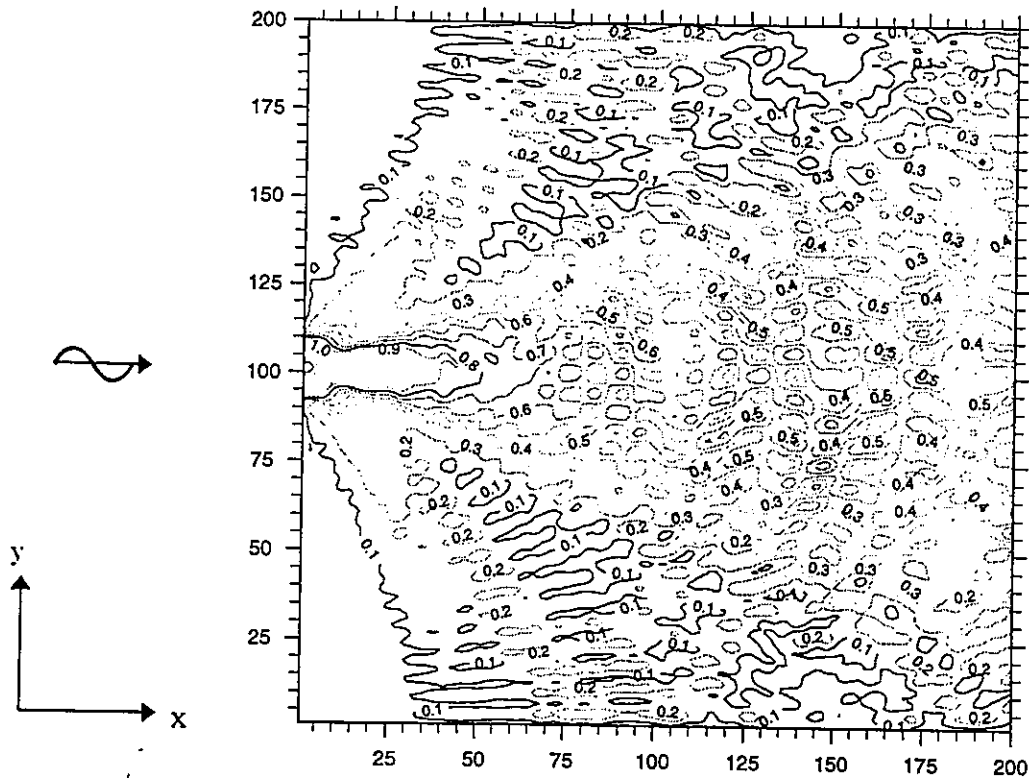
Fig. 3.12 - Breakwater gap width of two wave length. Wave diffraction diagram obtained with the hyperbolic model in the absence of sponge filters.
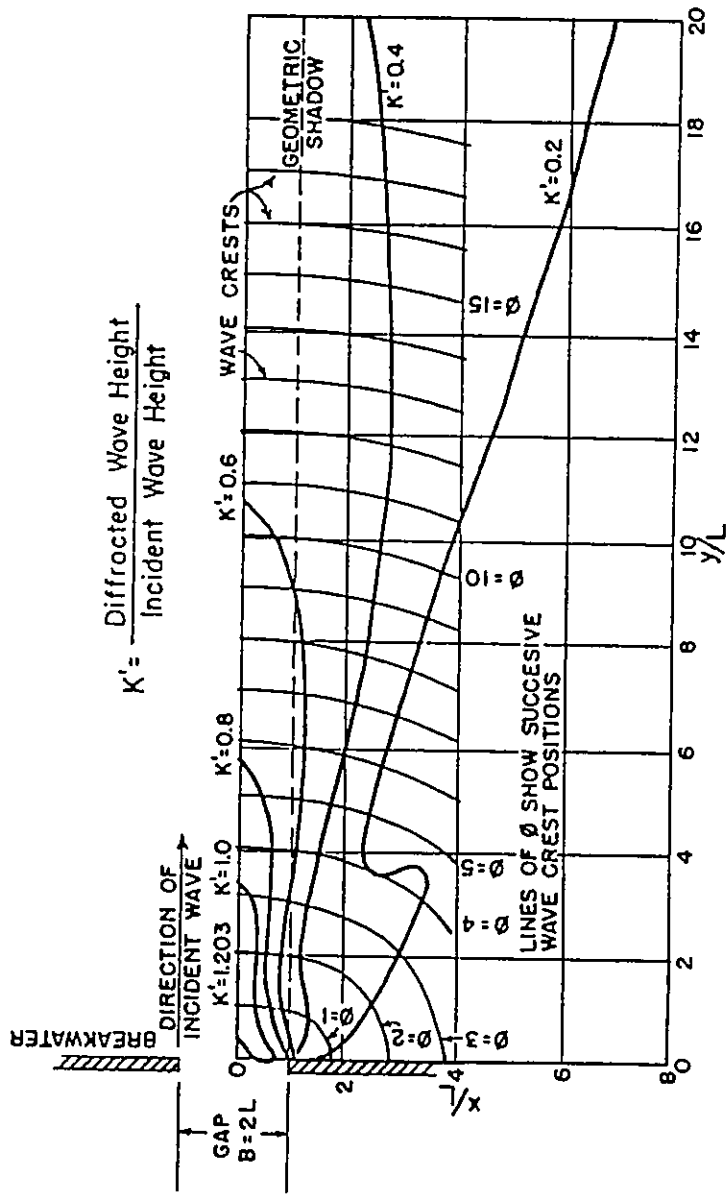
Fig. 3.13 - Breakwater gap width of two wave length. Wave diffraction diagram. Results obtained by Johnson (1952).

First order radiation BC
First order radiation BC+Spongr Layers
Wiegel (1962)

Normalised wave height

0.80
0.70
0.60
0.50
0.40
0.30
0.20
0.10
0.00

0   200   400   600   800   1000   1200   1400   1600   1800   2000

y in metres
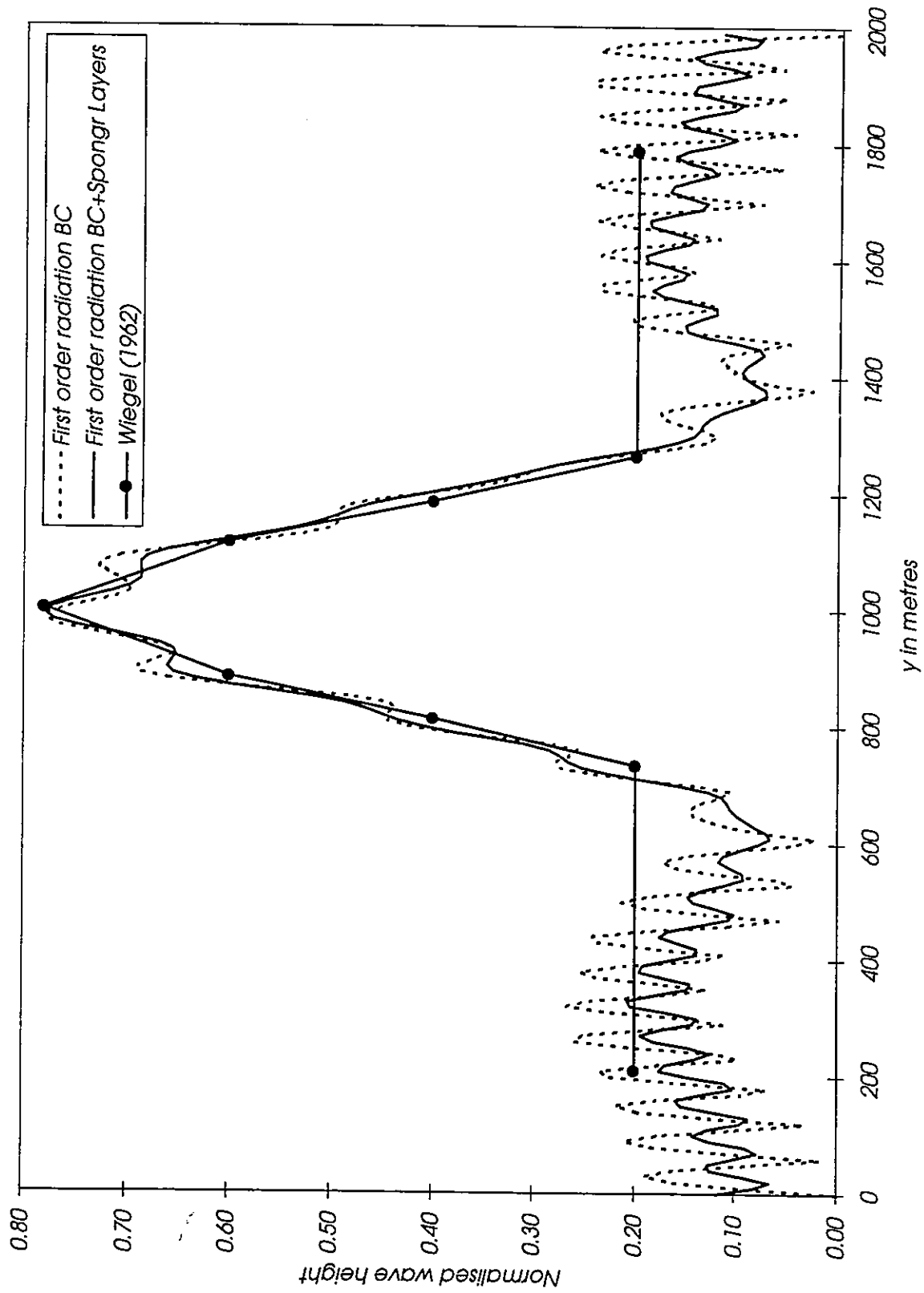
Fig. 3.14 - Normalised wave height at a distance x = 6 L behind the breakwater gap width of two wave length.
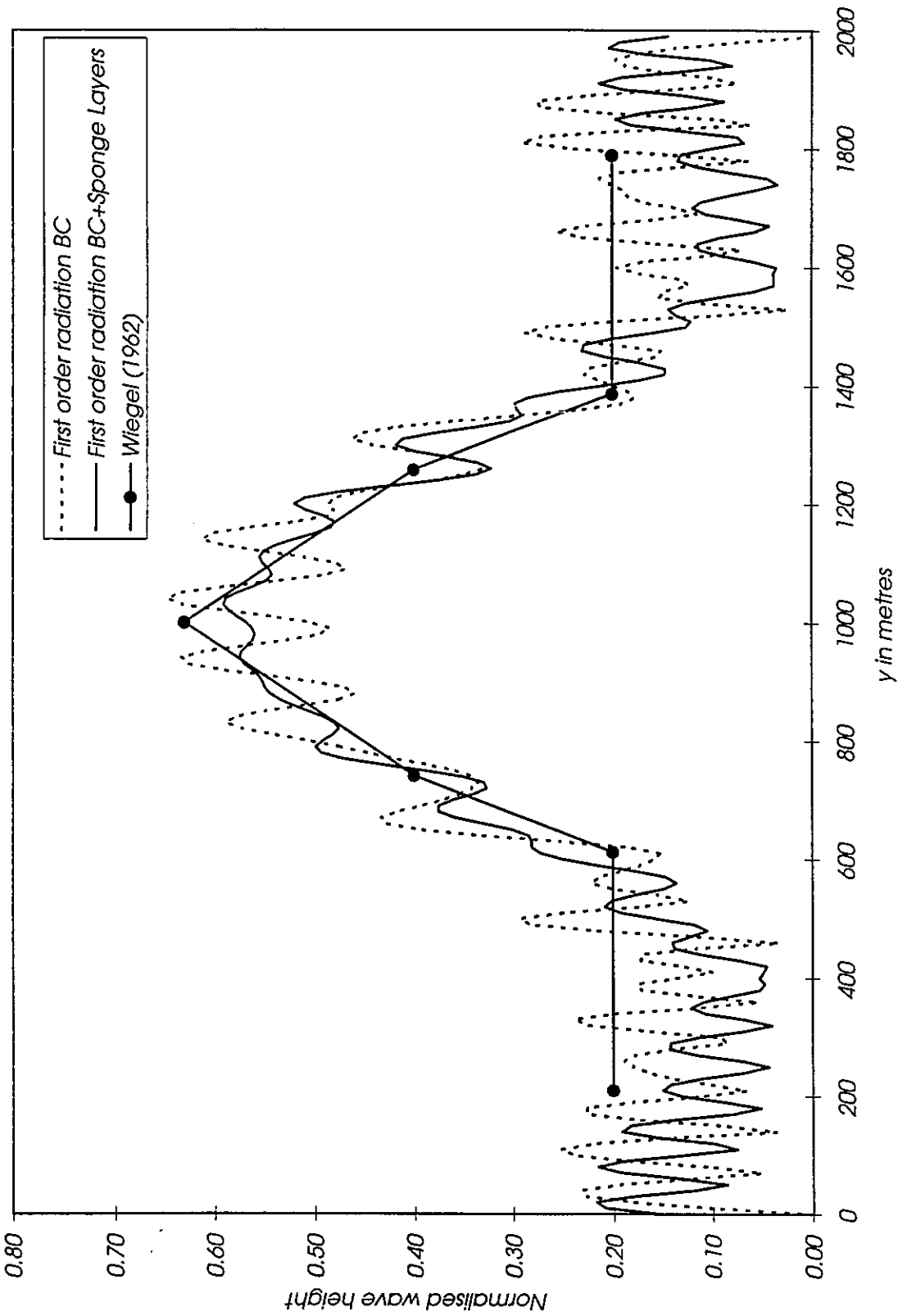
Fig. 3.15 - Normalised wave height at a distance x = 10 L behind the breakwater gap width of two wave length.
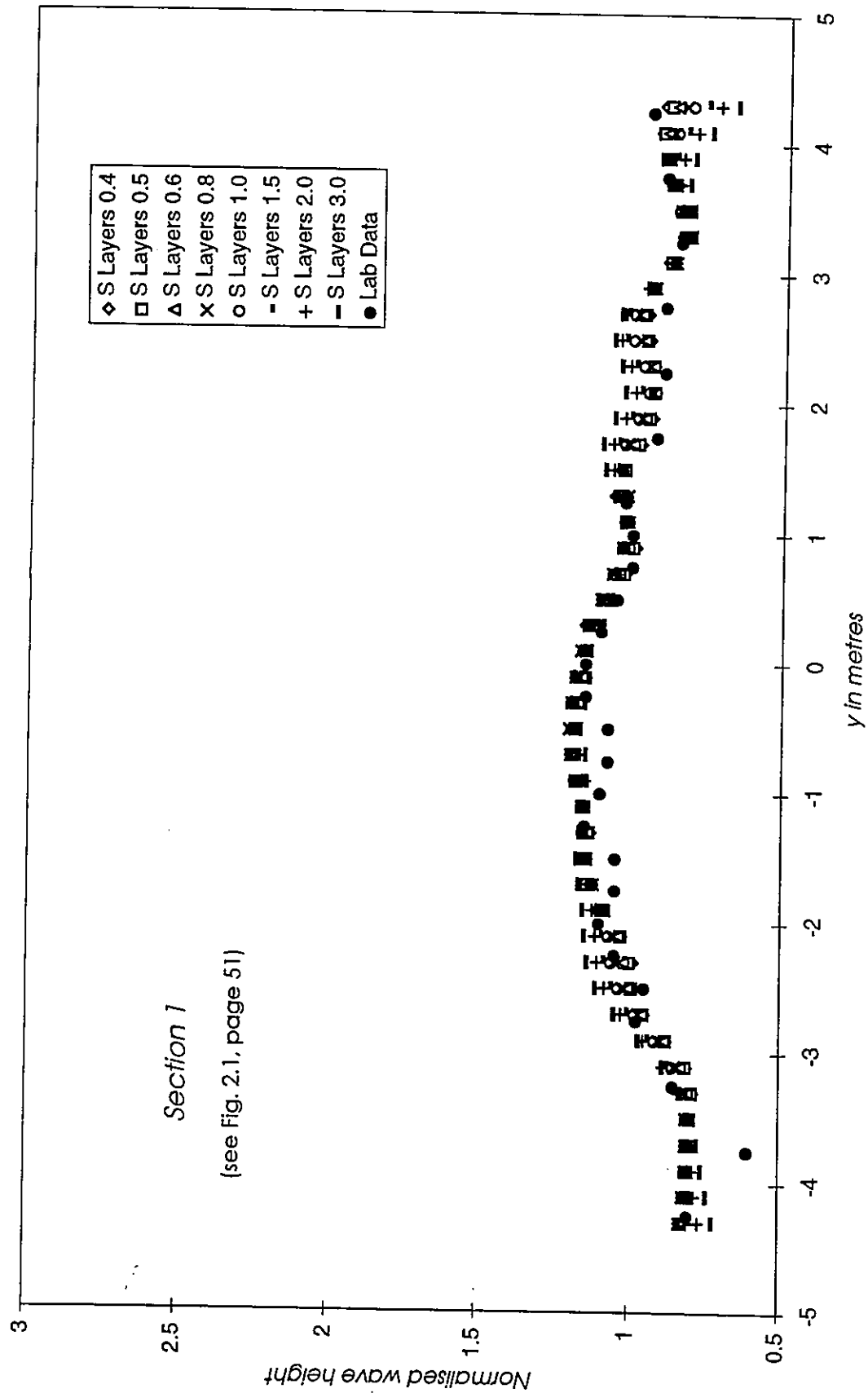
Fig. 3.16.1 – Comparison between experimental data of Berkhoff et al (1982) and results from the elliptic model with sponge filters. Section 1.
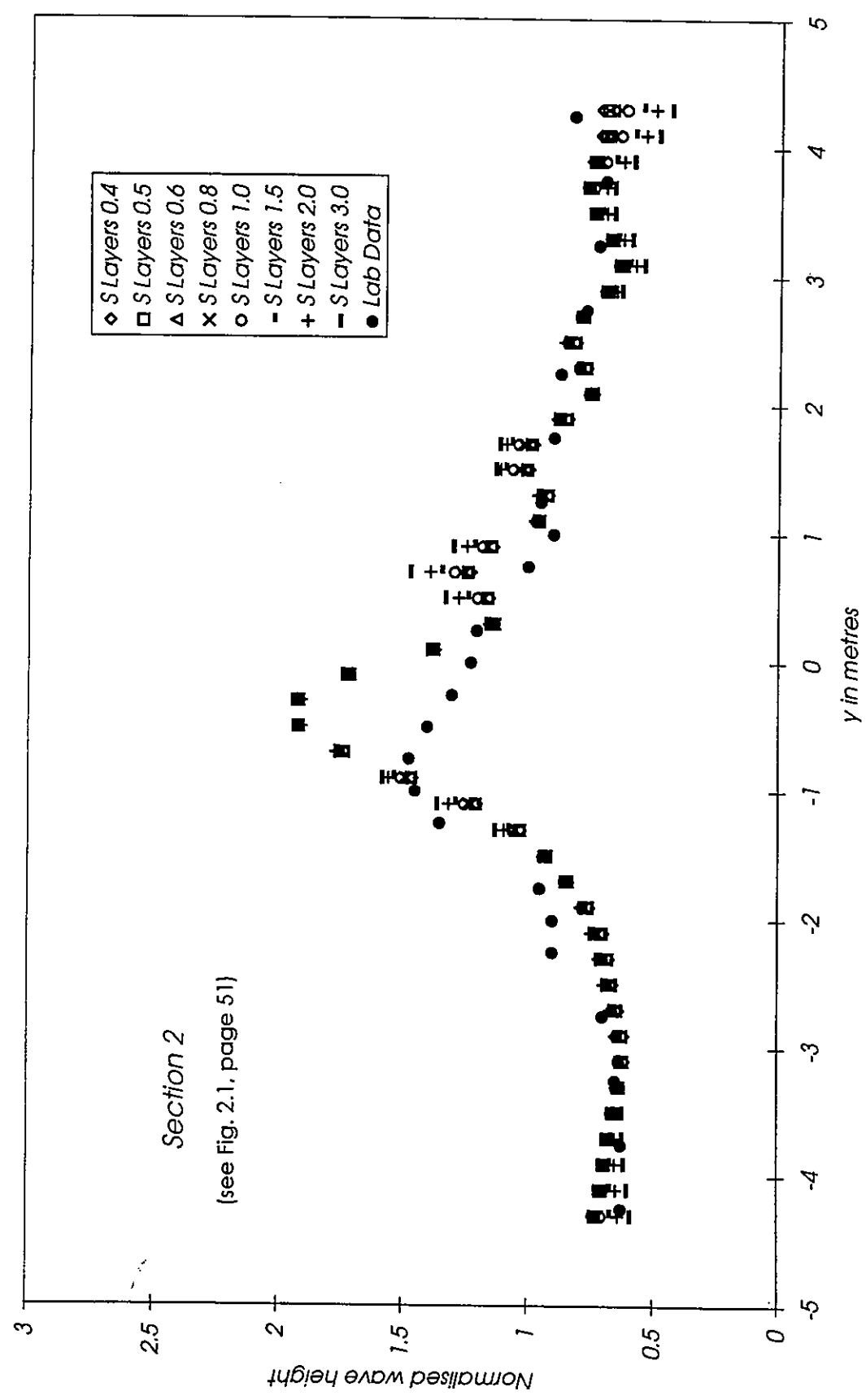
Fig. 3.16.2 - Comparison between experimental data of Berkhoff et al (1982) and results from the elliptic model with sponge filters. Section 2.
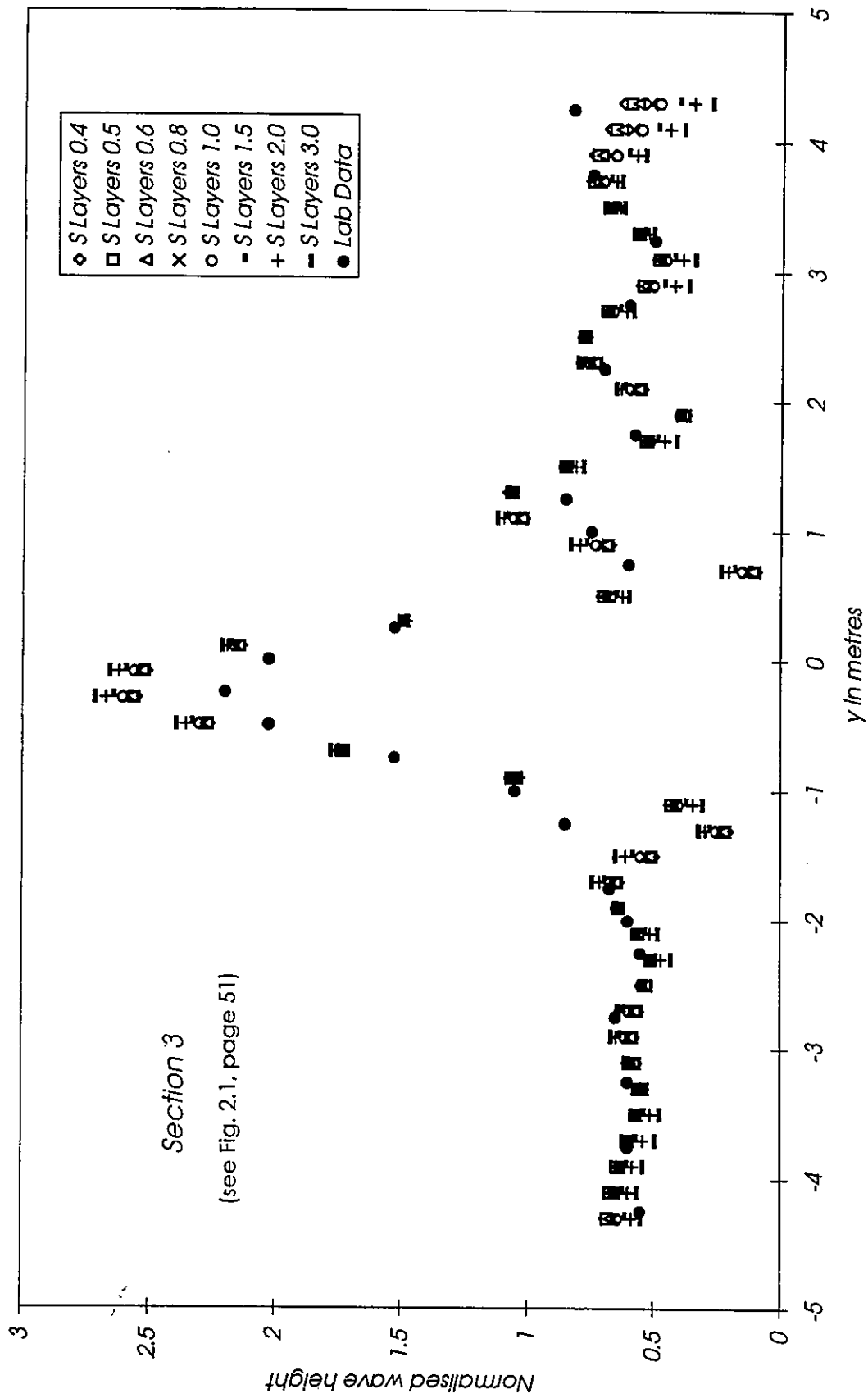
Fig. 3.16.3 – Comparison between experimental data of Berkhoff et al (1982) and results from the elliptic model with sponge filters. Section 3.
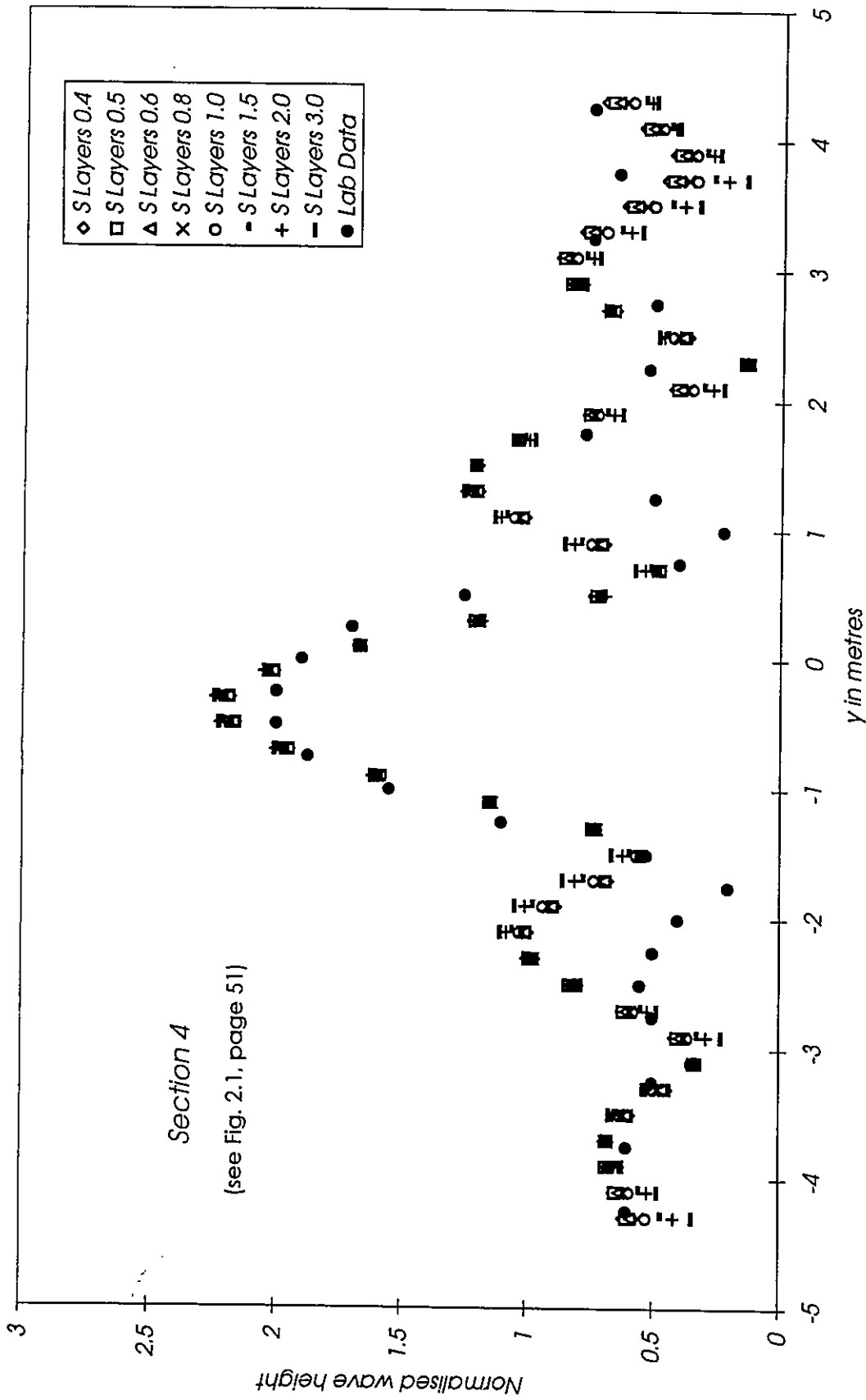
Fig. 3.16.4 - Comparison between experimental data of Berkhoff et al (1982) and results from the elliptic model with sponge filters. Section 4.

Section 5

(see Fig. 2.1, page 51)

◇ S Layers 0.4
□ S Layers 0.5
△ S Layers 0.6
× S Layers 0.8
○ S Layers 1.0
− S Layers 1.5
+ S Layers 2.0
− S Layers 3.0
● Lab Data

Normalised wave height

y in metres
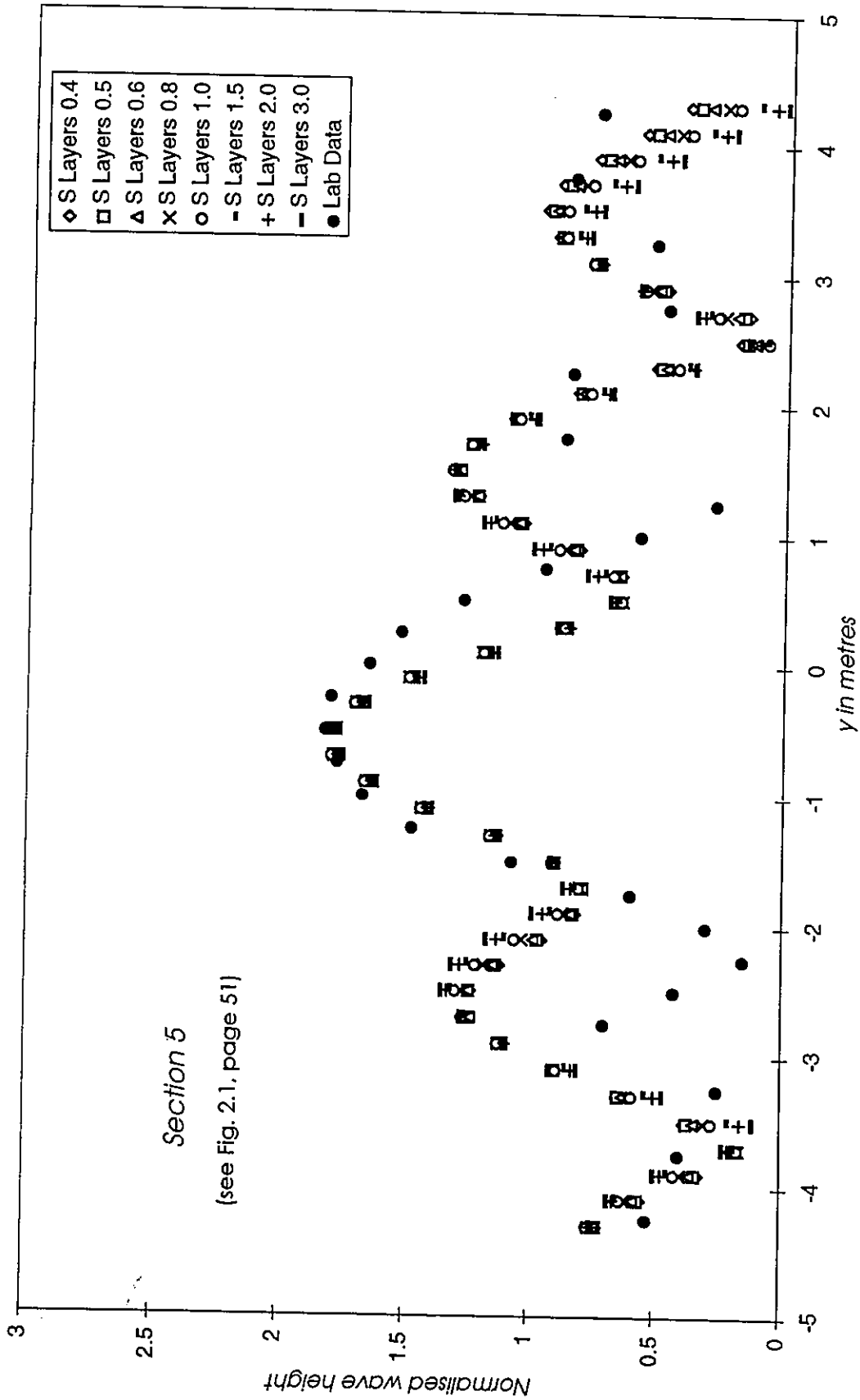
Fig. 3.16.5 - Comparison between experimental data of Berkhoff et al (1982) and results from the elliptic model with sponge filters. Section 5.
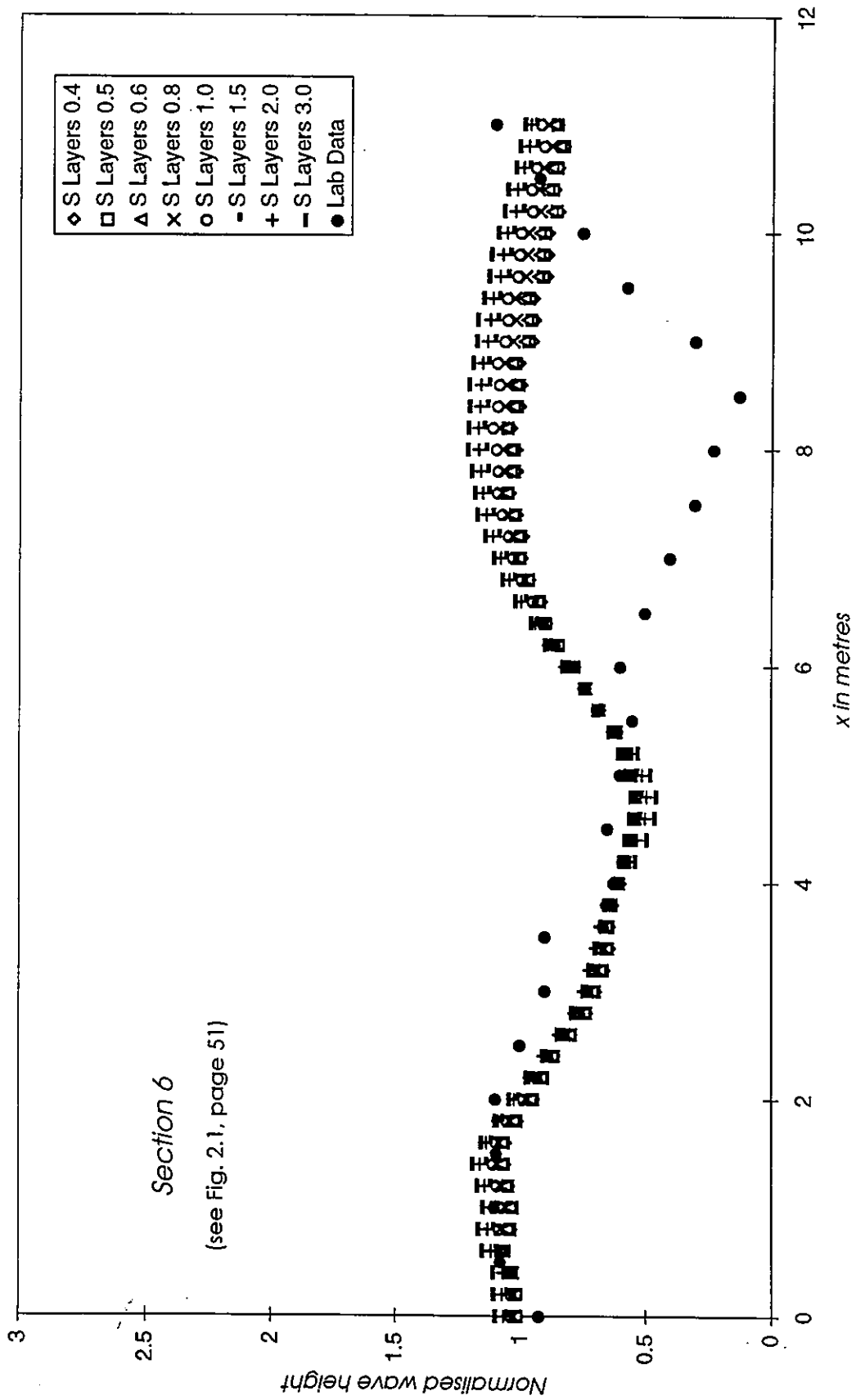
Fig. 3.16.6 - Comparison between experimental data of Berkhoff et al (1982) and results from the elliptic model with sponge filters. Section 6.
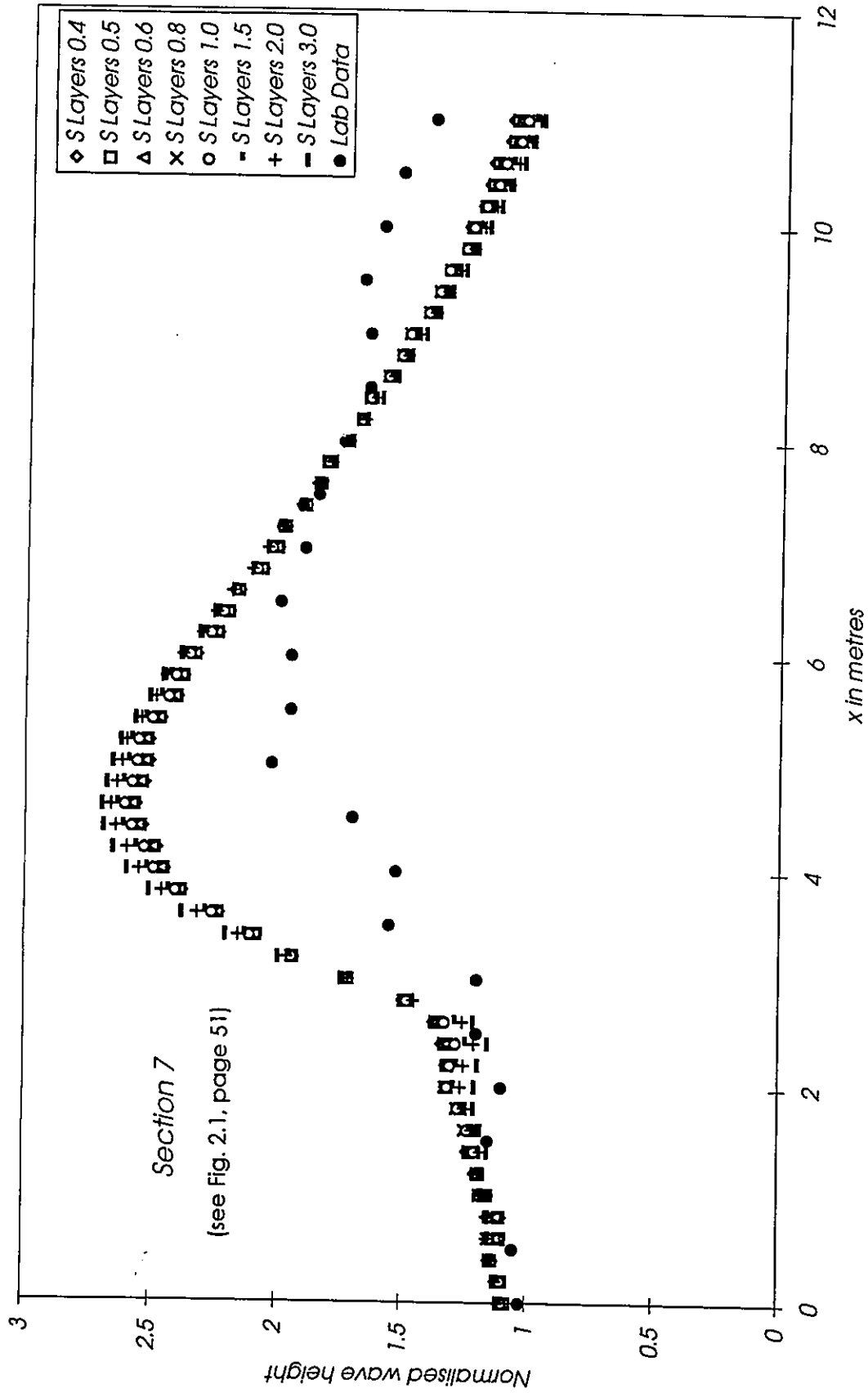
Fig. 3.16.7 - Comparison between experimental data of Berkhoff et al (1982) and results from the elliptic model with sponge filters. Section 7.
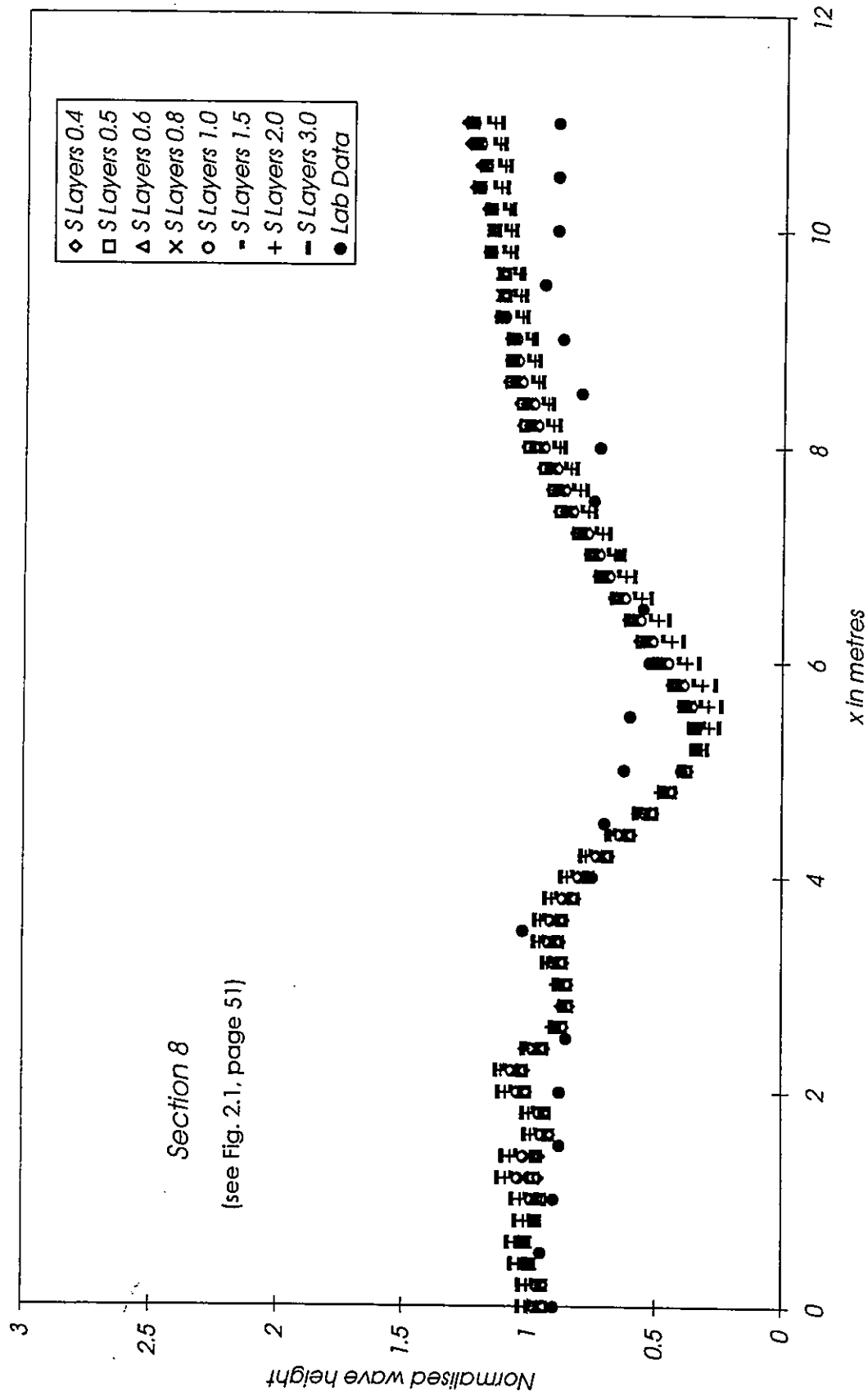
Fig. 3.16.8 - Comparison between experimental data of Berkhoff et al (1982) and results from the elliptic model with sponge filters. Section 8.
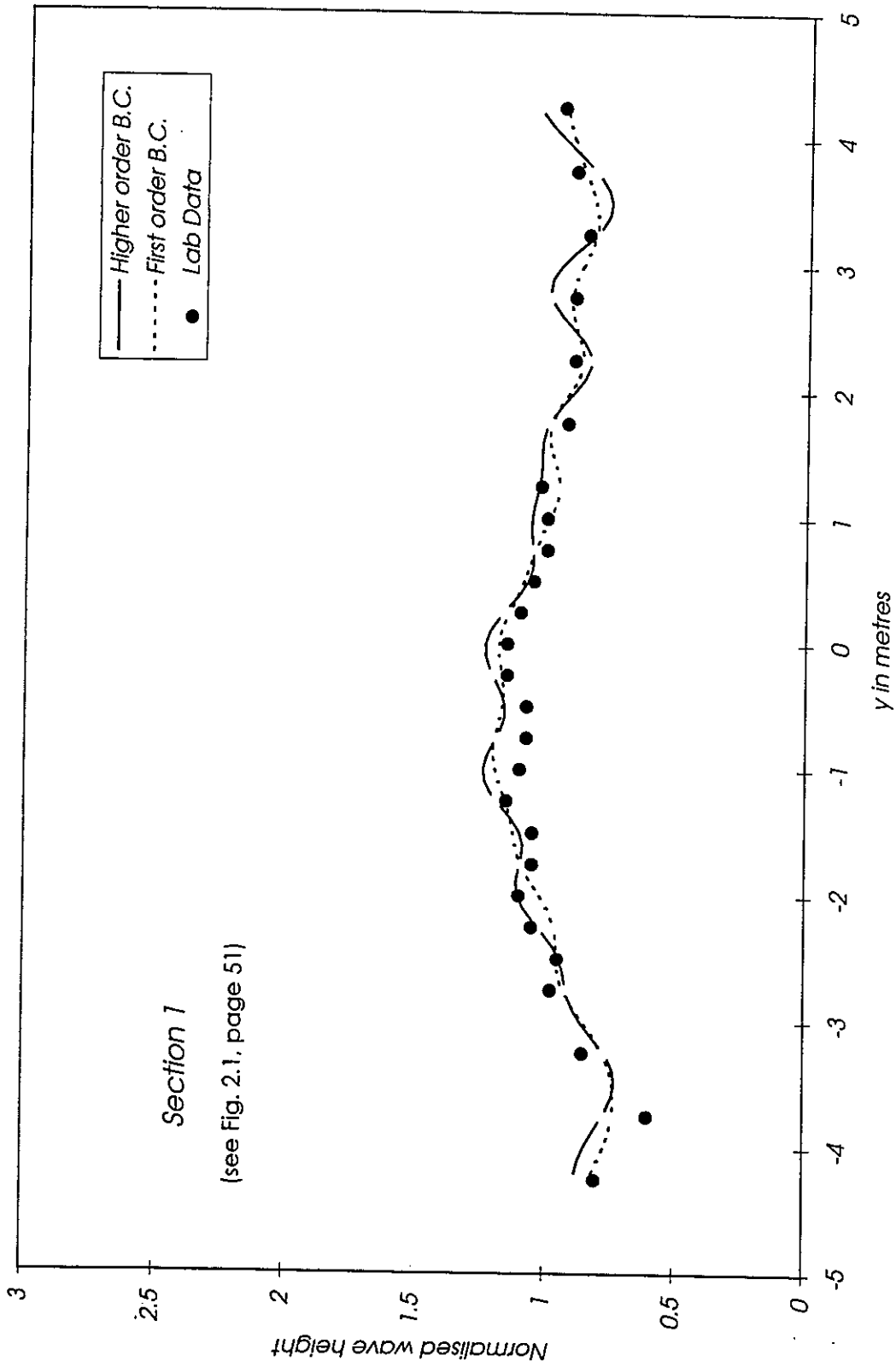
Fig. 3.17.1 - Comparison between experimental data of Berkhoff et al (1982) and results from the elliptic model with higher order boundary conditions. Section 1.
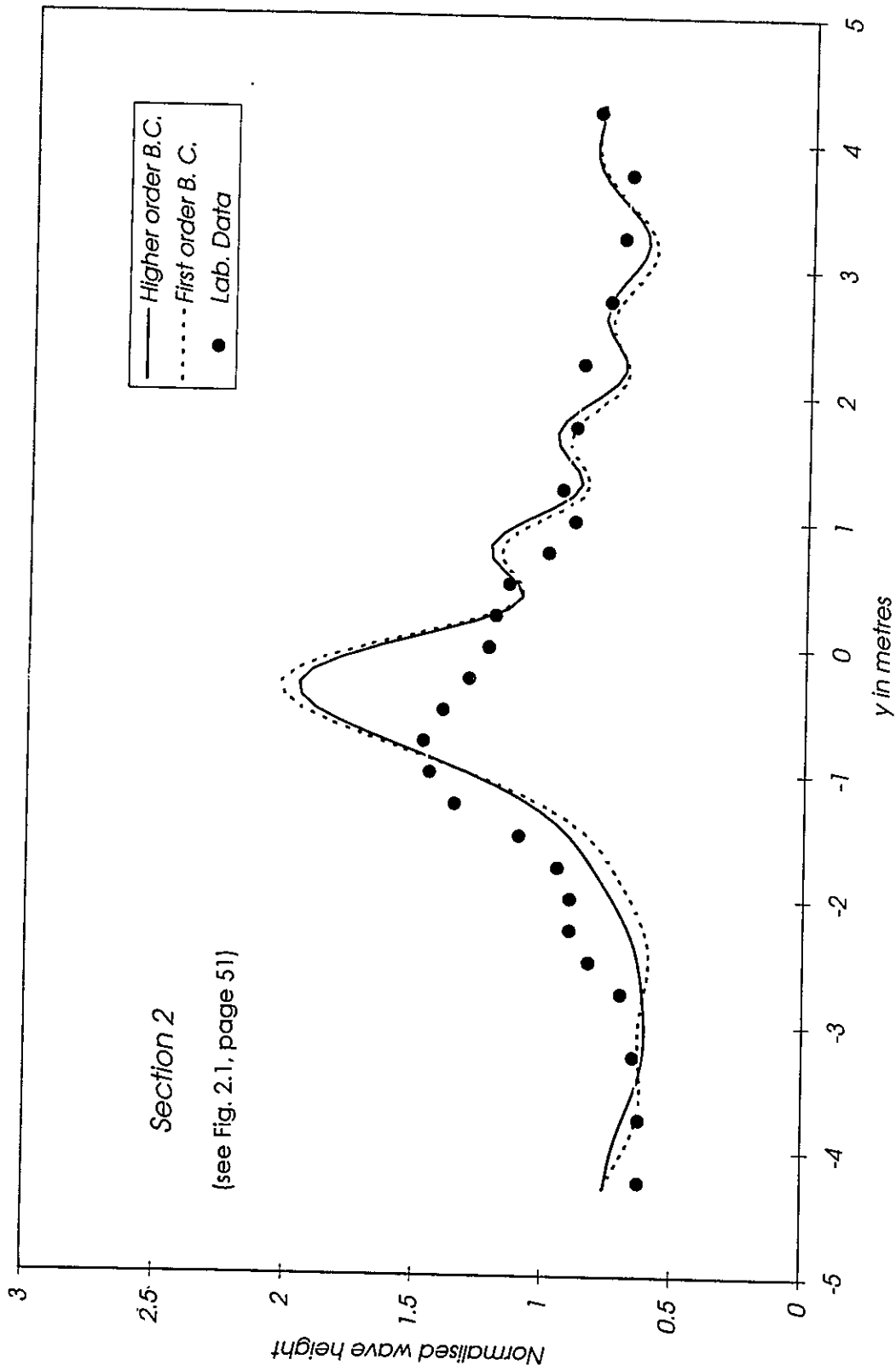
Fig. 3.17.2 - Comparison between experimental data of Berkhoff et al (1982) and results from the elliptic model with higher order boundary conditions. Section 2.
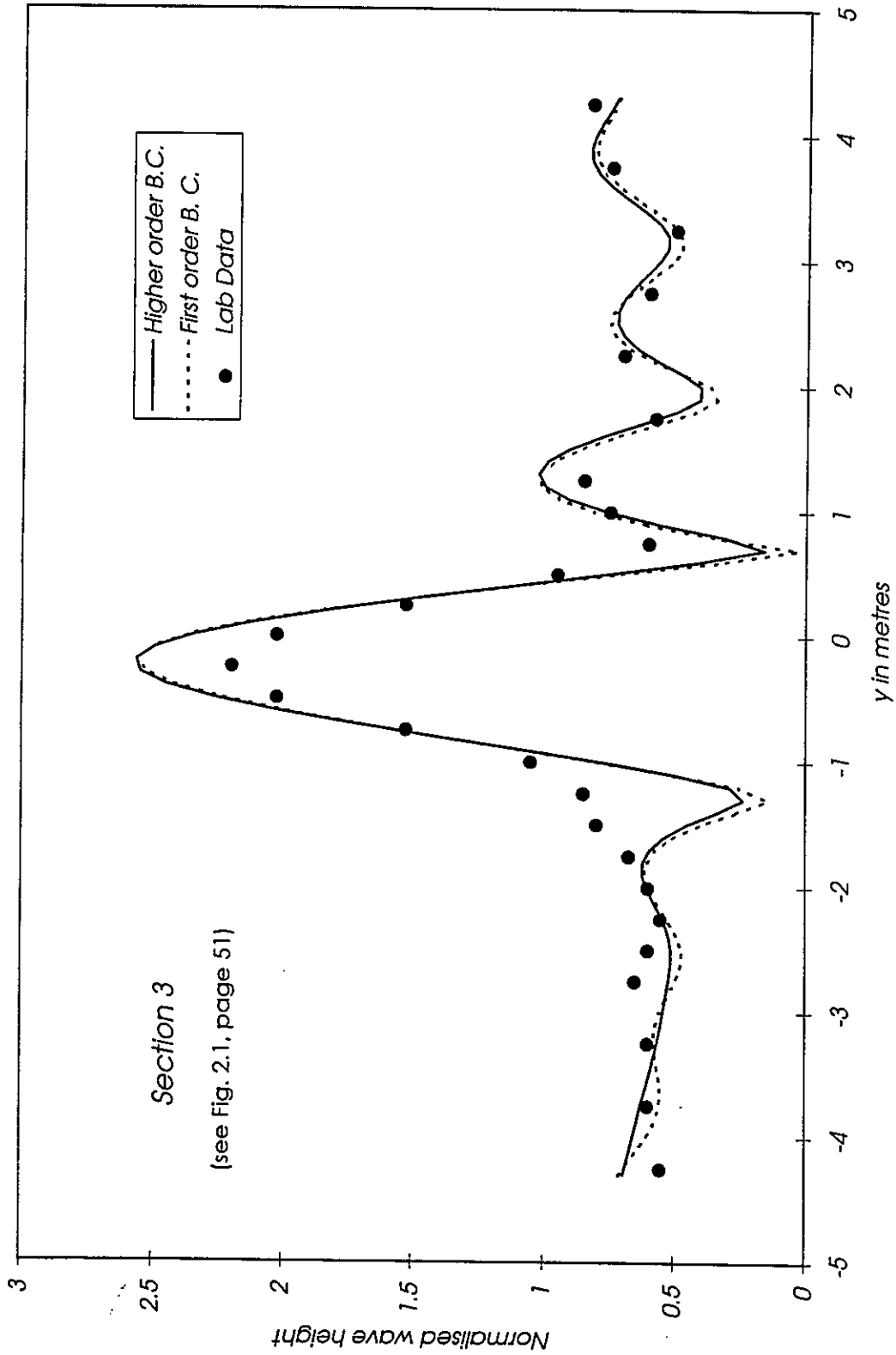
Fig. 3.17.3 - Comparison between experimental data of Berkhoff et al (1982) and results from the elliptic model with higher order boundary conditions. Section 3.
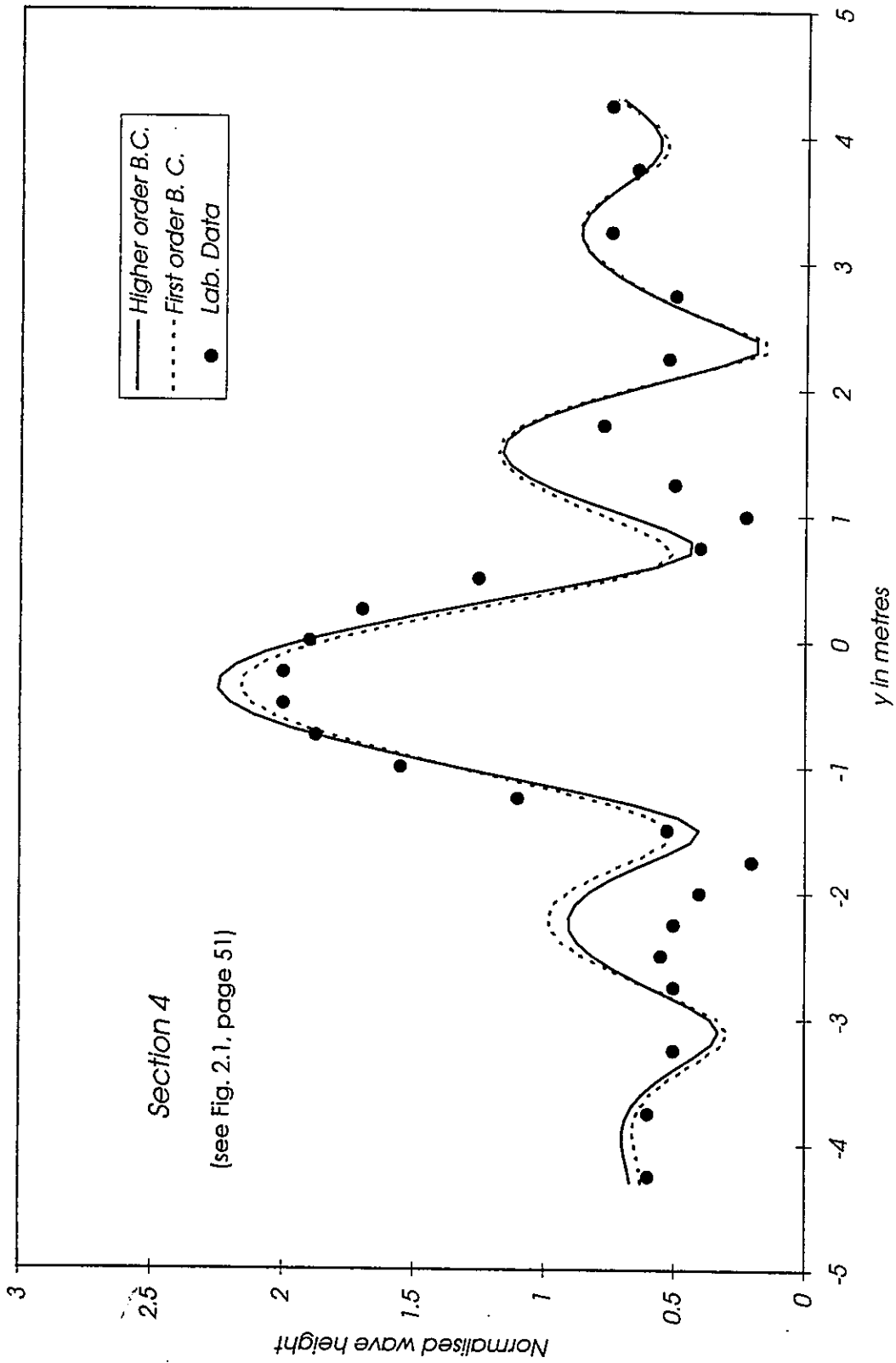
Fig. 3.17.4 - Comparison between experimental data of Berkhoff et al (1982) and results from the elliptic model with higher order boundary conditions. Section 4.
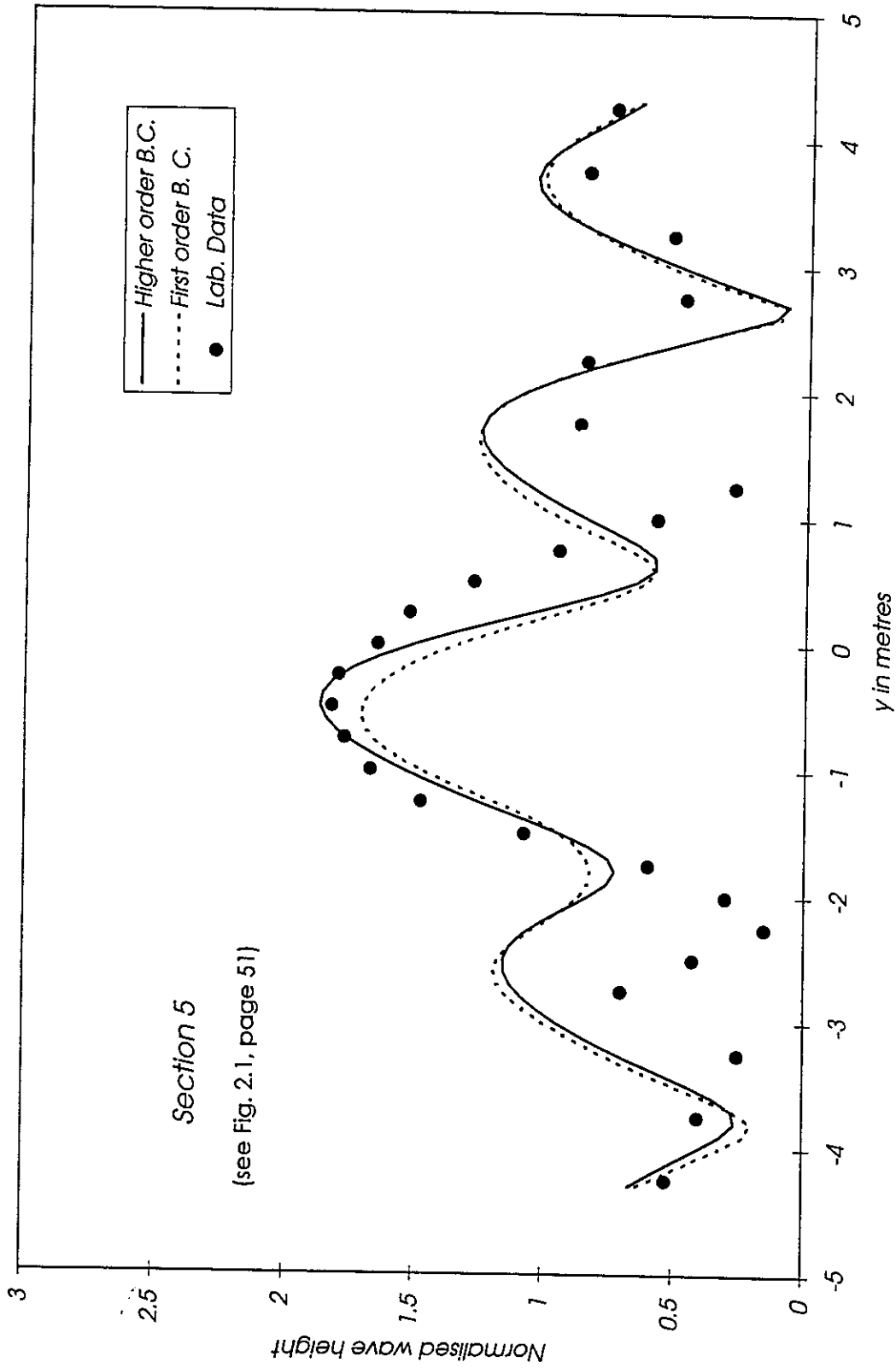
Fig. 3.17.5 - Comparison between experimental data of Berkhoff et al (1982) and results from the elliptic model with higher order boundary conditions. Section 5.
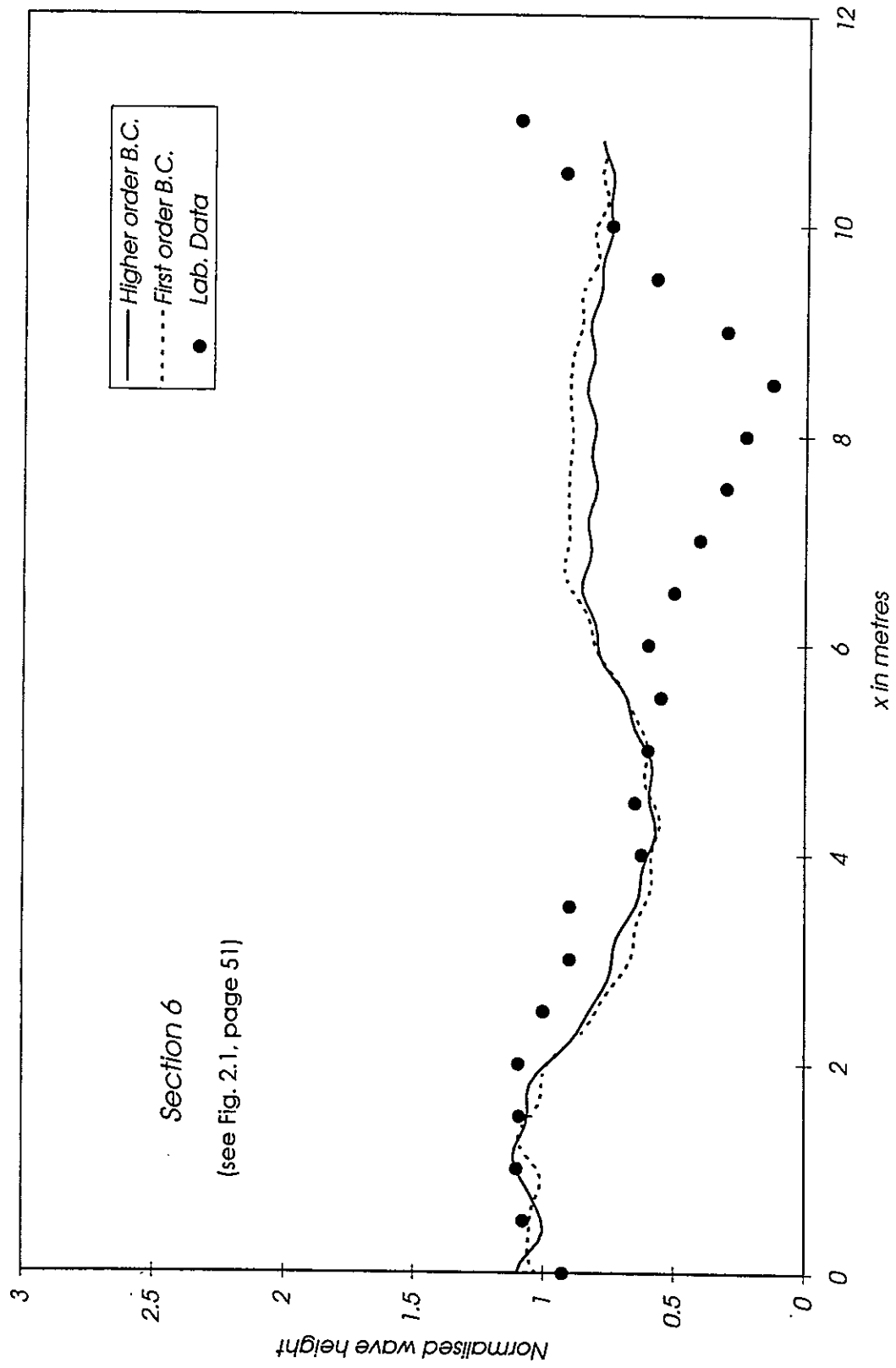
Fig. 3.17.6 - Comparison between experimental data of Berkhoff et al (1982) and results from the elliptic model with higher order boundary conditions. Section 6.
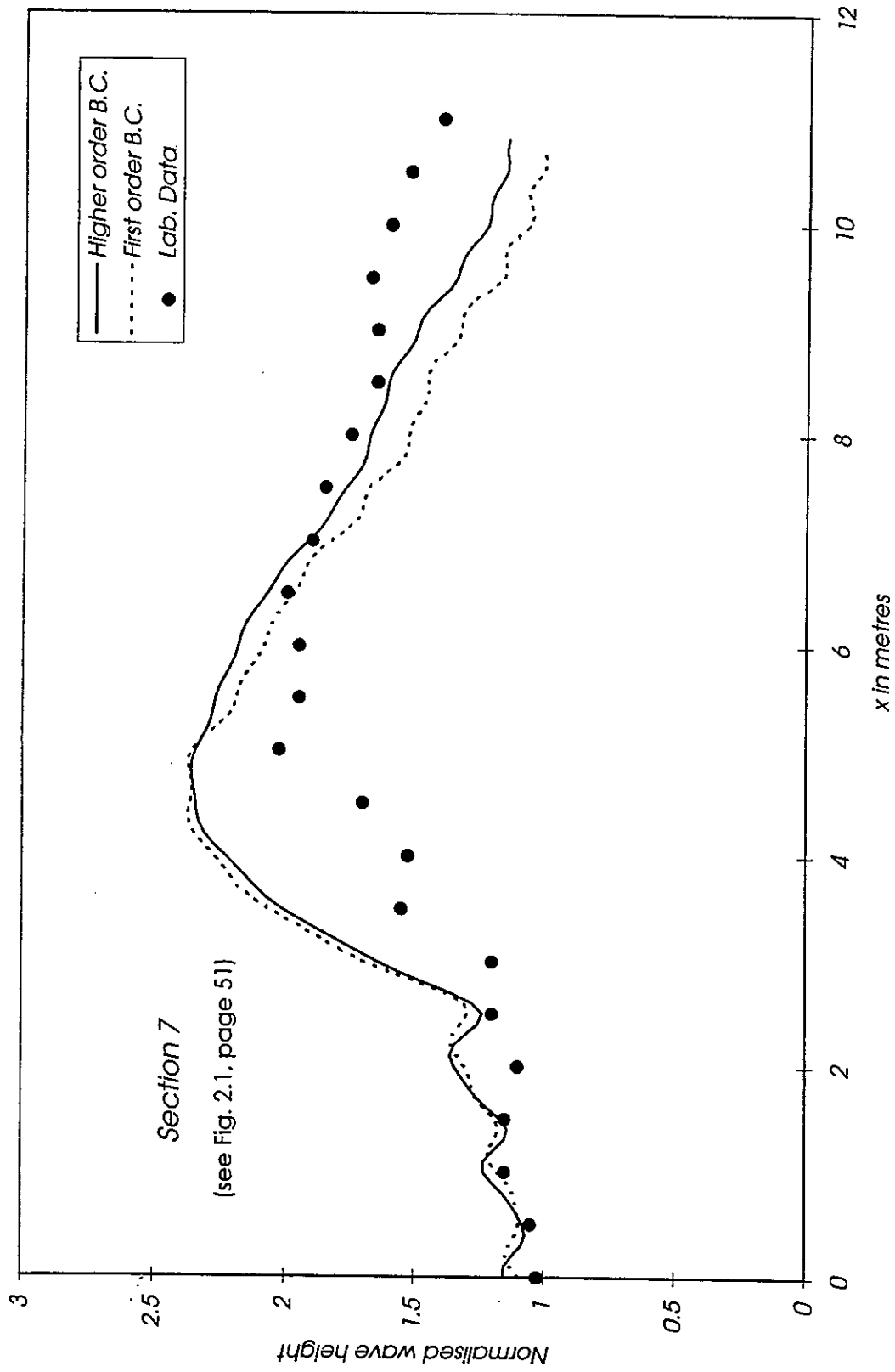
Fig. 3.17.7 – Comparison between experimental data of Berkhoff et al (1982) and results from the elliptic model with higher order boundary conditions. Section 7.
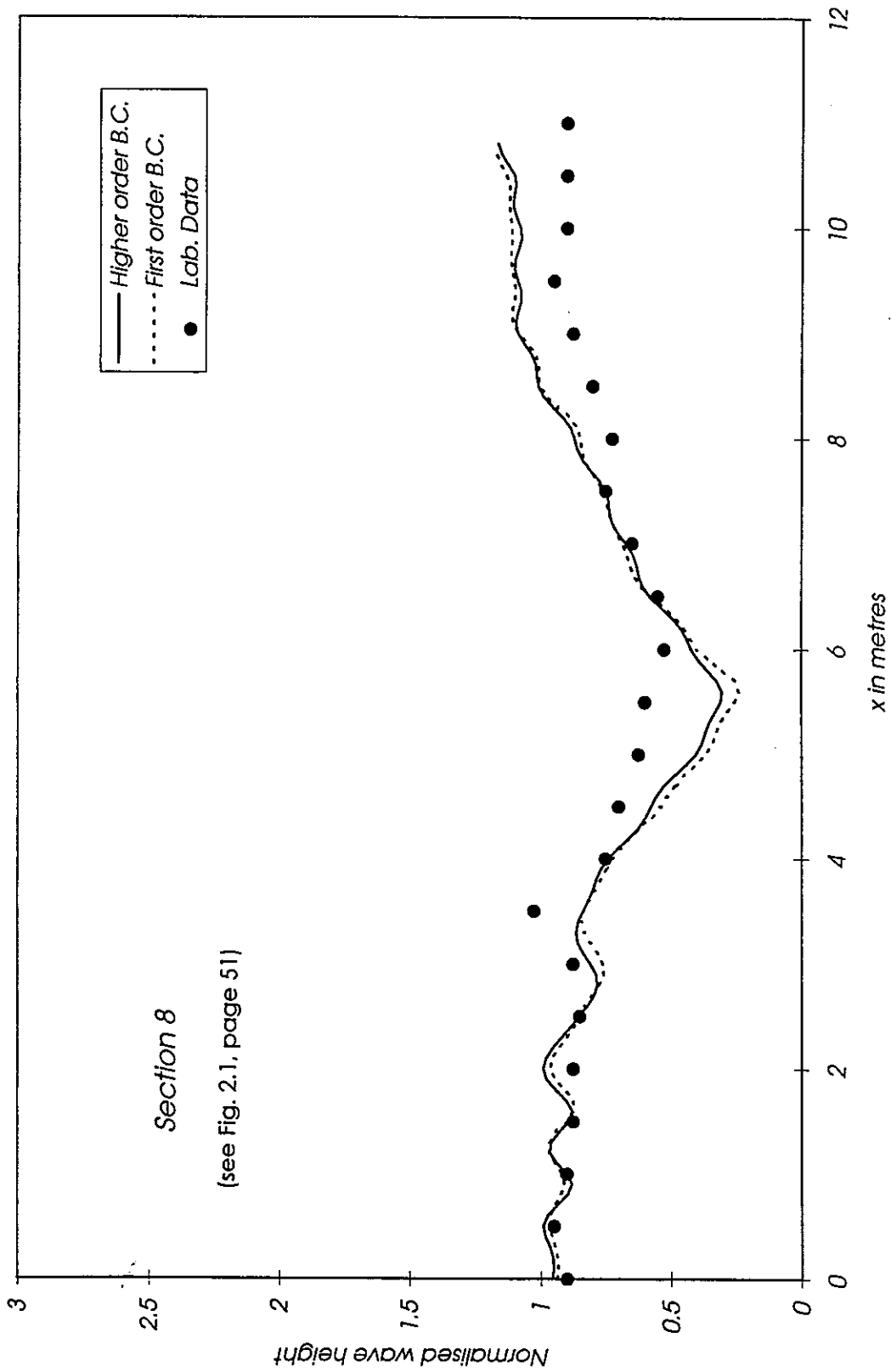
Fig. 3.17.8 - Comparison between experimental data of Berkhoff et al (1982) and results from the elliptic model with higher order boundary conditions. Section 8.

> ## Chapter 4
>
> # The Mild-Slope Equation Solved by a Multigrid Technique

4.1 - Introduction

The objective in this chapter is to develop an alternative numerical model that can overcome the difficulties of the model proposed by Li and Anastasiou (1992) for solving the non-linear form of the mild-slope equation by a multigrid technique. The difficulties of the previous model was in regard to the application of a relaxation method at each grid level. The iterative method proposed was the Gauss Seidel method which is not strictly applicable as the governing equation does not produce a diagonally dominant matrix. An appropriate iterative method is here proposed and its suitability for the solution of the mild-slope equation by a multigrid technique will be investigated. Such a formulation might incur a smaller computational cost than the model developed in chapter 2 and, therefore, might be a more efficient alternative for treating monochromatic wave propagation. It follows that its extension to a numerical model for irregular wave propagation might be more appropriate.

The chapter is organised as follows:

• Section 4.2 deals with a description of the non-linear form of the mild-slope equation which is the governing equation of the numerical model proposed in the present chapter.

• In section 4.3 a model based on the multigrid technique is proposed. A subsection presents and discusses the theoretical concepts of this numerical

technique and another subsection describes its implementation for the formulation described in section 4.2.

- Numerical tests performed to verify the model are described in section 4.4, and based on their results, a discussion of the applicability of the model is finally presented.

- A summary of the key points closes this chapter in section 4.5.

4.2 - The non-linear mild-slope equation

A review of mathematical models for the solution of the mild - slope equation has already been done in chapter 2. A qualitative comparison between these models was also made by summarising not only the physical constraints or limitations but also the associated numerical and computational difficulties. Hence this chapter will deal straight away with the description of the formulation that will be the governing equation of the proposed model.

The reduced form of the mild-slope equation is

$$\nabla^2\phi + k_c^2\phi = 0 , \qquad (4.1)$$

similar in form to the Helmholtz equation, where

$$k_c^2 = k^2 - \frac{\nabla^2\left(CC_g\right)^{0.5}}{\left(CC_g\right)^{0.5}} \qquad (4.2)$$

and k is the local wave number governed by the dispersion relation

$$\omega^2 = gk \tanh(kh) . \qquad (4.3)$$

Equation (4.1) can be transformed by introducing a logarithmic function Ψ, that varies slower than the velocity potential function and relates with this last one as follows:

$$\phi = e^{\Psi} . \qquad (4.4)$$

Thus, setting

$$\phi = Ae^{is} \qquad (4.5)$$

yields

$$\Psi = \ln(A) + is \qquad (4.6)$$

where A is the wave amplitude and s is the phase function, s = k.x.

Consequently taking into account the identity:

$$\frac{1}{\phi}\nabla^2\phi = \nabla^2(\ln\phi) + (\nabla\ln\phi)^2, \qquad (4.7)$$

equation (4.1) can be written as:

$$\nabla^2\Psi + \nabla\Psi.\nabla\Psi + k_c^2 = 0 \qquad (4.8)$$

As Radder (1979) and Li and Anastasiou (1992) claimed, the advantage of using a model based on equation (4.8) is that due to the fact that Ψ varies slower than ϕ, reasonably good results can be obtained with only two to three grid nodes per wave length. This fact is a remarkable advantage in terms of computational economy. However it should be borne in mind that for a rapidly varying bathymetry or areas were reflections occur, a larger number of grid points per wave length needs to be used.

4.3 - A multigrid model for the mild-slope equation

4.3.1 - The multigrid technique

The multigrid technique, became a popular numerical tool in the last two decades, used to solve efficiently not only boundary value problems as also initial value problems. It is a Multi - Level Adaptive Technique as some authors call it. Basically, the multigrid technique is based on the idea of solving a discrete system of equations by working on a sequence of grids, or levels, of increasing spacing and taking advantage from interactions between the approximated solutions obtained at each level. The discrete system of equations is derived from a continuous problem by a technique like finite elements or finite differences and the interactions between the hierarchy of grids is usually done by transferring the residual from one grid to the other.

It was applied to initial value problems by authors like Jameson (1983,1986) to solve the Euler equations and on boundary value problems by authors like Brandt (1977)

to predict the approximate solution of the so called Singular Perturbation Difference Equations which have the form

$$e\nabla^2 U + aU_x + bU_y = F,$$ (4.9)

where U, U_x, U_y are the unknown and its derivatives in the x and y directions, respectively, and e, a, b and F are known coefficients that can be real or complex. Using Brandt's (1977) nomenclature the technique can be described as follows: Having a set of uniform square grids

$$G^0, G^1, ..., G^M,$$ (4.10)

all approximating the same domain Ω with corresponding grid sizes

$$h_0 > h_1 > ... > h_M$$ (4.11)

that have the grid size ratio

$$h_{k+1} : h_k = 1 : 2,$$ (4.12)

the differential problem of the form

$$LU(x) = F(x) \quad \text{in } \Omega, \qquad \Lambda U(x) = P(x) \quad \text{on the boundary } \partial\Omega$$ (4.13)

can be approximated by a finite differences discretisation on each grid G^k as

$$L^k U^k(x) = F^k(x) \quad \text{for } x \in G^k, \qquad \Lambda^k U^k(x) = P^k(x) \quad \text{for } x \in \partial G^k.$$ (4.14)

The solution for the discrete problem in the coarser grid G^0, approximates the solution for the discrete problem in the finest grid G^M, which is the grid we are interested to solve the problem in.

For an approximate solution u^k at a grid level G^k the discrete problem stands

$$L^k u^k = F^k - f^k, \qquad \Lambda^k u^k = P^k - p^k$$ (4.15)

where f^k and p^k represent the residual functions. Assuming L and Λ linear and the exact solution

$$U^k = u^k + V^k,$$ (4.16)

then the correction V^k satisfies the residual equations

$$L^k V^k = f^k \qquad \Lambda^k V^k = p^k.$$ (4.17)

Finally the residuals f^k and p^k can be transferred from one grid level to another by a transfer operator I^k_{k+1} or I^{k-1}_k as follows

$$f^k = I^k_{k+1}\left(f^{k-1} - L^{k+1}V^{k-1}\right), \qquad p^k = I^k_{k-1}\left(p^{k-1} - \Lambda^{k-1}V^{k-1}\right)$$ (4.18)

or

$$f^{k+1} = I^{k-1}_k\left(f^k - L^k V^k\right), \qquad p^{k-1} = I^{k-1}_k\left(p^k - \Lambda^k V^k\right).$$ (4.19)

The advantages of the multigrid method are related to the two main steps of the overall process:

The first step involves the descent process, meaning moving from the finest grid to coarser grids. The system is relaxed on the finest grid and then the residual is transferred to the next coarser grid using a restriction operator (like injection or full weighting). This process is repeated until the coarsest grid is reached. The advantage of this procedure is that the convergence process is accelerated.

The standard iterative methods used to relax the system of equations possess the smoothing property (property of eliminating the oscillatory modes or high frequency modes) but leave the low frequency components of the error relatively unchanged. In other words, the standard iterations converge very quickly as long as the error has high frequency components but the low frequency components are much slower to eliminate. When passing from a fine grid to a coarser grid a mode becomes more oscillatory, meaning that smooth modes on a fine grid look less smooth on a coarser grid. So, passing the error after eliminating the oscillatory components to the next coarser grid means the error is being eliminated by a much quicker process than using only one single grid.

The second step involves the ascent process, meaning moving from the coarsest grid to the finer grids. In relation to a more robust iterative method what was just said for the descent process is not so important because the method can be also effective in eliminating the smooth or low frequency components of the error. Thus, solving the system on the coarser grid (that involves a considerably reduced number of grid nodes than the finest grid), then transferring the residual by a transfer operator (like nested iteration) to the next finer grid and relaxing again a few times to obtain a more accurate solution can also accelerate the convergence process.

4.3.2 - The multigrid technique applied to the mild-slope equation

Li and Anastasiou (1992) developed a numerical model where the multigrid technique was applied to solve equation (4.8) that was discretised by a finite differences technique. In the model the Gauss elimination direct method was used for the coarsest grid if necessary, while on the other grid levels the iterative Gauss

Seidel method was applied. The success of the above model is due to two aspects. Firstly there are no constraints or physical limitations in the formulation, like the ones usually associated with the more economic models like the parabolic model (Radder, 1979). Secondly only a small number of grid nodes per wave length are required (2 or 3), in order to obtain reasonably accurate results. Li and Anastasiou (1992) claimed significant computational speed advantages of this model when compared with the elliptic and hyperbolic models described in section 2.2.1 of chapter 2, which required at least a minimum of eight nodes per wave length. Their model was verified for Berkhoff's shoal and the results obtained showed good agreement with measured results. The shortcoming of this model include the fact that the governing equation does not produce a positive definite square matrix for practical cases. Consequently, the iterative Gauss Seidel method cannot converge. To overcome this difficulty Li and Anastasiou (1992) suggested solving the problem directly at the coarsest grid level using the Gauss elimination, as said before. However, if a suitable iterative method is implemented instead of the Gauss Seidel method then the resulting numerical model would take full advantage of the multigrid technique, and thus would be more efficient. Such a method is proposed here.

Equation (4.8) is the governing equation and can be approximated using the finite differences technique as follows (Li and Anastasiou, 1992)

$$-4V_{i,j}^n + V_{i-1,j}^n + V_{i-1,j}^n + V_{i,j-1}^n + V_{i,j-1}^n + a.V_x^n + b.V_y^n = f_k \tag{4.20}$$

where

$$a = h_k^2 \left(\Psi_{i-1,j}^{n-1} - \Psi_{i-1,j}^{n-1}\right)\!\big/\!\left(2h_m\right)$$
$$b = h_k^2 \left(\Psi_{i,j-1}^{n-1} - \Psi_{i,j-1}^{n-1}\right)\!\big/\!\left(2h_m\right) \tag{4.21}$$

i and j are the indices of the grid nodes in the x (direction normal to the shore)and y (longshore direction) co-ordinates respectively. k is the current grid level with a grid cell spacing h_k. m is the finest grid level with a grid cell spacing h_m. and V_x^n and V_y^n are the partial derivatives of the residual V^n with respect to x and y. As the index n represents the iteration cycle, the quantities a and b are known from the previous iteration cycle therefore remove the non-linear character of the problem transforming the governing equation into a linear system of equations. To improve

the stability of the iterative scheme Li and Anastasiou (1992) suggest the use of an upwind scheme for V_x^n and V_y^n.

Regarding the boundary conditions the problem was formulated as follows:

- Offshore / driving boundary

  The incident wave field is assumed known and therefore $\Psi = \ln(A) + is$, where A is the wave amplitude and s is the phase function.

- Shore / downstream boundary

  First order radiation boundary condition

  $$\frac{\partial \Psi}{\partial x} = ik \cos\alpha,$$ (4.22)

  where the wave angle α at an arbitrary point on the boundary is obtained from the deep water angle α_0 by Snell's law

  $$\frac{\sin\alpha}{L} = \frac{\sin\alpha_0}{L_0},$$ (4.23)

  L is the wave length and the subscript 0 denotes deep water conditions.

- Lateral / downstream boundaries

  First order radiation boundary conditions

  $$\frac{\partial \Psi}{\partial y} = ik \cos\alpha.$$ (4.24)

  Similar to the shore boundary, but now the direction of the boundary is x therefore, α is now the angle between the incident wave and the direction normal to the boundary, y.

4.4 - Numerical tests

Once again Berkhoff's shoal from Berkhoff et al (1982) was chosen to be the case to validate the multigrid model here developed to solve the mild-slope equation. The bathymetry and incident wave conditions are described in section 2.4.1 of chapter 2 and therefore will be omitted.

Four different numerical schemes, each with a different number of grid levels were applied. The number of grid levels tested was 3, 4, 5 and 6, and for all of them the finest grid allows about 5 nodes per wave length. The numerical domains considered have an area of 22.0*22.0 m² for a grid spacing where $\Delta x = \Delta y$. The finest grid has a total of 65*65 grid nodes. According to the explanation given in section 4.3.1, the next coarser grids have a total of 33*33, 17*17, 9*9, 5*5 and finally 3*3 grid nodes.

The objective of this numerical experiment is to investigate how the number of grid levels influences the accuracy and efficiency of the model. The two iterative methods described in chapter 2, the Bi-CGSTAB and the GMRES methods, were implemented to relax the system at each grid level. Both were used to solve iteratively the linear system of equations generated by equation (4.20) together with the boundary conditions described in section 4.3.2. The Bi-CGSTAB did not show convergence for the above formulation and the GMRES showed a non-monotonic convergence after reaching a certain residual. The computed results are presented in terms of normalised wave height in Figs. 4.1.1 to 4.1.8, for the eight sections behind the shoal as defined in chapter 2, and they were obtained with the model where the GMRES method was implemented, for a residual of order 10⁻³. It was observed that the computational cost in terms of total number of global iterations and also relaxations on each grid level decreases as the number of grid levels increase. For 3 grid levels the computational cost was about twice as much as for 6 grid levels, which proves the efficiency of the multigrid technique when applied to this particular formulation. Interactions between approximated solutions obtained at each grid level in a hierarchy of grids generate a faster process of convergence than the simple use of the most refined grid for relaxation of the linear system of equations.

The analysis of the computational results plotted for the 8 sections behind the shoal suggests that the numerical model here proposed based on the non - linear formulation of the mild - slope equation expressed by equation (4.8) can predict reasonably well wave transformation caused by a complex bathymetry. The model is sensitive to the focusing region that occurs behind the shoal due to refraction effects and to the consequent wave decay that occurs further away from the centre of the shoal due to the dominance of the diffraction process. The solutions for

the area at the left side of the focusing region show a good agreement with the laboratory data, and in fact, the results for this area are quite similar to the solutions obtained for the linear models proposed in chapter 2, as it can be confirmed by observing the results along section 6. However, the focusing region is slightly overpredicted in the region at the right side behind the shoal. This can be seen in sections 2, 3, 4, and 5, and confirmed along section 8. The reason for this is that although the numerical scheme is robust enough, it did not attain sufficiently accurate results, due to the fact that the convergence process was limited by a residual of the order of 10^{-3}, as mentioned before. Nevertheless, although the convergence process of the 4 models was stoped for the same value of the residual, much better solutions are obtained as the number of grid levels increases. The numerical model that makes use of a hierarchy of 6 grid levels is the one that gives the best approximate solutions. The computational results obtained show that an increase in the number of grid levels improves the accuracy of the solutions allowing a better agreement with the experimental data. Another observation mentioned before, is that an increase in the number of grid levels not only allows an improvement in the results but also decreases the total computational cost as it decreases the total number of global and grid level iterations.

An attempt to understand why the Bi-CGSTAB method cannot be applied and the GMRES method can only be applied under certain limitations was done. Several recent publications based on research done on the subject were studied aiming to take into account the most recent developments. A group of mathematicians (Barret et al, 1996) wrote about algorithms employed for solving iteratively a linear system: " ...Yet when the matrix is nonsymmetric or indefinite, or both, it is difficult to predict which method will perform best, indeed, converge at all. Attempts have been made to classify the matrix properties for which a particular method will yield a satisfactory solution, but "luck" still plays a large role. ...". This suggests that other methods like the Krylov Subspace Methods should be tried because the results obtained here are encouraging. Another alternative here suggested is to explore efficient solutions using sophisticated poly-iterative methods. Very recently good progress has been achieved in this area. A poly-iterative solver consists of applying different algorithms simultaneously to the system, in the hope that at least one will converge to the solution. Although this approach has merit in a sequential computing environment, it is even more valuable in a parallel computing

environment because by combining global communications the cost of several methods can be reduced to that of a single method. A successful numerical experiment was obtained by using three algorithms simultaneously.

4.5 - Closure

This chapter dealt with the numerical modelling of a non - linear transformed form of the mild - slope equation. This approximation was derived based on the idea of using a function which is less rapidly varying than the wave potential, therefore requiring a smaller minimum number of grid nodes per wave length to achieve the same accuracy. The non - linear equation was discretised using a finite difference technique to generate an approximate formulation which is linear and can be solved using an iterative method. In order to accelerate the convergence process of the iterative method a multigrid technique was implemented. Numerical experimentations to validate the model showed that the model is robust in predicting regular wave transformation in the nearshore region and that an increase of the number of grid levels used within the model accelerates the process of convergence, proving therefore the efficiency of the multigrid technique when applied to this particular non - linear formulation of the mild -slope equation. An increase of the number of grid levels not only accelerated the convergence process but also improved the accuracy of the results. The reason why the present model will not be extended into a numerical model for irregular wave propagation assuming a linear superposition of independent spectral components is because, despite being faster than the model developed in chapter 2, it does not generate as accurate a solution. Accuracy plays a crucial role in a numerical model for irregular wave propagation which is based on a component approach because errors arising from each component accumulate, smearing the final result.
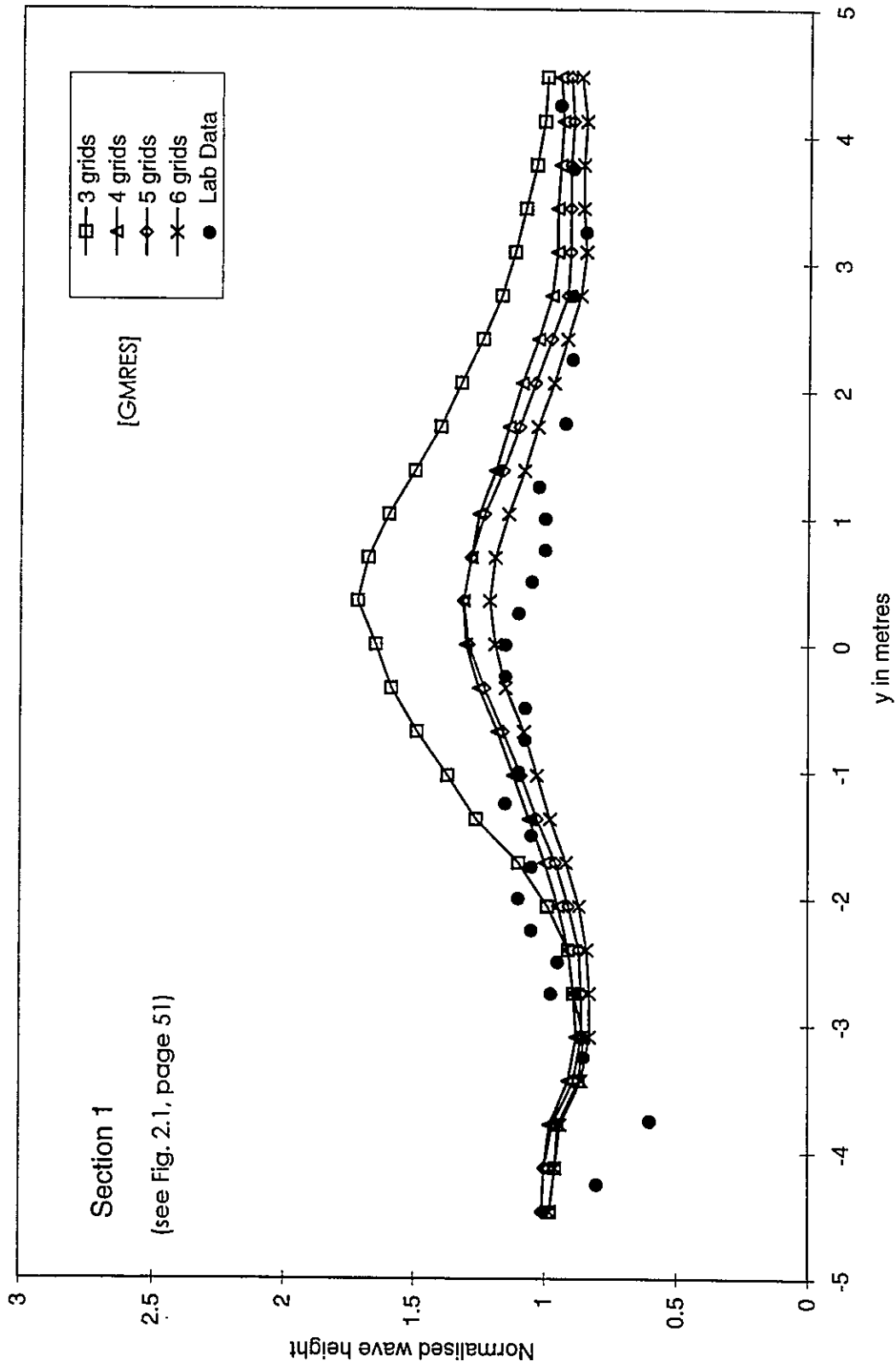
Fig. 4.1.1 - Comparison between experimental data of Berkhoff et al (1982) and results obtained from the 4 numerical models based on a multigrid technique. Section 1.
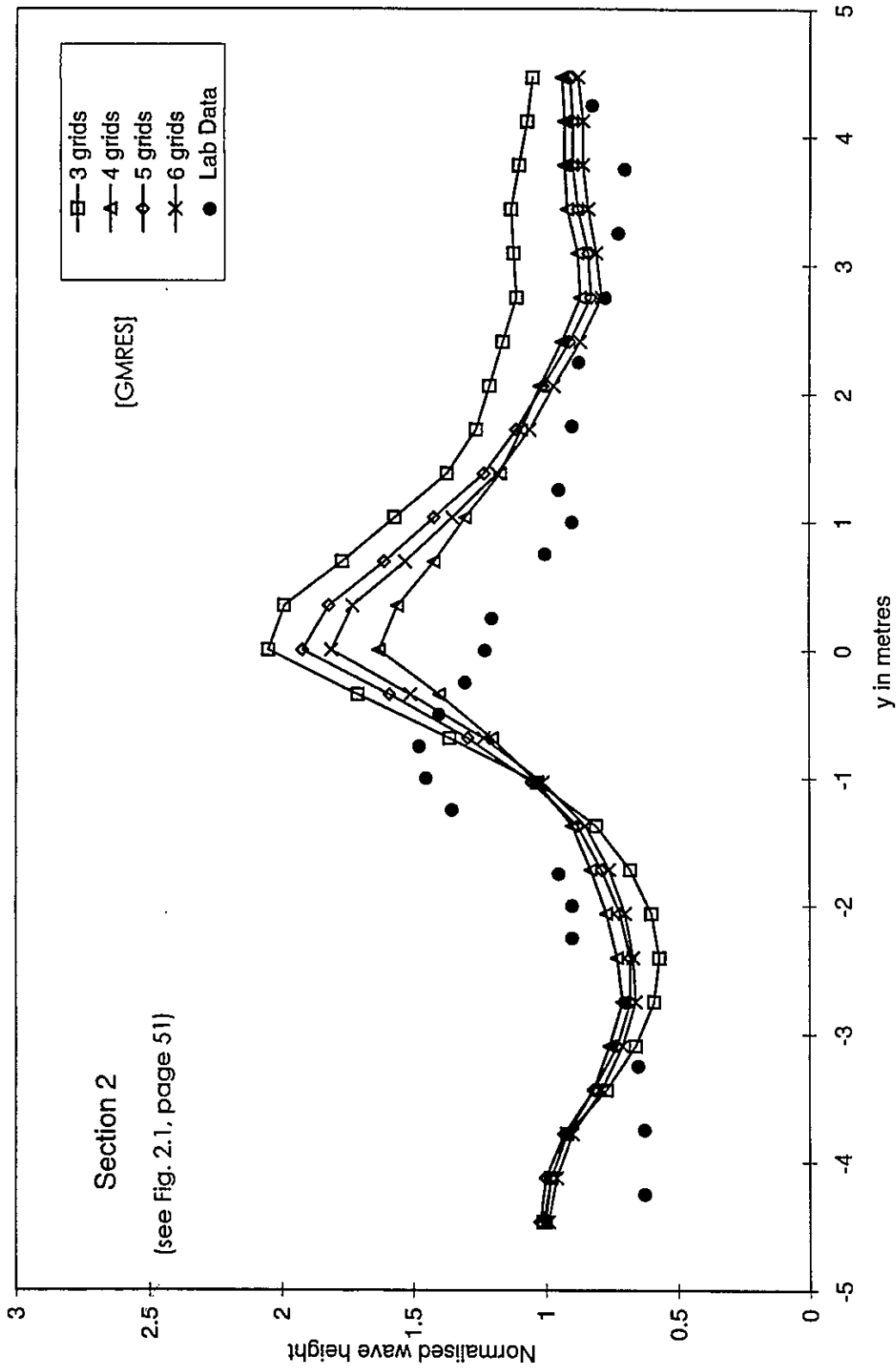
Fig. 4.1.2 - Comparison between experimental data of Berkhoff et al (1982) and results obtained from the 4 numerical models based on a multigrid technique. Section 2.
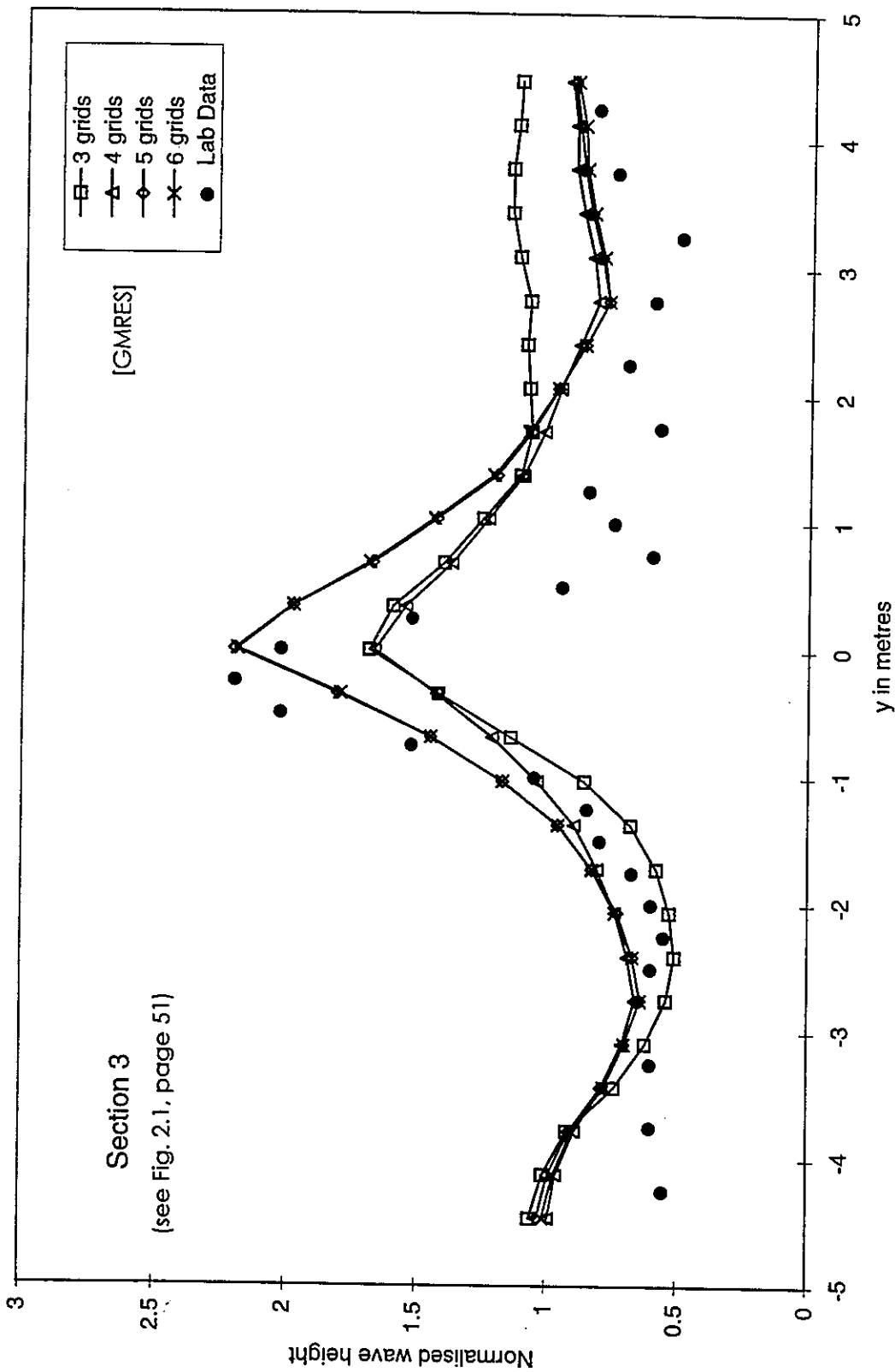
Fig. 4.1.3 - Comparison between experimental data of Berkhoff et al (1982) and results obtained from the 4 numerical models based on a multigrid technique. Section 3.
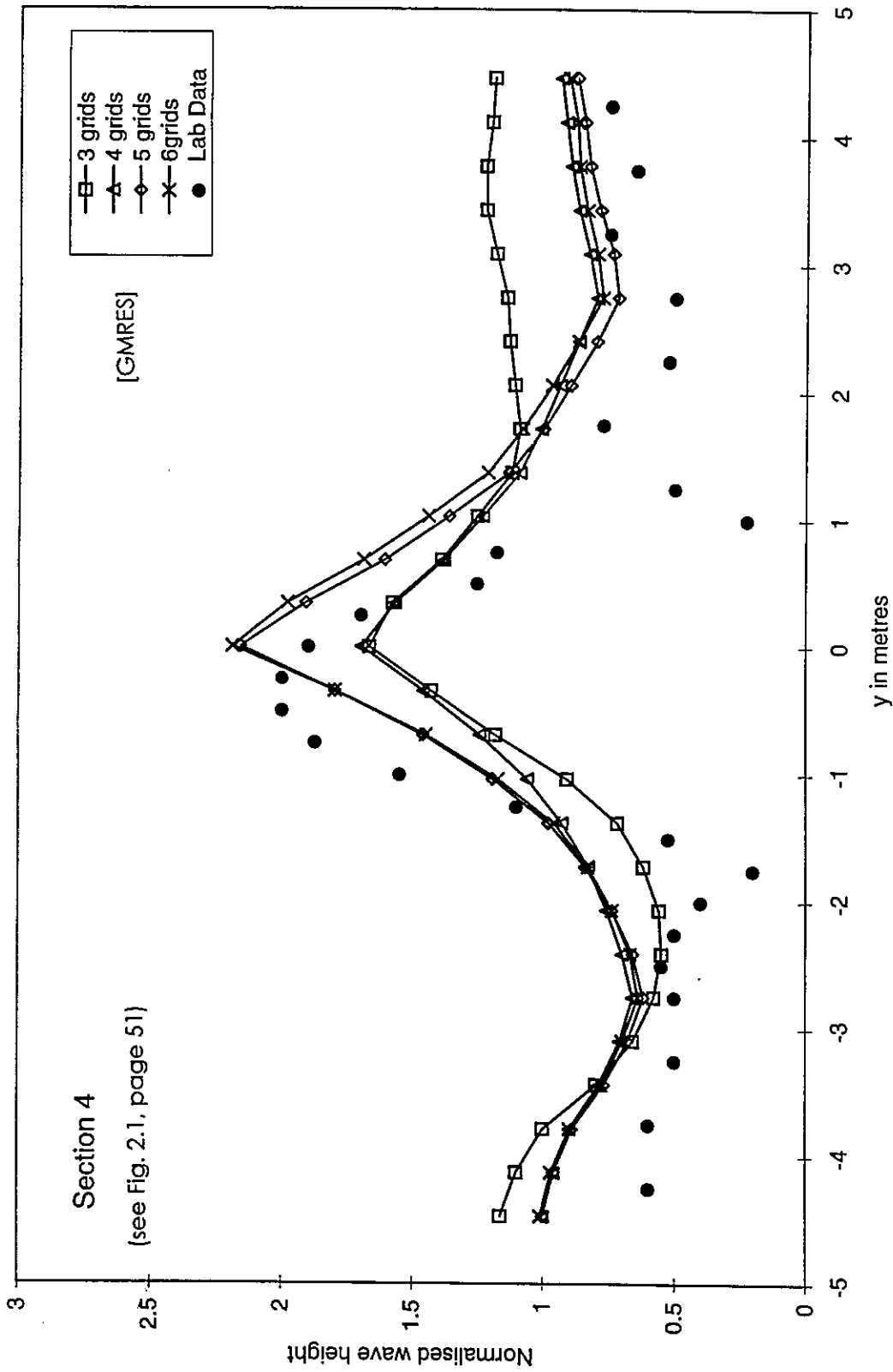
Fig. 4.1.4 - Comparison between experimental data of Berkhoff et al (1982) and results obtained from the 4 numerical models based on a multigrid technique. Section 4.
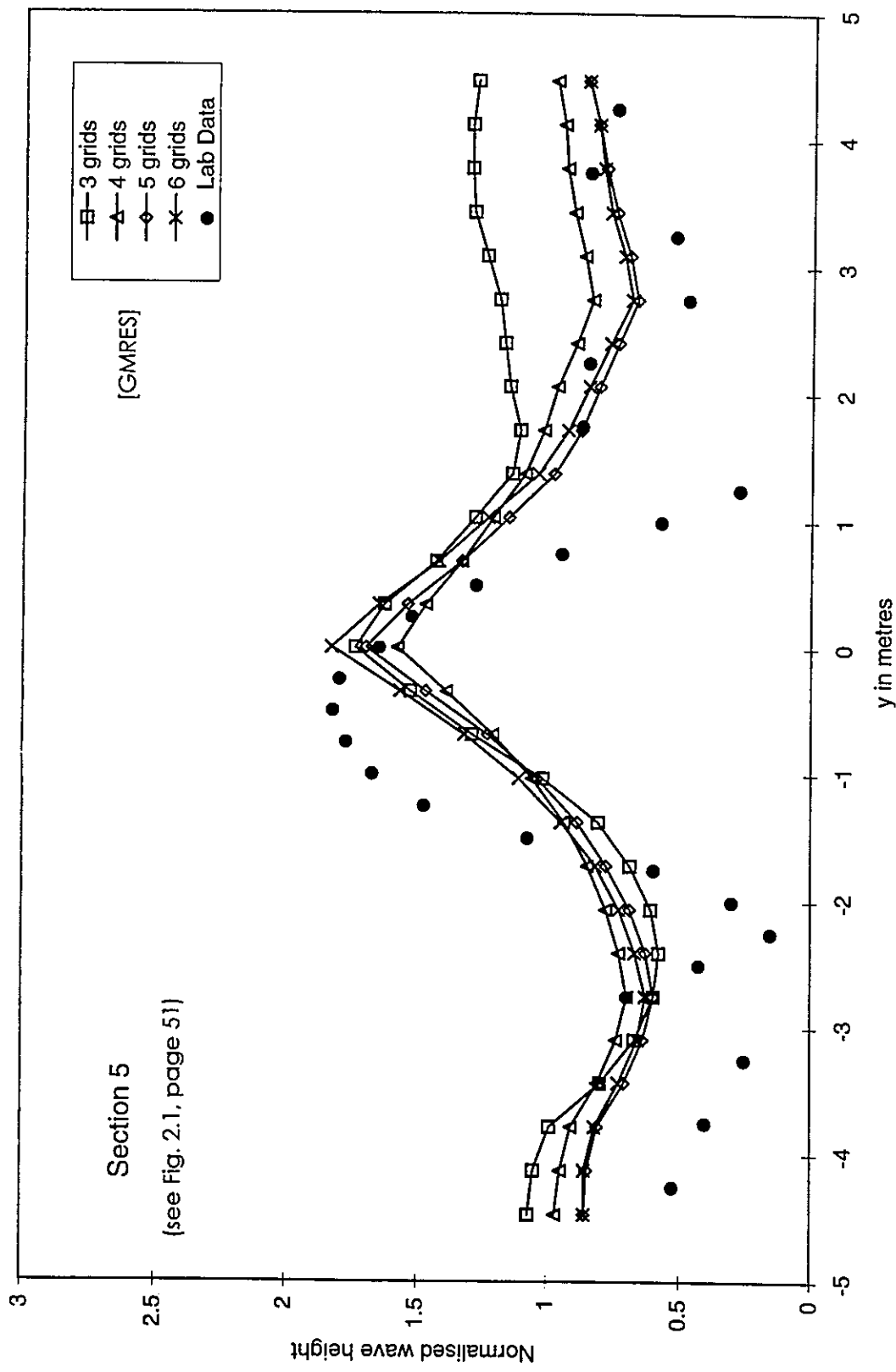
Fig. 4.1.5 - Comparison between experimental data of Berkhoff et al (1982) and results obtained from the 4 numerical models based on a multigrid technique. Section 5.
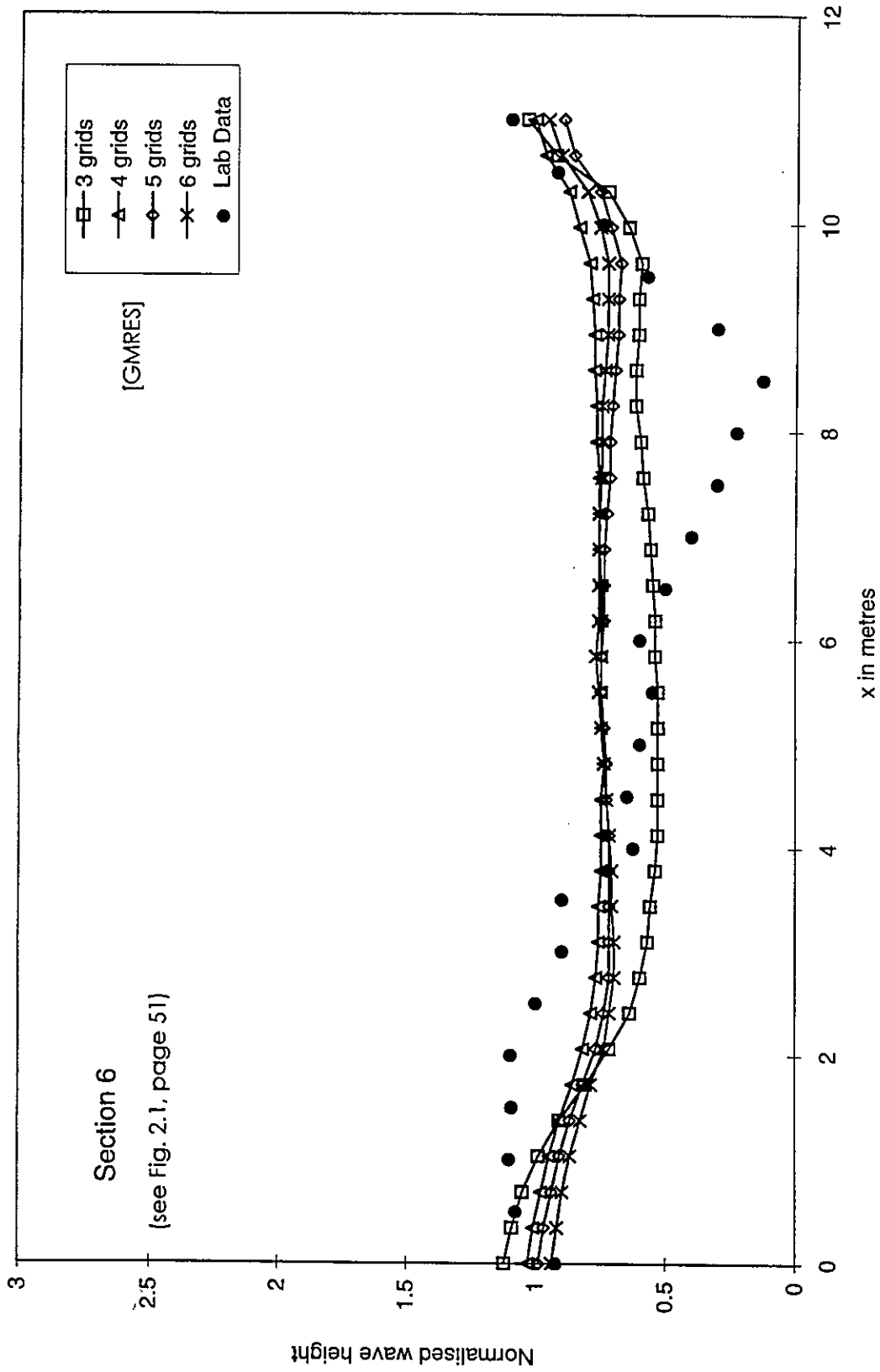
Fig. 4.1.6 - Comparison between experimental data of Berkhoff et al (1982) and results obtained from the 4 numerical models based on a multigrid technique. Section 6.
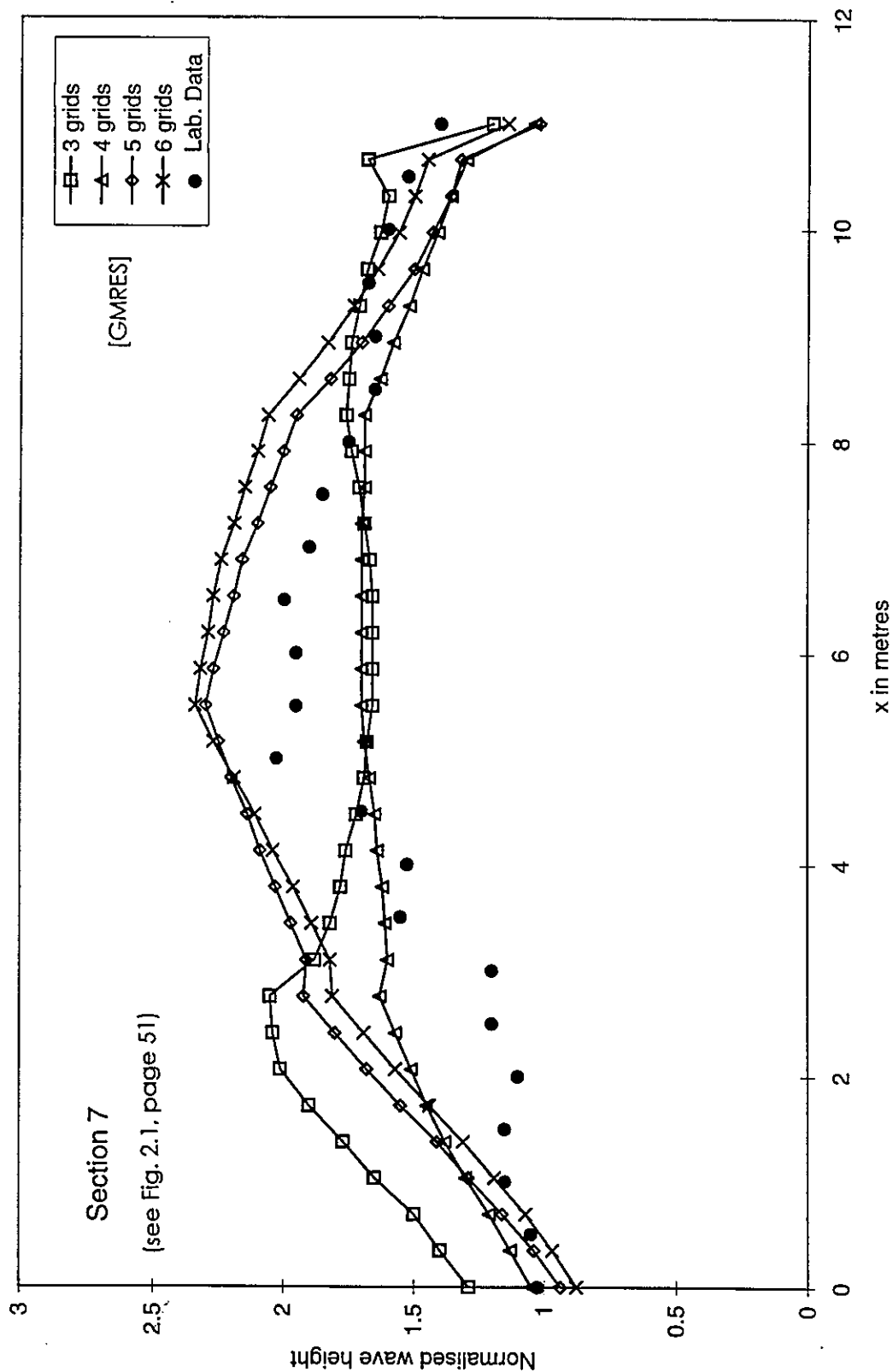
Fig. 4.1.7 - Comparison between experimental data of Berkhoff et al (1982) and results obtained from the 4 numerical models based on a multigrid technique. Section 7.
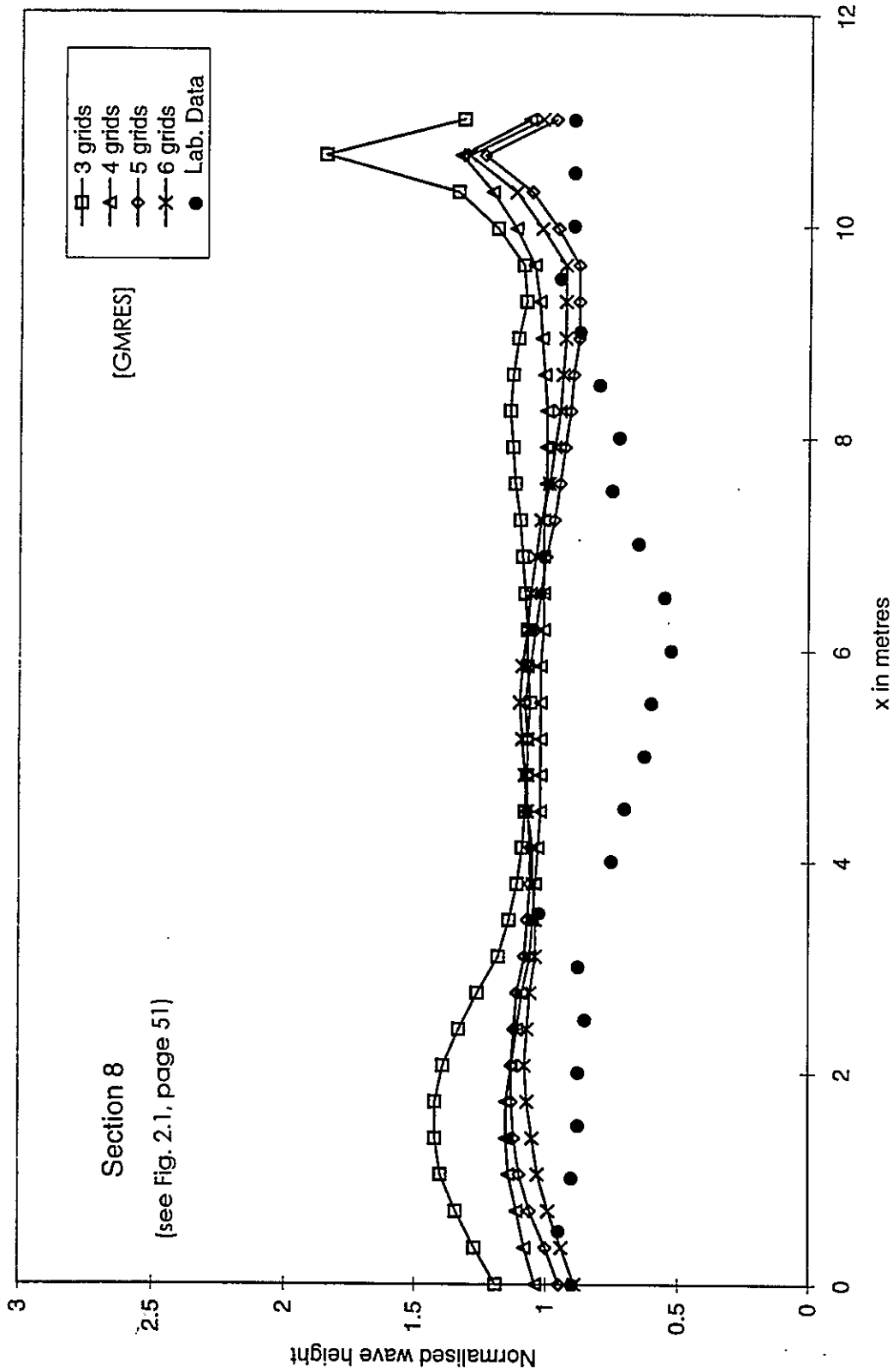
Fig. 4.1.8 - Comparison between experimental data of Berkhoff et al (1982) and results obtained from the 4 numerical models based on a multigrid technique. Section 8.

Chapter 5

Modelling of Irregular Waves

5.1 - Introduction

The objective of this chapter is to create a numerical model for irregular wave propagation. The model is based on the numerical model developed in chapter 2 for monochromatic waves and it can simulate irregular wave transformation due to the processes of refraction, diffraction and reflection.

The chapter is organised as follows:

- The following section introduces the subject of modelling irregular waves in the nearshore region and the associated theoretical concepts.
- In section 5.3 a discussion based on a literature survey of the existing numerical models for irregular wave generation and propagation is presented.
- Section 5.4 proposes a numerical model for irregular wave propagation. The methodology used for the discretisation of the directional spectra and the generation of irregular components is explained together with the mathematical treatment given to the wave components.
- Section 5.5 describes the tests performed to validate the model developed in the previous section and presents the results obtained. The model is validated by comparing computational results with data obtained from a laboratory experiment. Finally a discussion of the model performance is also done in this section.
- Section 5.6 presents a critical summary of the work developed in this chapter. It also establishes a link with the work presented in the next chapter with a view to improving the present numerical model for irregular wave propagation.

5.2 - Theoretical concepts

Physical oceanographers were the first who used the concept of random waves. Only later did engineers become aware of the importance of wave irregularity and its relevance in engineering applications. Gradually in the late 80's nearshore random wave models started to appear and laboratory experiments with irregular waves were conducted by several workers in the field of coastal engineering.

The first attempt to treat sea waves as a random process when considering the mathematical modelling of wave propagation was based on propagating a monochromatic wave of height equal to the significant wave height (one of the various statistical measures of sea waves, widely chosen to be a representative sea state) and period equal to a certain representative period that can be determined from gauge records by methods like the zero crossing method. Now it is known that this approach can give erroneous results when predicting wave climate in the nearshore region and, therefore, it is important to develop a numerical method for irregular wave propagation that allows a more realistic prediction.

Goda (1985) compared results obtained for monochromatic and irregular wave transformation over a spherical shoal and in the vicinity of a breakwater. The computation of random wave refraction has the effect of smoothing the spatial variation in wave height due to the presence of various directional and frequency components. Diffraction is badly treated when considering regular waves because wave height is underestimated in the sheltered area behind the breakwater resulting in bad design and eventually failure of the structure. Diffraction is particularly sensitive to the characteristics of wave spectra, especially to the directional spreading of wave energy. Although these results were obtained from a theoretical approach, meaning that there was no data to verify them, they generally agree with observations done later by other authors.

Vincent and Briggs (1989) have demonstrated by wave tank experiments that monochromatic models can significantly over predict the maximum amplification of irregular waves due to bathymetry variations. The differences between monochromatic and spectral models are most pronounced where bathymetric features lead to strong wave convergence. They concluded from the case of

irregular waves propagating over an elliptic shoal that monochromatic waves may overestimate the maximum amplification of irregular waves in convergence zones and underestimate wave heights in shadow zones by up to a factor of two, and that wave height patterns were sensitive to the incident wave height and frequency spectrum, but particularly to the breadth of the directional spreading function. These experiments motivated the development of mathematical models (that will be discussed in the next section) for irregular wave propagation because now there was available experimental data for comparison and validation.

The concept of the spectrum was discovered by Newton and extended to many physical problems, including the sea. It is a technique of decomposing a complex physical phenomenon into individual components. For the case of sea waves, it can be analysed by assuming that the sea state consists of an infinite number of wavelets with different frequencies and directions.

The theory of wave spectra is based on the assumption that the random sea is stationary, ergodic and Gaussian. Stationary, meaning that the joint probability function of the surface displacement is invariant to the addition of a constant time to all the times t_1, t_2, ..., t_n, that is the statistical properties of $\eta(x,t)$ are independent of the origin of time measurement. Ergodic, meaning that the time averaged statistics for the surface displacement at a certain spatial location is equal to those of the joint probability function of the surface displacement. Gaussian, meaning that the surface displacement follows a Gaussian distribution. One should bear in mind that this last assumption is not applicable for shallow waters but it is essential to decompose the random sea waves into an infinite number of components of linear and independent behaviour. The assumption of a Gaussian distribution is associated with symmetry about the still water level, which is realistic for small amplitude waves, especially in deep water. However, observations in the nearshore region show waves with high crests and shallow troughs and an additional asymmetry with respect to a vertical line passing trough the crest.

The three dimensional spectrum $S(k,\omega)$ is the Fourier transformation of the covariance of the auto-correlation function of the surface elevation $\eta(x,t)$ that describes the ocean surface. The auto-correlation function is a measure of the

connection between the two values $\eta(x,t)$ and $\eta(x+r,t+\tau)$ of the random variable η and is defined as

$$\chi(r,t) = \overline{\eta(x,t)\,\eta(x+r,t+\tau)}. \tag{5.1}$$

The three dimensional spectrum is

$$S(k,\omega) = (2\pi)^{-3} \iint \int_{-\alpha}^{\infty} \chi(r,\tau)\ \exp(-i\,(k\cdot r - \omega t))\ dr d\tau\, d\omega\,, \tag{5.2}$$

and if the wave field is homogeneous (homogeneous meaning that the joint probability function of the surface displacement is invariant to the addition of a constant horizontal vector to all the space points) the Fourier transformation of the covariance is the wave number spectrum, S(k), defined as

$$S(k) = (2\pi)^{-2} \int \int_{-\infty}^{\infty} \chi(r)\ \exp(-ik\cdot r)\ dr\ dk\,. \tag{5.3}$$

Nevertheless, one should bear in mind that the nearshore wave field is not always homogeneous and different components might not be uncorrelated. In fact, the propagation of irregular wave trains in shallow water is a non-linear process where substantial cross spectral energy transfer can take place over relatively short distances. This process involves the generation of bound sub - and super - harmonics and near - resonant triad interactions, defined as the energy exchange between three interacting wave modes. Battjes and Beji (1992) have done laboratory experiments to observe spectral evolution in the nearshore region but the interaction process is still not clearly understood.

The wave number spectrum,

$$S(k) = S_1(k,\alpha), \tag{5.4}$$

can be transformed into the directional frequency spectrum,

$$S_1(k,\alpha) = S_2(\omega,\alpha), \tag{5.5}$$

by using the dispersion relationship

$$\omega^2 = g k\ \tanh(kh)\,. \tag{5.6}$$

The directional frequency spectrum is a two dimensional spectrum and can be constructed according to the empirical relationship

$$S(\omega,\alpha) = S(\omega)\ G(\omega,\alpha) \tag{5.7}$$

where $S(\omega,\alpha)$ is the directional wave spectrum, $S(\omega)$ is the frequency spectrum and $G(\omega,\alpha)$ is a spreading function.

The directional wave spectrum represents the distribution of wave energy in the frequency domain, (ω) and direction, (α).

Several authors like Bretschneider (1968), Pierson and Moskowitz (1964), Hasselmann et al (1973), and others deduced water wave frequency spectra from observations. The spectral shape depends on factors like the geographical location, duration of wind action, fetch, and wind speed, existence of swell and stage of growth and decay of a storm. The water depth is another factor that can also determine the spectral shape because a range of physical effects are dependent on the water depth. In deep water (kd $\geq$ 1) the waves are mainly influenced by three physical processes: wave growth by wind, dissipation of energy by white-capping and non-linear quadruplet wave-wave interactions. In water of intermediate depth (kd $\cong$ 1) additional effects become important such as bottom friction, depth and current refraction, diffraction and reflection by obstacles. In shallow water (kd $\leq$ 1) also the effects of wave breaking, triad interactions and the effects of wave - current interaction become noticeable.

The main effect of bottom friction is that it reduces wave energy in the lower frequencies, thus decreasing the mean wave period, whereas quadruplet wave-wave interactions increase the mean wave period. Non - linear interactions between quadruplets and triads conserve energy therefore they do not affect the total amount of energy but only the spectral shape. Recent experiments by Battjes and Beji (1992), indicate that the wave breaking process does not change the shape of the spectrum. Instead non-linear triad wave-wave interactions change the spectral shape by the generation of both lower and higher harmonic components.

Although the spectral shape depends on the above factors a characteristic property associated with the spectral energy also plays an important role. It is the saturation condition. Once the spectrum becomes saturated, the continuing input from the wind is lost by wave breaking, and by energy transfer from one component to another. The saturation range expresses an equilibrium between energy loss and gain.

Regarding the directional distribution of wave energy, it was found to be more difficult to measure in the field. Nevertheless, some authors proposed expressions for the spreading function depending initially only on the wave direction and later on the wave frequency as well.

The normalised spreading function satisfies

$$\int_{-\pi}^{\pi} G(\omega,\alpha)d\alpha = 1.$$ (5.8)

In the sea, spectra with one peak frequency, two peak frequencies (bi-modal) or even three peak frequencies (tri-modal) can be observed. However, due to the process of frequency dispersion that takes place because of the fact that the low frequency components propagate faster than the high frequency components, the spectrum that reaches the nearshore region has commonly a narrow frequency range (it is narrow banded). A narrow band spectrum results in a variation of the surface elevation corresponding to a regular sinusoidal wave with slowly varying envelope and phase. Thus, under the assumption that waves are a narrow band normal process with zero mean and variance, it can be concluded that the wave amplitude A follows a Rayleigh distribution. What happens in practise is that the assumption of a narrow band spectrum leads to a very small probability that the maximum of the wave profile is allocated elsewhere than the wave crest, therefore the wave envelope represents the amplitude of individual waves where the probabilities of wave crests and troughs are symmetric. Thus, $H = 2A$ and the wave height H, is preferred rather than the amplitude A.

Based on the above assumption, useful statistical parameters can be derived. One of them, that will be later used in this chapter is the significant wave height, estimated as

$$H_s \approx H_{m0} = 4\sqrt{m_0} = 4\sqrt{\left(\int_0^\infty S(\omega)d\omega\right)}.$$ (5.9)

The significant wave height H_s, defined as the average of the highest one third of wave heights, is approximately equal to H_{m0}, except when the water depth is very small or the waves are very steep. H_{m0} is an energy based significant wave height determined as four times the square root of the area contained under the energy spectrum $S(\omega)$.

All the theoretical concepts that have been described thus far are important for the understanding of the two following sections because they constitute the theoretical basis underlining the mathematical modelling.

5.3 - Available models for irregular waves

The numerical modelling of random waves can be done by two approaches: the spectrum approach which is the transformation of a number of point values of the wave number spectrum S(k), and the component approach which is the transformation of independent volumes that are the same as regular waves.

The first method, the spectrum approach, is based on wave ray theory. Energy is conserved along the wave rays when waves are subjected to refraction or shoaling. Assuming a steady state condition the two dimensional spectrum is transformed in space using the equation

$$C_g \left[\cos\theta \frac{\partial(CC_g S)}{\partial x} + \sin\theta \frac{\partial(CC_g S)}{\partial y} + \frac{1}{C} \left(\sin\theta \frac{\partial C}{\partial x} - \cos\theta \frac{\partial C}{\partial y} \right) \frac{\partial(CC_g S)}{\partial\theta} \right] = N$$

(5.10)

where θ is the angle between the normal to the local bottom contours and the wave direction, S is the two dimensional spectrum $S(\omega,\alpha)$ and N is a source term. This formulation is derived from the energy balance equation for a steady state condition. Initially this theory was applied by Longuet - Higgins (1957), and later Karlsson (1969) and Goda and Suzuki (1975) further developed the idea of applying the energy balance equation expressed in terms of the directional spectrum. After Bouws and Battjes (1982) further developed the idea of the ray line as a characteristic line, the model allowed for refraction, shoaling and crossing waves. Nevertheless, this method has been mostly applied in deep waters, where it is more appropriate as it includes a source term allowing to incorporate the most important physical processes responsible for wave behaviour in deep ocean, such as atmospheric transfer (wind input), non-linear wave-wave interaction and energy

dissipation. Three groups of wave prediction models, known as first, second and third generation models, based on the wave energy equation have been successfully used for deep water. Several of the authors that are responsible for their development formed The SWAMP Group (1985). A more detailed description of these models will be done in the next chapter. This method will not be further pursued due to its limitations to treat the phenomenon of wave transformation in the nearshore region, as diffraction and reflection are not considered.

The component approach is based on the assumption of linear and independent behaviour of each individual spectral component. The sea surface is represented by a linear superposition of many harmonics travelling in various directions. An illustration of such a superposition where 13 elementary individual components sum to form the final wave profile is shown in Fig. 5.1. The total wave energy considered for the range of integration in the azimuth set [-π/2, π/2], is

$$\text{Total energy } E = m_0 = \int_0^\infty \int_{-\pi/2}^{\pi/2} S(\omega, \alpha) \partial\omega \partial\alpha \, , \qquad (5.11)$$

and can be considered as the summation of a finite number of spectral energy components or volumes:

$$\text{Total energy } E = \sum_{i=1}^n E(\omega_i, \alpha_i) \qquad (5.12)$$

$$= \sum S(\omega, \alpha) \Delta\omega \Delta\alpha \, . \qquad (5.13)$$

Each component can be associated with a regular wave by

$$S(\omega, \alpha) \Delta\omega \Delta\alpha = \frac{a_i^2}{2} \, . \qquad (5.14)$$

where a_i is considered to be the wave amplitude of each individual small amplitude wave with a certain frequency and direction of propagation. Based on this mathematical assumption that allows the manipulation of the spectra concept the water surface can be written as

$$\eta(x, y, t) = \sum_{i=1}^n a_i \cos[\omega_i t - \phi_i - k_i(x\cos\theta_i + y\sin\theta_i)] \, . \qquad (5.15)$$

The component approach method has been applied successfully to simulate directional waves over large coastal areas using a linear model based on the mild-slope equation. However, almost all the models developed up to now are based on

a parabolic approximation which as explained before approaches the phenomenon with physical limitations, neglecting the important processes of diffraction and reflection in the direction of wave propagation. Although it is understandable why only the parabolic approximation has been used, which is due to the fact that it is the one that generates the most economic model in terms of computational cost, the disadvantage is that it has a high cost in terms of representation of wave transformation.

Regarding the propagation of spectral components the main difficulty is to create a model that combines a good simulation of the physics involved and computational economy. Another important aspect to consider and evaluate is the minimum number of individual spectra components required in order to obtain good results. In all cases an optimal distribution between directional and frequency components is sought.

One of the pioneering models for irregular wave transformation in the nearshore region under the assumption of linear superposition of wave components was that of Isobe (1987). The random sea was chosen to be represented by a Bretschneider-Mitsuyasu-type frequency spectrum with a Mitsuyasu-type directional distribution function. The number of frequency and directional components used to simulate a random sea were 7 and 15, respectively. The model was based on a parabolic approximation of the mild-slope equation and verified for diffraction cases for which (Goda et al, 1978) analytical solutions were available for comparison, and for Berkhoffs et al (1982) shoal for which numerical and experimental results were available. For the diffraction cases the results showed good agreement with Goda's results for random waves, and for the Berkhoff's shoal the wave height amplification behind the shoal was not so large as for regular waves, although not much detail was presented for this case.

Grassa (1990), was one of the authors who proposed an extension of the parabolic approximation derived by Radder (1979) to irregular waves. He compared two methods for the simulation of irregular directional waves, both of the component approach type. These methods differ in the technique used to discretise the wave spectrum: one is based on components of equal energy and the other on components resulting from a constant frequency increment discretisation of the

spectrum. Very little improvement is obtained with more than 100 components and the differences between results from both methods of discretisation vanish as the number of components increases. However equalised energy discretisation gives, from the point of view of propagation, a more reliable representation of irregular waves than constant step methods, in particular if the number of wave components is not high. This can be a very important factor when dealing with a model built up from the elliptic form of the mild-slope equation. Therefore, equalised energy discretisation is a more advantageous method for discretising the spectrum and for obtaining the individual wave components. Hence it will be used in the model proposed in the next section. Grassa (1990) also compared his numerical results obtained from the parabolic model (with 10 frequency and 10 directional components, totalling 100 individual components) with the results obtained by Vincent and Briggs (1989) from laboratory experiments. He emphasised the fact that it is more important to use a larger number of directional components compared with the number of frequency components in order to obtain reliable results, particularly in cases involving diffraction.

Ilic and Chadwick (1995) studied irregular wave transformation in the vicinity of a detached breakwater. They applied a model proposed by Li (1994) for monochromatic waves based on a time dependent evolution equation derived from the original mild-slope equation. The model was extended to irregular waves under the assumption of linear superposition of equal energy spectral components. Tests performed making use of 7 frequency components and 4 directional components suggested that the number of directional components was insufficient. The numerical results were verified by comparison with data obtained from field measurements. In agreement with Goda's observations directional spreading was found to have a more important role than frequency spreading in determining wave heights in the diffraction zone.

A different numerical model also based on a time dependent form of the mild-slope equation was derived by Kirby et al (1992). The model was verified for 3 of the cases tested in the laboratory experiments of Vincent and Briggs (1989). The narrow frequency spectrum was discretised into five components with equal band widths, using therefore a constant step method discretisation. Although the number of directional components used is not mentioned the results presented show that

increasing directional spreading leads to much less spatial wave height variation induced by localised topographic irregularities.

Panchang et al (1990) chose the parabolic formulation proposed by Radder (1979) to propagate the individual spectral components. Once more the model was verified by comparison with the laboratory results obtained by Vincent and Briggs (1989) for the elliptic shoal. The model was tested for some of the cases for which laboratory data was available. The three cases where wave breaking should be taken into account were excluded because their model did not incorporate the phenomenon. The TMA spectrum was represented by 15 frequency components and 41 and 21 directional components for broad and narrow directional spectra, respectively. The linear superposition of the results showed that the model gives satisfactory results despite its physical limitations due to its parabolic formulation.

A common point obtained from all the above research works, which also agrees with Goda's observations mentioned earlier, is that directional spreading has been found to play a more important role than frequency spreading for a better simulation of irregular wave propagation.

A remark that seems appropriate to make here is that almost all the existing numerical models for irregular wave propagation based on the mild - slope equation are governed by a formulation that is a parabolic approximation of the equation. This is due to the fact that it is the most economic approach in terms of computational cost. Nevertheless there is a certain paradox here because the parabolic approximation imposes certain limitations in terms of dealing with wave direction (a main direction is required therefore components with large angle of incidence cannot be properly simulated); restriction of diffraction to the normal of the direction of propagation; and reflection in the direction of propagation. Thus it leads one to consider that theoretically it is the least appropriate model to apply for irregular waves. Because of these considerations a different model for irregular waves is proposed in the next section.

5.4 - A numerical model based on the mild-slope equation

This section proposes a numerical model for irregular wave transformation in the nearshore region that overcomes the limitations implicit in the numerical models based on the parabolic approximation of the mild slope equation. A governing equation based on an elliptic form was chosen as the basis of the model. This decision was one of the motivation factors for the research work presented in chapter 2, where 2 efficient numerical models for regular waves were investigated. The model here developed is based on the numerical formulation described in chapter 2 which generates a robust model for monochromatic waves. It is an accurate model that treats the phenomenon of wave propagation without any loss of the physics involved. Because a linear superposition of independent spectra components will be used to simulate irregularity, it is very important to have accuracy for each transformed component otherwise errors derived from each component would accumulate and would smear the final result. The governing equation is equation (2.2) and the boundary conditions are first order radiation boundary conditions formulated by equations (2.6), (2.8) and (2.10). The governing equation together with the boundary conditions are discretised by a finite differences technique resulting in the linear system of equations formed by equations (2.5), (2.7), (2.9), (2.11) and (2.12) that is solved by the iterative Bi-CGSTAB method. The same convergence criterion and order of accuracy as described in chapter 2 are used here.

The spectral discretisation will be done using a component approach (according to the discussion in the previous section), therefore the directional spectra will be considered transformed in a finite number of equal volumes corresponding to equal energy components. Each component will represent a regular wave that will be transformed within a numerical domain making use of the mild-slope equation based on the principle of conservation of energy. The reason why this discretisation method was chosen is based on the very interesting work done by Grassa (1990) described in the previous section where it can be seen that a method based on equal energy components is more successful than a constant step method when a small number of directional components is used.

The directional wave spectrum $S(f,\alpha) = S(f)G(f,\alpha)$, can be expressed in terms of wave frequency f, instead of the angular frequency ω, using the relation $\omega = 2\pi\, f$. Considering a cut - off for the extreme values within the frequency range and that $G(f,\alpha)$ is a normalised spreading function for directional distribution, the variance of the surface elevation or zero order moment of the frequency spectrum, which represents the total wave energy, can be calculated as

$$m_0 = \overline{\eta^2} = \lim_{t_0 \to \infty} \frac{1}{t_0} \int_0^{t_0} \eta^2 dt \,. \tag{5.16}$$

For a certain number of spectral components of equal energy N_f, and a number of directional components N_α, the directional spectrum will be discretised as follows:

- f_i satisfies: $\int_{f_{min}}^{f_i} S(f)df = \left(\dfrac{m_0}{N_f}\right)(i - 0.5)$

    for $f_i \in [f_{min}, f_{max}]$ and $i = 1, ..., N_f.)$ (5.17)

- α_{ij} satisfies: $\int_{\alpha_{min}}^{\alpha_{ij}} G(f,\alpha)d\alpha = \left(\dfrac{1}{N_\alpha}\right)(j - 0.5)$

    for $\alpha_{ij} \in [\alpha_{min}, \alpha_{max}]$, $i = 1, ..., N_f$ and $j = 1, ..., N_\alpha.$ (5.18)

To each energy component corresponds a individual regular wave of frequency f_i, direction α_j and amplitude a_{ij} that can be written as

$$a_{ij} = \sqrt{2\, S(f_i)\, G\!\left(f_i,\alpha_{ij}\right)\, \Delta f_i\, \Delta\alpha_{ij}} \tag{5.19}$$

or

$$a_{ij} = \sqrt{\frac{2\, m_0}{N_f N_\alpha}} \,. \tag{5.20}$$

Each component is then transformed over the numerical domain as a regular wave, according to the description done in the first paragraph, and finally the resulting wave height H_s, at any location of the domain is calculated as

$$H_s^2 = 2 \sum_{i=1}^{N_f N_\alpha} H_i^2 \,. \tag{5.21}$$

The final results are then presented in terms of amplification factor or normalised wave height which is the ratio of the transformed wave, as calculated by equation (5.21), to the incident wave, as calculated by equation (5.9).

5.5 - Numerical tests

In order to verify the developed model, tests were performed and results compared with the laboratory results obtained by Vincent and Briggs (1989) for directionally spread irregular waves passing over a submerged elliptic mound. The bathymetry is similar to that used by Berkhoff et al (1982) with the exception that for the present case the elliptic shoal is in a region of constant depth equal 45.72 cm and not over a slope. The minimum depth occurs above the centre of the shoal and is 15.24 cm. The shoal boundary perimeter is defined by

$$\left(\frac{x}{3.05}\right)^2 + \left(\frac{y}{3.96}\right)^2 = 1.$$ (5.22)

The elevation at any point in the shoal cross section E_s is given in meters by

$$E_s = -0.4572 + 0.7620\sqrt{1 - \left(\frac{x}{3.81}\right)^2 - \left(\frac{y}{4.95}\right)^2}.$$ (5.23)

The bottom layout can be seen in Fig. 5.2.

The numerical domain was set to cover an area of (220×200) grid nodes in the x and y directions which are the direction normal to shore and the longshore direction, respectively. The domain is built up from square cells with dimensions $\Delta x = \Delta y = 0.1$ m. The centre of the shoal was positioned at 7.0 m from the offshore boundary and 10.0 m from each of the lateral boundaries, with its largest axis parallel to the offshore boundary. A representation of the numerical domain, the location of the shoal and the position of the sections where laboratory measurements were taken is shown in Fig. 5.2. An important remark is that although 8 sections were described as locations where laboratory measurements were recorded, Vincent and Briggs (1989) only published data correspondent to section 4, located behind the shoal. Nevertheless it is a location of focused waves and therefore crucial for the verification of the numerical model here proposed.

The irregular offshore sea state was represented by a Texel, Marsen and Arsloe (TMA) Spectrum, which is a representation of spectral distribution of energy in finite water depth,

$$S(f) = \alpha g^2 (2\pi)^{-4} f^{-5} \exp\left\{-1.25\left(\frac{f_m}{f}\right)^4 + (\ln\gamma)\exp\left[\frac{-(f-f_m)^2}{2\sigma^2 f_m^2}\right]\right\}\Phi(f,h).$$

(5.24)

where:

α = Phillips constant, taken as 0.00155.

f_m = peak frequency, taken as $\dfrac{1}{1.05T_m}$ for T_m = 1.3 sec.

γ = peak enhancement factor, taken as 2 and 20 for the broad and narrow frequency spectrum.

σ = shape parameter, taken as $\begin{cases} 0.07 & \text{if} \quad f < f_m \\ 0.09 & \text{if} \quad f \geq f_m \end{cases}$

Φ = factor that incorporates the effect of depth h.

$$\Phi = \begin{cases} 0.5(\omega_h)^2 & \text{for } \omega_h < 1 \\ 1 - 0.5(2-\omega_h)^2 & \text{for } 1 \leq \omega_h \leq 2 \\ 1 & \text{for } \omega_h > 2 \end{cases}$$

for $\omega_h = 2\pi f \sqrt{\dfrac{h}{g}}$.

ω_h will be considered for offshore, with $f = f_m$ giving ω_h = 0.99 and thus Φ = 0.5.

Two different frequency spectra were considered. One narrow, for γ = 20 and one broad, for γ = 2, both shown in Fig. 5.3, where the spectral components used to represent the frequency spectrum are also plotted. The lower and upper limits considered for the frequency spectrum were 0.5 Hz and 2.0 Hz, respectively. These limits are consistent with Panchang's et al (1990) limits used in a parabolic model mentioned in the previous section. Vincent and Briggs (1989) used the same lower cut - off but an upper cut - off of 1.5 Hz. Each frequency component was then calculated by equation (5.17).

Similarly, two spreading functions, one narrow and one broad, were used in conjunction with S(f) to obtain the two dimensional directional spectra.

The directional spreading function derived from a Fourier series is

$$G(f,\alpha) = \frac{1}{2\pi} + \frac{1}{\pi}\sum_{j=1}^{J}\exp\left[-\frac{(j\sigma_m)^2}{2}\right]\cos j(\alpha - \alpha_m)$$ (3.25)

where σ_m is the spreading parameter, taken as 10° and 30° for a narrow and broad spreading function, respectively, as shown in Fig. 5.4. In the same figure the point values used to represent the directional components can also be seen. α_m is the mean wave direction, equal to 0° and J, taken here as 20 (consistently with Panchang's et al (1990) numerical experiment), is an arbitrary number of harmonics chosen to represent the Fourier series. For the narrow spreading function the range of values considered for the azimuth is within the range -45° < α < 45° because G(f,α) is practically zero outside this range. For the wide spreading function the range of values considered for the azimuth is within the range -90° < α < 90°. Each directional component was then calculated by equation (5.18).

Vincent and Briggs (1989) considered 17 different cases from which 3 include the dissipative non - linear process of wave breaking. These last three will be considered in the next chapter while the others will be dealt with here. Vincent and Briggs observed that for some of the irregular wave propagation cases tested in the laboratory occasional superposition of waves induced some breaking in the vicinity of the mound. Therefore, it was decided that these cases were not appropriate to verify the present model as the results cannot be compared with confidence. The cases will be refer to as M for monochromatic input wave, U for unidirectional input spectrum, N for input directional spectra with narrow directional spreading and B for input directional spectra with broad directional spreading. A summarised description of the test conditions can be seen in Table 5.1:

Case ID	Type	Period (sec)	Height (cm)	α	γ	σ_m (deg)
M2	Mono	1.30	2.54	—	—	—
U3	Spec	1.30	2.54	0.00155	2	0
N3	Spec	1.30	2.54	0.00155	2	10
B3	Spec	1.30	2.54	0.00047	2	30
U4	Spec	1.30	2.54	0.00047	20	0
N4	Spec	1.30	2.54	0.00047	20	10
B4	Spec	1.30	2.54	0.00047	20	30

Table 5.1. Test conditions for non-breaking series.

Based on the fact that an elliptic model can involve a high computational cost (in terms of time) for irregular waves as several spectral components should be propagated over the computational domain (Fig. 5.2), the choice of the number of frequency and directional components is quite important. There should be a compromise between having a minimum number of components in order to have a reasonable computational cost, and a sufficient number of components that give a good representation of the frequency and directional spreading. Thus 8 frequency components and 8 directional components was the number chosen to represent the directional spectra, making a total of 64 components. This choice seems to be ideal when considering the discussion of the subject in section (5.3).

In order to evaluate the performance of the numerical model for the above 7 cases the computational results are presented in terms of the normalised wave height, that is the ratio of the transformed wave height to the incident wave height, H/H_i. The wave height refers to a representative wave, and for these cases it was chosen to be the significant wave height. Vincent and Briggs (1989) reported that the period pattern showed little variation when the wave transformation process was occurring in the physical experiment. Two dimensional (2D) contour plots for the whole numerical domain and graphs for 6 sections that can be localised in Fig. 5.2 are presented because they seem to be the best way to show the results obtained. Results for section 4 are treated with particular attention because this section is the one where experimental data is available for comparison. For this section each case is verified against laboratory data for validation.

It was observed that as the frequency component increases in value, the iterative process requires a larger number of iterations to satisfy the accuracy criteria imposed. The number of iterations increases about 4 times from the smallest to the largest component. This confirms the expectations because as the frequency increases (or the period decreases) the wave length decreases and therefore the wave steepness, H/L, increases, its value becoming less legitimate to use based on small amplitude wave theory.

The 2D contour plots are shown for each of the above cases from Fig. 5.5 to Fig. 5.11. From the observations of the 2D contours conclusions regarding wave pattern and wave height amplification factor (or normalised wave height value) can be summarised as follows:

- Wave pattern

  The 2D contour plots show 3 distinct wave patterns regarding the convergence in the region behind the shoal. The first pattern can be observed for the cases with a broad frequency spectra, U3, N3 and B3. The focusing area is more extended in the x direction (normal to the shore) than for the rest of the cases. The second pattern can be observed for the monochromatic case, M2, and the unidirectional narrow frequency spectra, U4, where the focusing region is quite localised in a certain area just behind the shoal, particularly for the monochromatic case. The third pattern can be observed for the cases with a narrow frequency spectra and directional spreading, N4 and B4. The focusing region behind the shoal is more localised or more concentrated to a certain area than the broad frequency spectra cases (U3, B3 and N3), meaning that is more similar to the second pattern. Nevertheless, for these two cases the wave pattern shows a non - monotonic or sharp variation caused by the presence of the shoal which is extended to a larger area of the domain distant from the shoal.

- Wave height amplification

  Regarding the amplification of the wave height due to the existence of the shoal it can be observed that the monochromatic case, M2, is the case that gives the smallest value for the normalised wave height at the two sides of the shoal. The narrow frequency spectra with directional spreading cases, B4 and N4, are the ones which show the highest amplification of the wave height just behind the shoal and the less smooth variation of its value within the region affected by the presence of the shoal. The results obtained with the broad frequency spectra

cases, U3, B3 and N3, are the ones which present the smallest difference between the maximum and the minimum values of the normalised wave height, that is which appear to be less perturbed in passing over the shoal. The unidirectional cases, U3 and U4, show a smoother variation of the normalised wave height than the monochromatic case M2. Results for case U4 are generally higher than for the case U3 for the area affected by the presence of the shoal.

More about the performance of the model with respect to each case can be observed from the results plotted for each of the 6 sections (Fig. 5.12 to Fig. 5.17). The results for the cases with directional spreading are not absolutely symmetric for each side of the shoal due to the introduction of a small numerical error when each directional component is generated. This happens because the process used to generate each direction is a cumulative process so that the numerical error introduced when the total area is divided into components is minimised and thus produces the best representation of the spreading function. The same idea was applied to generate the frequency spectral components. The three sections in the y direction (shore direction), sections 3, 4 and 5, confirm the observations from the 2D contour plots. The maximum amplification factor at the edge of the shoal (section 3) is minimum for the broad frequency spectra cases, U3, B3 and N3, and the monochromatic case, M2. The lowest value at the shoal sides can be seen for the monochromatic case, M2. Then advancing behind the shoal in the direction of propagation, for all the cases the peak amplification factor is decreased and the lowest value at the two regions to the side is increased. However, the decrease of the maximum value is larger for the narrow frequency spectra particularly when in the presence of directional spreading and for the monochromatic case, for which the peak, which before was higher than for the broad frequency spectra, now becomes smaller. While this occurs, the profile pattern changes smoothly for the broad frequency spectra cases whereas for the narrow frequency spectra with directional spreading and monochromatic cases the changes in the profile pattern are bigger. It can be seen from sections 4 and 5 that for these last three cases the focusing area enlarges to the sides. The three sections in the x direction, sections 6, 7 and 8, confirm the smoothest variation of the broad frequency spectra. For the narrow frequency spectra with directional spreading the increase of spreading in terms of direction seems irrelevant at least when 8 directional components are used with 8 frequency components because the results obtained for the cases B4 and N4,

although not coincident, are not different enough to be distinguishable in the plots. For the broad frequency spectra with directional spreading the increase of the directional range still does not seem to make a big difference for cases B3 and N3. Nevertheless when comparing these cases with the unidirectional cases directional spreading is important. This can be seen in Figs. 5.18 and 5.19, which are relative to section 4. The two graphs of narrow and broad frequency cases were plotted separately for a better visualisation and investigation of the influence of directional spreading. These results lead to the conclusion that although directional spreading is important, 8 components are not enough for a good representation of the effects of directional spreading.

Now that the sensitivity of the model for the 7 cases has been established, and before more considerations and conclusions are established, it is necessary to evaluate how close the numerical results are to the experimental data obtained. In order to validate them comparisons were made for section 4, for which laboratory data is available. Plots can be seen from Fig. 5.20 to Fig. 5.26 for the 7 cases. The computational results for the monochromatic case, M2, seen in Fig. 5.20, and the unidirectional cases U3 (Fig. 5.21) and U4 (Fig. 5.24) show very good agreement with the laboratory data. In fact, only the peak of the convergence region behind the shoal is slightly underpredicted, about 15%, for the monochromatic case M2 and about 7% for the narrow frequency spectra, U4. The broad frequency spectra case, U3, shows an excellent agreement along the whole section. These results confirm the expectation that using narrow frequency spectra shows a performance which stands between the performance of the broad frequency spectra and the monochromatic case. The cases involving directional spreading do not show such good agreement in the focusing region, particularly the cases with broad directional spreading, B3 (Fig. 5.23) and B4 (Fig. 5.26), for the peak of the focusing region. In fact, what can be observed from the laboratory data is that directional spreading decreases the amplification behind the shoal. Waves are less disturbed by the presence of the shoal meaning that a smoother variation of the amplification factor can be observed in this region. It is interesting to observe that for the broad frequency spectra cases, B3 and N3, the model smoothes the two sides of the focusing region in agreement with the laboratory data. Although the same can also be observed in the experimental results for the narrow frequency cases, B4 and N4, the model does not reproduce this behaviour and thus, it shows a pattern more

similar to the monochromatic case. This fact indicates that the model is sensitive to frequency spreading. The biggest difference between the computational results and the laboratory data can be observed for the broad directional spectra cases, B3 and B4 at the peak of the focusing area. For the narrow frequency spectra with narrow directional spreading case, N4, the peak of the convergence region overpredicts the laboratory results by about 13%. For the narrow frequency spectrum with broad directional spreading case, B4, the peak of the convergence region overpredicts the laboratory result by about 70%. For the broad frequency spectra with narrow directional spreading case, N3, the peak of the convergence region overpredicts the laboratory result by about 48%. For the broad frequency spectra with broad directional spreading case, B3, the peak of the convergence region overpredicts the laboratory result by about 85%. These trends confirm that the number of directional components required to simulate directional spreading should be larger than the number of frequency components required to simulate frequency spreading.

Some of the differences that can be observed between the numerical results and the laboratory data may be attributed to non - linear effects which are not simulated in the numerical experiment as we are dealing with a linear model; accumulation of error due to the superposition of the independent components; the fact that the laboratory data contains a roughly 5% variability about average values; the fact that the input frequency spectra and spreading function were not always exactly replicated between laboratory experiment and calculations; constraints implicit in the physical model that influence the process of wave transformation like the fact that the wavemaker had a finite length restricting the region in the basin over which homogeneity can be assumed; the fact that although the cases where breaking was observed to occur in the vicinity of the shoal were excluded, with irregular waves random superposition can cause wave breaking that would not occur with small monochromatic waves; and finally due to an insufficient number of directional components.

Based on observation of the results of the tests done to validate the model and the evaluation of its performance for each input case it can be summarised that:
- the model gives good results in general because the focusing region is reduced with distance from the shoal;

- The model is sensitive to frequency spreading and directional spreading;
- 8 frequency spectra components are enough to evaluate the influence of frequency spreading and obtain good results. This conclusion is supported by the results obtained for the unidirectional cases and by the differences between the narrow and broad frequency cases with the same directional spreading function;
- 8 directional components are not enough to simulate directional spreading because the computational results obtained with broad and narrow directional spreading functions are almost the same.

5.6 - Closure

In this chapter a numerical model for irregular wave propagation was proposed. It is based on a linear superposition of independent spectral components each of which is propagated as a monochromatic wave using the accurate model developed and validated in chapter 2. An investigation of boundary conditions was made in chapter 3 in which one of the objectives was to improve the accuracy of the model developed in chapter 2. Nevertheless, it was observed that sponge filters are not as efficient for this model as they proved to be for the hyperbolic model, and that higher order boundary conditions require a more complicated stencil that incurs a higher computational cost. Bearing in mind that a large number of components is required to simulate a random sea, the model here applied was based exactly on the model developed in chapter 2. The results obtained proved that the model gives good approximate solutions when a reasonable number of spectral components is used and that the monochromatic representation can lead to erroneous results. The number of directional components required is higher than the number of frequency components. This investigation showed that the model is appropriate to deal with irregular wave transformation, thus making it worthwhile to improve it by introducing the important process of breaking as it will be done in the next chapter.

surface elevation

Final wave profile

time

1
2
3
4
5
6
7
8
10
12

Spectral components

Amplitude^2

1   3   5   7   9   11   13

Energy spectrum
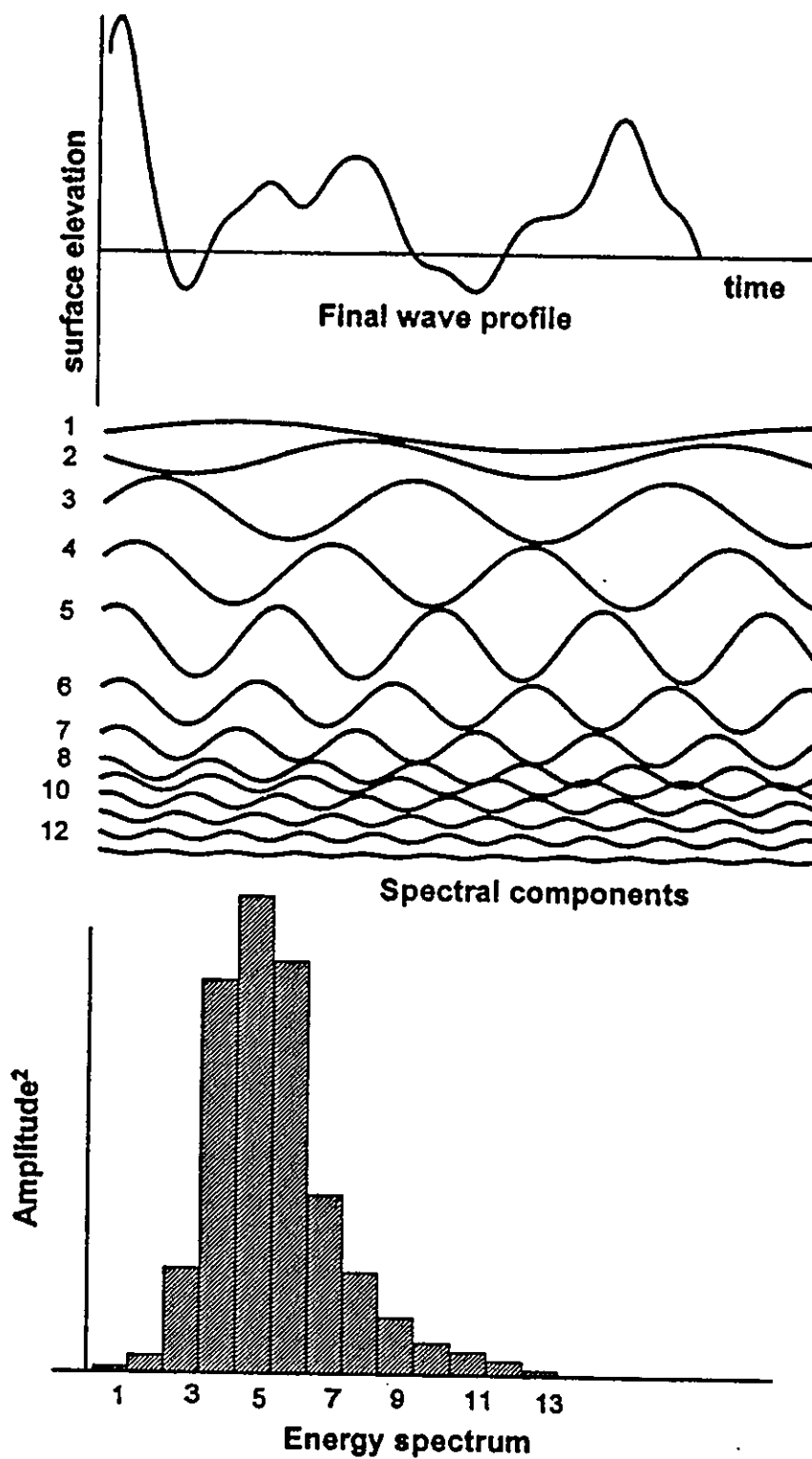
Fig. 5.1 - Superposition of spectral components and resulting spectrum (from Massel, 1996).

PROFILE

Shoal Thickness:

$$-0.4572 + 0.7620\sqrt{1-\left(\frac{x'}{3.81}\right)^2 - \left(\frac{y'}{4.95}\right)^2}$$

x' in m

Shoal boundary perimiter:

$$\left(\frac{x'}{3.05}\right)^2 + \left(\frac{y'}{3.96}\right)^2 = 1$$

y' in m

Outside shoal:
h = 0.4572 m

CONTOUR

y (in m)

x (in m)
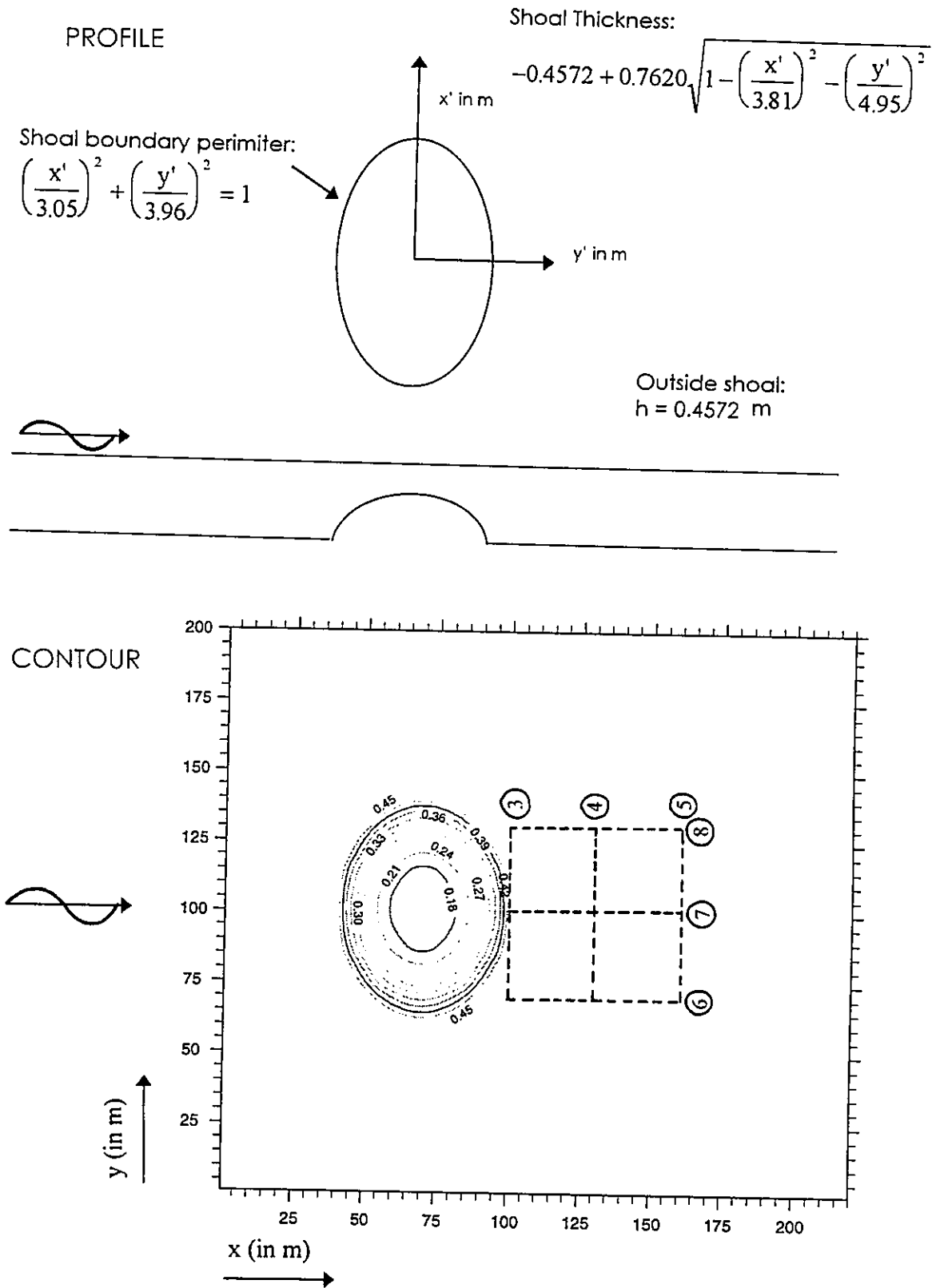
Fig. 5.2 - Elliptic shoal over uniform depth; model bathymetry.
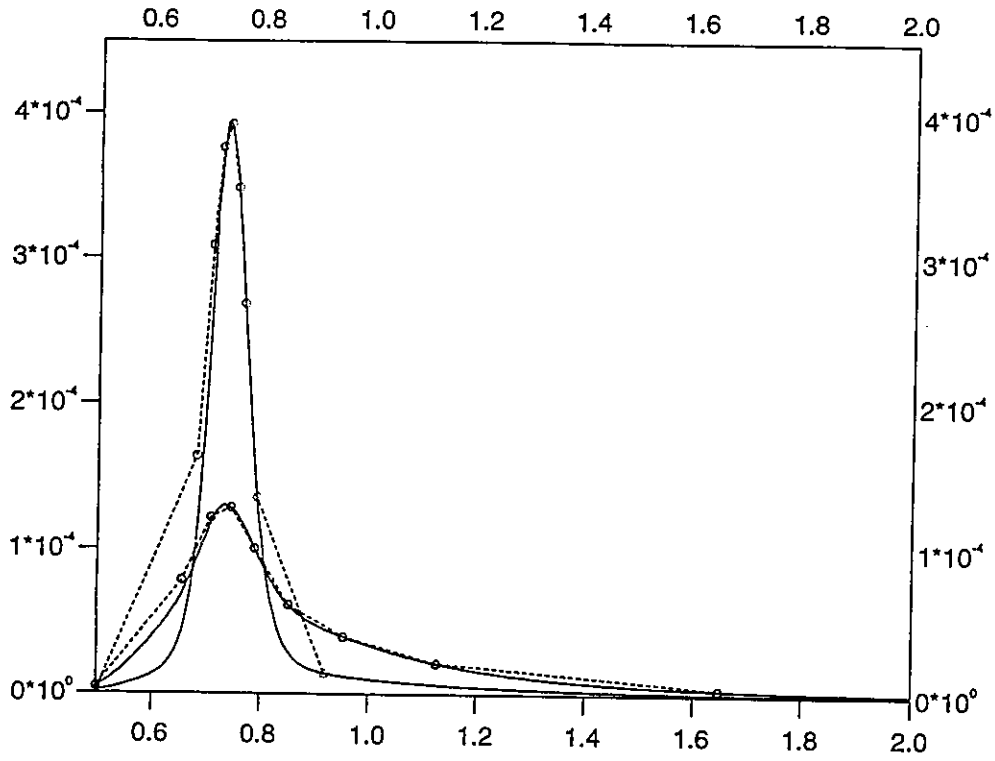
Fig. 5.3 - Wave spectra and calculated components.
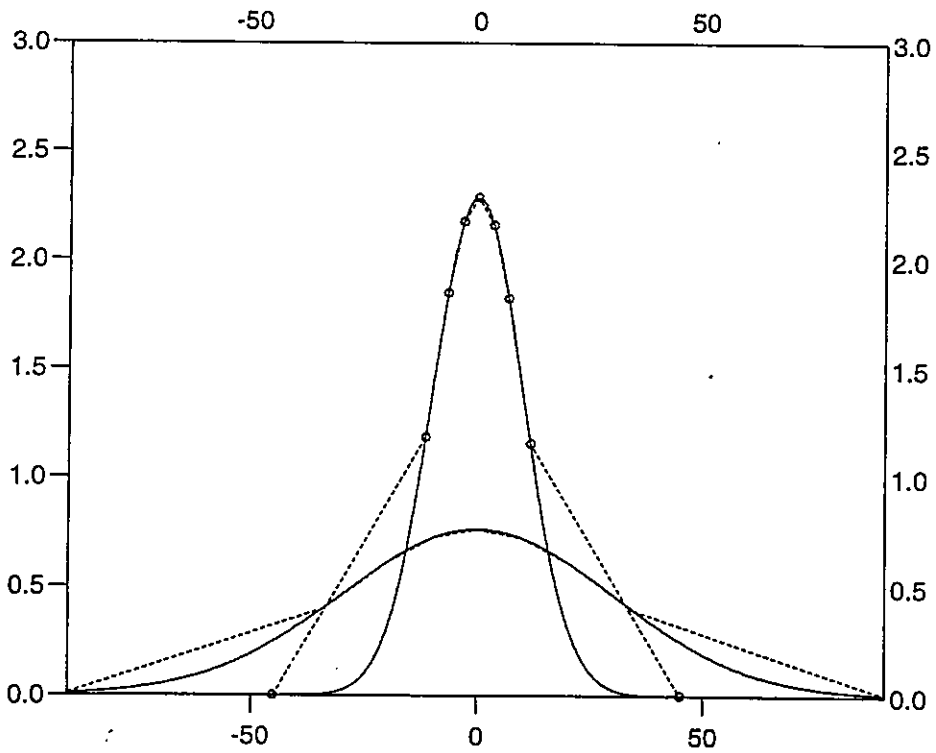
Fig. 5.4 - Angular spreading functions for directional spectra and calculated
components.
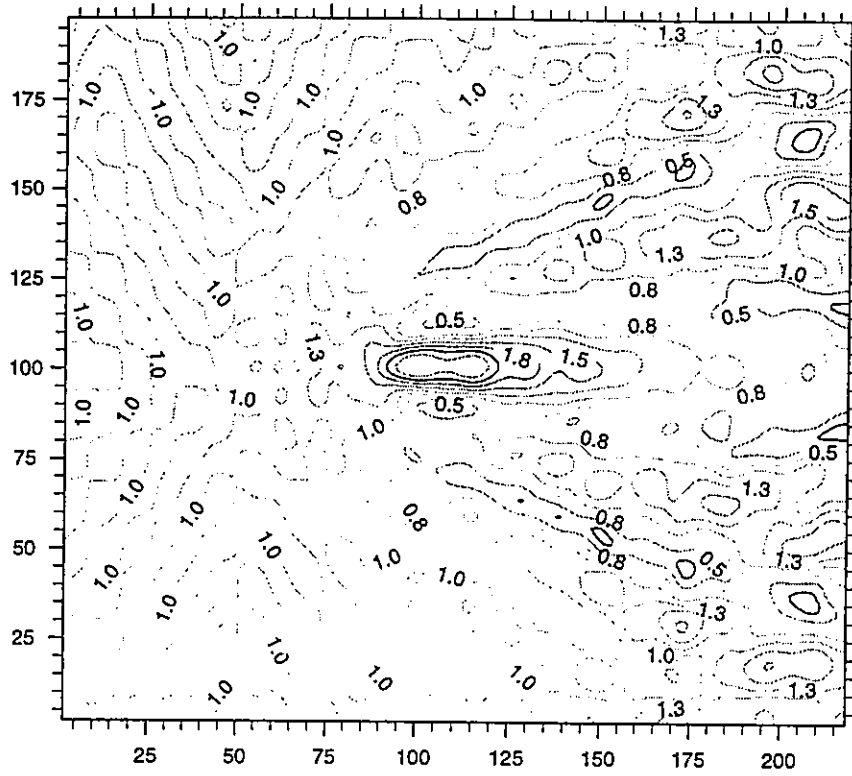
Fig. 5.5 - Normalised wave height contours for case M2.
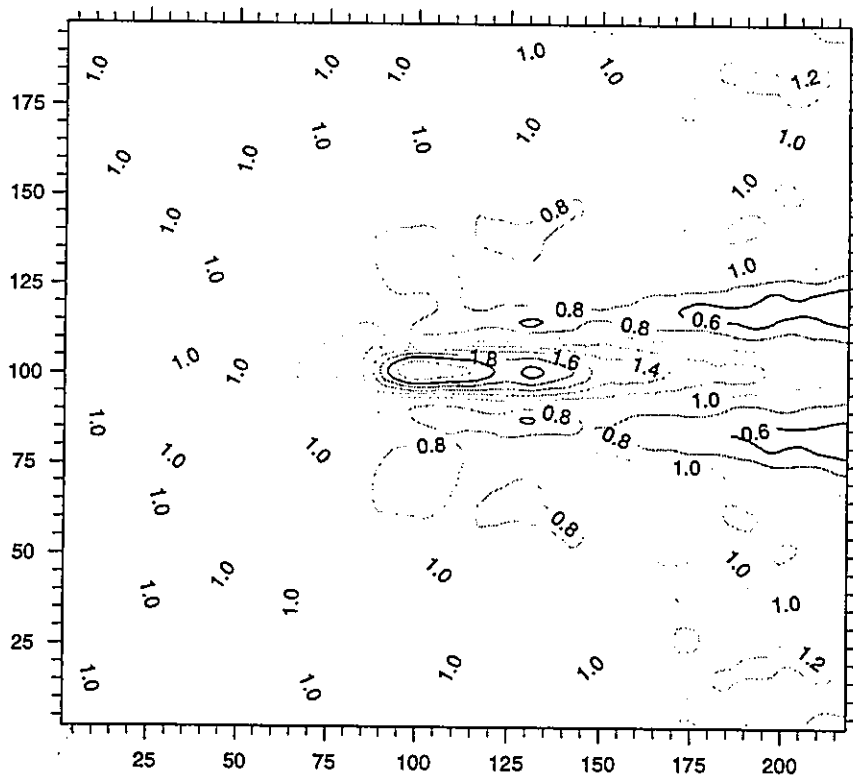
Fig. 5.6 - Normalised wave height contours for case U3.
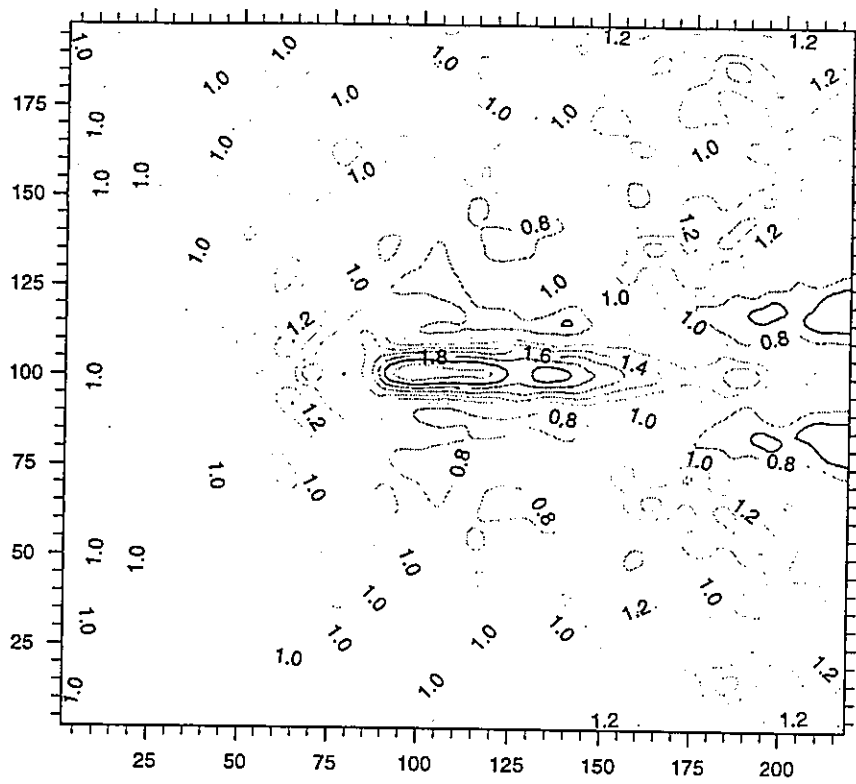
Fig. 5.7 - Normalised wave height contours for case N3.
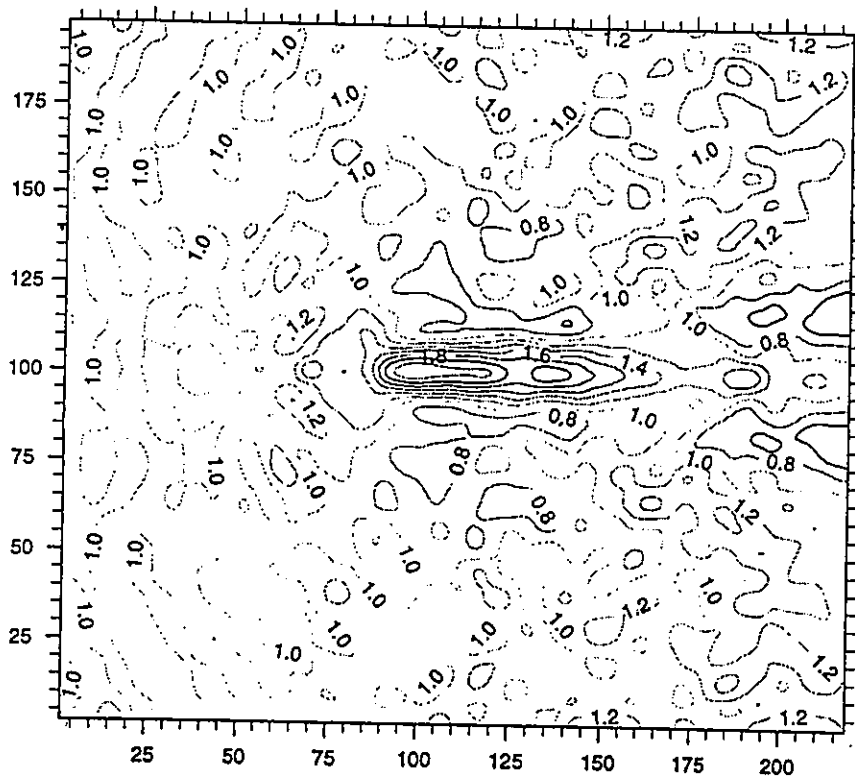
Fig. 5.8 - Normalised wave height contours for case B3.
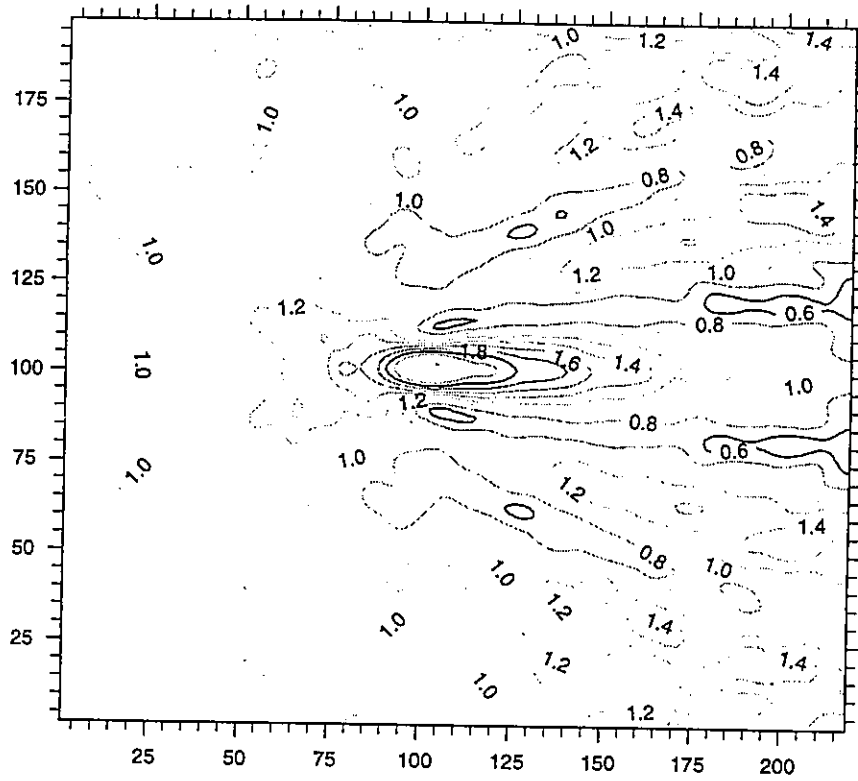
Fig. 5.9 - Normalised wave height contours for case U4.
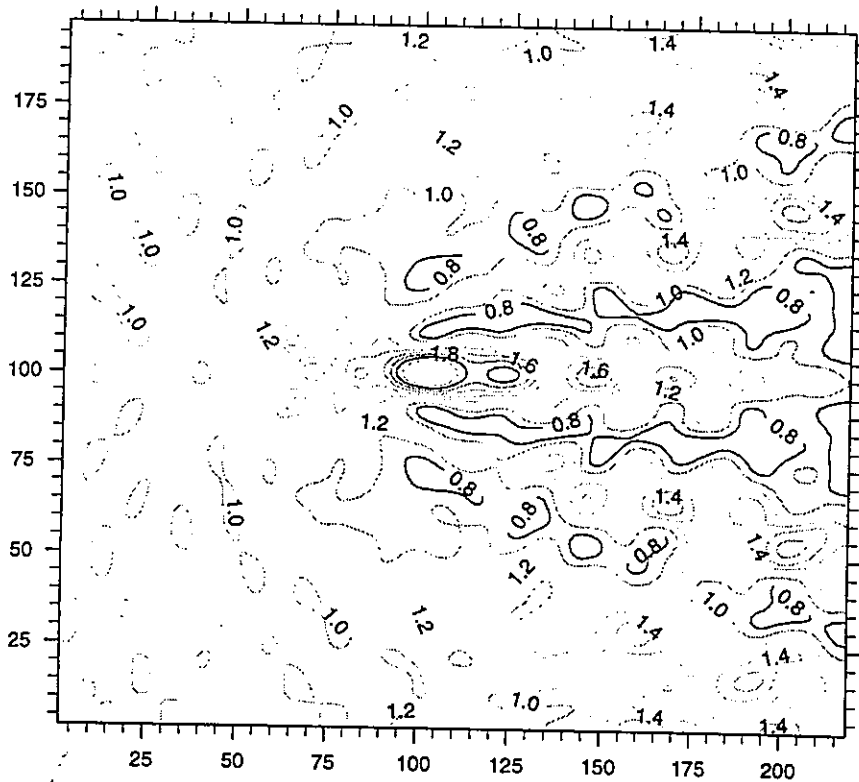
Fig. 5.10 - Normalised wave height contours for case N4.
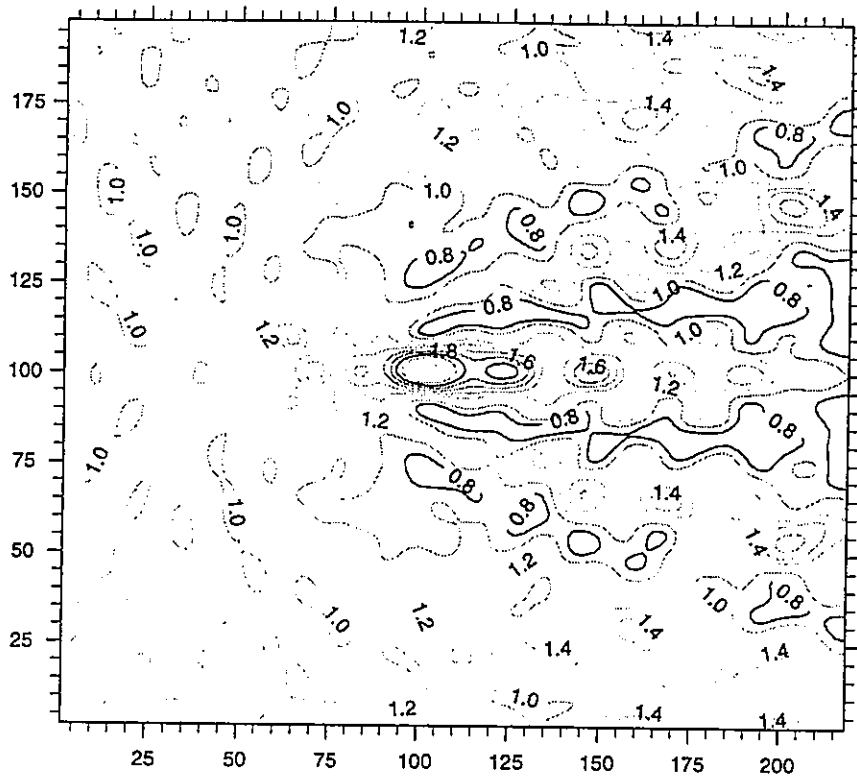
Fig. 5.11 - Normalised wave height contours for case B4.
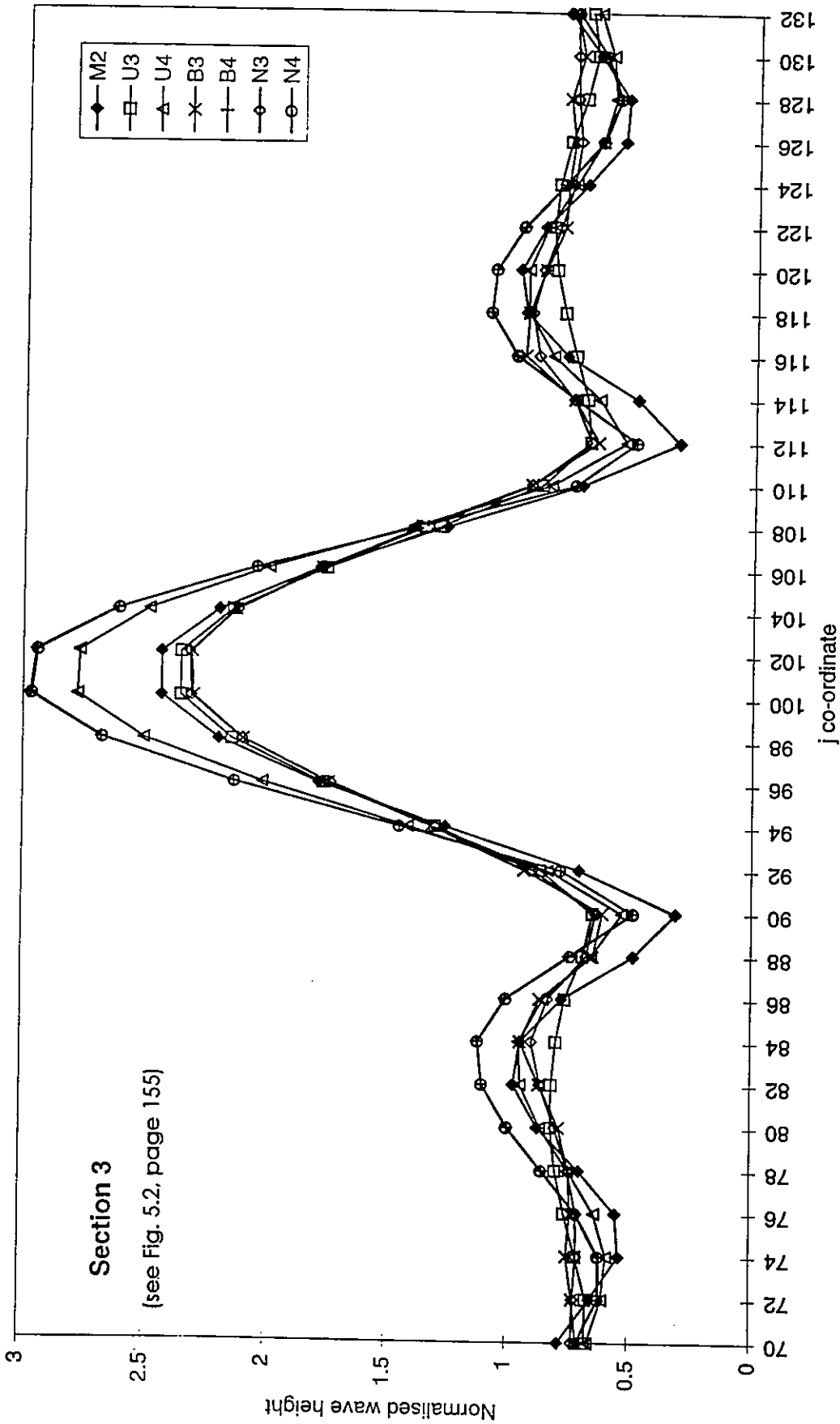
Fig. 5.12 - Computational results for section 3.
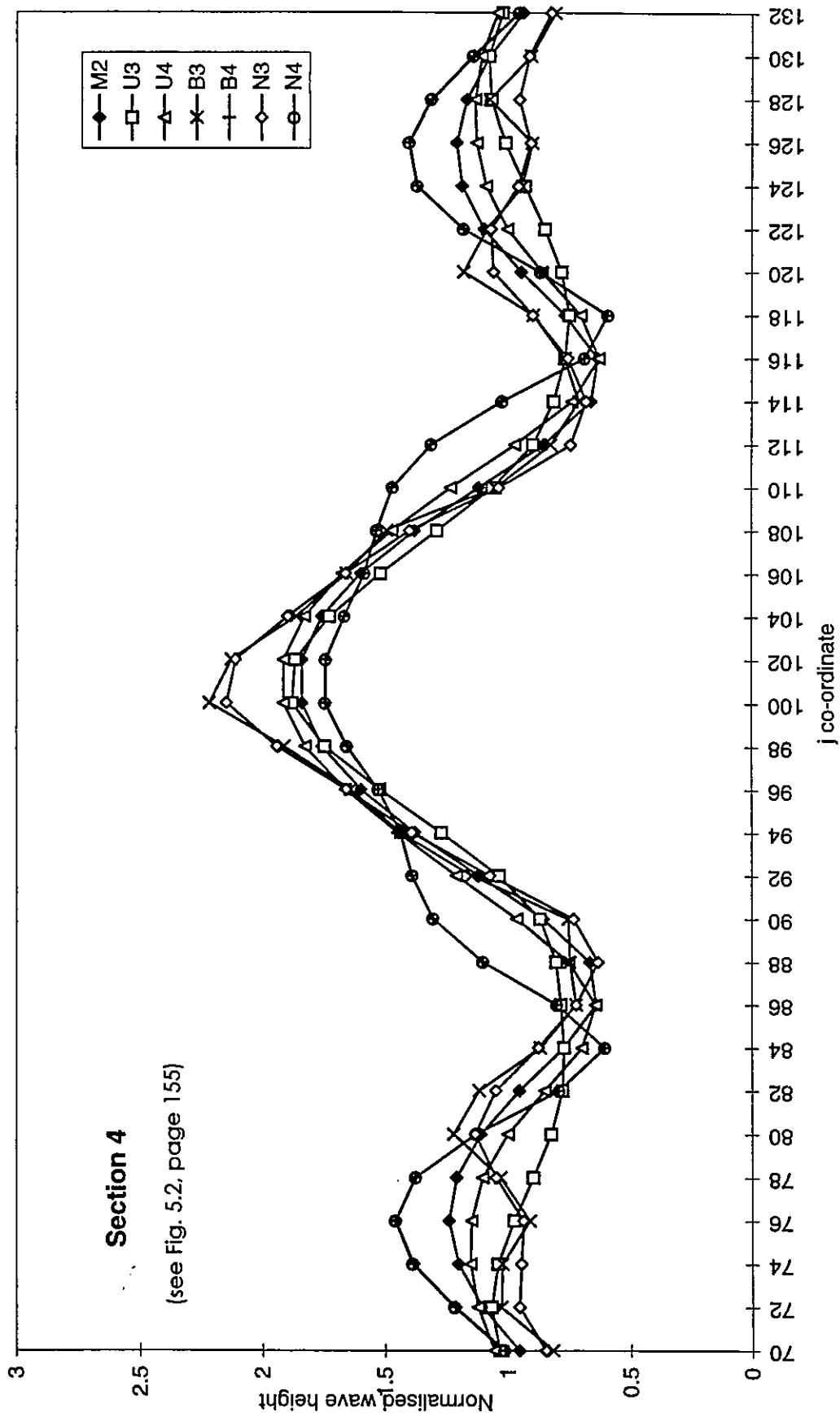
Fig. 5.13 - Computational results for section 4.
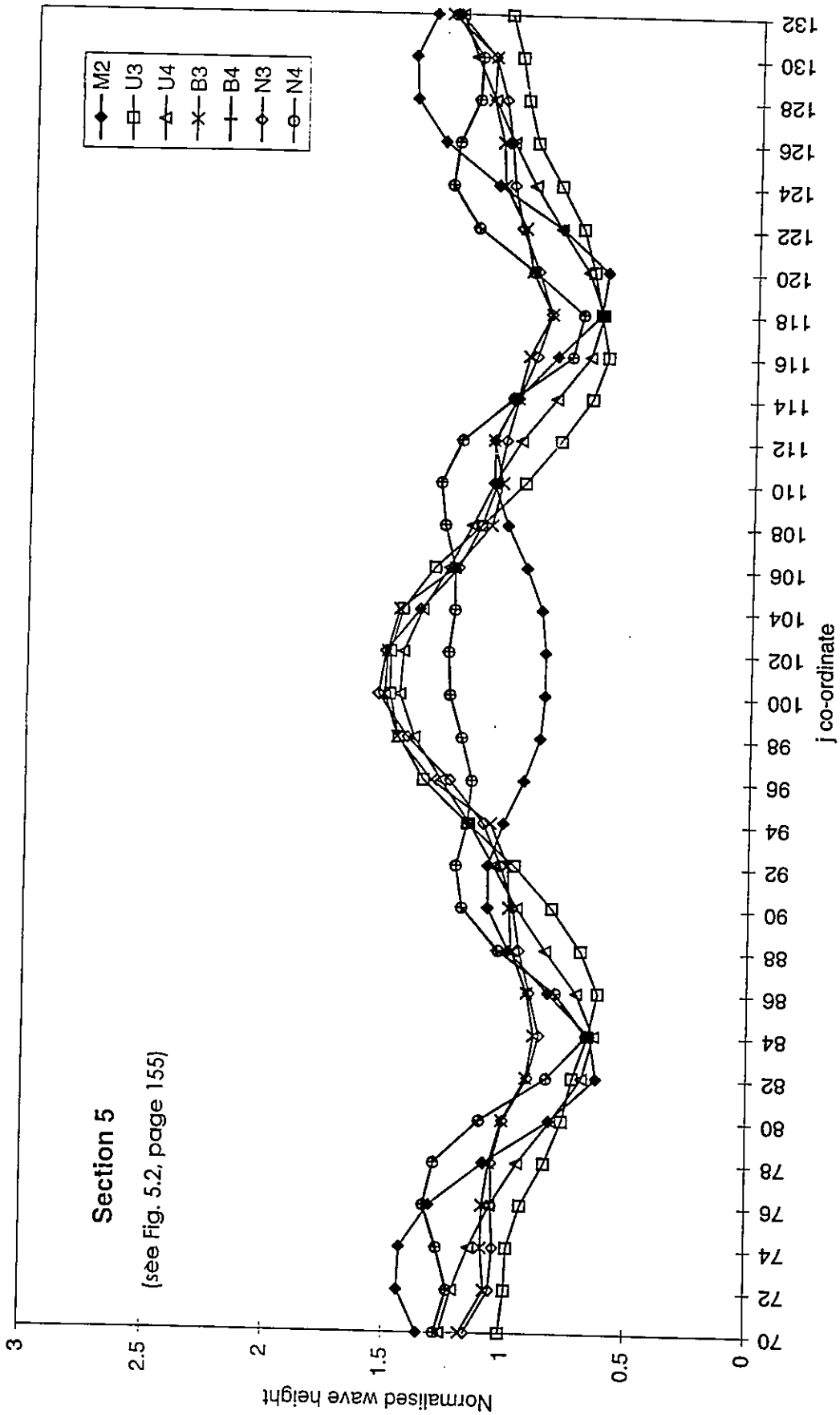
Fig. 5.14 - Computational results for section 5.
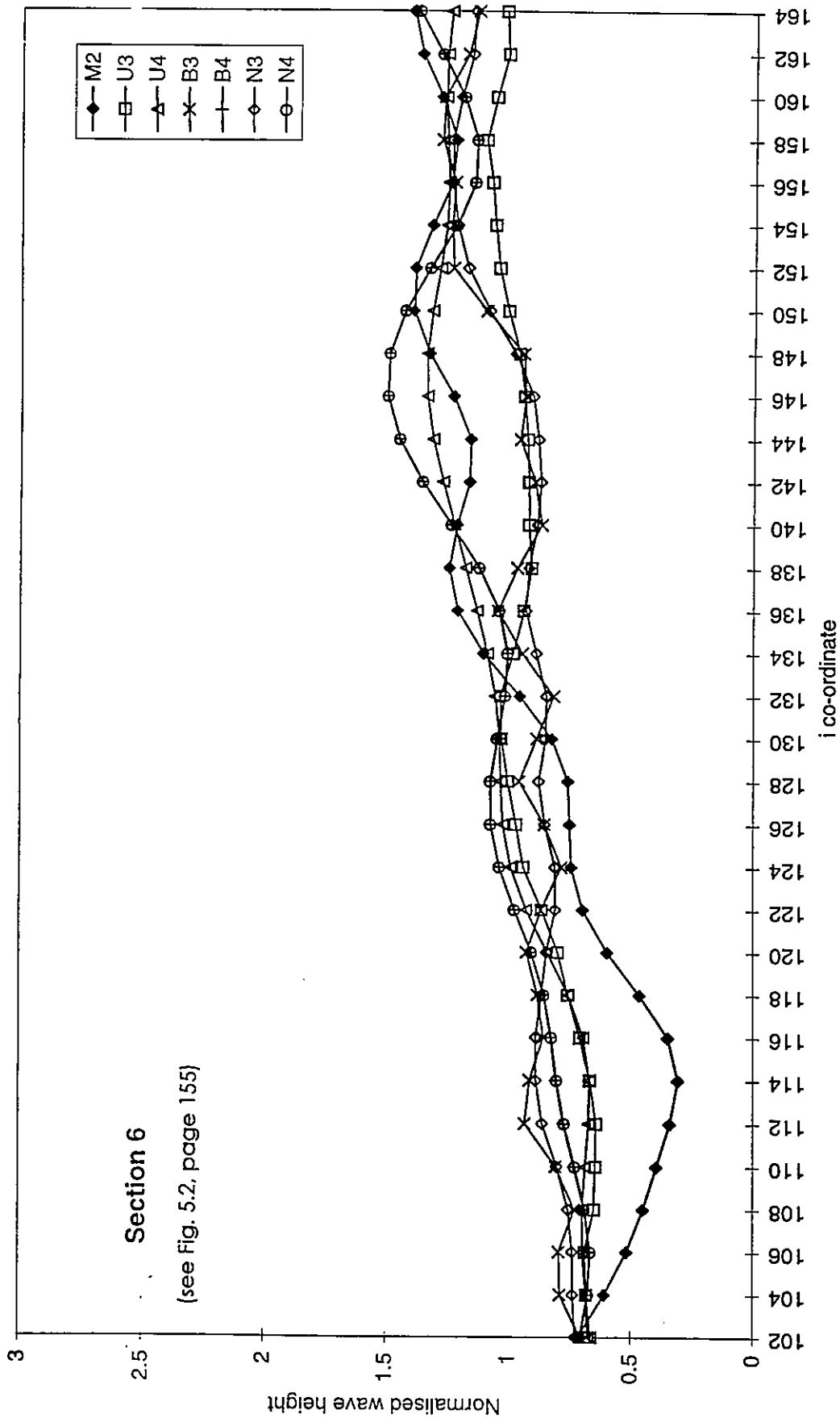
Fig. 5.15 - Computational results for section 6.
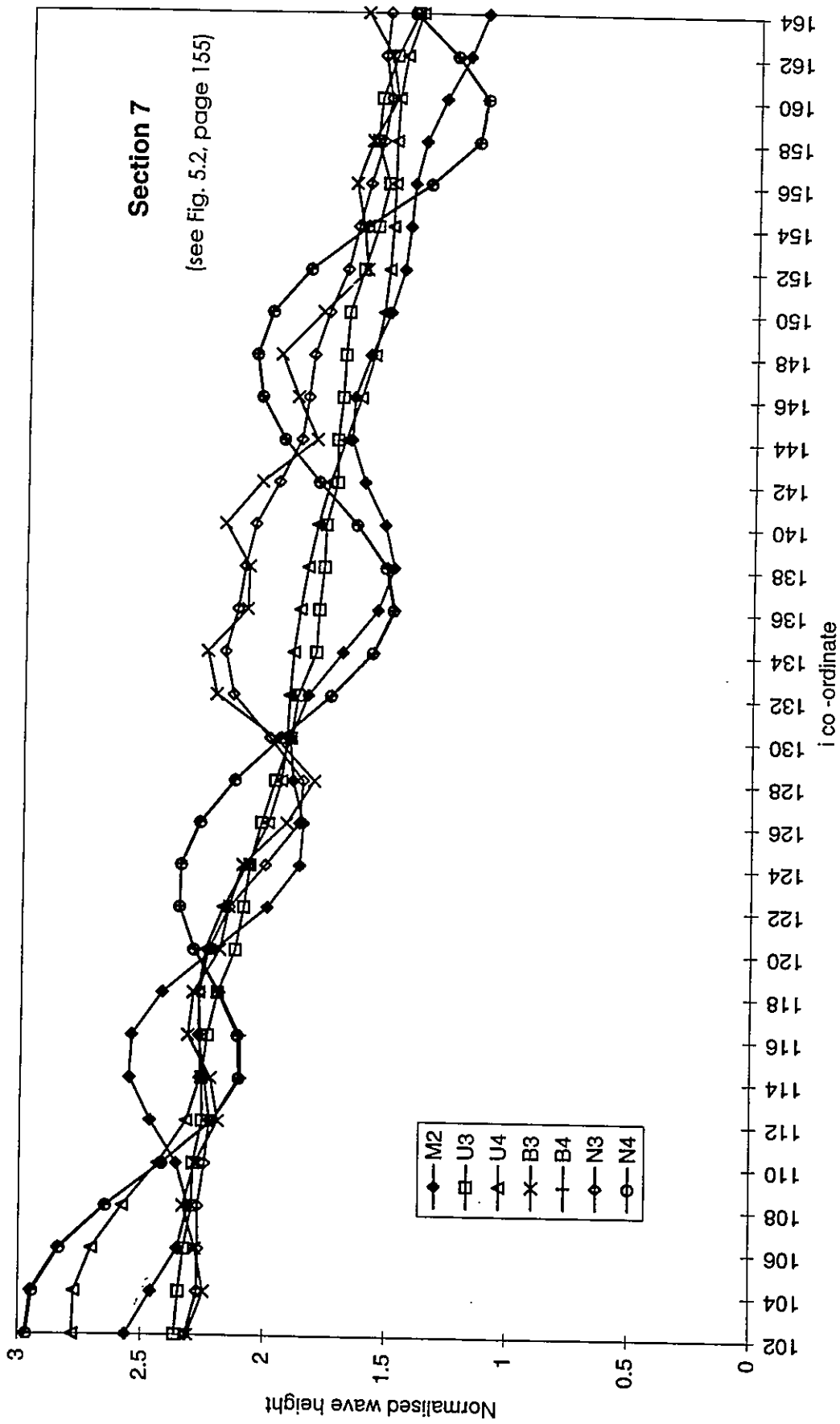
Fig. 5.16 - Computational results for section 7.
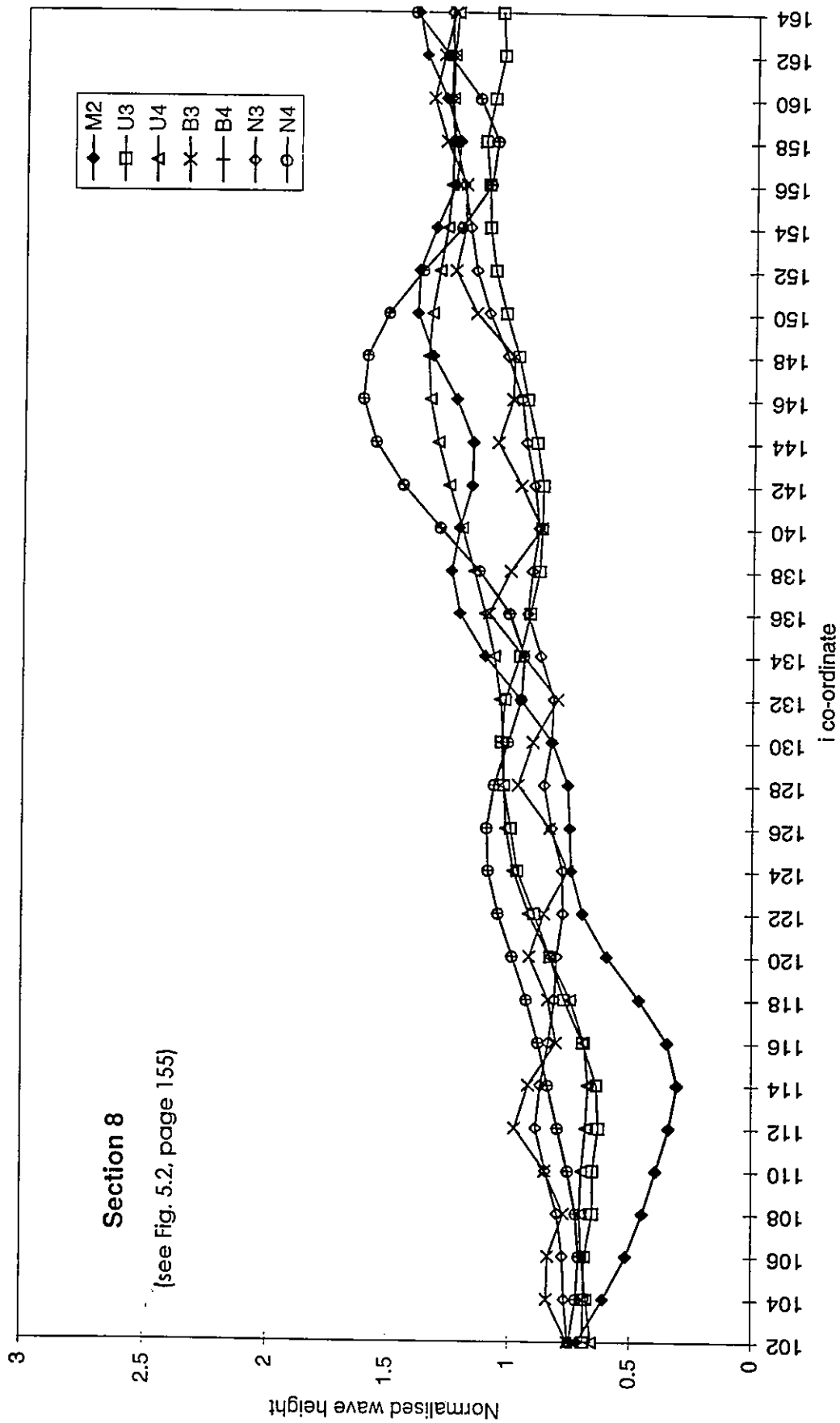
Fig. 5.17 - Computational results for section 8.
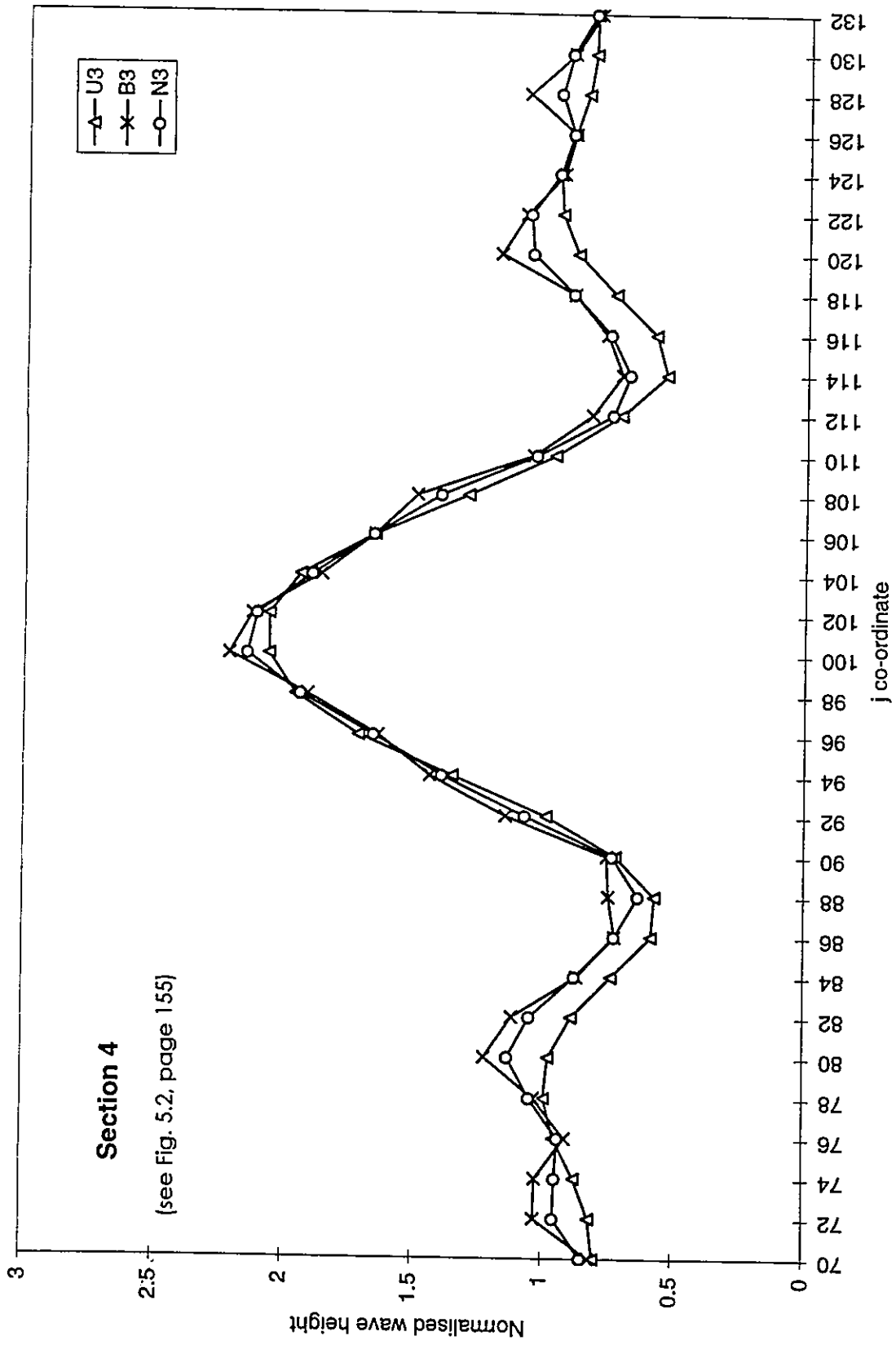
Fig. 5.18 - Computational results for the broad frequency spectra cases.
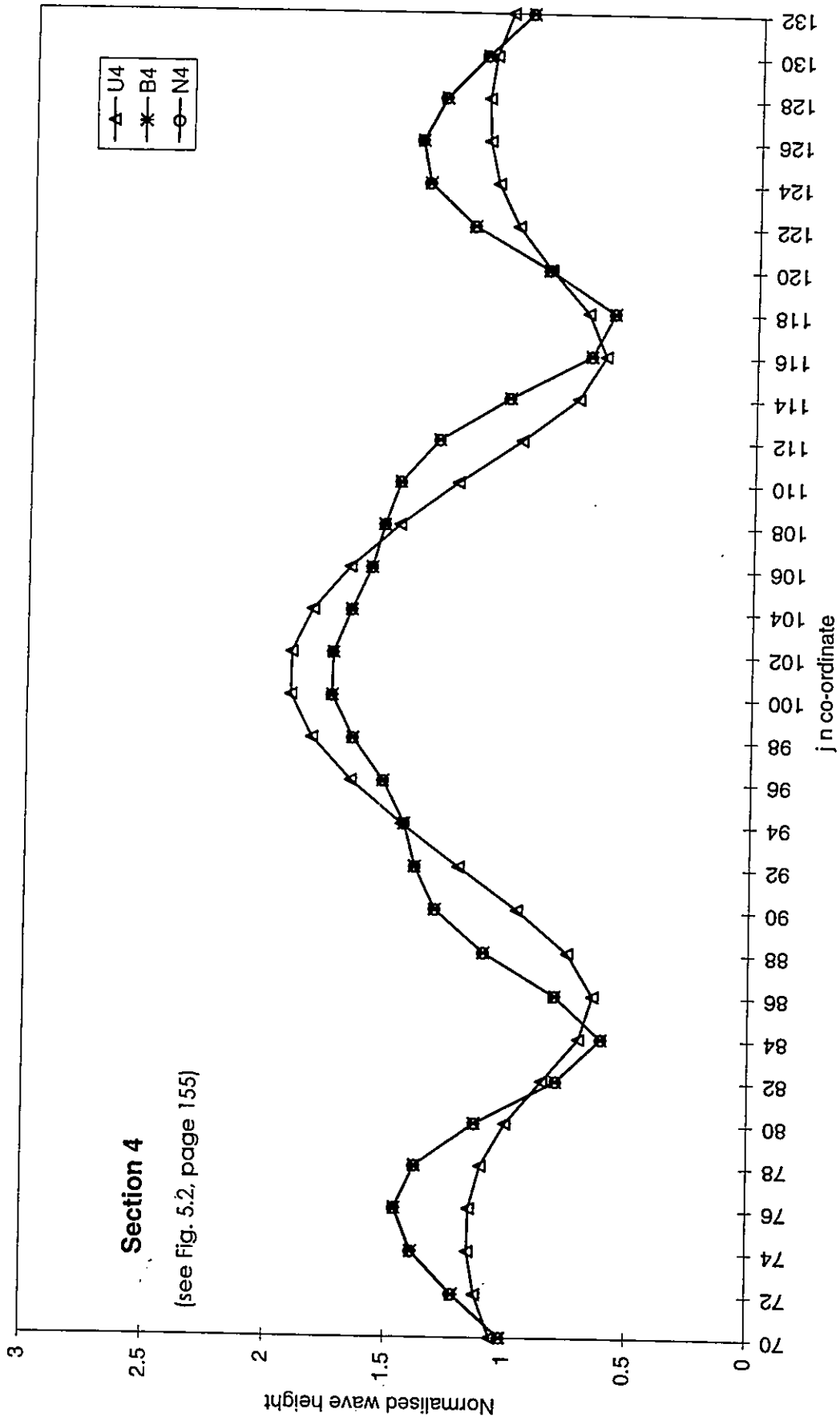
Fig. 5.19 - Computational results for the narrow frequency spectra cases.
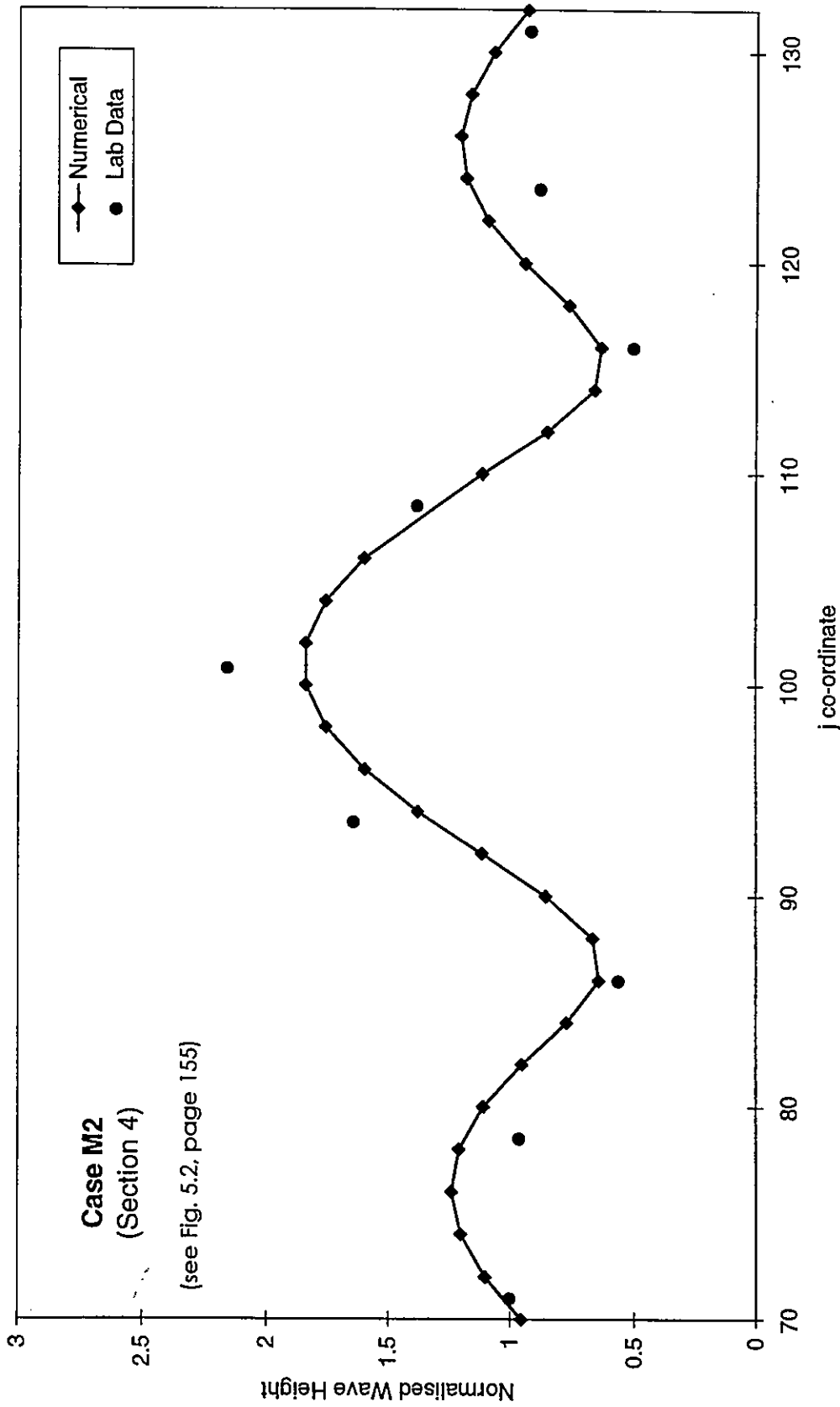
Fig. 5.20 - Comparison between experimental data of Vincent and Briggs (1989) and computational results for case M2. Section 4.
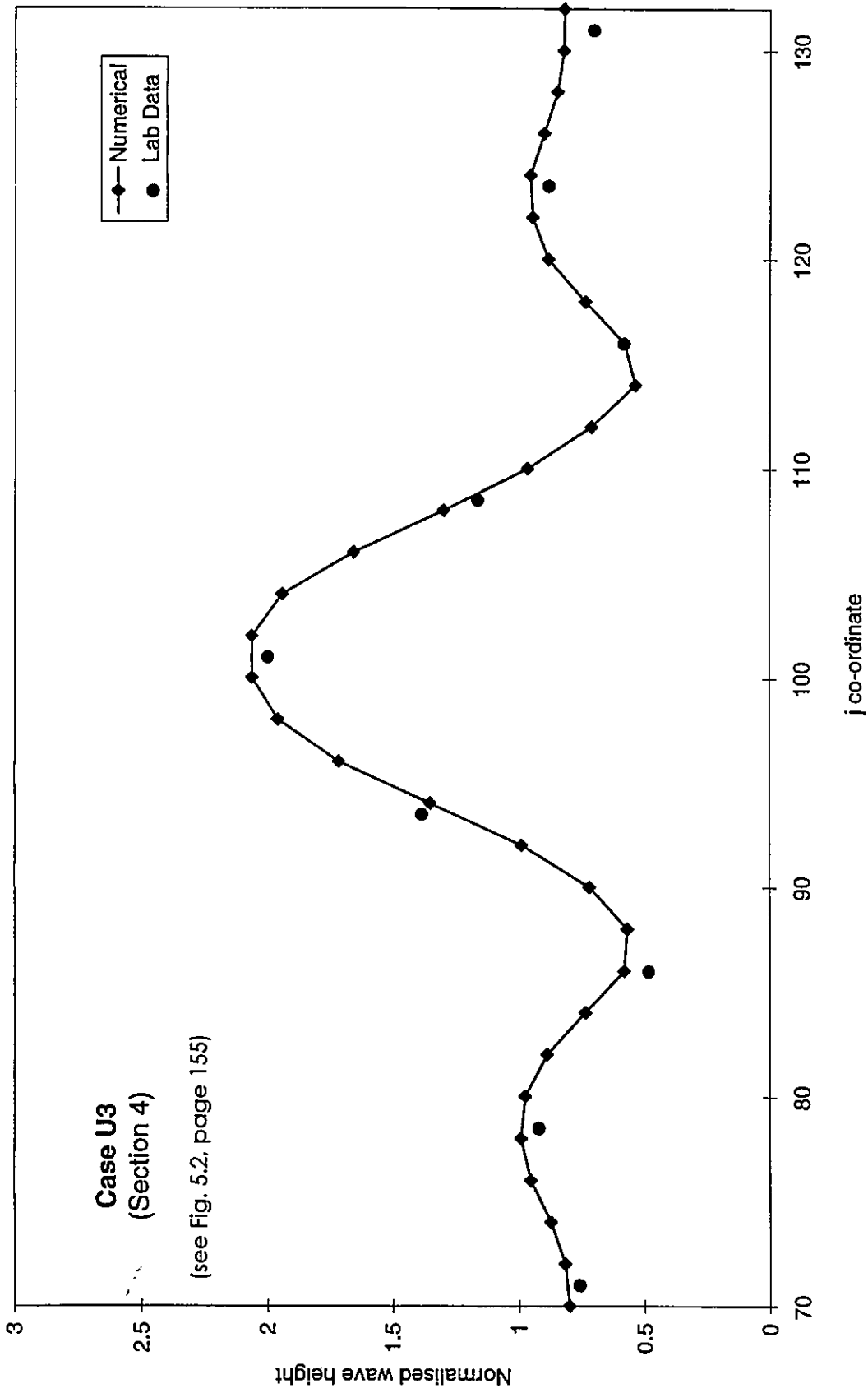
Fig. 5.21 - Comparison between experimental data of Vincent and Briggs (1989) and computational results for case U3. Section 4.
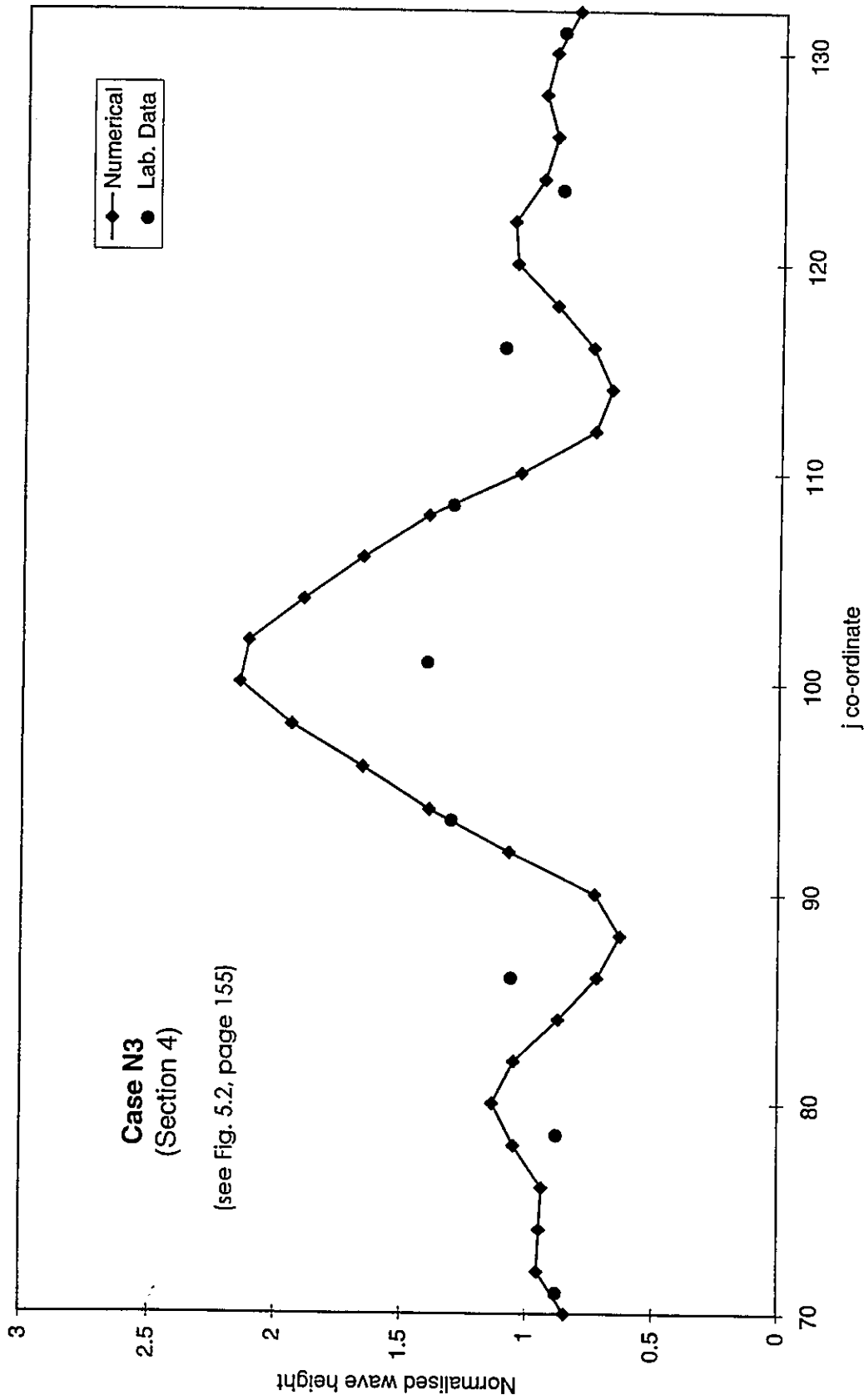
Fig. 5.22 - Comparison between experimental data of Vincent and Briggs (1989) and computational results for case N3. Section 4.
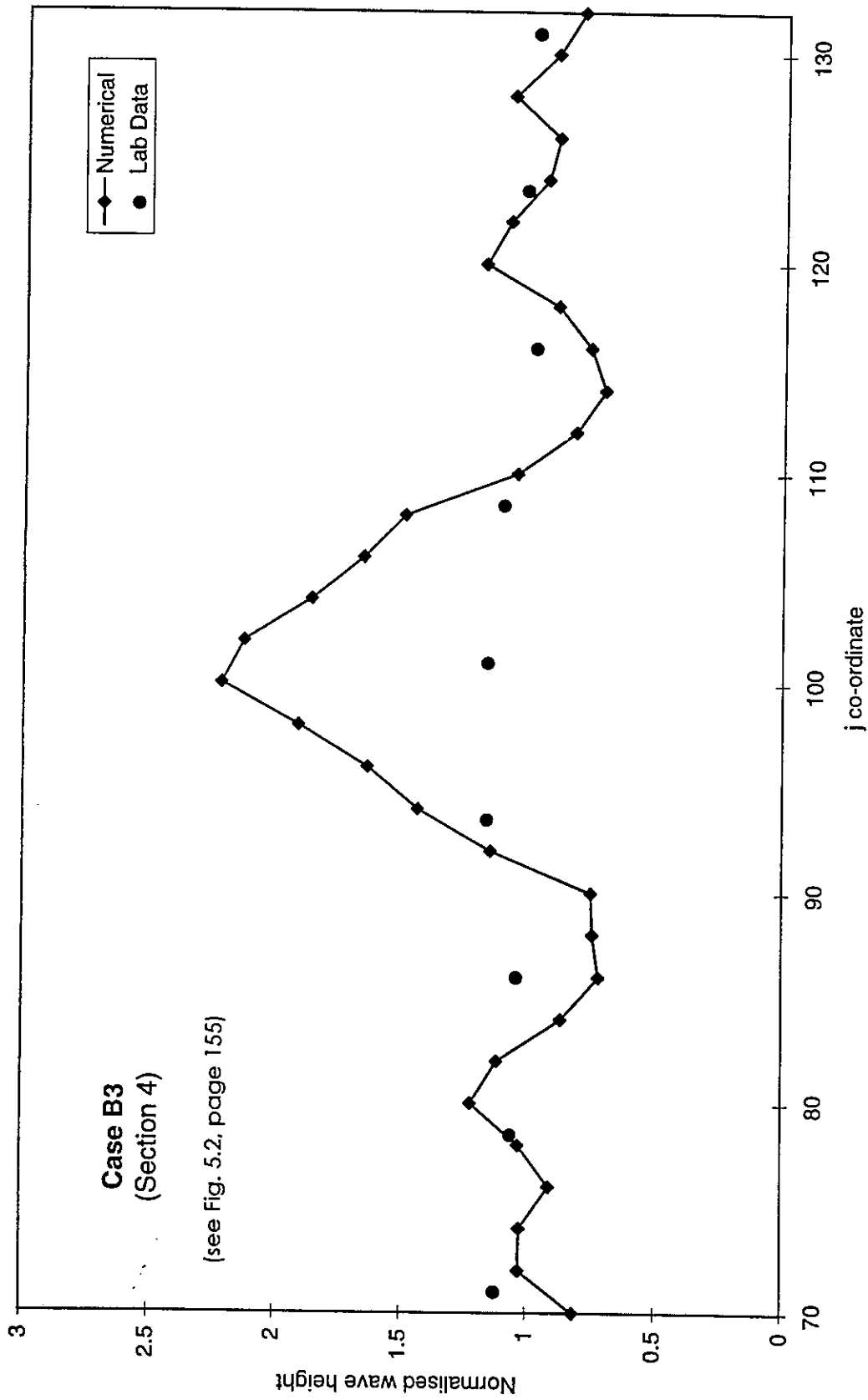
Fig. 5.23 - Comparison between experimental data of Vincent and Briggs (1989) and computational results for case B3. Section 4.
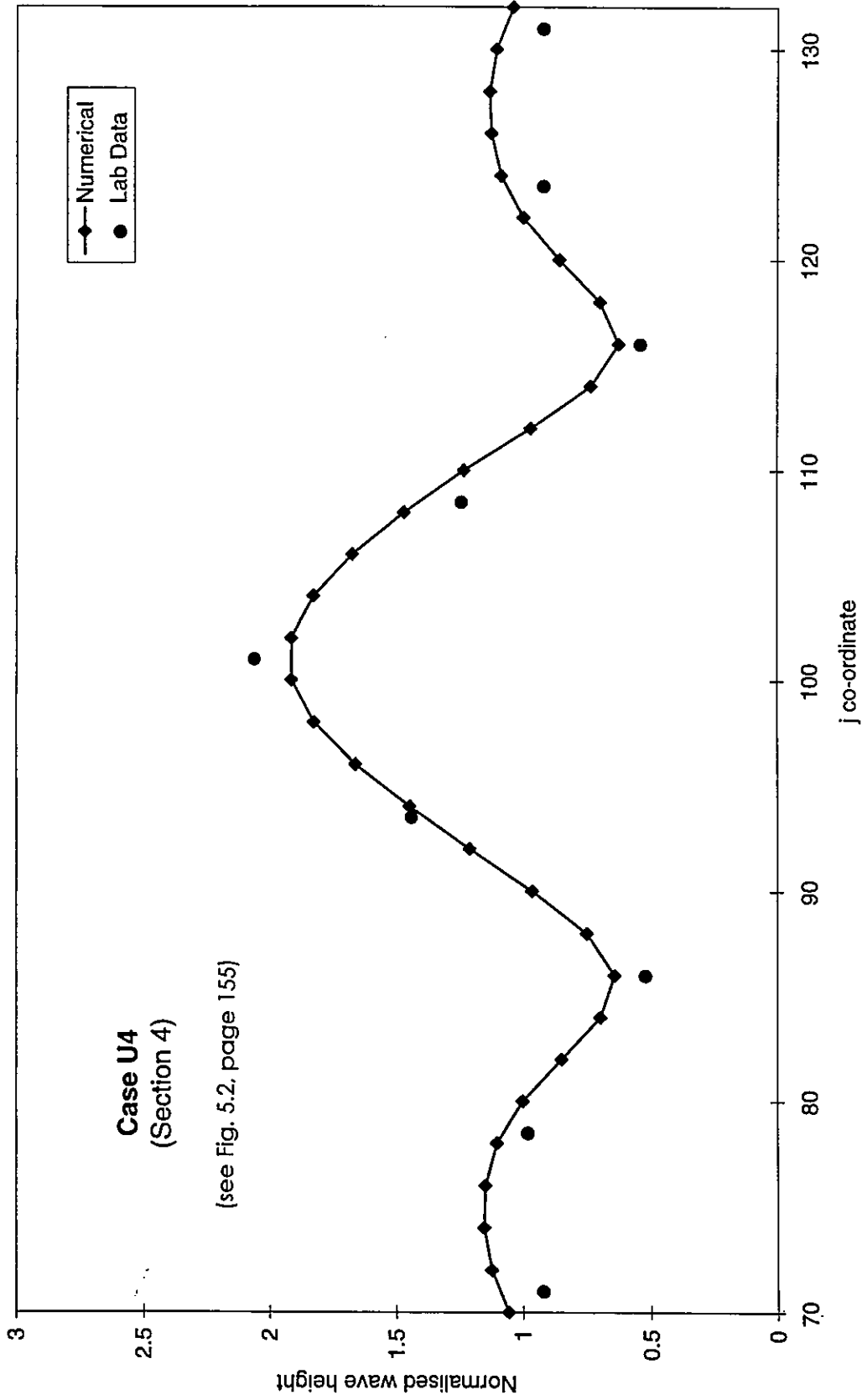
Fig. 5.24 - Comparison between experimental data of Vincent and Briggs (1989) and computational results for case U4. Section 4.
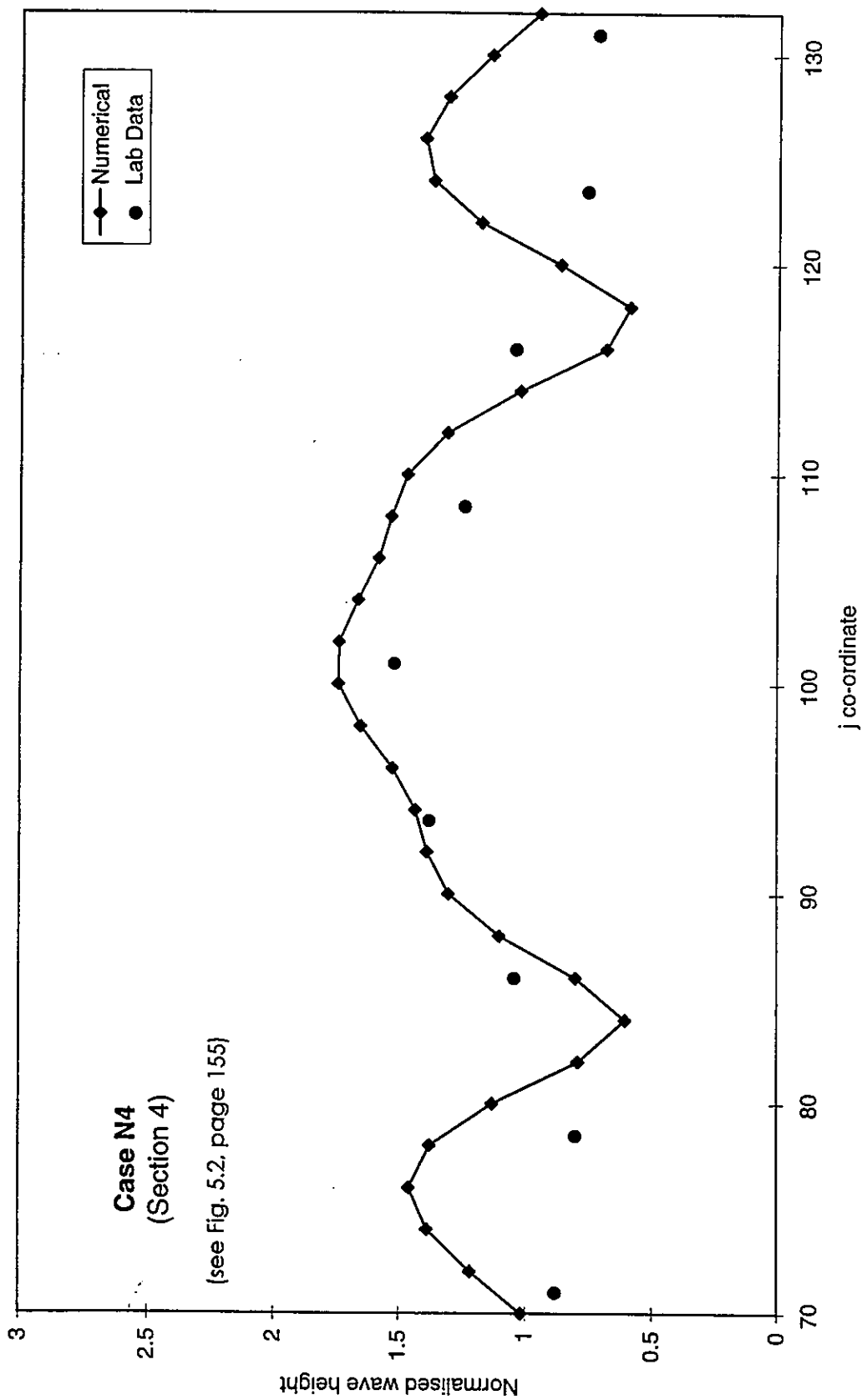
Fig. 5.25 - Comparison between experimental data of Vincent and Briggs (1989) and computational results for case N4. Section 4.
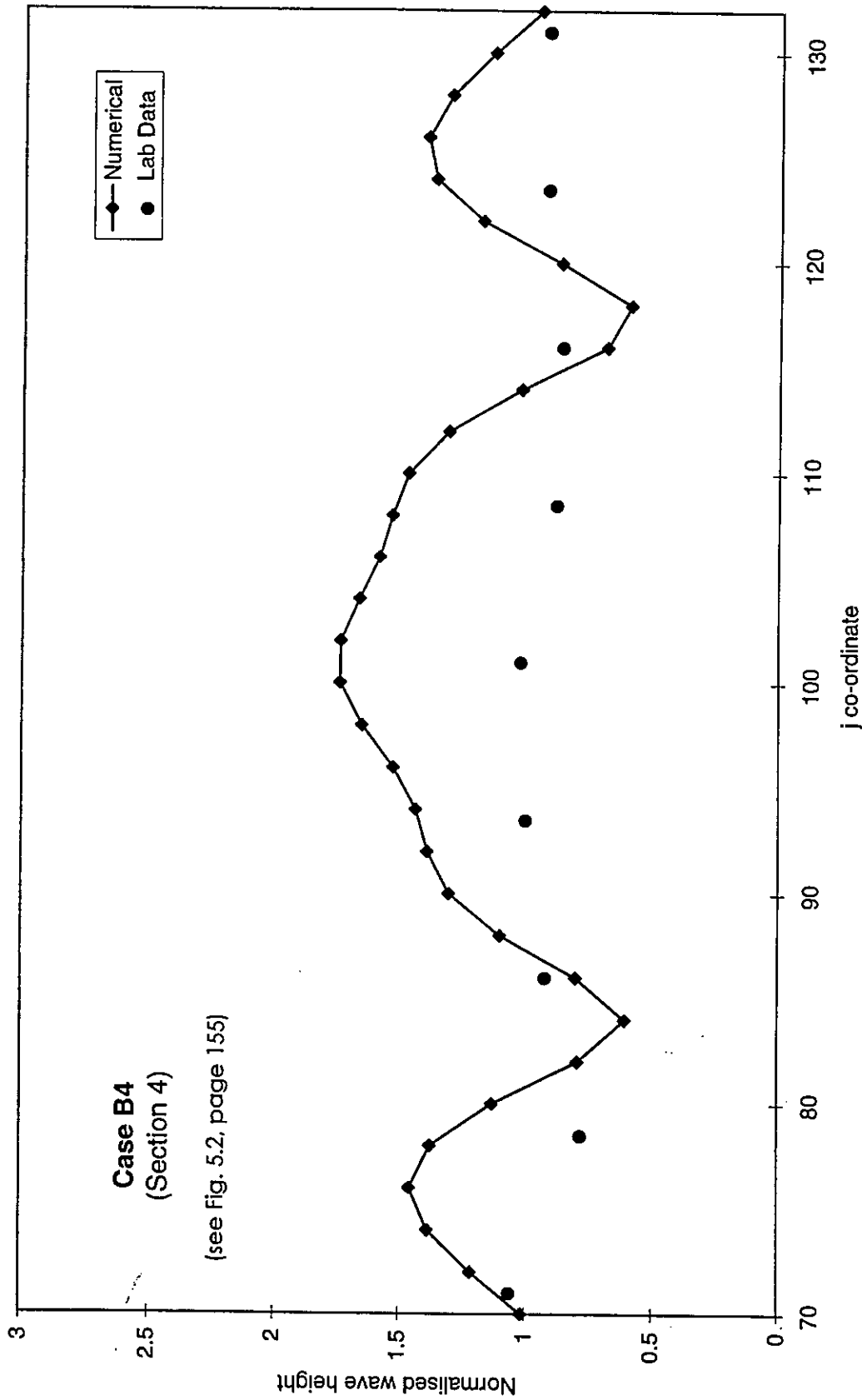
Fig. 5.26 - Comparison between experimental data of Vincent and Briggs (1989) and computational results for case B4. Section 4.

Chapter 6

Modelling of the Wave Breaking Phenomenon

6.1 - Introduction

In this chapter the objective is to incorporate the phenomenon of random wave breaking into the numerical model developed in the previous chapter.

The chapter is organised as follows:

*   The following section introduces the subject of wave breaking and gives a detailed description of the phenomenon.
*   Section 6.3 presents a description and discussion of the different criteria that have been used to describe regular wave breaking.
*   In section 6.4 the methods used to predict random wave breaking are reviewed.
*   Section 6.5 proposes 2 different methods to predict random wave breaking and their incorporation into the numerical model for irregular waves developed in the previous chapter.
*   Tests to validate the numerical model proposed in the previous section are described in section 6.6. The computed results of the tests are compared with available data from Vincent and Briggs's (1989) laboratory experiments. A discussion on the performance of the model is then presented.
*   Finally a critical summary regarding the research work developed within this chapter is done in the last section of this chapter, section 6.7.

6.2 - The physics of wave breaking

In the nearshore region there is another important process that determines wave transformation besides shoaling, refraction, diffraction and reflection: it is wave dissipation due to wave breaking. Wave dissipation or decay in the nearshore region is due to bottom friction, percolation through a porous bottom and wave breaking. Unless we are in the presence of a very muddy bed, the first two processes can be neglected as authors like Thornton and Guza (1983) or Dally et al (1985) suggest.

Wave breaking is extremely important not only when considering wave propagation onto a beach where it plays a very important role in transporting sediments and in the generation of currents but also for designing coastal structures, where a prediction of the maximum wave height is of paramount importance to a project.

Wave breaking is a non - linear phenomenon that occurs on the so called surf zone. The surf zone is the area limited by the shoreline and the wave breaking line, which can be considered as the offshore line at which, waves start breaking in progressing towards the shore. The physical phenomenon can easily be identified by its visual characteristic which is the wave crest curling over the surface. The fluid motion in breaking random waves is highly complex and precise mathematical description of the phenomenon is a difficult task although attempts have been made to do so using linear and non - linear theories. Basically quantitative knowledge on breaking waves has been obtained empirically. For the highly non - linear phenomenon of wave breaking the fluid accelerations no longer can be assumed to be small compared to gravity nor is the particle velocity small compared to the phase velocity. The particle orbits are not closed and generate an excess momentum flux, or radiation stress, in the direction of wave propagation after averaging over a wave period (Southgate, 1986). When waves break this excess momentum flux is released generating the wave - induced currents (longshore and cross-shore) and the wave set - up.

Knowledge about breaking waves initially derived from particular attention devoted to regular wave studies. Thus, concepts like breaking point, which can be defined as the point of maximum wave height or the point when the first water particle comes

out of the wave crest according to the breaking criterion under consideration, cannot be so clearly defined for irregular waves.

Waves break in different ways depending on wave height, wave period, beach slope and wind effects (qualitatively so well known by surfers). Based on observations, authors like Galvin (1972), Peregrine (1983), Southgate (1988) and Smith and Kraus (1991) have identified 4 types of breaking according to their visual characteristics (Fig. 6.1):

- Spilling: White water appears at the wave crest and spills down the front face of the wave. The upper 25% of the front face may become vertical before breaking. Usually occurs on flat or gently sloping beaches.

- Plunging: The whole front face of the wave steepens until vertical; the crest curls over the front face and falls into the base of the wave, sometimes proceeded by the projection of a small jet. Usually occurs on moderate steep beaches.

- Collapsing: The lower part of the front face of the wave steepens until vertical, and this front face curls over as an abbreviated plunging wave. Minimal air pockets and usually no splash - up is observed. This type lies between the two previous types, and many times the distinction is not clear.

- Surging: The wave slides up the beach with little or no bubble production. The water surface remains almost plane, except where ripples may be produced on the beach face. Usually occurs on very steep beaches.

These properties of breaking waves in the surf zone appear to be governed by the parameter ξ_0 defined as

$$\xi_0 = \frac{\tan\beta}{\sqrt{\frac{H}{L_0}}},$$ (6.1)

or the inshore parameter ξ_b defined as

$$\xi_b = \left(\frac{H_b}{L_0}\right)^{-0.5}.$$ (6.2)

Thus, the following classification of breaker types can be established:

- surging or collapsing if $\xi_0 > 3.3$ or $\xi_b > 2.0$.
- plunging if $0.5 < \xi_0 < 3.3$ or $0.4 < \xi_b < 2.0$.
- spilling if $\xi_0 < 0.5$ or $\xi_b < 2.0$.

When breaking occurs the particle motion undergoes a transformation from irrotational to rotational motion generating vorticity and turbulence. Until the present date no theoretical model allows an accurate estimation of wave height reduction. Such a model would be based on a rotational analysis allowing to calculate the mean velocity field through the water column during the rapid transformation process of the motion. As no such model exists, a proper determination of energy dissipation and radiation stress can not yet be done. One step necessary in order to overcome this unsolved problem is to understand qualitatively the mechanisms and processes governing the mean flow just after breaking and this was done by Basco (1985) (Fig. 6.2). He described with a reasonable depth the mechanisms involved in the breaker types that most commonly occur in the surf zone: spilling and plunging. He further developed some research work done by Svendsen (1984), who introduced some fundamental concepts in wave breaking analysis like the surface roller (secondary vortex that propagates forward with a bore - like motion and has a similar scale as the plunger vortex which is left behind), and spatial sub - zones (transition, inner and swash zone) within the surf zone (uniform beach) where a sequence of visual transformation of the broken wave can be identified. Another contribution done by Basco (1985), even more important than the first one, was the identification of a secondary wave that can be generated when breaking occurs. Although this fact can only be supported by visual observations, Basco suggested a very convincing explanation: the plunger vortex (rotating fluid mass system generated by the overturning jet) that translates backwards acts like a wave paddle over the fluid between itself and the roller vortex that propagates forward, generating a secondary wave with kinematics completely different from the original wave. Although further investigation is necessary to prove this theory, it seems quite plausible and it can be the explanation as to why we can see waves reforming after breaking.

Besides the mechanisms involved in the physical process of wave breaking there are two other aspects where some progress has been achieved in the understanding of the breaking phenomenon. They regard turbulence generation and spatial distribution of the different stages of evolution of the phenomenon. Regarding the first aspect, once again an accurate quantitative knowledge is not yet established, however turbulence is produced, convected, diffused and dissipated when breaking occurs. Dissipation happens through two main areas: the outer radius of

the plunger vortex that translates backwards, and at the interface between the surface roller or vortex that propagates forward and the water below. An interesting estimate, suggested by Svendsen (1984), is that only about one - third of the energy that corresponds to a 35% drop in wave height in the outer or transition region (first sub - zone in the surf zone, where rapid transitions of the wave shape occur) is due to real energy dissipation. The other two - thirds of wave height decrease are due to redistribution of energy (and momentum). Potential energy is converted into forward momentum flux that is concentrated in the surface roller or vortex. Without doubt Svendsen (1984) undertook a crucial investigative work that enormously contributed to the understanding of the surf zone. However, his theory was developed for the inner zone (sub-zone that follows the transition zone, where a rather slow change in the wave shape can be observed, the wave front resembles a bore, and the wave to water depth ratio is almost constant). Therefore the above remarks regarding the wave height decrease within the transition zone were derived based on deductions resulting from the analysis of the wave before the breaking point and within the inner region, where in fact Svendsen's theory gives excellent results for wave height and set - up.

With regard to the spatial distribution of the different stages of evolution of the phenomenon, different classifications have been proposed by a number of authors. For example, Seyama and Kimura (1988) divided the surf zone into two regions (plunging and bore region), and called the area just before breaking the shoaling region. They considered the point between the plunging and the bore region to be around the point where $h/h_b = 0.6$. However, in being consistent with the points considered when describing turbulence (previous paragraph), the classification that seems more practical and better describes the wave shape evolution is the one attributed to Stive (1984). The outer zone is the region delimited from the breakpoint (where the overturning of the jet starts) and the point where the water depth ratio is almost constant. Within this region rapid transitions of the wave shape are observed. There follows the inner region where a rather slow change in the wave shape occurs and the wave front resembles a bore. Finally immediately shorewards is the run - up region where the shoreline is visible and the flow can be characterised by a quasi - steady breaking motion, like a bore, independent of the breaker type.

6.3 - Modelling regular wave breaking

The phenomenon of wave breaking was described and discussed in the previous section, based on state of the art work to the present date. In this section breaking will be discussed under the perspective of modelling the phenomenon.

Modelling wave decay due to dissipation through breaking is a complex task, therefore the initial approach taken by researchers in the field achieved reasonable results under the assumption of the waves being regular. In this section a literature survey is done in order to understand how the problem was approached and to enable further study of the more complex problem that is the phenomenon of random wave breaking.

The pioneer researchers who model wave transformation by breaking realised that a criterion to determine its occurrence had to be established. As breaking depends on variables like bottom slope, wave steepness and wave form, criteria based on limiting the wave height, the wave steepness or even the wave crest velocity where established. Miche (1944) was one of the first authors who suggested a criterion where wave stability depends on the wave steepness, H/L. Using Stokes wave theory he proposed the formulation

$$\frac{H}{L} = 0.142 \tanh\left(\frac{2\pi d_b}{L_b}\right)$$ (6.3)

valid for any water depth. For deep water it reduces to H/L=0.142 and for shallow water to H/L=0.78. In fact, this conclusion was in agreement with the ideas of Michell (1893) who, considering a maximum crest angle of 120°, found the same criterion for deep water where there is no influence of the bottom slope on the wave kinematics.

More recently authors (e.g. Battjes and Janssen, 1978; Holthuijsen et al, 1989; Anderson et al, 1991) used a modified Miche - type relation:

$$H_b = 0.88 \, k^{-1} \tanh\left(\frac{\gamma k h}{0.88}\right)$$ (6.4)

where γ is a wave height to water depth ratio. Battjes and Stive (1984) investigated the influence of the bottom slope and the incident wave steepness on this last

parameter and they found it independent of the bottom slope. They proposed the expression

$$\gamma = 0.5 + 0.4\tanh\left(33\frac{H_0}{L_0}\right).$$

(6.5)

Another criterion is the breaker height to breaker depth ratio. McCowan (1891) studied the phenomenon based on solitary wave theory and he found a value for the breaker wave height inferior to the one derived from equation (6.3). He suggested the constant value $H_b/d_b = 0.78$. Although this formulation is not the most accurate to predict wave breaker height because important factors like wave steepness are not taken into consideration, it is very much used in numerical models to predict wave transformation in the nearshore region. This fact is due to the simplicity involved in its incorporation in models and to the fact that it provides reasonable prediction of wave decay in a surf zone where the water depth is monotonically varying. Based on the same theory, Munk (1949) derived a different expression

$$\frac{H_b}{H_0} = \frac{1}{3.3(H_0 \cdot L_0)^{\frac{1}{3}}}$$

(6.6)

from where the breaker height for a non-refracted wave can be derived. This criterion does not seem a very good suggestion as the breaker height only depends on deep water parameters and therefore does not allow a wave to reform and eventually to break more than once.

Another, different, group of formulations was suggested by several authors. They all consider the influence of the bottom slope and the first one was derived by Le Mehaute and Koh (1967)

$$H_b = 0.76\,H_0\left(\frac{H_0}{L_0}\right)^{-0.25} m^{\frac{1}{7}},$$

(6.7)

where m is the bottom slope.
Later, Weggel (1972) proposed a relation, also including the effects of bottom slope, in order to estimate the maximum breaker height that a coastal structure might be subjected to

$$\frac{H_b}{d_b} = \frac{1}{0.64\left(1 + e^{-19.5m}\right)} + 4.46\left(1 - e^{-19m}\right)\frac{H_b}{T^2} \qquad (6.8)$$

This criterion has been widely used in coastal engineering practice and is recommended in the US Army's Shore Protection Manual. Smith and Kraus (1991) extended the data set used by Weggel (1972) to deeper waters and found the formulation

$$\frac{H_b}{d_b} = \frac{1.12}{\left(1 + e^{-60m}\right)} + 5.00\left(1 - e^{-43m}\right)\frac{H_0}{L_0}, \qquad (6.9)$$

that is valid for $0.0007 \leq H_0/L_0 \leq 0.0921$ and $1/80 \leq m \leq 1/10$.

As it can be realised, different formulations have been suggested for determining the wave breaker height. The existence of such a vast number of formulations can be due to basically 2 factors: some simply differ because they were derived from different data sets and therefore are valid for different water depth ranges; and another important factor is that the above formulations were derived to fit data measured using different wave measurement systems.

All the previous formulations are based on the concept of limiting directly the wave height. However, a different type of models is based on the wave energy equation from where energy dissipation by breaking can be estimated. The wave energy equation can be expressed as

$$\frac{\partial}{\partial x}(E\,C_{gx}) = -\varepsilon \qquad (6.10)$$

where E is the mean wave energy density, C_{gx} is the shoreward component of the group velocity, and ε is the energy dissipation per unit surface and per unit of time due to wave breaking.

The most popular model is the one where broken waves are treated as bores (hydraulic jumps that translate in the direction of the initial wave), for spilling and plunging breakers. Based on this theory the energy dissipation rate can be considered as

$$\varepsilon = \frac{1}{4}\rho g\frac{(h_2 - h_1)^3}{h_2 h_1}Q \qquad (6.11)$$

where Q is the discharge across the bore, $Q = v_1 h_1 = v_2 h_2$ and v_1 and v_2 the relative flow velocities to the shock discontinuity. Authors like Hwang and Divoky (1970), Battjes (1986), Battjes and Janssen (1978) and Thornton and Guza (1983) considered $Q = Ch/L$ with $C = \sqrt{gh}$. Assuming $(h_2 - h_1)^3 = H^3$ and $(h_2 h_1) \approx h^2$ they derived the following expression for the energy dissipation rate

$$\varepsilon = B\frac{1}{4}\rho g\frac{H^3}{hT}$$ (6.12)

where B is a parameter that evaluates the suitability of the assumption that the bore resembles a hydraulic jump. Obviously for the theoretical hydraulic jump B would be equal to 1. The validation of this theoretical model was done by authors like Stive (1984) for a mild beach slope of 1:40. He measured the flow fields of a hydraulic jump and a regular broken wave and realised that the mean wave energy dissipation rate was underestimated from the hydraulic jump formulation by 30 to 50% (Svendsen et al, 1978, reported a value of 20 to 30%), which can be explained by the effects of the turbulent flux of momentum. However he observed a close resemblance between the two flow fields and so he decided to readjust the formulation and create a new model where instead of the empirical parameter B he now had two different parameters, one concerning the energy dissipation rate and the other the wave set - up. Comparisons between his numerical results and the experimental data now showed a good estimation of the wave height but poor prediction of the wave set - up. Summarising, it can be said that authors who applied the formulation based on the bore model reported a reasonable success. Between these authors are Battjes (1986), Stive (1984) and Yamaguchi (1986) who applied the model for regular waves.

The bore model approaches the phenomenon more accurately than the previous model strictly based on limits of wave condition because it is derived from a physical concept. It should also give a better evaluation of wave decay because the wave height is proportional to wave energy. Besides it can be applied without the constraints of the previous model where most of the formulations derived are valid for monotonically varying sea beds. However, when considering its incorporation into a wave propagation model, there still remain two unsolved

problems associated with the exact location of initiation of wave breaking, and value of the empirical parameter B.

Aiming to develop a more accurate wave breaking model where the energy dissipation rate was given by the hydraulic jump approximation, Svendsen (1984) thought that an extended form of the energy balance would allow a better description of the reformed wave height and the mean water level. He thought that this would be achieved if the wave energy equation would include an extra term besides the energy flux and the energy dissipation (as equation 6.10). This extra term is associated with the radiation stress. His idea was based on the fact that when breaking occurs part of the wave energy is converted into forward momentum flux in the vortex roller, therefore increasing the radiation stress, which is associated with a similar increase in the energy flux. He suggested the following expression for the wave energy equation

$$\frac{\partial}{\partial x}(EC_{gx}) + \frac{\partial}{\partial x}(E_r C) = -\varepsilon \qquad (6.13)$$

where the second term concerns the energy flux carried by the surface roller, that is

$$E_r = \rho \frac{AC}{2T} \qquad (6.14)$$

with A the roller area (A $\approx$ 0.9H^2), C the phase velocity and T the wave period.
In fact, this makes sense, because an increase in the energy flux due to the vortex roller requires an equivalent increase in the absolute value of the dissipation rate, which is in agreement with his experimental results mentioned 2 paragraphs before. Although this formulation improves wave height estimates in the inner surf zone it does not give satisfactory results for the set - up.

Two other types of models based on the wave energy equation should be mentioned. The differences between them and the bore model concern the expression proposed for wave energy dissipation. One of them can be called a turbulent model and the other a stable wave height model. The first is based on the concept that turbulence is the main mechanism of dissipation in the surf zone and that turbulence is statistically isotropic. Based on this idea Mizuguchi (1980) proposed the following formulation

$$\varepsilon = \frac{1}{2}\rho g \, \nu \, (k \, H)^2 \qquad (6.15)$$

where k is the wave number and v is the molecular viscosity for irrotational flows. However he replaced the molecular viscosity v by the turbulent eddy viscosity v_e which is based on the wave and beach profile characteristics and can be written as

$$v_e = v_{eB}\left(\frac{H - c'd}{\gamma h}\right)^q$$ (6.16)

where v_{eB} is v_e at the breaker line, c' is the ratio between the wave height and the water depth in the wave recovery zone of a constant depth beach, γ is the breaker depth index described before and q an empirical parameter.

Another turbulent model for a turbulent flow that considers waves and currents was proposed by Izumiya and Horikawa (1984). The wave motion was assumed to be irrotational. The following expression was proposed

$$\varepsilon = \frac{\gamma \beta}{\rho^{1 2}}\left(\frac{E}{h}\right)^{3 2}\left(\frac{2C_g}{C} - 1\right)^2$$ (6.17)

where γ is the breaker depth index and β a non-dimensional coefficient dependent on the wave characteristics and on the mean water depth. The product $\gamma\beta$ is given by

$$\gamma \beta = \beta_0 \sqrt{\frac{C_g E}{C\rho gh^2} - 0.09}$$ (6.18)

with $\beta_0 = 1.8$.

Finally the stable wave height model, is a particular model based on the idea of wave height stabilisation at some value in a uniform depth after wave breaking. This idea came out from laboratory and real sea data observations, therefore the model describes intuitively the transformation of regular waves in the surf zone. The model was proposed by Dally (1980) who claimed good agreement with laboratory results (Dally et al, 1984, 1985). However the model requires to be calibrated for a pair of empirical parameters which does not make the model as simple and as easy to apply as the author claims.

A good description of the phenomenon of wave breaking should allow us to predict its spatial occurrence, the reformed wave height and the mean water level. None of the above models does this, although as it was said, some of them approach the

physical phenomenon more empirically than others. However, there is one aspect that none of the existing models up to the present date considers, which is the steepness of the reformed wave that can generate waves breaking more than once in the surf zone.

6.4 - Modelling irregular wave breaking

Modelling random waves is a complex task and that is because the concept of breaking point is difficult to quantify, non - linear wave interactions that influence the breaking process are not well understood, and much of the knowledge derived from investigating the breaking phenomenon is empirical.

It is very obvious intuitively that approaching the phenomenon of wave breaking assuming that the waves are monochromatic would lead to erroneous estimates. In fact this was observed by Vincent and Briggs (1989) who by performing laboratory experiments were able to compare results for both cases and conclude about the differences.

The first attempt to incorporate the influence of randomness in the breaking phenomenon in models of wave propagation was done by applying a certain breaking criterion derived empirically to a representative parameter of the sea state, like the significant wave height. More recently, a different approach has been proposed. This approach consists of applying a breaking criterion to waves discretised by a component approach method, that is, to individual wave components, under the assumption of their linear superposition. In fact the model developed for this work which will be described in the next section proposes two criteria based on this approach. The following paragraphs are dedicated to describing both of the approaches starting from the empirical formulation applied to a monochromatic wave representative of the sea state.

Goda (1975) was one of the first authors who suggested a formulation for wave breaking considering the phenomenon of wave propagation as a random process.

The criteria determines that the breaker height at a given water depth is a function of L₀ and m,

$$\frac{H_b}{d_b} = A \frac{L_0}{d_b}\left\{1 - \exp\left[-B\frac{\pi d_b}{L_0}\left(1 + Km^s\right)\right]\right\} + C$$

(6.10)

where A=0.17, B=1.5, C=0, K=15 and s=4/3. Izumiya and Isobe (1986) further investigated Goda's expression for non-uniformly sloping beaches and proposed that under these circumstances, the bottom slope m, to be considered should be a value defined as the mean slope in the distance 5d_b offshore from the breakpoint. Moreover, Seyama and Kimura (1988) set - up irregular wave breaking experiments on uniformly sloping beaches and found a new set of coefficients for equation (6.10), under the consideration that the value for water depth is not the still water depth as considered in the above equation but a value accounting for the differences of the crest and trough amplitudes of non - sinusoidal waves. They obtained the coefficients A=0.16, B=0.8, C=0.2, K=15 and s=4/3. Although Goda's formulation, equation (6.10), was based on a large number of data carefully analysed and therefore making it reliable, when this criterion is used in connection with linear theories, the breaking point is predicted a little bit shoreward of the true breaking point. This is due to the fact that linear wave theories underpredict the wave height increase just prior to the breaking point. To overcome this difficulty, Watanable et al (1984) reanalysed Goda's criterion and proposed to use the ratio of water particle velocity at still water level, u_b to wave celerity, c_b , as a breaker index. This criterion was originally given in a graphic form but for the convenience of numerical calculation Isobe (1987) proposed the following formula

$$\frac{u_b}{c_b} = 0.53 - 0.3\exp\left(-3\sqrt{d_b/L_0}\right) + 5\, m^{1.5}\exp\left(-45\left(\sqrt{d_b/L_0} - 0.1\right)^2\right).$$

(6.11)

Another group of formulations proposed concern a breaking criteria based on energy considerations. One of the first proposals was done by Komar and Gaughan (1972), who derived the following expression from experimental data:

$$H_b = K\, g^{0.2}\left(H_0 T\right)^{0.4}.$$

(6.12)

were k = 0.39 from best fitting to experimental data.

Izumiya and Horikawa (1984) introduced the concept of critical wave energy at breaking, E_c. They derived an expression for the maximum wave energy that a wave can reach without breaking,

$$\frac{E_c}{\rho g d^2} = \frac{1}{1+a(H/d)_c}\left(\frac{H}{d}\right)_c^2 U_{rc}^{-1/2}\left[1-\frac{2}{1+a(H/d)_c}U_{rc}^{-1/2}\right] \qquad (6.13)$$

where $(H/d)_c$ should be calculated from Goda's expression, equation (6.10), $a=0.33$ and U_{rc} is the Urssel number,

$$U_{rc} = 2\pi A\frac{L_0}{d}\left(\frac{H}{d}\right)_c. \qquad (6.14)$$

An interesting approach is based on the idea of associating limiting wave relations with joint distributions of wave heights to obtain a random wave transformation model inside the surf zone. As it was explained in the previous chapter, the wave height, H, can be assumed to follow a Rayleigh distribution and so breaking can be simulated by truncating the tail of the Rayleigh distribution. Different breaking criteria (Fig. 6.3) were suggested by different authors and they are briefly summarised as follows:

- Collins (1970) and Battjes (1972) used a sharp cut - off of the Rayleigh probability density function, with all waves that are breaking or have already broken having heights equal to H_b. Differences arise from using different breaking criteria.

- Kuo and Kuo (1974) also used a sharp cut - off at H_b but, assuming that broken waves are smaller than H_b, they redistributed them across the range of wave heights in proportion to the probability of unbroken waves at each height.

- Goda (1975) assumed wave breaking to occur in a range of wave heights (H_{b1} H_{b2}) with a linearly varying probability. According to the author, breakers are spread over a certain range to account for the variability of breaker heights, and to partially compensate for the inaccuracy of using a single wave period. Broken waves are redistributed in proportion to the probability of unbroken waves, thus resulting in a gradual cut - off of the initial probability density function.

Although these models are based on interesting theoretical considerations they were intuitively derived because some of the assumptions, like redistribution of wave heights, have not been confirmed yet. The main shortcoming of these models is that they were derived for a monotonically varying water depth and therefore cannot be applied to non - monotonically depth decreasing surf zones. Furthermore the Rayleigh distribution may be only correctly applied to linear waves and so would not be expected to work for waves near breaking in the surf zone.

Two other models were based on the same assumption, that is that the wave height follows a Rayleigh distribution which is truncated by breaking, but they have one point in their favour which is that they are wave energy equation models. They have a better physical support than the wave limitation condition models so are more reliable. One of them was developed by Battjes and Janssen (1978) who assumed that: the probability function for the lower, non - broken waves, is the same as it is in the absence of breaking, that is of Rayleigh type; there is a maximum value of the wave height, H_m, possible to occur at each depth; and that broken waves continue to propagate with the same wave height, H_m. Based on these assumptions and on the fact that the broken wave dissipates with a bore - like motion they derived the following expression for the energy dissipation rate:

$$\varepsilon = B \frac{1}{4} \rho g \frac{f_p}{h} H_m^3 Q_b$$

(6.15)

where Q_b is the probability of occurrence of broken waves and is governed by the formulation

$$\frac{1 - Q_b}{\ln Q_b} = -\left(\frac{H_{rms}}{H_m}\right)^2 .$$

(6.16)

The model was applied (with B=1, fully developed bore) to an extensive set of experimental and field data for purposes of calibration and verification (Battjes and Stive, 1984, 1985) showing a generally good agreement and a high degree of realism.

The other model based on the wave energy equation method was proposed by Thornton and Guza (1983). They analysed a large number of field data at the coast of California which led them to conclude that the use of the Rayleigh distribution gives a reasonable description of waves in the surf zone. Based on that, they

expressed the distribution of breaking wave heights, $p_b(H)$, as a weighting of the Rayleigh distribution, $p(H)$, for all waves:

$$p_b(H) = W(H)\, p(H) \tag{6.17}$$

where $W(H)$ is the weighting function, desired to be as simple as possible to give a good fit of $p_b(H)$ to the observed distributions, such as

$$W(H) = \left(\frac{H_{rms}}{\gamma h}\right)^n \left\{ 1 - \left[1 + \left(\frac{H_{rms}}{\gamma h}\right)^2 \right]^{-5.2} \right\}. \tag{6.18}$$

with $\gamma=0.42$ and $n=4$.

Model results were compared with both laboratory and field data. The accuracy of the model was dependent on the parameter B.

Both last models have given good predictions and are built up from simple ideas. Nevertheless, they both depend on empirically determined parameters, thus requiring calibration.

From now on the attention will be focused on the other breaking approach mentioned at the beginning of the section. It assumes that at each location the sea state can be represented by a linear superposition of individual monochromatic components therefore the remaining problem when considering breaking is to either implement a breaking criterion that can be applied to each individual component on each location in the surf zone or to calculate the total amount of dissipation for each location in the surf zone and then distribute it between the individual components. Isobe (1987) attempted to implement the first alternative. He developed an irregular wave propagation model based on a parabolic approximation of the mild - slope equation that is applied to each individual wave component. In the surf zone, energy dissipation is modelled based on the wave energy equation, equation (6.11), for each component. The energy dissipation rate, ε, for each component is assumed to be proportional to its energy,

$$\varepsilon = f_D E, \tag{6.19}$$

where f_D is the dissipation rate factor for irregular waves that can be written as

$$f_D = Q_b f_D' \tag{6.20}$$

with Q_b as the probability of breaking waves and f_D' a modified dissipation rate factor for regular waves.

On the assumption that the distribution of u/C of individual waves can be approximated by the Rayleigh distribution, Q_b can be calculated as

$$Q_b = \left[1 + 2.004\left(\frac{\gamma_b}{\gamma_{1/3}}\right)^2\right]\exp\left[-2.004\left(\frac{\gamma_b}{\gamma_{1/3}}\right)^2\right]$$ (6.21)

with γ_b given by equation (6.11) and $\gamma_{1.3}$ representing the significant value of the ratio of water particle velocity to wave celerity without breaking.

The modified dissipation rate factor for regular waves is calculated based on

$$f_D^I \propto \sqrt{\gamma - \gamma_r}$$ (6.22)

where γ is the ratio of water particle velocity to wave celerity and γ_r the same ratio at the wave recovery zone. In his numerical experiment Isobe used experimental data obtained for constant bottom slopes to calculate a certain number of parameters involved in the calculation of γ and γ_r, together with the assumption that the ratio of water particle velocity to wave celerity at the breaking point for individual waves is 20% smaller than that for regular waves, therefore $\gamma_b = 0.8\,\gamma_b{}'$.The last assumption was made without any basis of scientific support because, although the breaker height of an individual wave component of irregular waves is known to be smaller than that of regular waves, a quantitative evaluation has not yet been done. A simple application of the model was performed for a plane sloping beach, but no comparisons were made.

6.5 - Implementation of the breaking phenomenon in the numerical model

The numerical model for irregular wave transformation where the breaking phenomenon will be implemented is the model described in the previous chapter. The randomness of the sea is simulated by frequency and directional independent components which are treated as monochromatic waves and transformed within the numerical domain by means of the governing equation, which is the elliptic form of the mild - slope equation. The directional spectra was chosen to be discretised using the criterion of equal energy components because, as it was mentioned in the previous chapter, it gives a better simulation of the random sea particularly if a small number of components is used. At each location the water

surface elevation is assumed to be equal to a linear superposition of that arising from each individual spectral component.

As it was discussed in the previous section, wave dissipation by breaking has never been implemented successfully in a numerical model based on the mild - slope equation for irregular wave transformation. In this section two proposals to simulate the phenomenon are suggested. The first is based on the idea of calculating the energy dissipated by each component at each location, and the second involves calculating the total energy dissipation at each location and then distributing it to the different components. The following paragraphs are dedicated to describing both approaches.

The idea for the first method was developed based on the acknowledgement of the research work done by the SWAMP group. They are a group of researchers who do ocean wave modelling based on the idea that the evolution of a surface wave field in space and time is governed by the basic transport or energy balance equation

$$\frac{\partial S}{\partial t} + v \cdot \nabla S = N = S_{in} + S_{nl} + S_{ds}$$ (6.23)

where $S = S(f, \alpha; x, t)$ is the two dimensional (2D) wave (surface variance) spectrum, dependent on frequency f and propagation direction α, which varies with x, t on space - time scales large compared with a typical wave length or period; $v = v(f,\alpha)$ is the (deep water) group velocity; and the net source function N is represented as the sum of the input S_{in} by the wind, the non - linear transfer S_{nl} by resonant wave - wave interactions and the dissipation S_{ds}. In fact, several wave prediction models have been proposed based on the above formulation but the authors who gave an essential contribution and provided a broader theoretical framework for later models were Phillips (1958) and Miles (1957) with the concept of the equilibrium range of the spectrum, and Hasselmann (1960) with the analysis of the non - linear energy transfer due to resonant wave - wave interactions.

In the present work all the interest is concentrated around the last term in equation (6.23), which is the dissipation term, S_{ds}. This term includes dissipation by bottom friction, bed percolation and breaking. Before further comments are done regarding energy dissipation in the nearshore region it is important to summarise the

wave - bottom interaction mechanisms and evaluate their importance in terms of wave energy variation. These interaction mechanisms are basically five: scattering caused by bottom irregularities, sediment suspension, motion of a soft bottom, percolation through a porous bottom and friction in the turbulent bottom boundary layer. The first process results in a local redistribution of wave energy and the last four are dissipative. Concerning the dissipative processes the first is not well known, the second is only significant when in the presence of a mud bottom, whereas the other two are common in coastal areas. Percolation is important for coarse sand, but friction dominates for fine sand or when sand ripples are present. Laboratory experiments for a regular progressive wave with H = 2 m , T = 8 sec, and h = 7 m give the relative changes in the mean energy flux over one wave length due to turbulent bottom friction and percolation to be 1.7% and 0.06% respectively (Svendsen and Jansson, 1982). Based on this experiment it seems a reasonable decision to neglect the last two dissipative processes and therefore attribute all the dissipation to the breaking phenomenon. This will be done here.

Several of the researchers mentioned above (SWAMP group) proposed different formulations for the energy dissipation term which differ due to different derivation conditions. However, analysis of all the above formulations proposed reveals that they have one thing in common which is that energy dissipation is proportional to: the 2D wave spectrum, S(f, α); the frequency component, f, to the power of m; and the peak frequency, f_p, to the power of n.

Hasselmann and Hasselman (1983) proposed a formulation for the energy dissipation for wave growth in shallow water:

$$S_{ds} = -c_0 \left(\frac{E \omega_p^{-4}}{g^2} \right)^6 \frac{\omega^{-4}}{\omega_p^{-3}} S(f,\alpha)$$

(6.24)

where $c_0 = 1.2 \times 10^9$, E is the total variance, $\omega_p = 2\pi f_p$ is the peak angular frequency and g the gravitational acceleration. This formulation will be used in the model because of its simplicity and also because, although several other authors proposed different formulations for shallow water, there is nothing at the present date that would lead us to think that this expression is not appropriate for the nearshore region or that the other formulations are better. Thus, a model in which the energy dissipated by each spectral component is calculated based on the above formulation was developed. Each spectral component is propagated as a

monochromatic wave using the linear model based on the elliptic form of the mild slope equation with first order radiation boundary conditions. Then, an energy dissipation term, $S_{ds_{ij}} \Delta f_i \Delta \alpha_j$, where

$$S_{ds_{ij}} = -c_0 \left(\frac{m_0 (2\pi f_p)^4}{g^2} \right)^6 \frac{(2\pi f)^4}{(2\pi f_p)^3} S(f_i, \alpha_j),$$

(6.25)

associated with each transformed spectra component, ij, is calculated and subtracted from the energy associated to each transformed spectral component, which is

$$\frac{a_{ij}^2}{2} = S(f)_{ij} \Delta f_i \Delta \alpha_j.$$

(6.26)

This method does not take into account parameters like wave steepness or bottom slope which are important factors known to influence wave breaking. However, it is noted again that it is difficult to determine the influence of those parameters when considering such small components, and also that no research work is known to have been done in this area. From now on this numerical model will be refered to as the model with the first breaking criterion.

Another idea also proposed here is based on a different approach of modelling the breaking phenomenon, and involves the calculation of the energy dissipation rate at each location and then distributing it between the different spectral components. The numerical model for wave transformation in the nearshore region where this method is implemented is based on the model developed in the previous chapter. The modification done concerns the introduction of a dissipation term in the governing equation. The idea of linear superposition of independent spectral components which are then propagated as a regular wave remains the same. Based on the extensive literature survey done before, and in agreement with the comments made during its description (sections 6.2 and 6.3), it has been concluded that the best approach for calculating the spatial distribution of the energy dissipation is the wave energy equation under the assumption that the breaking wave resembles a bore (hydraulic jump). The assumptions made in order to apply the model legitimately are that: the probability function for the lower, non - broken waves, is the same as it is in the absence of breaking, that is the Rayleigh distribution; there is a maximum value of the wave height, H_m, possible to occur at each depth;

and that broken waves carry on propagating with the same wave height, H_m. The energy dissipation can now be expressed by

$$\varepsilon = B\frac{1}{4}\rho g\frac{f_p}{h}H_m^3 Q_b \qquad (6.27)$$

as derived by Battjes and Janssen (1978) and the probability of occurrence of broken waves is given by Q_b that can be calculated by the following expression:

$$\frac{1-Q_b}{\ln Q_b} = -\left(\frac{H_{rms}}{H_m}\right)^2 . \qquad (6.28)$$

This method was chosen with confidence because its verification was done using a large range of laboratory and field data (as mentioned in section 6.3) and good results were obtained.

The initial step towards obtaining the energy dissipation rate at each location is to find the maximum wave height value possible to occur at that same location. This is done assuming a cut off of the Rayleight distribution and the expression used to calculate the value of H_m is

$$H_m = 0.88 \, k_p^{-1} \tanh(\gamma \, k_p h / 0.88) \qquad (6.29)$$

where k_p is the wave number correspondent to the peak frequency, γ is a Miche (1944) type parameter which for shallow water has been considered equal to the constant value of 0.78 based on McCowan (1891) suggestion derived from solitary wave theory.

The next step is to calculate Q_b, that is the probability of occurrence of H_m at each location and is done by solving equation (6.28), where H_{rms} can be estimated as

$$H_{rms} = \sqrt{8}\sqrt{m_0} \qquad (6.30)$$

with m_0 the total wave energy as described by equation (5.11).

Thus equation (6.28) can be written as

$$Q_b = 1 + \left(\frac{\sqrt{8}\sqrt{m_0}}{H_m}\right)^2 \ln Q_b \qquad (6.31)$$

which is a non - linear equation that is solved by the Newton Raphson method. This method is very efficient if the first approximate solution is close to the exact solution and, as a good approximate solution can be easily estimated, this method was chosen to be used in the present work.

Finally for the wave with energy per unit surface and unit time,

$$E = \rho g \frac{H^2}{8},$$ (6.32)

the energy dissipation rate factor f_D, can be calculated at each location by

$$f_D = \frac{\varepsilon}{E} = 2Q_b f_p \frac{H_m^2}{H^2}$$ (6.33)

where H is a representative wave height, here chosen to be the significant wave height, $H_{1/3}$. The empirical factor B, which is used to represent the bore conditions, was here taken as 1, meaning that we are dealing with a fully developed bore.

Now that the energy dissipation rate is calculated at each location the remaining problem is to distribute it to each spectral component. This is done by assuming that the dissipation is proportional to the 2D wave spectrum times the angular wave frequency to the power of 4. Once again this decision was based on observation of the estimates proposed for the energy dissipation term in equation (6.24) by the SWAMP group. Thus,

$$f_{D_{ij}} \propto f_D \frac{\omega_i^4 S(f_i, \alpha_j)}{\sum_{i=1}^{N_f} \sum_{j=1}^{N_\alpha} \omega_i^4 S(f_i, \alpha_j)}.$$ (6.34)

The dissipation term, $\dfrac{i\omega f_{D_{ij}} \phi}{CC_g}$, was then incorporated into the mild - slope equation that can now be written as

$$\nabla^2 \phi + k_c^2 \phi = 0$$ (6.35)

with

$$k_c^2 = k^2 - \frac{\nabla (CC_g)^{1/2}}{(CC_g)^{1/2}} + \frac{i\omega f_{D_{ij}}}{CC_g}.$$ (6.36)

From now on this numerical model will be refered as the model with the second breaking criterion.

6.6 - Numerical tests

In order to validate both numerical models, that is, to evaluate and compare their performance regarding modelling of the breaking phenomenon, 2 different cases for which laboratory data is available were tested.

The data used here are the results of laboratory tests performed by Vincent and Briggs (1989) for irregular waves. The bathymetry consists of an elliptic shoal, whose larger axis is parallel to the offshore boundary, placed in a region of constant water depth. The bathymetry and the input irregular offshore sea state were the same as for the cases reported in the previous chapter. Thus, more details regarding the bathymetry can be found in the previous chapter, section 5.4: the shoal geometry is given by equation (5.22), the elevation at any point over the shoal is given by equation (5.23), the uniform depth outside the shoal is 45.72 cm and finally a sketch of the bathymetry can be seen in Fig. 5.2. The input spectrum was the TMA spectrum and the spectral distribution of energy in finite water depth is expressed by equation (5.24). The directional spreading function derived from a Fourier series is expressed by the formulation (5.25). The two cases here simulated numerically are: the propagation of a directional spectrum with a broad frequency spreading (Fig. 5.3) and a broad directional spreading (Fig. 5.4), named B5; and a directional spectrum with a narrow frequency spreading (Fig. 5.3) and a narrow directional spreading (Fig. 5.4), named N5. The test conditions for the breaking series are summarised in the following table:

Case ID	Type	Period (sec)	Height (cm)	α	γ	σ_m (deg)
B5	Spec	1.30	19.00	0.08650	2	30
N5	Spec	1.30	19.00	0.02620	20	10

Table 6.1 Test conditions for the breaking series

Like the tests for the non - breaking cases performed in the previous chapter, 8 frequency components and 8 directional components were combined so that a total of 64 spectra components were considered to represent the offshore sea state. The computational results are presented in terms of the normalised wave height or amplification factor. 2D contour plots for the whole computational domain (Fig. 6.4

to 6.7) and 6 sections (Fig. 6.8 to 6.13) allocated in the region behind the shoal (Fig. 5.2) were chosen to give the best visualisation and evaluation of the results. Again, as for the non -breaking cases, there is only laboratory data available for section 4.

The 2D contour plots show that for the 2 cases, B5 (Figs. 6.4 and 6.5) and N5 (Figs. 6.6 and 6.7), and both criteria, the focusing area behind the shoal is still evident. The wave pattern does not differ much between the cases and the amplification factor is generally higher for the second breaking criterion than for the first. The 6 sections (Fig. 6.8 to 6.13) behind the shoal allow a better evaluation of the results and the differences between the two methods. When comparing case B5 to case B3 and case N5 to case N4, the difference concerns the value of the incident wave height that before was 2.54 cm and now is 19.0 cm so that breaking occurs. It can be observed that for the wave breaking cases the results are definitely much smoother than for the non - breaking cases and also the amplification factor is reduced for the breaking cases, particularly with the first breaking criterion. When comparing the computational results obtained for both cases, B5 and N5, for each section, it can be observed that frequency and directional spreading have the effect of reducing the disturbance caused by the presence of the shoal, although the second criterion seems to be less sensitive to that. For each section and each case the first criterion gives lower results than the second criterion. For section 4 the computational results obtained from both models overpredict the peak amplification factor. Concerning the two sides, they show good agreement for case B5 and again overestimation of the results for case N5. In fact, what can be observed is that the laboratory data for this particular section show that the wave height does not vary much along the section. This is not achieved with either of the numerical models proposed here. The reason for this behaviour is that the model does not consider non - linear effects, like wave interactions and bottom friction which, as said before, does not usually represent such an important influence on wave decay but might be considerable for this particular experimental bathymetry when a wave reaches a height of 19.0 cm, and the effects of large scale breaking. The differences between both cases were expected and confirm some conclusions stated in the previous chapter that frequency and directional spreading tend to neutralise the effect of the presence of the shoal, that is, the waves tend to be less disturbed when passing over the shoal. Differences between the computational results obtained from both criteria are due to the different approach used to model the phenomenon. The second approach

assumes that all dissipation due to breaking occurs over the shoal, whereas the first approach assumes that dissipation due to breaking occurs proportionally to the wave height and therefore not only over the shoal but also over the focusing area behind the shoal. This explains why the solutions obtained with the first breaking criterion are lower than the ones obtained with the second criterion for the region behind the shoal.

6.7 - Closure

In this chapter two numerical models of wave propagation in the nearshore region were developed and tested. Both models are an extension of the model developed in the last chapter in the sense that the process of random wave breaking is incorporated in that model. Two different ideas based on a different approach of the phenomenon were implemented. One is based on the concept of breaking each independent spectral component, and the other on the concept of breaking the total propagating wave and then distributing the dissipated energy among the independent spectral components. Tests were done to verify both models and evaluate their performance. The model based on the concept of breaking each independent wave component produced results that agree better with the laboratory data available for comparison. Not much research work has been done in this area so the idea of attributing a certain amount of wave energy dissipation to a spectral component is an innovation in the area of modelling wave propagation in the nearshore region. As mentioned before, the breaking process has been implemented in numerical models in which the mild - slope equation is the governing equation, simply by treating the propagating wave as a monochromatic wave, representative of the sea state, and usually applying a wave height to water depth ratio breaking criterion. Thus, although in fact there is not much laboratory or field data available regarding the process of random wave breaking, it is very important that the phenomenon is included in numerical models for irregular wave transformation in the nearshore region. That is the reason why it was considered so important that the above two proposals were tested.
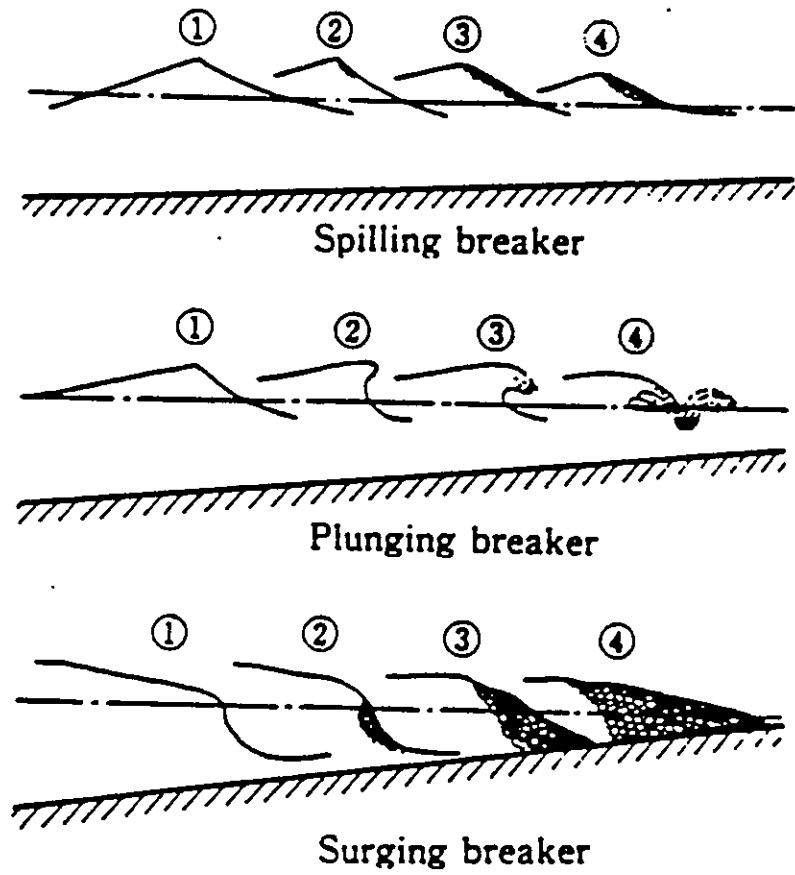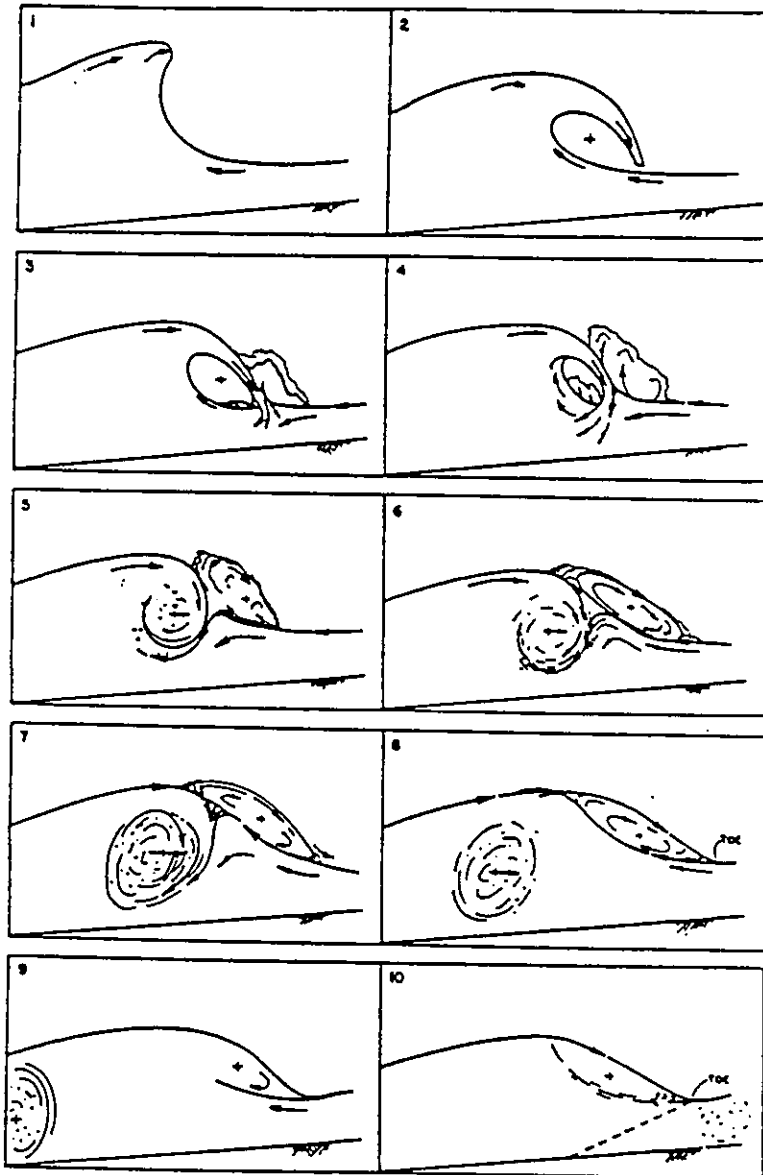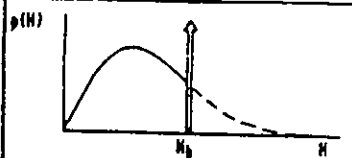
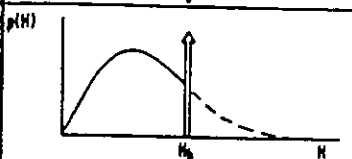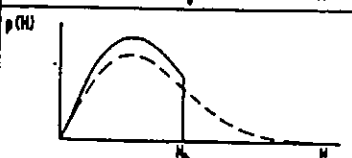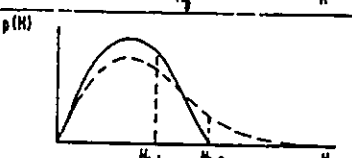Fig. 6.1 - Breaker types (from Horikawa, 1988).

Fig. 6.2 - Schematic sequence of breaking wave events (from Basco, 1985).

AUTHOR	DISTRIBUTION	SHOALING	BREAKER CRITERIA
COLLINS (1970)	$p(H)$	LINEAR	$\frac{H_b}{H_d} = 0.76\beta^{1/7}(H_d/L_d)^{-1/4}$ (AFTER LeMEHAUTE AND KOH, 1967)
BATTJES (1972)	$p(H)$	LINEAR	$H_b = \frac{0.88}{k}\ \text{TANH}\left(\frac{\gamma}{0.88}kh\right)$
KUO and KUO (1974)	$p(H)$	LINEAR	$H_b = 0.63h$
GODA (1975)	$p(H)$	NONLINEAR (SHUTO, 1974)	$\frac{H_b}{H_d} = A\frac{L_d}{H_d}\left\{1-\exp\left\{-1.5\frac{h}{H_d}\frac{H_d}{L_d}\left(1+K\tan^{p}\beta\right)\right\}\right\}$ (AFTER GODA, 1975)

The dotted lines represent the original Rayleigh distributions and the heavy lines represent the modified distributions.

Fig. 6.3 - Modified probability density functions due to wave breaking (from Thornton and Guza, 1983).
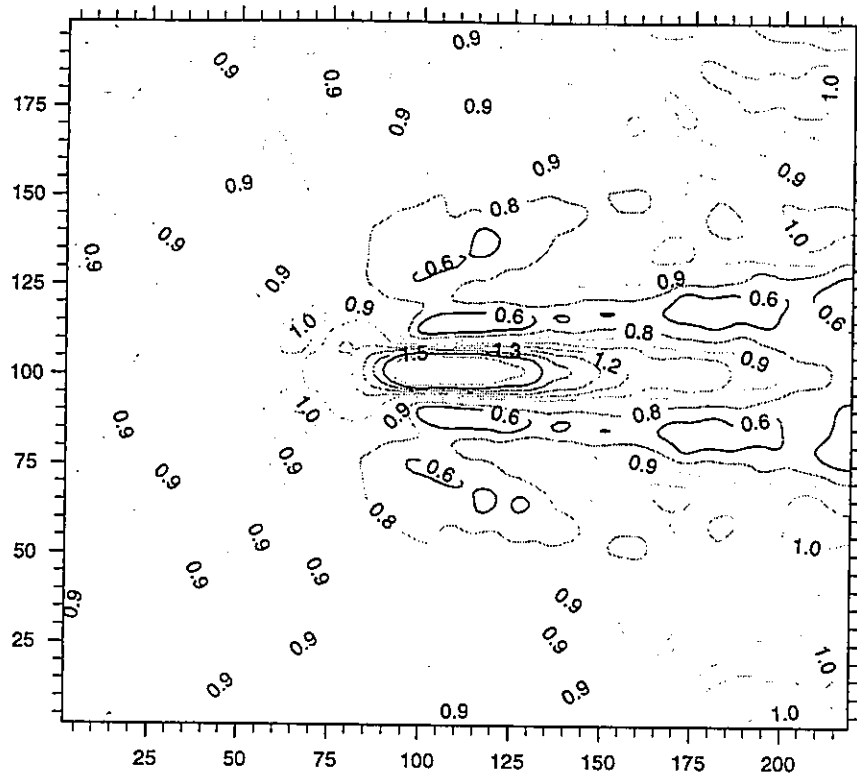
Fig. 6.4 - Normalised wave height contours for case B5 with first breaking criterion.
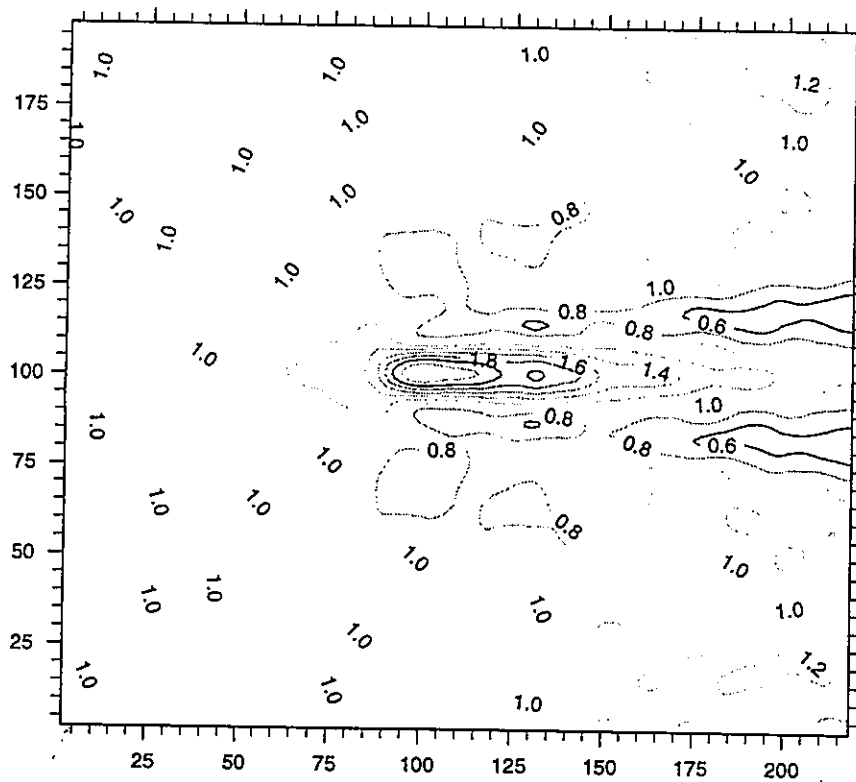

Fig. 6.5 - Normalised wave height contours for case B5 with second breaking criterion.

Fig. 6.6 - Normalised wave height contours for case N5 with first breaking criterion.
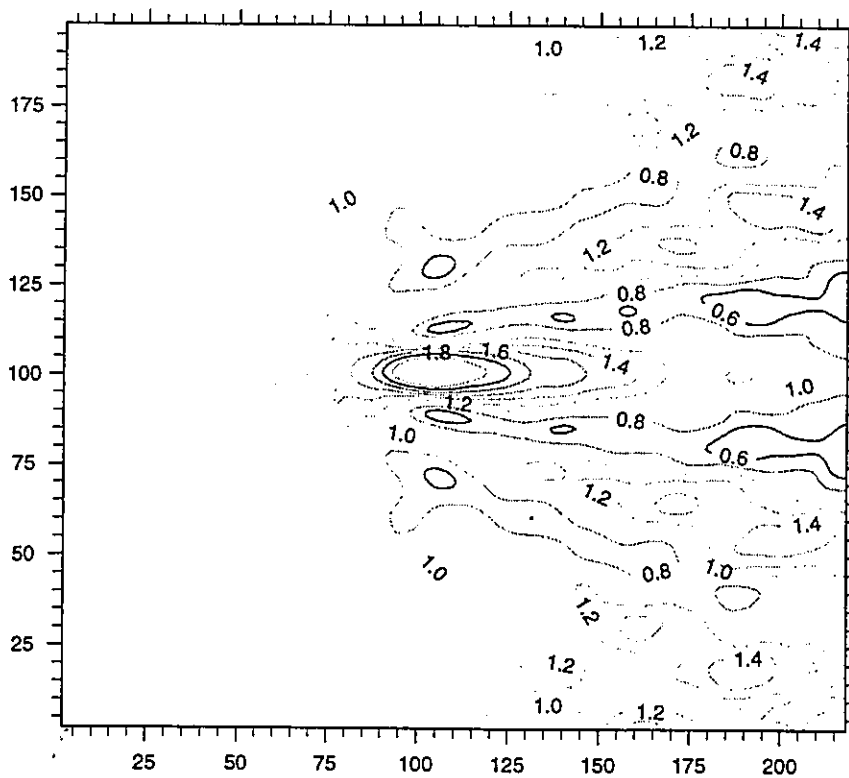
Fig. 6.7 - Normalised wave height contours for case N5 with second breaking criterion.
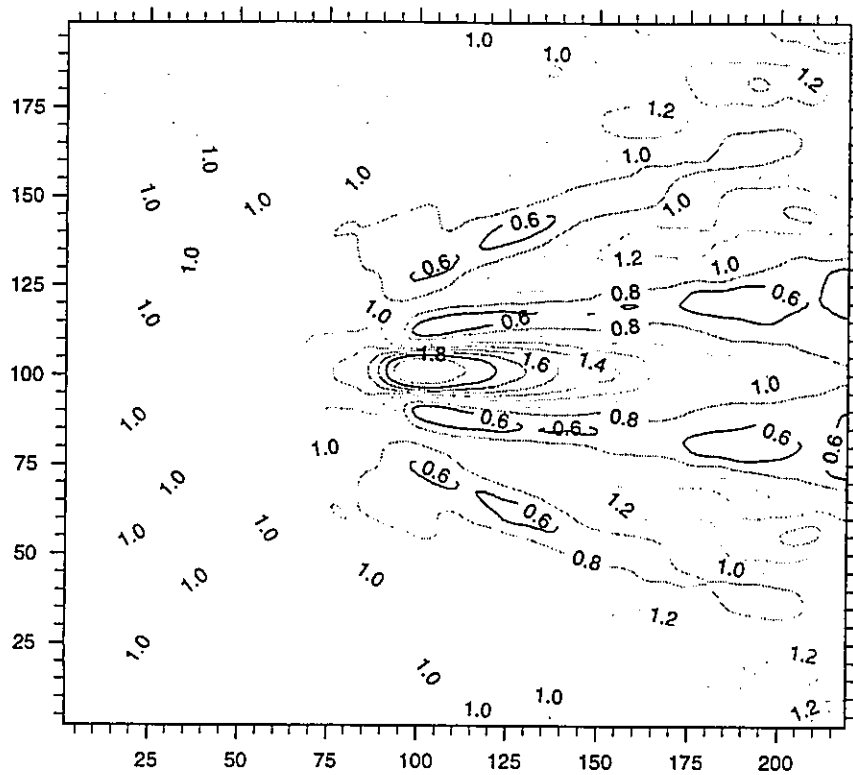
Case B5
(Section 3)

(see Fig. 5.2, page 155)

—✳— 1 st criterion
—△— 2 nd criterion

Normalised wave height

j co-ordinate

Fig. 6.8 - Computational results for case B5. Section 3.
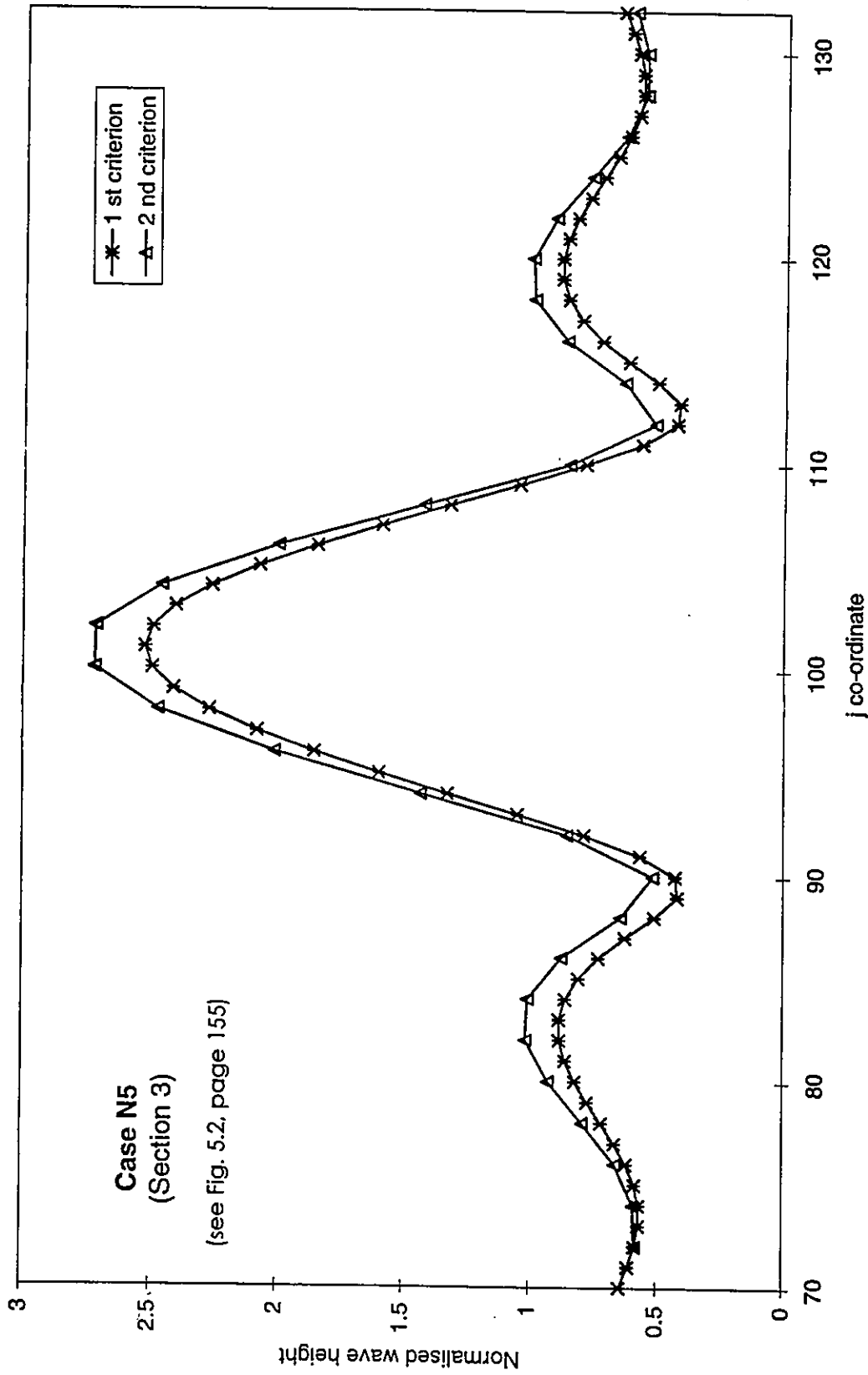
Fig. 6.9 - Computational results for case N5. Section 3.
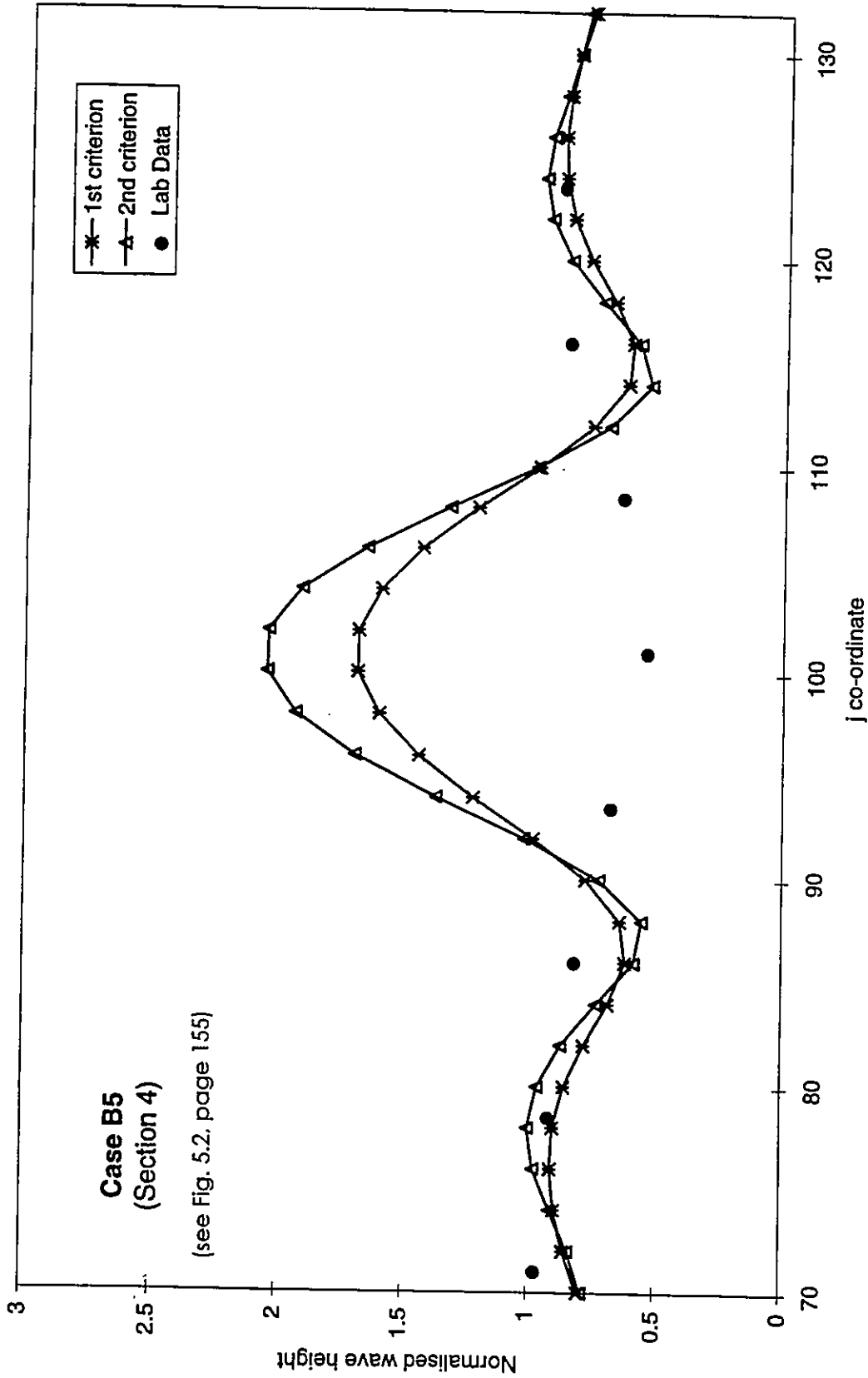
Fig. 6.10 - Comparison between experimental data of Vincent and Briggs (1989) and computational results for case B5. Section 4.
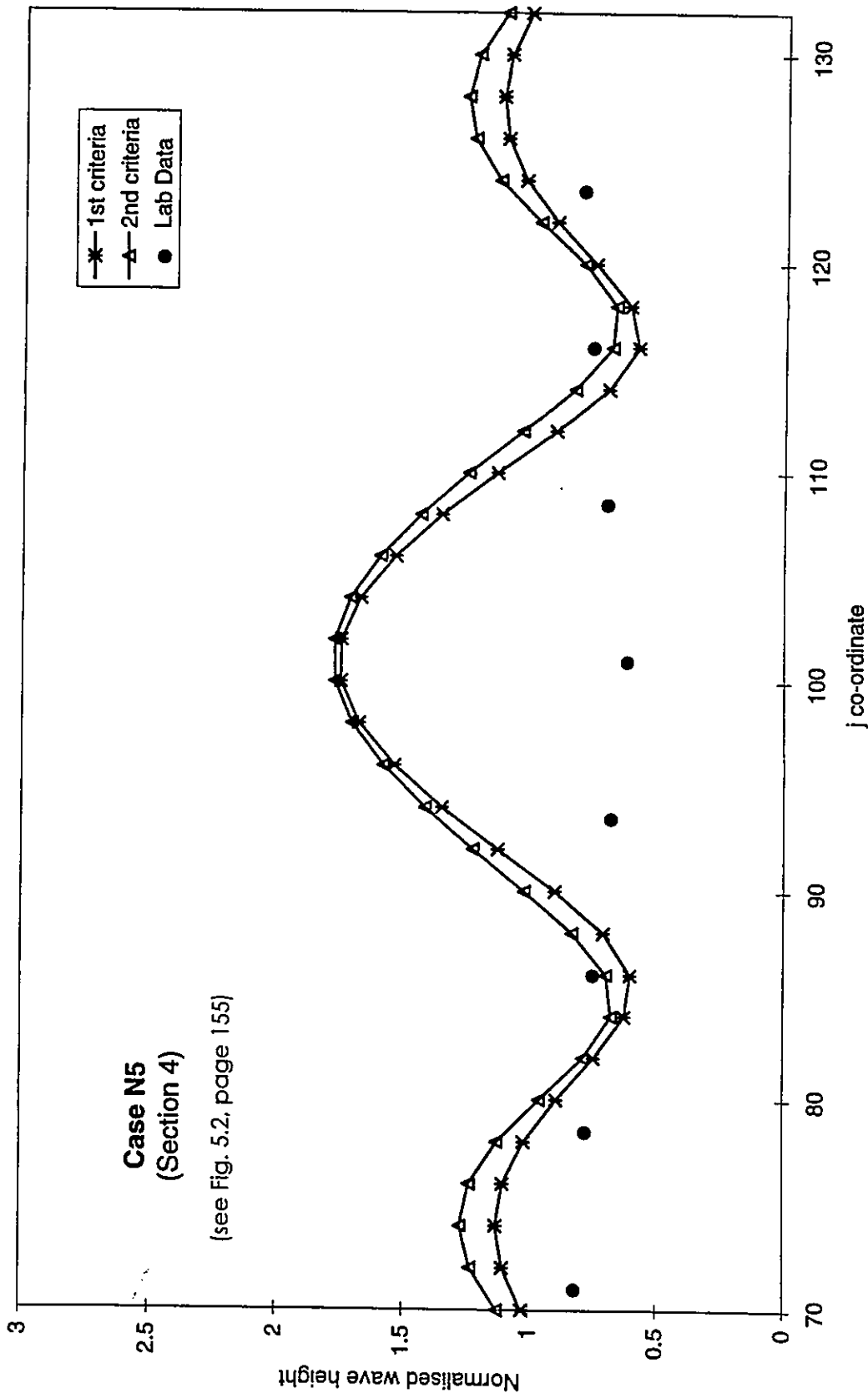
Fig. 6.11 - Comparison between experimental data of Vincent and Briggs (1989) and computational results for case N5. Section 4.

Case B5
(Section 5)

(see Fig. 5.2, page 155)

Fig. 6.12 - Computational results for case B5. Section 5.

Fig. 6.13 - Computational results for case N5. Section 5.

Case B5
(Section 6)

(see Fig. 5.2, page 155)

1 st criterion
2 nd criterion

Normalised wave height

i co-ordinate

Fig. 6.14 - Computational results for case B5. Section 6.
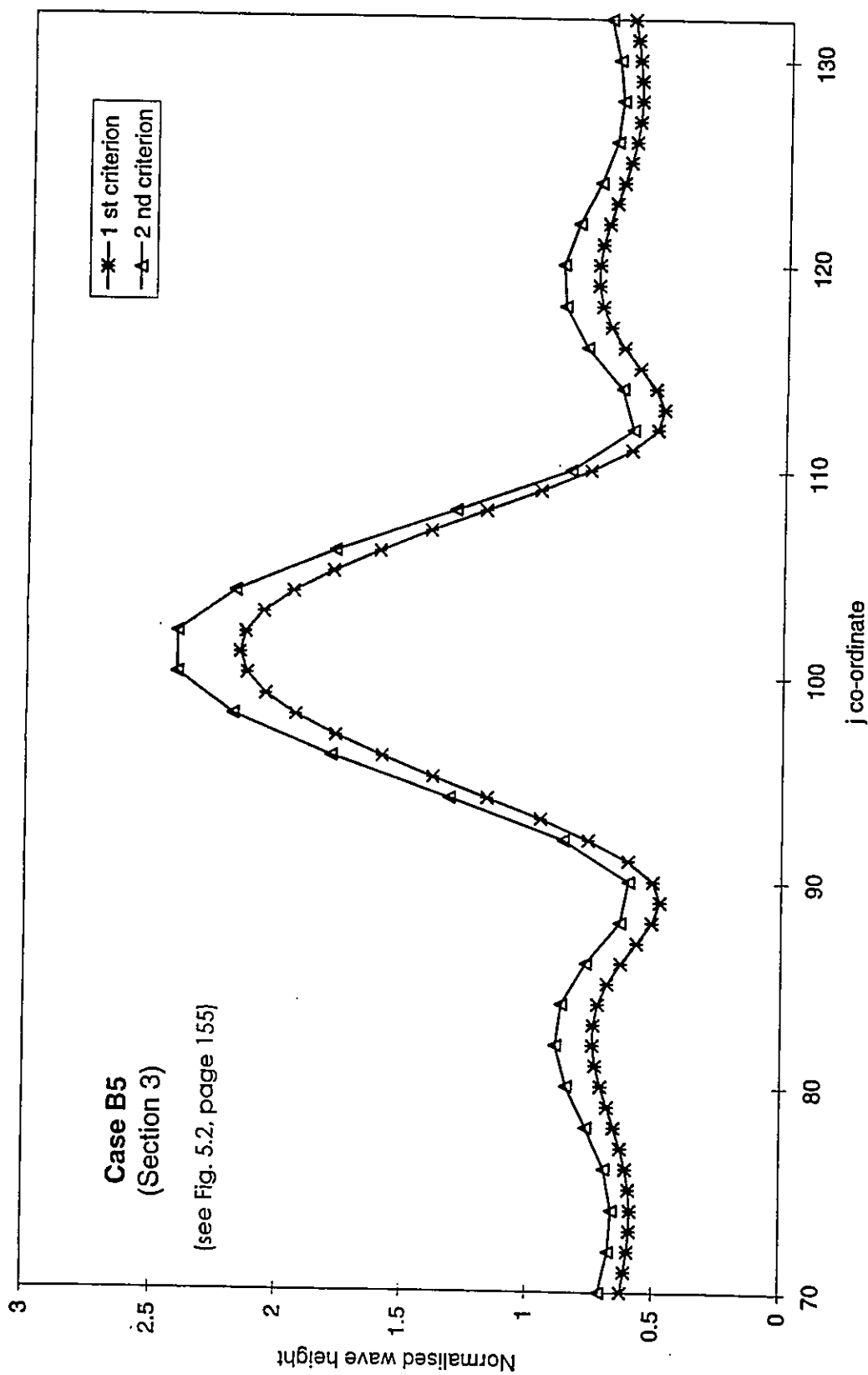
Fig. 6.15 - Computational results for case N5. Section 6.

Fig. 6.16 - Computational results for case B5. Section 7.
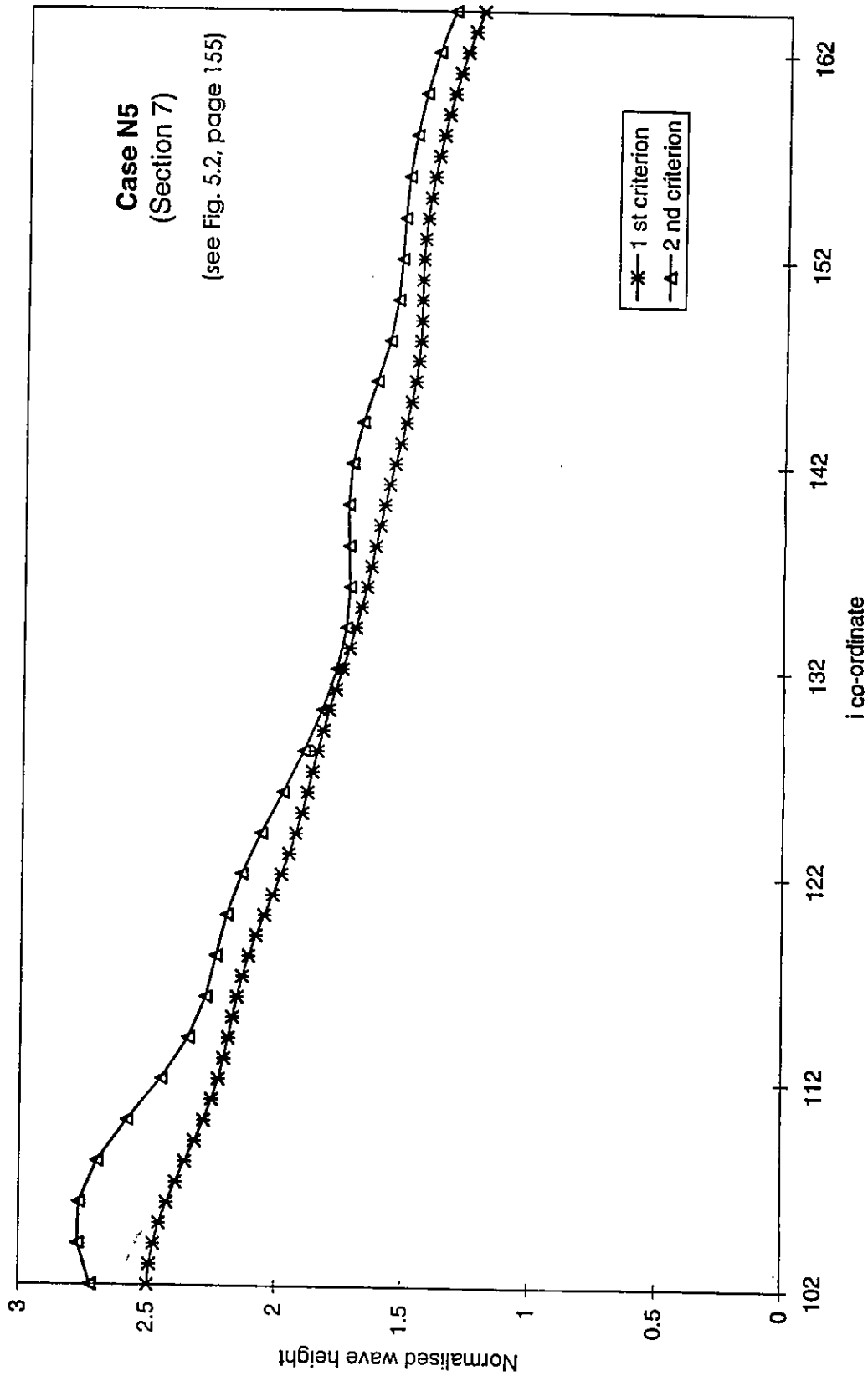
Fig. 6.17 - Computational results for case N5. Section 7.
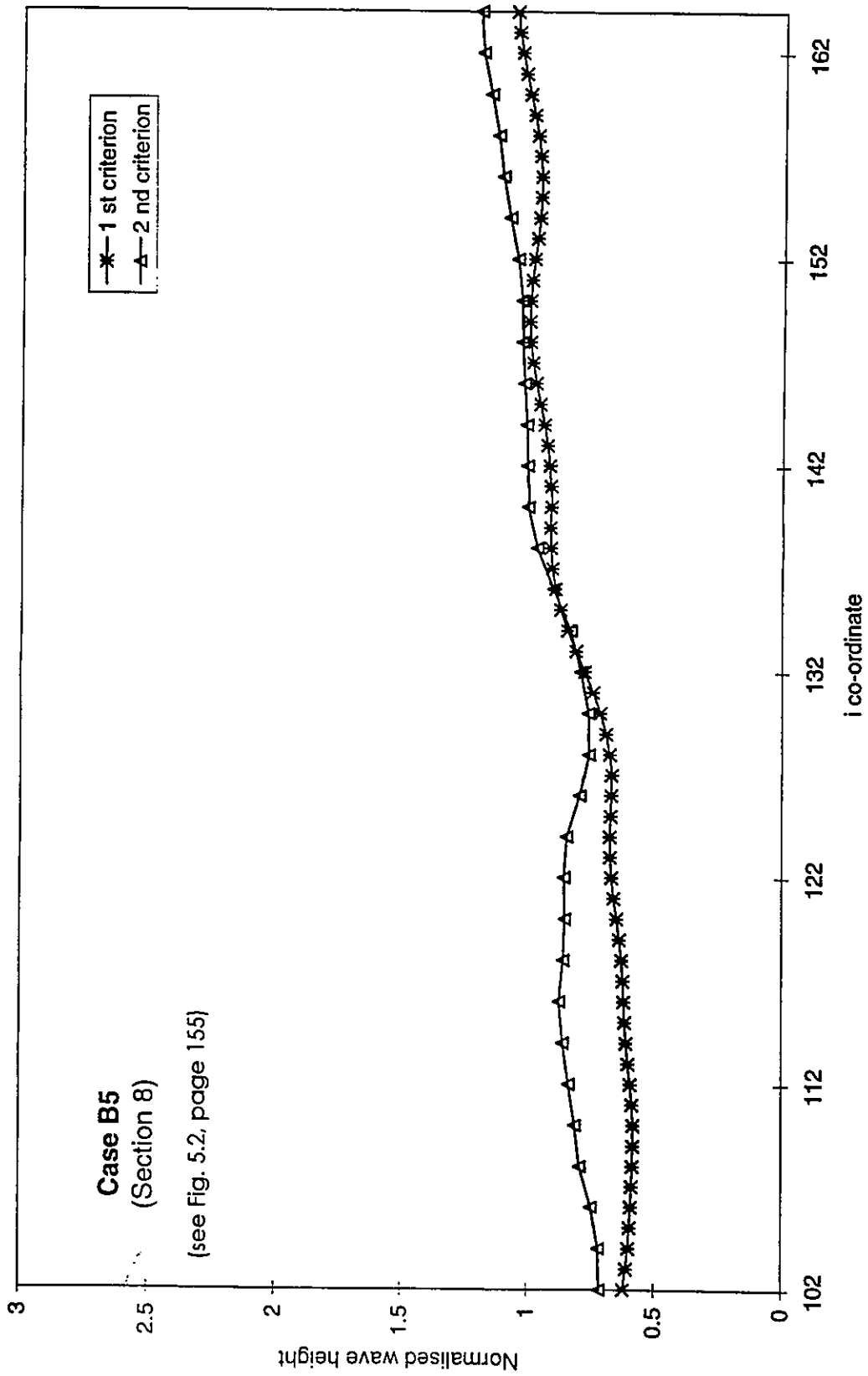
Fig. 6.18 - Computational results for case B5. Section 8.
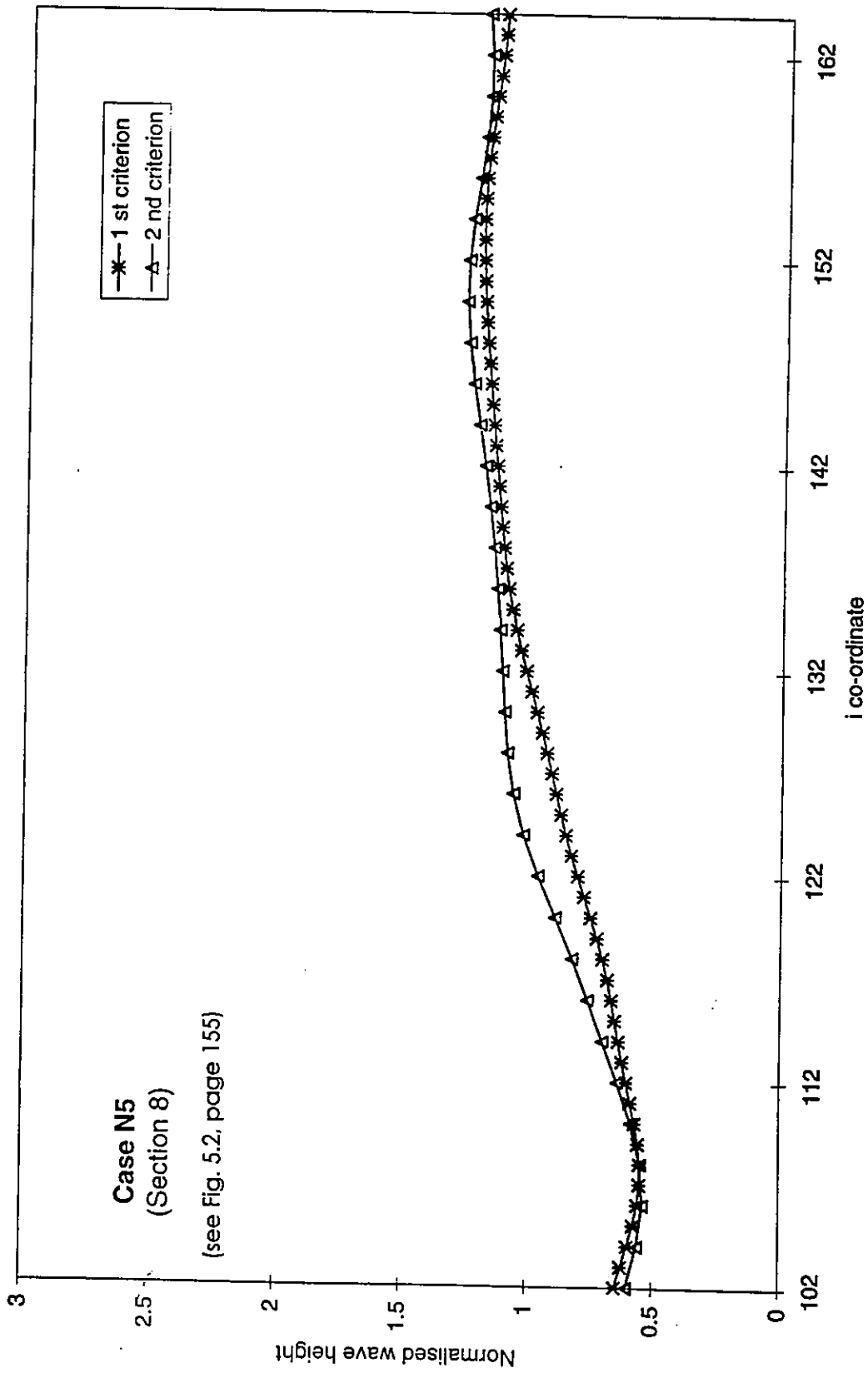
Fig. 6.19 - Computational results for case N5. Section 8.

Chapter 7

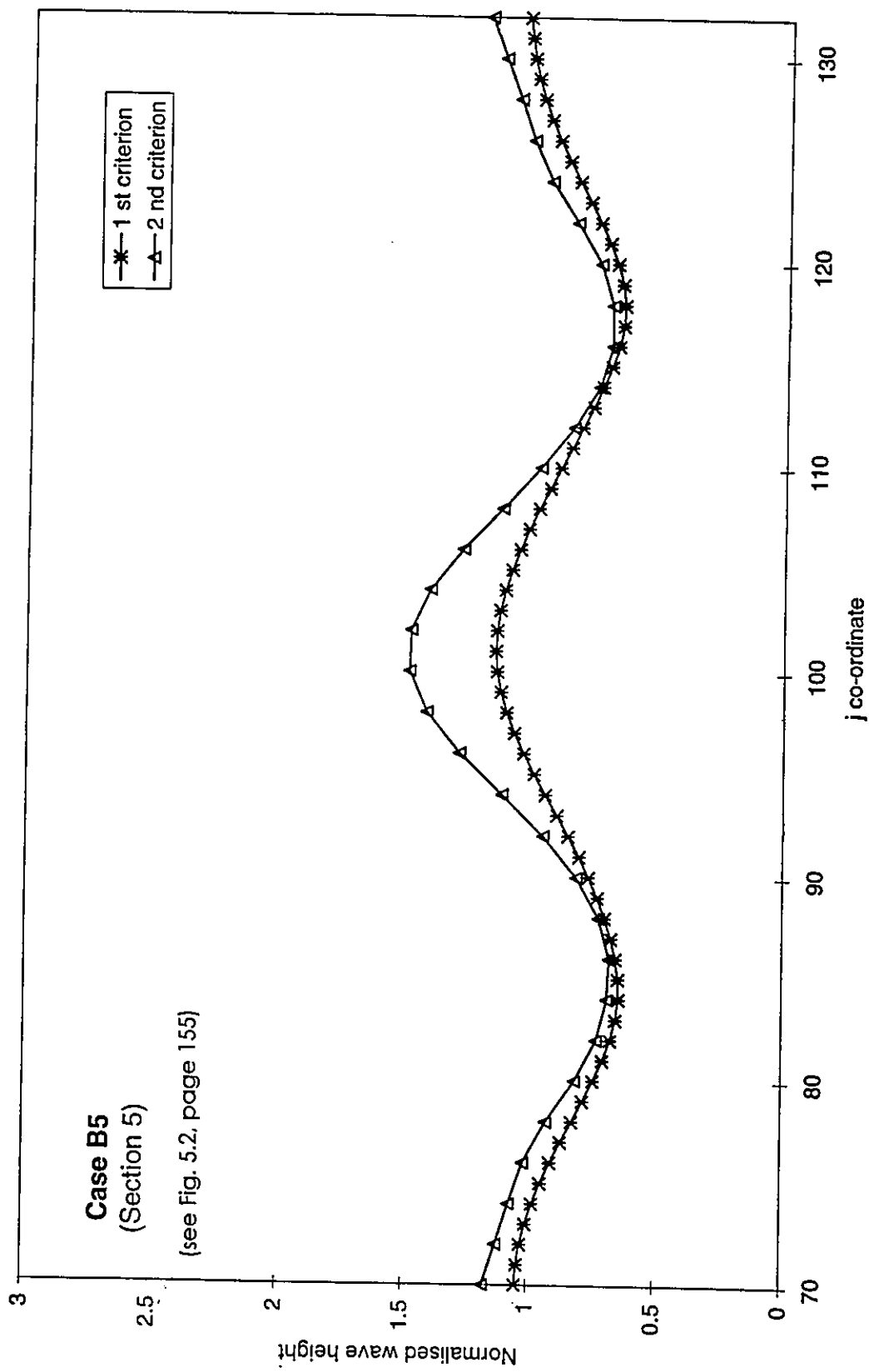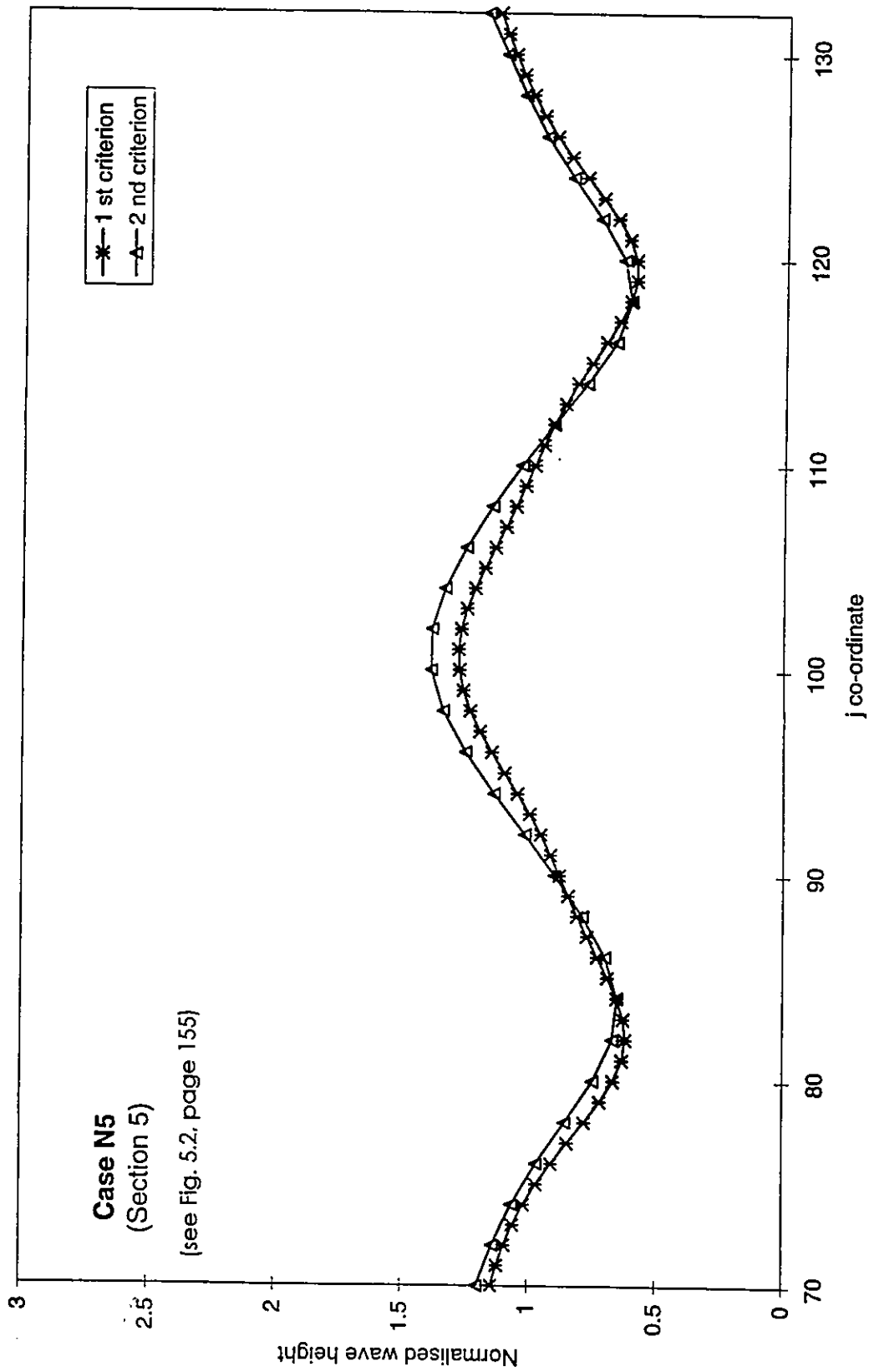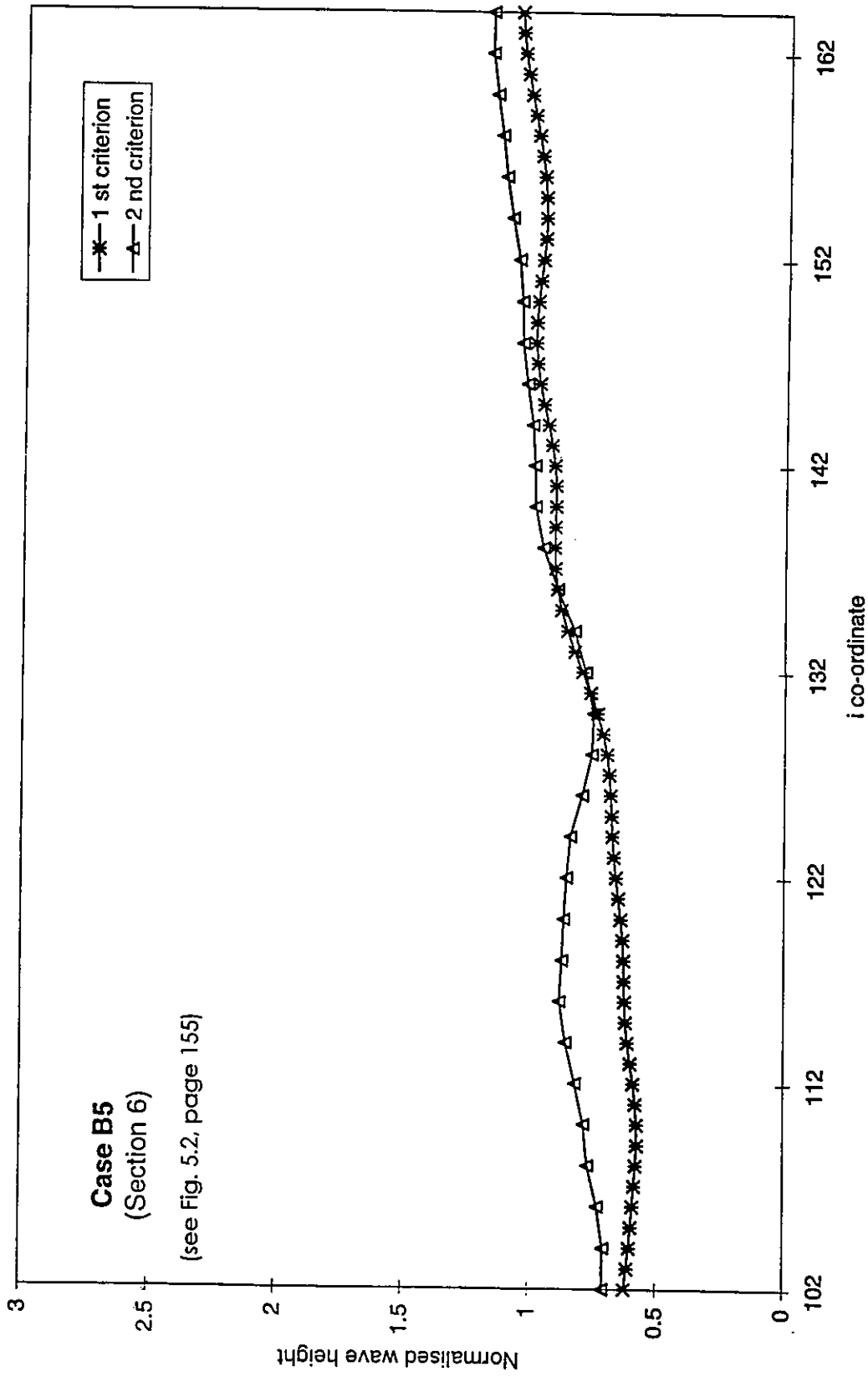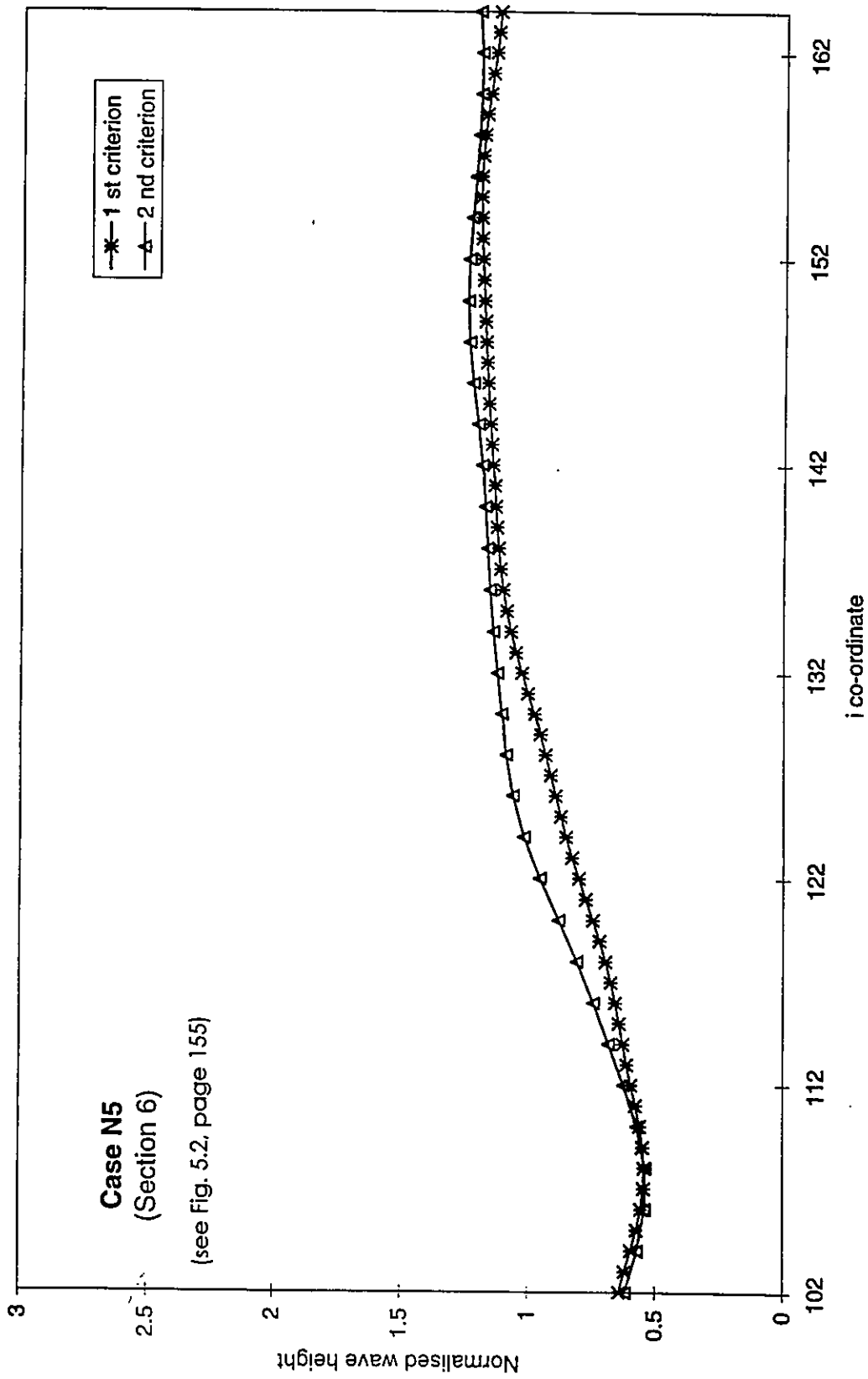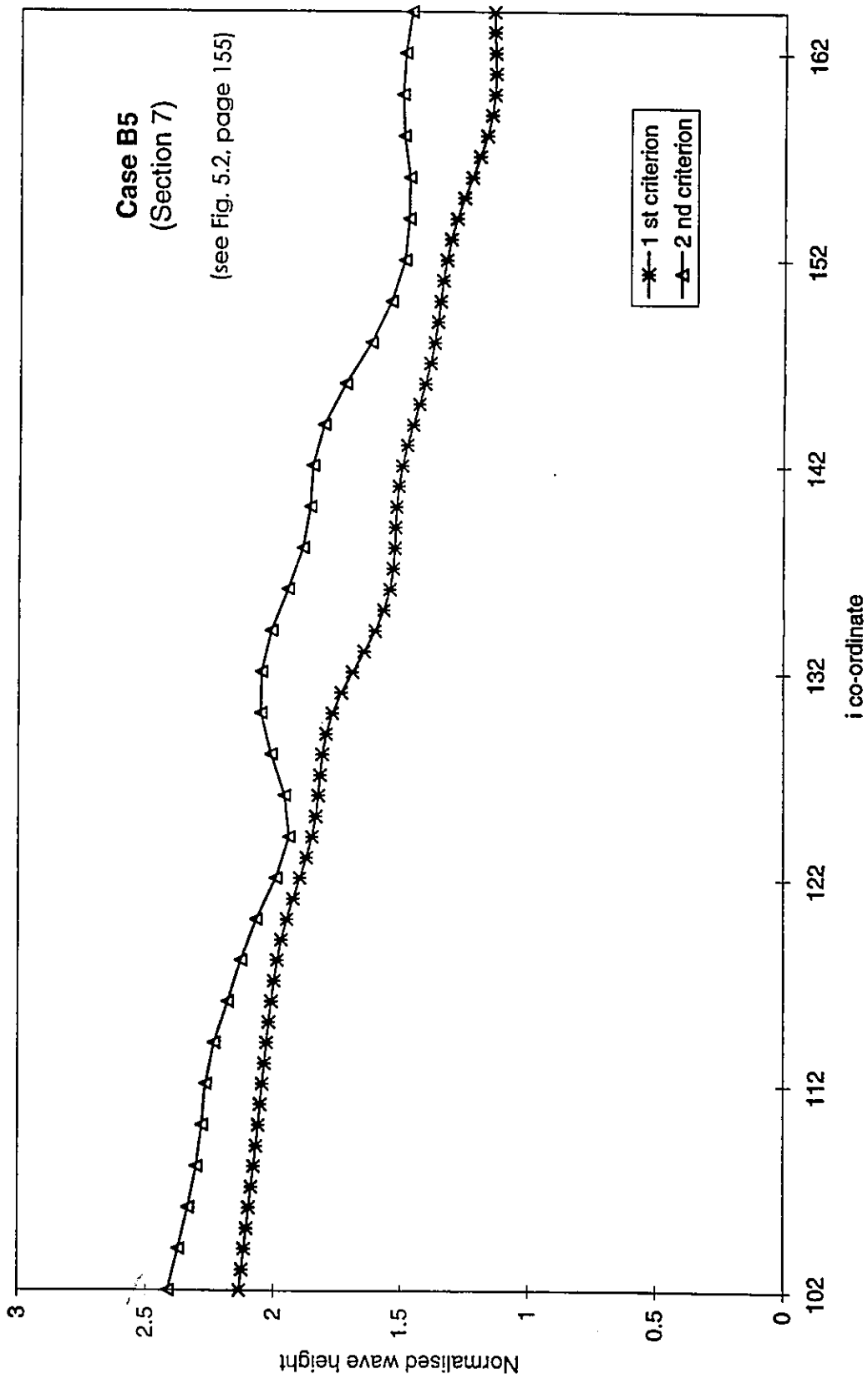Conclusions and

Recommendations for Further Work

7.1 - Conclusions

The phenomenon of regular and irregular wave transformation in the nearshore region was investigated in the previous five chapters of the present work. Several aspects associated with the process of wave transformation have been addressed from the theoretical and numerical point of view using the mild - slope equation as the modelling equation. Its elliptic formulation was judged as superior in comparison with the hyperbolic and parabolic formulations, due to its higher computational efficiency for particular cases, and better simulation of the physics involved. In the present section a number of conclusions are drawn with regard to the results obtained from the work undertaken.

1) Aiming to simulate the sea state using linear superposition of results from a monochromatic refraction - diffraction combined model, requires an efficient numerical model for monochromatic wave propagation in the nearshore region. Efficiency concerns a good representation of the physics involved in the phenomenon and simultaneously an economic computational approach, in terms of run - time and memory requirements. This can be achieved by developing a numerical model that predicts regular wave transformation in the nearshore region, including the processes of refraction, diffraction and reflection, which is based on the elliptic form of the mild - slope equation. Certain iterative methods produce the most economic solvers for the above formulation when applied to a large domain. It has been shown in this study that two Krylov

Subspace Methods, the Bi - Conjugate Gradient Method and the Generalised Minimum Residual Method generate suitable algorithms to satisfy the requirement of efficiency. They both produce robust models, capable of producing accurate solutions when applied for complex geometries.

2) A comparison between the performances of both algorithms showed that the Bi - Conjugate Gradient algorithm has a better convergence rate than the Generalised Minimum Residual algorithm. It is considerably faster, requiring about half of the computational time. Nevertheless, the Generalised Minimum Residual algorithm performs with a better stability, that is, it is characterised by monotonic convergence whereas the Bi - Conjugate Gradient algorithm shows a certain (small) instability within the convergence process.

3) An appropriate simulation of open boundary conditions is important for predicting correctly the characteristics of the wave field. If outgoing waves are not correctly simulated artificial reflections will be introduced into the numerical domain and generate numerical errors due to the presence of standing waves. This study showed that the success of their implementation within the numerical model is highly dependent on the formulation of the governing equation, that is, the suitability of the boundary conditions formulation depends on the mathematical model used and its evaluation should be done by numerical experimentation.

4) Sponge filters are a viable alternative for improving the efficiency of numerical simulation of open boundaries. They are applied in combination with first order radiation boundary conditions. This study showed that they are more suitable for the hyperbolic mathematical formulation of the mild - slope equation than for the elliptic formulation. Their inclusion in each of the models is done by introducing a dissipation term in the governing equation. A great improvement in the accuracy of the results was achieved with sponge filters implemented for the hyperbolic model. Sponge filters result in a certain wasted numerical domain in the area adjacent to the boundaries. Their successful application was achieved for a sponge width equal to only one wave length, for the case of the hyperbolic model.

5) An increase in the order of accuracy of the radiation boundary conditions is the other alternative for improving the efficiency of the numerical simulation of open boundaries because it generates a succession of boundaries more transparent to the passage of obliquely incident waves. The implementation of first order and the next higher order of accuracy radiation boundary conditions into the numerical model based on the elliptic form of the mild -slope equation confirmed that more accurate solutions are obtained. Nevertheless, it was also verified that they increase the computational cost of the model significantly.

6) A numerical model based on a transformed form of the mild - slope equation was successfully solved by a multigrid technique. The model was derived based on a non - linear formulation where the new wave function is less rapidly varying than the velocity potential leading to a smaller number for restriction of the minimum number of grid nodes per wave length. The multigrid technique applied to the numerical model solved by the Generalised Minimum Residual algorithm was shown to accelerate the convergence process of the iterative solver. An increase of the number of grid levels not only reduces the total number of global and grid level iterations but also improves the accuracy of the results.

7) A numerical model for irregular wave transformation in the nearshore region based on the linear superposition of monochromatic spectral components transformed using the linear numerical model developed in the initial part of this work, can describe the phenomenon of random wave propagation satisfactorily if a minimum number of frequency and directional components is used. Tests performed over a complex bathymetry proved that the number of directional components required is higher than the number of frequency components. This leads to the conclusion that such a requirement does not only apply to parabolic models, because they have limitations dealing with large wave angles since waves have to propagate according to a main direction, but it is also extended to an elliptic formulation. Eight frequency components are capable of representing correctly a broad frequency spectrum but the same number is not enough to represent a broad directional spreading function.

8) Wave breaking is one of the main processes that occurs in the nearshore region therefore it cannot be neglected when modelling wave transformation in such areas. In this work, two models based on the consideration of breaking of each individual spectral component were implemented in the numerical model previously developed for irregular waves. The results obtained from both models do not show good agreement with the observed results showing that a linear model cannot simulate correctly the process of random wave breaking which is highly non - linear and induces interactions between spectra components which are not taken into account in the present model. In addition the effects of large scale (area) breaking cannot be underestimated.

7.2 - Recommendations for further work

Based on the results of this study the following recommendations for further work can be made.

1) Since the elliptic form of the mild - slope equation can be solved efficiently, as it was proved in this work, an attempt to include non - linear effects into the numerical model for monochromatic wave propagation should be done to achieve more realistic solutions. A proposal is to implement Kirby and Dalrymple's (1986) non - linear dispersion relation.

2) A numerical model for irregular waves based on the linear superposition of spectral components propagated using a non - linear model for monochromatic waves (as suggested above) is required. The effects, in terms of improving the accuracy, by using such model would more than compensate the consequences that are imposed by using a restricted number of spectral components to represent the sea state, therefore allowing a more economic numerical model.

3) There is a clear need for experimental results on the breaking of random waves and a full analysis of the phenomenon integrated in the context of random wave propagation.

4) More insight into the process of random wave breaking and its inclusion into numerical models for irregular wave propagation in the nearshore is required. The existing models require additional information about interactions between spectral components induced by energy dissipation by wave breaking.
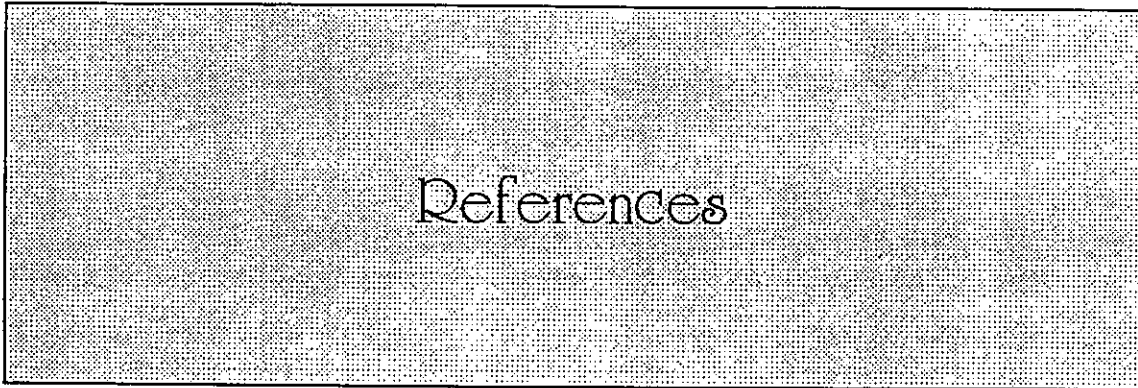
Anderson, O. H., Hedegaard, I. B. and Deigaard, R. ; 1991;
Model for morphological changes in the coastal zone;
MAST G6 - M.

Barret, R., Berry, M., Dongarra, J., Eijkhout, V., Romine, C.; 1996;
Algorithmic Bombardment for the Iterative Solution of Linear Systems - a Poli-Iterative
Approach;
Journal of Computational and Applied Mathematics, vol. 74, no. 1-2, pg 91-109.

Basco, D. R. ; 1985;
A qualitative description of wave breaking;
J. of Waterway, Port, Coastal and Ocean Eng., vol. 111, no. 2, pg 171 - 187.

Battjes, J. A. ; 1972;
Set - up due to irregular waves;
Proc. 13th ICCE, Vancouver, ASCE, vol. 3, pg 1993 - 2004.

Battjes, J. A. ; 1986;
Energy dissipation in breaking solitary and periodic waves;
Delft University of Technology, rep. nr. 86 - 5.

Battjes, J. A. and Beji, S; 1992;
Breaking waves propagating over a shoal;
Proc. 23rd ICCE, Venice, Italy, ASCE, vol. 1, pg 42 - 50.

Battjes, J. A. and Janssen, J. P. F. M.; 1978;
Energy loss and set - up due to breaking of random waves;
Proc. 16th ICCE, Hamburg, ASCE, vol. 1, pg 569 - 587.

Battjes, J. A. and Stive, M. J. F.; 1984;
Calibration and verificationof a dissipation model for random breaking waves;
Proc. 19th ICCE, Houston, ASCE, vol 1, pg 649 - 660.

Battjes, J. A. and Stive, M. J. F.; 1985;
Calibration and verificationof a dissipation model for random breaking waves;
J. of Geophysical Res., vol. 90, C5, pg 9159 - 9167.

Bayliss A.,Gunzburger M. and Turkel E.;1982;
Boundary Conditions for the Numerical Solution of Elliptic Equations in Exterior Regions;
SIAM J. Appl. Math., Vol. 42, No. 2, pg 430-451.

Berkhoff, J.C.W.; 1972;
Computation of combined refraction-diffraction;
Proc. 13th ICCE, Vancouver, ASCE, pg 471-490.

Berkohoff, J. C. W.; 1976;
Mathematical Models for Simple Harmonic Linear Water Waves. Wave refraction and Diffraction;
Publ. no. 163, Delft Hydraulics Laboratory, Delft, The Netherlands.

Berkhoff,J. C. W., Booy, N. and Rader, A. C.; 1982;
Verification of numerical wave propagation models for simple harmonic water waves;
Coastal Eng., vol. 6, pg 255-279.

Bettess, P. and Zienkiewicz, O. C.; 1977;
Diffraction and Refraction of Surface Waves Using Finite and Infinite Elements;
International Journal for Numerical Methods in Engineering, vol. 11, pg 1271-1290.

Booij, N.; 1981;

Gravity waves on water with non - uniform depth and current;

PhD thesis presented to the technical University of Delft, at Delft, The Netherlands.

Booij, N.; 1983;

A note on the accuracy of the mild-slope equation;

Coastal Eng., vol. 7, pg 191-203.

Bouws, E. and Battjes, J. A.;1982;

A Monte Carlo approach to the computation of refraction of water waves;

J. Geophysical Res., 87(C8), pp. 5718 - 5722.

Brandt A.; 1977;

Multi - Level Adaptive Solutions to Boundary - Value Problems;

Mathematics of Computation, Vol. 31, No. 138, pg 333-390.

Bretschneider, C. L.; 1968;

Significant waves and wave spectrum;

Ocean Industry, Feb., pg 40-46.

Chapman, D. C.;1985;

Numerical Treatment of Cross-Shelf Open Boundaries in a Barotropic Coastal Ocean
Model;

J. Phys. Oceanography, 15, pg 1060-1075.

Collins, J. I.; 1970;

Probabilities of breaking wave characteristics;

Proc. 12th ICCE, Washington, ASCE, vol. 1, pg 399 - 414.

Copeland, G.J.M.; 1985;

A numerical model for the propagation of short gravity waves and the resulting
circulation around nearshore structures;

Ph.D. Thesis, Dept. of Civil Engineering, University of Liverpool.

Copeland, G.J.M.; 1985;

A practical alternative to the "mild-slope" wave equation;

Coastal Eng., vol. 9, pg 125-149.

Daily, W. R.; 1980;

A numerical model for beach profile evolution;

MSc thesis, Dep. of Civil Eng., University of Delaware, USA.

Daily, W. R., Dean, R. G. and Dalrymple, R. A.; 1984;

A model for breaker decay on beaches;

Proc. 19th ICCE, Houston, ASCE, vol. 1, pg 82 - 98.

Daily, W. R., Dean, R. G. and Dalrymple, R. A.; 1985;

Wave height variation across beaches of arbitrary profile;

J. of Geophysical Res., vol. 90; C6, pg 11917 - 11927.

Dalrymple, R. A., Kirby J. T. and Hwang, P. A.; 1984;

Wave diffraction due to areas of energy dissipation;

J. Waterway, Port, Coastal and Ocean Eng., ASCE, vol. 110, pg 67 - 79.

Dean, R. G. and R. A. Dalrymple; 1984;

Water Wave Mechanics for Engineers and Scientists;

Prentice-Hall, Inc., Englewood Cliffs, New Jersey 07632, USA.

Dong, P. Al-Mashouk, M.; 1989;

Comparison of transient and steady state wave models for harbour resonance;

Proc. Conf. on Hydraulic and Environmental Modeling of Coastal, Estuarine and River Waters, Bradford, pg 233-244.

Ebersole, B. A.; 1985;

Refraction-Diffraction Model for Linear Water Waves;

J. Waterway Port Coastal Ocean Eng.,ASCE, vol. 111, pg 939-953.

Engquist, B. and Majda A.; 1977;

Absorbing Boundary Conditions for the Numerical Simulation of Waves;

Mathematics Computation, Vol 31, No 139, pg 629-651.

Fletcher, R. ;1976;

Conjugate gradient methods for indefinite systems;

Lecture Notes in Math., 506, pg 73-89.

Galvin, C. J.;1972;

Wave breaking in shallow water;

R. E. Meyer (Editor), Waves on beaches and resulting sediment transport. Academic Press, pg 413 - 456.

Goda, Y.; 1983;

A unified nonlinearity parameter of water wave;

Rep. Port, Harb. Res. Inst.,Japan, 22, pg 3-30.

Goda, Y.; 1975;

Irregular wave deformation in the surf zone;

Coastal Engineering in Japan, vol. 18, pg 13 - 26.

Goda, Y.; 1985;

Random Seas and Design of Maritime Sructures;

University of Tokyo Press, Japan.

Grassa, J. M.; 1990;

Directional Random Waves Propagation on Beaches;

Proc 22nd ICCE, The Netherlands, ASCE, vol. 1, pg 798 - 811.

Hamm, L., Madsen, P. A. and Peregrine, D. H.; 1993;

Wave transformation in the nearshore zone: a review;

Coastal Engineering, vol. 21, no. 1 - 3, pg 5 - 39.

Hasselman, S. and Hasselman, K.; 1983;

Integration of the spectral transport equation with exact and parametrical computational of the nonlinear energy transfer;

Proc. Symp. Wave Dynamics and Radio Probing of the Ocean Surface, Miami, Plenum Press.

Hasselman, K. et al.; 1973;

Measurements of wind - wave growth and swell decay during the Joint North Sea Wave Project (JONSWAP);

Deutsche Hydr. Zeit, Reihe A (8º), no. 12.

Holthuijsen, L. H., Booij, N. and Herbers, T. H. C.; 1989;

A prediction model for stationary, short - crested waves in shallow water with ambient currents;

Coastal Eng., vol. 13, pg 23 - 54.

Houston, J. R. ; 1981;

Combined Refraction and Diffraction of short waves using the finite element method;

Appl. Ocean Res., 3(4), pg 163-170.

Hwang, L - S. and Divoky, D.; 1970;

Breaking wave setup and decay on gentle slopes;

Proc. 12th ICCE, Washington, ASCE, vol. 1, pg 337 - 389.

Ilic, S. and Chadwick, A.; 1995;

Evaluation and Validation of the Mild Slope Evolution Equation Model Using Field Data;

Coastal Dynamics' 95, pg 149-160.

Ippen, A. T. and Y. Goda; 1963;

Wave-induced oscillations in harbours: the solution for a rectangular harbour connected to the open-sea;

Hydrodynamics Lab., M.I.T., T.R. no. 59.

Isobe, M.; 1987;

A parabolic model for the transformation of irregular waves due to refraction, diffraction and breaking;

Coastal Eng. in Japan, vol. 30, no. 1, pg 33 - 46.

Israeli, M. and Orszag, S. A.; 1981;

Approximation of Radiation Boundary Conditions;

J. Computational Physics 41, pg 115-135.

Ito, Y. and Tanimoto, K.; 1972;

A method of numerical analysis of wave propagation-application to wave diffraction and refraction;

Proc. 13th ICCE, Vancouver, ASCE, pg 403-522.

Izumiya, T. and Horikawa, K.; 1984;

Wave energy equation applicable in and outside the surf zone;

Coastal Engineering in Japan, vol. 27, pg 119 - 137.

Izumiya, T. and Isobe, M.; 1986;

Breaking criterion on non - uniformly sloping beach;

Proc. 20th ICCE, Taipei, ASCE, vol. 1, pg 318 - 327.

Jameson, Antony; 1983;

Solution of the Euler Equations for Two Dimensional Transonic Flow by a Multigrid Method;

Applied Mathematics and Computation, 13, pg 327-355.

Jameson, A. and Yoon, S.; 1986;

Multigrid Solution of the Euler Equations Using Implicit Schemes;

AIAA, vol. 24, no 11, pg 1737-1743.

Johnsen, M. and Lynch, D. R.; 1994;

A second - order radiation boundary condition for the shallow water wave equations on two - dimensional unstructured finite element grids;

International Journal of Numerical Methids in Fluids, vol. 18, pg 575 - 604.

Johnson, J. W.; 1952;

Generalized Wave Diffraction Diagrams;

Proceedings, Second Conference on Coastal Engineering, Council on Wave Research, Berkeley, pg 6-23.

Johnson, J. W.; 1953;

Engineering Aspects of Diffraction and Refraction;

Transactions, American Society of Civil Engineers, Vol 118, pg 617-652.

Karlsson, T.; 1969;

Refraction of continuous ocean wave spectra;

J. WPCOE, 95 (WW4), pg 437 - 448.

Kirby, J. T.;1984;

A note on linear surface wave - current interaction over slowly varying topography;

J. Geophys. Res., vol. 89, No C1: 745 - 747.

Kirby, J. T.;1989;

A Note on Parabolic Radiation Boundary Conditions for Elliptic Wave Calculations;

Coastal Engineering, vol. 13, pg 211-218.

Kirby, J. T., Lee, C. and Rasmussen, C.; 1992;

Time-Dependent Solutions of the Mild-Slope Wave Equation;

Proc. 23rd ICCE, Venice, ASCE, vol. 1, pg 391-404.

Komar, P. D. and Gaughan, M. K.; 1972;

Airy wave theory and breaker height prediction;

Proc. 13th ICCE, Vancouver, ASCE, vol. 1, pg 405 - 418.

Kuo, C. T. and Kuo, S. T.; 1974;

Effect of wave breaking on statistical distribution of wave heights;

Proc. 3rd Conf. on Civil Eng. in the Oceans, ASCE, New York, vol. 2, pg 1211 - 1231.

Larsen, J. and Dancy, H.; 1983;

Open boundaries in short wave simulations - a new approach;

Coastal Eng., vol. 7, pg 285-297.

Lee, J-J; 1971;

Wave-induced oscillations in harbours of arbitrary geometry;

J. Fluid Mech, vol. 45, part2, pg 375-394.

Le Mehaute, B. and Koh, R. C. Y.; 1967;

On the breaking of waves arriving at an angle to the shore;

J. Hydraulic Res., vol. 5, no. 1, pg 541 - 549.

Li, B.; 1994;

A generalized conjugate gradient model for the mild slope equation;

Coastal Eng., vol. 23, pg 215-226.

Li, B. and Anastasiou, K.; 1992;

Efficient elliptic solvers for the mild-slope equation using the multigrid technique;

Coastal Engineering, vol. 16, pg 245-266.

Longuet - Higgins, M. S.;1957;

On the transformation of a continuous spectrum by refraction;

Proc. Cambridge Phil. Soc. 53, pg 226 - 229.

Madsen, P. A. and Larsen, J.; 1987;

An efficient finite-difference approach to the mild-slope equation;

Coastal Eng., vol. 11, pg 329-351.

Massel, S. R.; 1989;

Hydrodynamics of Coastal Zones;

Elsevier Oceanography Series.

McCowan, J.; 1891;

On the solitary wave;

Phil. Mag. J. Science, vol. 32, 5th series.

Miche, M.; 1944;

Mouvements ondulatoires de la mer en profondeur constant on decroissante;

Annales des Ponts et Chaussees.

Michell, J. H.; 1893;

On the highest waves in water;

Phil. Mag., vol. 36, 5th series, pg 430-437.

Miles, J. W.; 1957;

On the generation of surface waves by shear flow;

J. Fluid Mech., 3, pg 185 - 204.

Miles, J. and W. Munk; 1961;

Harbour paradox;

Proc. ASCE, J. Waterways Harbor Div., 87, pg 111-130.

Mizuguchi, M.; 1980;

An heuristic model of wave height distribution in surf zone;

Proc. 17th ICCE, Sidney, ASCE, vol. 1, pg 278 - 289.

Mei, C. C.; 1989;

The applied dynamics of ocean surface waves;

World Scientific.

Munk, W. H.; 1949;

The solitary wave theory and its applications to surf problems;

Annals of the New York Academy of Sciences, vol. 51.

Orlanski, I.; 1976;

A Simple Boundary Condition for Unbounded Hyperbolic Flows;

J. Comput. Physi., 21, pg 251-269.

Panchang, V. G., Cushman-Roisin, B. and Pearce, B. R.; 1988;

Combined Refraction-Diffraction of Short-Waves in Large Coastal Regions;

Coastal engineering, vol 12, pg 133-156.

Panchang, V. G., Pearce, B. R., Wei, G. and Cushman-Roisin, B.; 1991;

Solution of the mild-slope wave problem by iteration;

Applied Ocean Research, Vol. 13, No 4, pg 187-199.

Panchang, V. G., Wei, G., Pearce, B. R. and Briggs, M. J.; 1990;
Numerical simulation of irregular wave propagation over a shoal;
J. Waterway, Port, Coastal and Ocean Eng., ASCE, vol. 116, no. 3., pg. 324 - 340.

Penny, W. G. and A. T. Price; 1952;
The Diffraction Theory of Sea Waves by Breakwaters and the Shelter Afforded by
Breakwaters;
Philosophical Transactions, Royal Society, Series A, Vol 244, London, pg 236-253.

Peregrine, D. H.; 1983;
Breaking waves on beaches;
Ann. Rev. Fluid Mech., 15, pg 149 - 178.

Phillips, O. M.; 1958;
The equilibrium range in the spectrum of wind - generated ocean waves;
J. Fluid Mech., 4, pg 426 - 434.

Pierson, W. J., Jr. and Moskowitz; 1964;
A proposed spectral form for fully developed wind seas based on the similarity law
of S. A. Kitaigorodskii;
J. Geophys. Res., vol. 69, no. 24, pg 5181 - 5190.

Rader, A.C.;1979;
On the parabolic equation method for water wave propagation;
J. Fluid Mech., 95 (1), pg 159-176.

Romate J.E.; 1992;
Absorbing Boundary Conditions for Free Surface Waves;
J. Computational Physics, 99, pg 135-145.

Romate J.E. and Broeze J.;1992;
Absorbing Boundary Conditions for Free Surface Wave Simulations with Panel
Method;
J Computational Physics, 99, pg 146-158.

Saad, Y. and M. H. Schultz; 1986;

GMRES: a generalized minimal residual algorithm for solving nonsymmetric linear systems;

SIAM J. Sci. Stat. Comput., Vol. 7, No. 3, pg 856-869.

Santos, A. J. P. and Neves, R. J. J.; 1991

Radiative artificial boundaries in ocean barotropic models.

Computer Modeling in Ocean Engineering 91, pg 373-383.

Seyama, A. and Kimura, A.; 1988;

The measured properties of irregular wave breaking and wave height change after breaking on the slope;

Proc. 21st ICCE, Malaga, ASCE, vol. 1, pg 419 - 432.

Smith, R. and Kraus, N. D.; 1991;

Laboratory study of wave - breaking over bars and artificial reefs;

J. of Waterway, Port, Coastal and Ocean Eng., vol 117, no. 4, pg 307 - 325.

Smith , R. and Sprinks, T.; 1975;

Scattering of surface waves by a conical island;

J. Fluid Mech., Vol 72, pg 373-384.

Southgate, H. N.; 1988;

Wave breaking: a review of techniques for calculating energy losses in breaking waves;

Rep. SR 168, Hydraulics Research, Wallingford.

Stive, M. J. F.; 1984;

Energy dissipation in waves breaking on gentle slopes;

Coastal Eng., vol. 8, pg 99 - 127.

Stokes, G. G.; 1847;

On the Theory of Oscillatory waves;

Transactions of the Cambridge Philosophical Society, Vol. 8, pg 441-455.

Svendsen, I. A.; 1984;
Wave heights and set - up in a surf zone;
Coastal Eng., vol. 8, pg 303 - 329.

Svendsen, I. A. and Jonsson, I. G.; 1982;
Hydrodynamics of coastal waters;
Technical University of Denmark, 285 pg.

Svendsen, I. A., Madsen, P. A. and Buhr - Hansen, J.; 1978;
Wave characteristics in the surf zone;
Proc. 16th ICCE, Hamburg, ASCE, vol. 1, pg 520 - 539.

Tang, Y. and Grimshaw, R.;1996;
Radiation Boundary Conditions in Barotropic Coastal Ocean Numerical Models;
Journal of Computational Physics, 123, pg 96-110.

The SWAMP Group; 1985;
Ocean Wave Modelling;
Plenum Press.

Thornton, E. B. and Guza, R. T.;1983;
Transformation of wave height distribution;
J. Geophysical Res., vol. 88; no. C10, pg 5925 - 5938.

Tsay, T.-K. and Liu, P. L.-F.; 1983;
A finite element model for wave refraction and diffraction;
Appl. Ocean Res., 5 (1), pg 30-37.

U.S. Army Corps of Engineers; 1984;
Shore Protection Manual;
U.S. Army Engineer Waterways Experiment Station, USA.

Walker, H. F. and L. Zhou; 1994;
A simpler GMRES;
J. Numer. Linear Algebra Appl., 1, pg 571-581.

Watanable, A., Hara, T. and Horikawa; 1984;
Study on breaking condition for compound wave trains;
Coastal Eng. in Japan, vol. 27, pg 71 - 82.

Weggel, J. R.;1972;
Maximum breaker height;
J. Waterways, Harbors and Coastal Eng. Division, vol. 98, no. ww4, pg 529 - 547.

Wiegel, R. L.; 1962;
Diffraction of Waves by Semi-infinite Breakwater;
Journal, Hydraulics Division, American Society of Civil Engineers, Vol. 88, pg 27-44.

Williams, R. G., Darbyshire, J. and Holmes, P.; 1980;
Wave refraction and diffraction in a caustic region: a numerical solution and experimental vallidation;
Proc. Inst. Civil Eng., Part 2, 69, pg 635-649.

Van der Vorst, H. A.; 1992;
Bi-CGSTAB: a fast and smoothly converging variant of Bi-CG for the solution of nonsymmetric linear systems;
SIAM J. Sci. Stat. Comput., Vol 13, No. 2, pg 631-644.

Vincent, C. L. and Briggs, M. J.; 1989;
Refraction - Diffraction of Irregular Waves over a Mound;
J. of Waterway, Port, Coastal, and Ocean Eng. ASCE, vol. 115, no. 2, pg 269 - 284.

Yamaguchi, M.; 1986;
A numerical model of nearshore currents based on a finite amplitude wave theory;
Proc. 20th ICCE, Taipei, ASCE, vol. 1, pg 849 - 863.

Yoo, D. and O'Connor, B. A.;1986;
Mathematical modelling of wave - induced nerashore circulations;
Proc. 20th ICCE, Taipei, ASCE, vol. 2, pg 1667 - 1681.

Yoo, D. and O'Connor, B. A.;1988;

Diffraction of waves in caustics;

J. of Waterway, Port, Coastal, and Ocean Eng., ASCE, vol. 114, no. 6, pg 715 - 731.

Yoo, D., O'Connor, B. A. and McDowell, D. M.;1989;

Mathematical models of wave climate for port design;

Proceedings of the Institution of Civil Engineers, vol. 86, No. Jun, pg 513 - 530.

Zhao, Y. and Anastasiou, K.;1996;

Modelling of wave propagation in the nearshore region using the mild-slope equation with GMRES-based iterative solvers;

International Journal for Numerical Methods in Fluids, vol. 23, pg 397-411.